PERIODIC FLOW OF NON-NEWTONIAN FLUIDS ACROSS AN ARRAY OF CYLINDERS

Ph. D. THESIS

by

RAM PRAVESH RAM

DEPARTMENT OF CHEMICAL ENGINEERING
INDIAN INSTITUTE OF TECHNOLOGY ROORKEE
ROORKEE-247667, INDIA
AUGUST, 2017

PERIODIC FLOW OF NON-NEWTONIAN FLUIDS ACROSS AN ARRAY OF CYLINDERS

A THESIS

Submitted in partial fulfilment of the requirements for the award of the degree

of

DOCTOR OF PHILOSOPHY

in

CHEMICAL ENGINEERING

by

RAM PRAVESH RAM

DEPARTMENT OF CHEMICAL ENGINEERING
INDIAN INSTITUTE OF TECHNOLOGY ROORKEE
ROORKEE-247667, INDIA
AUGUST, 2017

INDIAN INSTITUTE OF TECHNOLOGY ROORKEE
ROORKEE

CANDIDATE'S DECLARATION

I certify that the work which is being presented in the thesis entitled "Periodic Flow of non-Newtonian Fluids Across an Array of Cylinders" is partial fulfilment of the requirements for the award of the Degree of Doctor of Philosophy and submitted in the Department of Chemical Engineering of the Indian Institute of Technology Roorkee, Roorkee is an authentic record of my own work carried out during a period from July, 2012 to August, 2017 under the supervision of Dr. A. K. Dhiman, Associate Professor and Dr. R. P. Bharti, Associate Professor, Department of Chemical Engineering, Indian Institute of Technology Roorkee, Roorkee.

The matter presented in the thesis has not been submitted by me for the award of any other degree of this or any other institute.

(Ram Pravesh Ram)

This is to certify that the above statement made by the candidate is correct to the best of our knowledge

(A. K. Dhiman)
Supervisor

(R. P. Bharti)
Supervisor

Dated: 21.8.2017

DEDICATED

TO

MY FAMILY

ACKNOWLEDGEMENT

I take this opportunity to express my heartiest and deepest sense of gratitude to those who helped me to complete my dissertation. This thesis would not have been possible without the support and meticulous guidance of my supervisors **Dr. A. K. Dhiman** and **Dr. R. P. Bharti,** Associate Professors, Department of Chemical Engineering, Indian Institute of Technology Roorkee. I take this opportunity to express my deepest sense of gratitude to such a sincere academician and generous guide who have been a source of inspiration and encouragement to me in completing this research work in its present form. I have a deep sense of admiration for his goodness and his anytime availability during this research work.

I express my sincere gratitude to **Dr. C. B. Mazumdar**, Head, Department of Chemical Engineering and **Dr. Bikash Mohanty**, Chairman, DRC for their continuous encouragement, inspiration and support. I am also thankful to **Dr. Shishir Sinha**, Chairman, SRC for their kind affection and support. I am also very very thankful to all the faculty members of the department and Institute for their inspiration, love and continuous support and especially my SRC members **Dr. (Mrs.) Shashi (Internal) and Dr. Manish Mishra (External)** for their continuous inspiration and support. I would also like to express my profound thanks to Deepak Kumar, Anirudh Sanyal, Asif, Neeraj, Akshay, Maaz, etc., whose friendship has always given me a mental support and whose communications, though from near and far places, have been great sources of inspiration. Also, my warmest thanks go to all my friends, seniors and colleagues at IIT Roorkee, whose names would form a big list, for their unparalleled company and valuable and timely assistance. I would also like to thank the office and technical staff of Chemical Engineering Department and especially Mr. Arun Dwivedi, Chaudhariji, Mr. Rajkumar Yadav and Vijay Singhji who extended all possible help during all stages of this research work.

In spite of all my efforts, this was not at all possible without the endless care, unfailing support and understanding of my dear wife Mrs. Sangita and my kids Aditya and Tejas who faced every difficult moment with me during my doctoral program smilingly and always stood along with me. I am deeply and thoroughly grateful to my parents for all their blessings, affection and well wishes for me who always give me courage and strength to face all the challenges in my life. I am also thankful to my big brother Sri Ashok Kumar who always takes care of me and other family members such as Mohnish, Sonia and relatives for their continuous love and moral support. Lastly, I am always thankful to the omnipresent, **GOD**, for providing me an opportunity, strength and ambiance to accomplish this work.

(**Ram Pravesh Ram**)

SYNOPSIS

The flow and thermal features of fluids across the periodic array of cylinders and/or over tube banks are considered as one of the classical problems in the fluid mechanics because of its widespread industrial applications. For instance, the flow of process streams in the shell side of tubular heat exchangers is often used to model the flow over the tube banks. Screens used to filter polymer melts are sometimes modeled as randomly oriented cylinders. Longitudinal flow over rod bundles is common in most fuel elements of nuclear power reactors where the main heat exchanging equipment is composed of a large number of parallel fuel rods arranged in a regular array. To allow sufficient and regularly distributed space for the coolant flow parallel to the axes of the fuel rods, suitable spacing devices are used, which also provide rigidity to the fuel element. Moreover, this flow arrangement is also found significant in the fluidized bed drying of fibrous materials, filtration of paper and pulp suspensions and biological systems, etc. (Duli et al., 1995; Martin et al., 1998; Vijaysri et al., 1999; Mandhani et al., 2002; Mangadoddy et al., 2004).

The above flow geometries are oriented in different geometrical arrangements in the process equipment such as heat exchangers, evaporators, boilers and condensers, etc. Typically, tube banks consist of square, triangular, rectangular and hexagonal array of cylinders. Amongst all these arrangements, the square array of cylinders is most popular and widely used because of its simple geometrical orientations. Because the physical geometry of interest, the expected patterns of the flow through an array of cylinders have a periodically repeating nature. The present work is devoted to the periodic flow of fluids across a square array of circular cylinders in cross-flow. Understanding of the flow and thermal features from such a system is always challenging, because the boundary layers are periodic and continuous which cause a great resistance to the flow of fluids. The kind of flow whether longitudinal or transverse, laminar or turbulent and the porosity of the cylinders (cylinder arrays are treated as porous media), are the other factors which further make the problem more stimulating to explore and investigate. For instance, in the case of transverse flow, the buoyancy acts perpendicular to flow direction, which enhances the rate of heat transfer. Few such examples are the air flowing horizontally over a heated pipe, steam leaving a boiler passes through a pipe where a fan blowing over it, etc. Other examples include the applications in solar thermal extraction system as well as some parts of electronic equipment cooling, etc. (Gowda et al., 1998; Soares et al., 2009; Daniel and Dhiman, 2013).

Furthermore, the non-Newtonian fluid (shear-thinning and shear-thickening) nature and the buoyancy induced flow are the additional factors which make the problems more intricate and ambiguous due to the direct impact of these parameters on the flow and thermal fields, drag

force and Nusselt number, etc. In fact, a thorough and in-depth understanding of the detailed kinematics of such a flow is germane to the development of a reliable methodology for the process equipment design. In other words, the flow and heat transfer characteristics across a periodic array of cylinders are one of the starving areas to be studied in fluid mechanics.

Owing to such an excellent industrial relevance, still very little is known about the flow and heat transfer characteristics across a periodic array of cylinders even with simple Newtonian kind of fluids (Koch and Ladd, 1997; Martin et al., 1998; Spelt et al., 2005b). Notwithstanding, in the literature, two distinct approaches/schemes are available to investigate such type of flow and thermal problems. In the first scheme, the field equations are solved for the different geometrical arrangements of a periodic array of cylinders/spheres with known geometrical configuration, whereas, in the second scheme, the assemblage of cylinders/spheres is modeled by using the approximate cell models where the modeling depends upon particle-particle interactions. For instance, a frictional pressure gradient over an assemblages of long cylinders was estimated by employing a most common velocity and stress-variational principle (Slattery, 1972). Further, free surface cell model (Happel, 1964) was used to determine the interferences amongst the cylinders. The drag on cylinders was described to gradually reduce under the analogous value of Newtonian fluids with an increasing shear-thinning behavior. Subsequently, the model equations were solved by using free surface cell models, zero vorticity cell model, etc. (Vijaysri et al., 1999; Shibu et al. 2001; Mandhani et al., 2002; Mangadoddy et al., 2004, etc.)

In summary, the critical review of the available literature on the periodic flow across an array of cylinders for Newtonian and non-Newtonian fluids suggests that insights for global engineering parameters such as the drag coefficients, pressure loss, permeability, Nusselt numbers, etc. using various cell models are available, but they are limited to lemianr creeping flow and low porosity of the cylinders. In fact, there is no literature which could reveal the flow and thermal features by using the direct periodic array of cylinders. Additionally, in case of mixed convection flow problems, negligible literature/studies are available to such flow geometries. These gaps in the literature motivated us to investigate the problems of forced and mixed convection across an array of cylinders to explore the features of Newtonian and non-Newtonian power-law fluids flow through such an industrially important flow geometry.

Therefore, with the aim of fulfilling the gap in the literature, this thesis is concerned with the numerical investigation of steady forced/mixed convection flow and heat transfer characteristics of Newtonian and non-Newtonian power-law fluids across an array of circular cylinders in a square arrangement.

Objectives of the thesis

The objectives of this thesis are to supplement the available knowledge through a CFD investigation for the wide ranges of pertinent dimensionless parameters such as fluid volume fraction, power-law index, Reynolds, Prandtl and Richardson numbers to explore the momentum and heat transfer characteristics of Newtonian and non-Newtonian fluids across a periodic array of circular cylinders in square configuration. Particularly, this dissertation has focused on an investigation of the five problems as mentioned in the following Table.

Table: Problems studied in this dissertation

S. No.	***Problems studied across a periodic array of cylinders in a square configuration***	***Ranges of physical parameters***
1.	Forced convection flow and heat transfer characteristics of Newtonian fluids	$0.70 \leq \phi_f \leq 0.99$ $0.70 \leq Pr \leq 100$ $1 \leq Re \leq 40$
2.	Forced convection flow characteristics of non-Newtonian power-law fluids	$0.70 \leq \phi_f \leq 0.99$ $1 \leq Re \leq 40$ $1 \leq Pr \leq 100$ $0.4 \leq n \leq 1.8$
3.	Forced convection heat transfer characteristics of non-Newtonian power-law fluids	$0.70 \leq \phi_f \leq 0.99$ $1 \leq Re \leq 40$ $1 \leq Pr \leq 100$ $0.4 \leq n \leq 1.8$
4.	Mixed convection flow and heat transfer characteristics of Newtonian fluids	$0.70 \leq \phi_f \leq 0.99$ $0.70 \leq Pr \leq 50$ $1 \leq Re \leq 40$ $0 \leq Ri \leq 2$
5.	Mixed convection flow and heat transfer characteristics of power-law fluids	$0.70 \leq \phi_f \leq 0.99$ $1 \leq Pr \leq 50$ $1 \leq Re \leq 40$ $0 \leq Ri \leq 2$ $0.4 \leq n \leq 1.8$
(ϕ_f : fluid volume fraction, Pr: Prandtl number, Re: Reynolds number, Ri: Richardson number and n: power-law index)		

The solution of aforementioned problems has been obtained by solving the modified form of Navier-Stokes equations with appropriate boundary conditions for the various cases and conditions with and without the use *of Boussinesq approximations* by using commercial CFD solver ANSYS Fluent (2009). An unstructured non-uniform grid consisting of triangular cells was generated by using a commercial grid tool GAMBIT. A finer mesh was generated near the cylinder surfaces to better resolve the sharper gradients. The 2-D, laminar and segregated solver

was utilized to simulate the incompressible flow on the collocated grid arrangement. A second order upwind scheme was used to discretize the convective terms appearing in both flow and thermal equations. A SIMPLE scheme was used to handle the pressure and velocity coupling. The double precision solver was used to improve the accuracy of solutions and the converged results were obtained when each of the continuity, momentum residuals reached in the order of 10^{-10} and energy residuals in the order of 10^{-14}. In view of all these facts, the above five problems are discussed herein for a brief overview of this dissertation:

1. Forced convection flow and heat transfer characteristics of Newtonian fluids across periodic array of circular cylinders

The forced convection flow and heat transfer characteristics of Newtonian fluids have been studied for the ranges of parameters as mentioned in Table. Particularly, the influences of flow governing parameters (Re, Pr and ϕ_f) on the local and global characteristics have been revealed. The numerical results suggest that for a given value of Reynolds number, the total drag coefficients decrease drastically as the fluid volume fraction increases. The importance of inertia diminishes with an increasing compactness of cylinders (i.e., the decreasing ϕ_f) because of the largest contribution of viscous dissipation in this limit in small gaps between the cylinders. Therefore, the friction drag is dominating over pressure drag. These features reveal that there is the strong dependence of drag coefficient on both fluid volume fraction as well as Reynolds number. In the case of heat transfer, for the fixed values of Reynolds and Prandtl numbers, the average Nusselt number increases with decreasing fluid volume fraction. This increase in average Nusselt number is greatly influenced by the interactions between the cylinders. Attempts are also made to interpret the average Nusselt number values in terms of the Colburn heat transfer factor (j_H) for their easy use in process engineering and design calculations. Further, the numerical results of individual and total drag coefficients and the average Nusselt number have been used to develop the simple correlations as a function of pertinent dimensionless variables (i.e., Re, Pr and ϕ_f) and results have been compared with the available literature which displayed an excellent agreement.

2. Forced convection momentum transfer characteristics of power-law fluids across periodic array of circular cylinders

Here, the flow features of power-law fluids have been displayed for the ranges of parameters as listed in Table. The results are presented in terms of streamlines, pressure coefficient and individual and total drag coefficients for the governing parameters. The dependence of individual

and total drag coefficients on the power-law index, fluid volume fraction and Reynolds number shows the non-monotonous behavior. For shear-thinning fluids (n < 1), the pressure drag coefficient dominates over friction drag coefficient; whereas, an opposite behavior was seen for the shear-thickening fluids (n > 1) except at Re = 40. Further, both of the individual and total drag coefficients were seen to increase and decrease with the increase in the power-law index over the range of fluid volume fraction ($0.70 \leq \phi_f \leq 0.90$) and ($0.92 \leq \phi_f \leq 0.99$), respectively. Strong interactions between the periodic cylinders were observed at the lower values of fluid volume fractions which diminish with the increasing value of fluid volume fractions. The results were further used to develop an empirical correlation for the pressure, friction and total drag coefficients to give an additional physical insight of this study. The results have been compared with the available literature which shows an excellent agreement.

3. Forced convection heat transfer characteristics of power-law fluids across periodic array of circular cylinders

In this part, the results have been discussed in terms of local and global characteristics of heat transfer such as isotherm patterns, local and average Nusselt numbers for the broad range of governing parameters (Table). The numerical results revealed the heat transfer enhancement of approximately 97% in the shear-thinning fluids among the lowest and the highest fluid volume fractions for the highest value of Pr and the lowest value of Re and n. Under the identical conditions, the enhancement was about 83% in the shear-thickening region. For the ranges examined herein, different levels of improvement in the average Nusselt number were noticed because of the shear-thinning and shear-thickening natures. The results were further used to develop an empirical correlation for the average Nusselt number and the Colburn heat transfer factor to give additional physical insight. Additionally, the present results have been compared with the available literature which displayed a good agreement.

4. Aiding buoyancy mixed convection characteristics of Newtonian fluids across periodic array of circular cylinders

Mixed convection features of Newtonian fluids have been studied under the aiding buoyancy conditions for the ranges of parameters stated in Table. The numerical results were observed to be the strongly dependent on the governing parameters (ϕ_f, Re, Pr and Ri). The drag coefficients were observed to be diminished with an upturn in Reynolds number and fluid volume fractions, whereas an opposite behavior was noticed with the rise in Prandtl number and buoyancy parameter (Ri). Further, the local and average Nusselt numbers were improved with increased

value of Prandtl and Reynolds numbers and surprisingly with the fluid volume fractions (ϕ_f) also, as opposed to decrease in forced convection case. Additionally, aiding buoyancy enhances both flow as well as heat transfer features. The strong influence of ϕ_f on results was observed relative to other parameters (Re, Pr and Ri). Moreover, at the higher values of ϕ_f , Re and Pr, a transient behavior was also noticed. Statistical correlations were developed for the total drag coefficient and average Nusselt number to gain the further physical insights. Finally, the results have been compared with the scant available literature which displayed an excellent agreement.

5. Aiding buoyancy mixed convection characteristics of power-law fluids across periodic array of circular cylinders

The mixed convection flow and heat transfer characteristics to non-Newtonian fluids across a periodic array of circular cylinders have been investigated numerically for a wide range of governing parameters (n, ϕ_f , Re, Pr and Ri) under the aiding buoyancy conditions (Table). The influences of these parameters on the streamlines, pressure coefficient, isotherm patterns and individual and total drag coefficients, local and average Nusselt numbers were explored and presented. The local flow phenomenon (streamlines, pressure coefficient and isotherm patterns) describes that the dense arrays offer higher resistances to flow of fluids and hence sparse array is required to minimize the flow resistances. Further, the drag coefficients decrease gradually with increasing value of Re for all the values of fluid volume fractions and power-law index. However, an increase in drag coefficients was observed with increasing value of Prandtl number in the mixed convection (Ri > 0) case as opposed to forced convection case (Ri = 0). The isotherm patterns reveal that the increasing inertial effects enhance the rate of heat transfer due to the dense clustering of the isotherms near the cylinder surfaces. The average Nusselt number was observed to be increased with the increasing values of ϕ_f , Re, Pr and Ri and the decreasing value of n (increasing shear-thinning behavior). A transient behavior was observed for both of the drag coefficients as well as average Nusselt number at higher fluid volume fractions and Reynolds numbers. Additionally, aiding buoyancy enhances both of the flow and thermal parameters in the vicinity of periodic cylinders. Moreover, statistical correlations for the drag coefficients and average Nusselt numbers are developed for gaining the more physical insight of the results.

In summary, the detailed insights of the forced and mixed (aiding buoyancy) convection flow and heat transfer characteristics have been gained and presented for both Newtonian and non-Newtonian power-law fluids for the wide ranges of flow governing parameters across a periodic array of circular cylinders in a square geometrical configuration.

TABLE OF CONTENTS

LIST OF FIGURES

LIST OF TABLES

NOMENCLATURE

A_i	Flow area (m^2)
C_D	total drag coefficient (-)
C_D^N	normalized total drag coefficient (-)
C_{DF}	friction drag coefficient (-)
C_{DF}^N	normalized friction drag coefficient (-)
C_{DP}	pressure drag coefficient (-)
C_{DP}^N	normalized pressure drag coefficient (-)
C_{DR}	drag ratio (-)
c_p	specific heat (J/kg K)
C_P	surface pressure coefficient (-)
D	cylinder diameter (m)
D_{hi}	hydraulic diameter (m)
E_{ij}	the rate of strain tensor (s^{-2})
F	the correction factor (-)
Fa	tube arrangement factor (-)
F_D	drag force per unit length of the cylinder (N/m)
F_{DF}	viscous drag force per unit length of the cylinder (N/m)
F_{DP}	pressure drag force per unit length of the cylinder (N/m)
g	gravitational acceleration (m/s^2)
Gi	grid sizes (i = 1, 2, 3 and 4)
Gr	Grashof number (-)
h	convective heat transfer coefficient (W/m^2K)
I_2	second invariant of rate of strain tensor (s^{-2})
k	thermal conductivity (W/m K)
L	cylinder spacing (m)
m	power-law consistency index (Pa s^n)
$\dot{m}$	mass flow rate (kg/s)
n	power-law index (-)
n_s	unit vector (m)
N_c	total number of grid points (-)

n_T	total number of tubes (-)
N	total number of nodes in the computational domain (-)
Nu	average Nusselt number (-)
Nu^N	normalized average Nusselt number (-)
Nu_L	local Nusselt number (-)
P	pressure (Pa)
$p(\theta)$	Surface pressure at an angle θ (Pa)
p_0	free stream pressure at the exit boundary (Pa)
P_{wi}	wetted perimeter (m)
Pe	Peclet number (-)
Pr	Prandtl number (-)
R	radius of cylinders (m)
Re	Reynolds number (-)
Ri	Richardson number(-)
S	surface area (m^2)
T	temperature (K)
T_i	inlet fluid temperature (K)
T_o	outlet fluid temperature (K)
T_w	cylinder wall temperature (K)
T_∞	bulk fluid temperature (K)
V	volume averaged velocity (m/s)
V_x and V_y	x- and y-components of velocity, respectively (m/s)
X^N, X^M	normalized parameters (-)
W	distance from the wall (m)

Greek symbols

α	thermal diffusivity (m^2/s)
β	coefficient of volumetric thermal expansion (1/K)
Δ	maximum grid spacing (-)
Δ	minimum grid spacing(-)
η	viscosity of fluids (Pa s)
η_a	apparent viscosity (Pa s)
$\dot{\gamma}$	rate of shear at any point in the fluid (s^{-1})

μ	viscosity of fluids (Pa s)
ϕ_f	fluid volume fractions (-)
ϕ_s	solid volume fractions (-)
ψ	stream function (m^2/s)
ψ_{min}	minimum value of stream function (m^2/s)
ψ_{max}	maximum stream function (m^2/s)
ρ	density of fluids (kg/m^3)
ρ_0	density of fluids at temperature T_0 (kg/m^3)
θ	surface angle (radian)
τ	extra stress tensor (Pa)
τ_{xx} , τ_{yx}	x- and y-component of shear stress (Pa)
τ_0	yield stress (Pa)
$\varepsilon_r(x)$	relative change (%)

Subscripts/superscripts

∞	Bulk
f	Fluid
s	Solid
max	Maximum
min	minimum
i	inlet
o	outlet

Abbreviations

CFD	Computational Fluid Dynamics
CV	Control Volume
FDM	Finite Difference Method
FEM	Finite Element Method
FVM	Finite Volume Method
LBM	Lattice Boltzmann Method
PDE	Partial Differential Equations

LIST OF PUBLICATIONS FROM THIS WORK

➢ Refereed International Journals

1. R. P. Ram, R. P. Bharti, A. K. Dhiman, "Forced convection flow and heat transfer across an in-line bank of circular cylinders" The Canadian Journal of Chemical Engineering 94(7), 1381-1395 (2016).

2. R. P. Ram, A. K. Dhiman, R. P. Bharti, "CFD investigation of heat transfer characteristics of non-Newtonian power-law fluids across a periodic array of circular cylinders in a square configuration" *(under review in Progress in Computational Fluid Dynamics).*

3. R. P. Ram, R. P. Bharti, A. K. Dhiman, "Transverse flow characteristics of power-law fluids across sparse periodic array of circular cylinders" *(under review in The Canadian Journal of Chemical Engineering).*

4. R. P. Ram, A. K. Dhiman, R. P. Bharti, "Mixed convection flow and thermal features across a periodic array of circular cylinders in cross flow with aiding buoyancy conditions" *(under review in International Journal of Thermal Sciences).*

5. R. P. Ram, R. P. Bharti, A. K. Dhiman, "Mixed convection flow and heat transfer characteristics of non-Newtonian fluids across an array of circular cylinders with aiding buoyancy" *(under review in Industrial and Engineering Chemistry Research).*

➢ International and National Conferences

6. Ram Pravesh, R.P Bharti, Amit Kumar Dhiman, "Periodic fluid flow across an array of cylinders" An International Conference on Advances in Chemical Engineering (ACE 2013)" organized by Chemical Engineering department, I.I.T. Roorkee during February 22-24, 2013. SOUVENIR, Paper ID: 00147.

7. Ram Pravesh, A. K. Dhiman, R. P. Bharti, "Estimation of drag coefficient for the fluid flow through periodic array of cylinders" CHEMCON 2013, 66th Annual Session of Indian Institute of Chemical Engineers (IICHE) organized at Institute of Chemical Technology Mumbai during December 27-30, 2013 (paper ID: FMC 051).

8. Ram Pravesh, R.P Bharti, A. K. Dhiman, "Flow of non-Newtonian fluids through periodic array of circular cylinders" 5th International and 41st National Conference on Fluid Mechanics and Fluid Power (FMFP 2014)" organized by Mechanical Engineering department, I.I.T. Kanpur during December 12-14, 2014 (Paper ID: FMFP-14-K1-103).

Chapter 1

INTRODUCTION

1.1 Motivation

The flow of fluids across periodic array of cylinders and/or over tube banks represent an idealization to many industrially important processes as encountered in chemical and allied industries, polymer industries as well as biological and food industries, etc. (Vijaysri et al., 1999; Prasad and Chhabra 2001; Shibu et al., 2001). Accordingly, these flow geometries are found significant in the design of several heat and mass transfer equipments, filtration of paper and pulp suspensions, autoclave processes, coating of textiles, fluidized bed drying of fibrous materials (e.g. coconut shell and rice husk, etc.), composite manufacturing and oil recovery, etc. (Sangani and Acrivos, 1982; Drummond and Tahir, 1984; Talwar and Khomami, 1995; Koch and Ladd, 1997; Mandhani et al., 2002; Mangadoddy et al., 2004; Spelt et al., 2005a, b). For instance, the flow of process streams in the shell side of tubular heat exchangers which also display the non-Newtonian behaviors are often used to model the flow from these geometries. Screens used to filter polymer melts are sometimes modeled as a randomly oriented cylinders. Further, longitudinal flow over tubes or rod bundles is common in most fuel elements of nuclear power reactors. In the principal heat exchanging equipment, the core is composed of a large number of parallel fuel rods arranged in a regular array. To allow sufficient and regularly distributed space for the coolant flowing parallel to the axes of the fuel rods, suitable spacing devices are used, which also provide rigidity to the fuel element, etc.

The above tube banks/flow geometries are oriented in different geometrical arrangements in process piping systems such as heat exchangers, evaporators, boilers and condensers, etc. Typically encountered arrangements found in tube banks consist of square, triangular, rectangular and hexagonal array of cylinders. Amongst all these arrangements, the square array of circular cylinders is most popular and widely used because of its simple geometrical orientation. Further, the flow which occurs through this geometry is repeating in nature over some module or periodic length and therefore is called as periodic flow. The present work is devoted to the periodic flow of fluids across a periodic array of circular cylinders in a square configuration. In fact, the flow and thermal features from such an industrially important geometry are one of the starving classical problems to be studied in fluid mechanics.

The common engineering problem of flow across a periodic array of cylinders is to investigate the nature of flow and heat transfer characteristics. Understanding of the flow and thermal features from such a system is always challenging, because the boundary layers are periodic and continuous which cause a great resistances to flow of fluids. The kind of flow whether longitudinal or transverse, laminar or turbulent along with the varying porosity of the cylinders (cylinder arrays are approximated as porous media) are the other factors which further make the problem more stimulating to explore and investigate. For instance, in case of transverse flow, the buoyancy acts perpendicular to flow direction, which enhances the rate of heat transfer. Few such examples are the air flowing horizontally over a heated pipe, steam leaving a boiler passes through a pipe where a fan blowing over it, etc. Other examples include the applications in solar thermal extraction system as well as some parts of electronic equipment cooling, etc. (Gowda et al., 1998; Soares et al., 2009; Daniel and Dhiman, 2013).

Furthermore, the non-Newtonian fluid (shear-thinning and shear-thickening) nature and the buoyancy induced flow are the additional factors which make the problems more intricate and ambiguous due to the direct impact of these parameters on the flow and thermal fields, drag force and Nusselt number, etc. In fact, a thorough and in-depth understanding of the detailed kinematics of such a flow is germane to the development of a reliable methodology for the process equipment design. In other words, the flow and heat transfer characteristics across a periodic array of cylinders are one of the starving areas to be studied in fluid mechanics.

Owing to such an excellent industrial relevance, still a very little is known about the flow and heat transfer characteristics across a periodic array of cylinders even with simple Newtonian kind of fluids (Koch and Ladd, 1997; Martin et al., 1998; Spelt et al., 2005b) and therefore, it's still an infancy area of research. Fortunately, over the past few decades, considerable research efforts have been made to this flow configuration to determine the local and global flow and heat transfer characteristics (streamlines, pressure and isotherm contours, individual and total drag coefficients, local and average Nusselt numbers, etc.) for the different ranges of parameters. Many reviews, books, survey articles (Zukaukas, 1987b; KaKac et al., 1987; Skartsis et al., 1992a; Ghosh et al., 1994; Perry, 1997) and research papers (Happel, 1959; Launder and Massey, 1978; Sangani and Acrivos, 1982; Drummond and Tahir, 1984; Edwards et al., 1990; Astrom et al., 1992; Ghaddar, 1995; Talwar and Khomami, 1995; Koch and Ladd, 1997; Martin et al., 1998; Spelt et al., 2005a, b, etc.) are present in the literature to display the above behaviour from these flow configurations. No doubt, most of these are concentrated on Newtonian fluid flow than the corresponding non-Newtonian flow. In fact, scant literature is available for the forced convection

flow and heat transfer features of non-Newtonian fluids to the periodic array of circular cylinders. Additionally, in the case of mixed convection flow and thermal problems, almost negligible literature/studies are available for the array of cylinders. These gaps in the literature motivated us to investigate the problems of forced and mixed convection across a periodic array of circular cylinders to reveal the features of Newtonian and non-Newtonian power-law fluids from such an industrially important flow geometries.

Therefore, the aim of this thesis is to fill up the gaps in the literature through a CFD investigation for the wide ranges of pertinent dimensionless parameters such as fluid volume fractions, power-law index, Reynolds number, Prandtl number and Richardson number to explore the momentum and heat transfer characteristics of Newtonian and non-Newtonian power-law fluids across a periodic array of circular cylinders in square configuration. The problem was modeled as a unit cell with symmetric and periodic boundary conditions and the governing equations (continuity, momentum and thermal energy) have been solved numerically. The study examined the dependence of local and global characteristics (i.e., streamlines, pressure and isotherm contours, pressure coefficients, individual and total drag coefficients and local and average Nusselt numbers, the Colburn j_H factor) to both of the Newtonian and non-Newtonian fluids.

1.2 Organization of thesis

This dissertation consists of ten chapters. Chapter 2 presents the fundamental concepts of periodic flow, a brief knowledge of different kinds of fluids, engineering parameters used in this study and the relevant literature review for the flow across a periodic array of cylinders and/or tube banks. It, in turn, facilitates the objectives of this dissertation based upon the gaps found in the literature. Chapter 3 discusses the problem description, mathematical modeling, governing equations and boundary conditions, etc. In Chapter 4, the solution methodology, choices of numerical parameters and grid independence test have been discussed. The five problems studied in this thesis have been thoroughly discussed in Chapters 5 to 9, which includes a brief description of problems, useful governing equations and validation/benchmarking of the results and finally the results and discussions. Lastly, Chapter 10 presents the concluding remarks and scope for the future works.

Chapter 2

FUNDAMENTAL CONCEPTS AND LITERATURE REVIEW

This chapter deals with the basic ideas about periodic flow across an array of cylinders including their various kinds and flow geometry to understand the elementary flow phenomena. Various dimensionless parameters used in this study have also been defined herein. It is followed by the relevant literature on the flow of Newtonian and non-Newtonian fluids across the periodic array of circular cylinders and/or over tube banks to discuss the latest development of forced and mixed convection flow and heat transfer characteristics.

2.1 Periodic flow

Periodic flow is defined in terms of periodically repeating nature, as shown in Fig. 2.1. The assumption of periodicity implies that the velocity components repeat themselves in space as follows:

$$u(\vec{r}) = u(\vec{r} + \vec{L}) = u(\vec{r} + \overrightarrow{2L}) = \cdots \quad (2.1a)$$

$$v(\vec{r}) = v(\vec{r} + \vec{L}) = v(\vec{r} + \overrightarrow{2L}) = \cdots \quad (2.1b)$$

$$w(\vec{r}) = w(\vec{r} + \vec{L}) = w(\vec{r} + \overrightarrow{2L}) = \cdots \quad (2.1c)$$

Where $\vec{r}$ is the position vector and $\vec{L}$ is the periodic length vector of the domain considered as shown in Fig. 2.1.

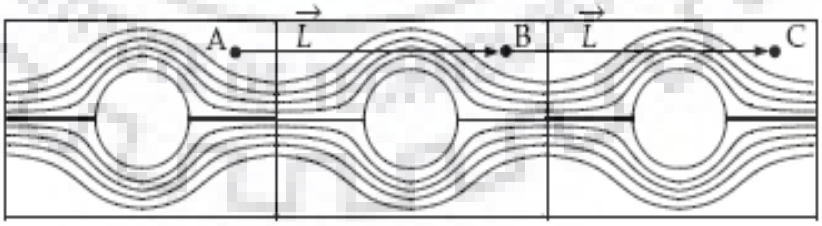

$$\begin{aligned} u_A &= u_B = u_C & \bar{p}_A &= \bar{p}_B = \bar{p}_C \\ v_A &= v_B = v_C & p_B - p_A &= p_C - p_B \end{aligned} \quad (2.2)$$

Figure 2.1: Schematics of periodic flow geometry (ANSYS Fluent, 2009)

The points A, B and C of length $\vec{L}$ in Fig.2.1 are the periodic length. The velocity and pressure are equal through these periodic length.

2.1.1 Types of periodic flow

In periodic flow, since the geometry as well as flow features are repetitive in nature and, therefore, based on these repetitions, it is categorized in two types as rotational and translational. In the first type, i.e., rotational, no pressure drop occurs across the periodic planes whereas, in the second type, i.e., translational, a pressure drop occurs across the translationally periodic boundaries which yield the fully developed or stream-wise periodic flow. Stream-wise periodic conditions exist when the flow pattern repeats over some periodic length L with a constant pressure drop across each repeating module along the stream-wise direction. In such a flow configuration, the geometry varies in a repeating manner along the direction of the flow leading to a periodically fully developed flow regime in which the flow pattern repeats in successive cycles and due to this feature, the modeling of periodic flow is straightforward. The examples of translational and rotational periodic planes are shown in Figs. 2.2 (a) and 2.2 (b), respectively.

(a) (b)

Figure 2.2: (a) Translational and (b) rotational periodic plane (ANSYS Fluent, 2009).

2.1.2 Various arrangements for periodic flow

The different kinds of flow arrangements for a periodic array of circular cylinders are presented herein according to their geometrical orientations. Fig. 2.3 represents a square arrangement of circular cylinders through which the fluid is flowing in the transverse direction. For instance, Fig. 2.3(a) shows the approach of fluid across a general square packing arrangement and Fig. 2.3 (b) displays the occurrence of periodic flow inside the tube bundles which are repeating in nature. Similarly, Fig. 2.4 (a) displays a general transverse flow for a triangular array and an example of hexagonal arrangement is shown in Fig. 2.4 (b).

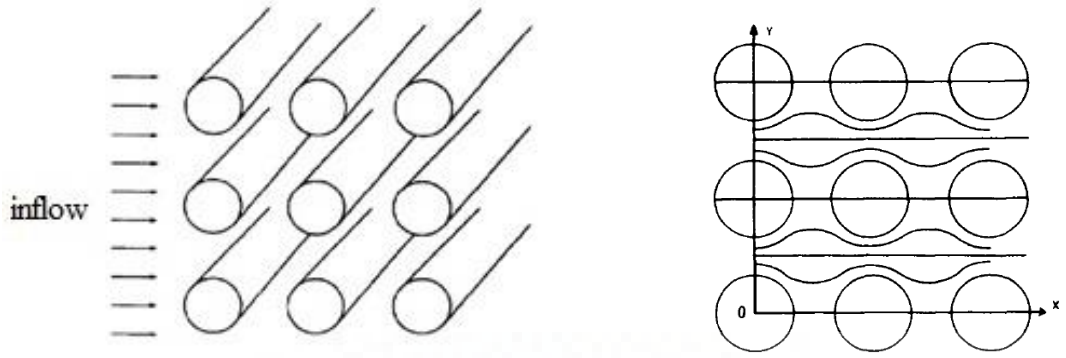

(a) (b)

Figure 2.3: General transverse flow across a regular array of cylinders for square arrangement (a) Bruschke and Advani, 1993 (b) Drummond and Tahir, 1984

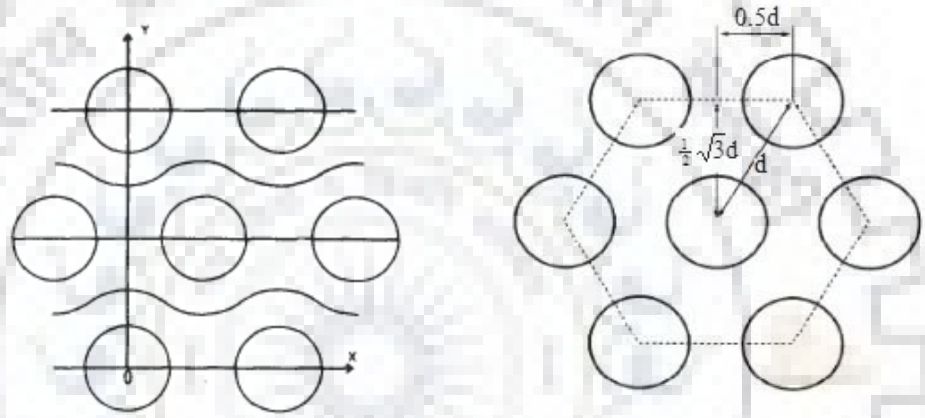

(a) (b)

Figure 2.4: (a) General transverse flow for a triangular array (Drummond and Tahir, 1984) and (b) an example of cylindrical tubes in hexagonal arrangement (Bruschke and Advani, 1993)

Notwithstanding, the possible geometrical arrangements of tubes inside the tube banks/rod bundles may be infinite, perhaps, three different kinds of arrangements are well-known under the assumption of equal tube diameters, namely (i) a regular triangular array of tubes (ii) a regular square array of tubes and (iii)) a circular array of tubes. Among all these three arrangements, the regular square array of tubes/rods contained in square channels is very common and most widely used (Fig. 2.5). Further, all these tube bundle arrangements are subdivided into three types of subchannels, e.g., central, wall and corner subchannels. The present study is concerned with square central subchannels.

The main geometrical parameters for tube bundles are the tube outside diameter D, the distance between the tube centers (pitch) L, the distance W from the wall which is equal to the tubes diameter plus the shortest distance between a rod and the channel wall, and the number of

tubes n_T in a tube bundle. Table 2.1 displays the types of subchannels, their flow areas and wetted perimeters for regular square arrays. The hydraulic diameter for each subchannel of Table 2.1 is determined by $D_{h,\,i} = 4A_i/P_{w,\,i}$; where, i is the kind of subchannel, e.g., square central, wall or square corner subchannel, etc.

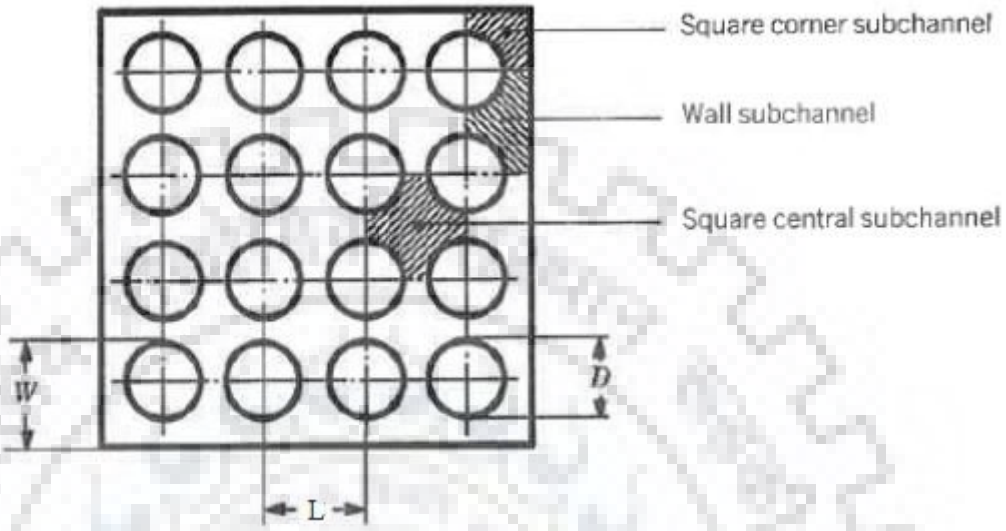

Figure 2.5: Typical geometrical arrangements of tube bundles for regular square arrays (KaKac et al., 1987)

Table 2.1: Geometrical parameters for square array of cylinders/rod bundles (adapted from KaKac et al., 1987)

Subchannels Type (i)	Number of tubes in tube bundles (n_i)	Flow Area (A_i)	Wetted Perimeter ($P_{w,\,i}$)
Total number of rods, $n_T = N^2$			
Central	$(N+1)^2$	$L^2 - \frac{\pi}{4}D^2$	πD
Wall	4(N-1)	$\left(W - \frac{D}{2}\right)L - \frac{\pi}{8}D^2$	$\frac{\pi}{2}D + L$
Corner	4	$\left(W - \frac{D}{2}\right)^2 - \frac{\pi}{16}D^2$	$\frac{\pi}{4}D + 2\left(W - \frac{D}{2}\right)$

Further, the geometrical arrangements for various type of cylinders arrays have been used in computational works using their pitches as shown in Figs. 2.6 (a-c) for the square, rectangular and triangular arrays of the cylinders, respectively. Also, for example, the expressions to calculate their flow area, wetted perimeters and number of tubes etc. have been shown in Table 2.1 for the square array of cylinders/tube bundles.

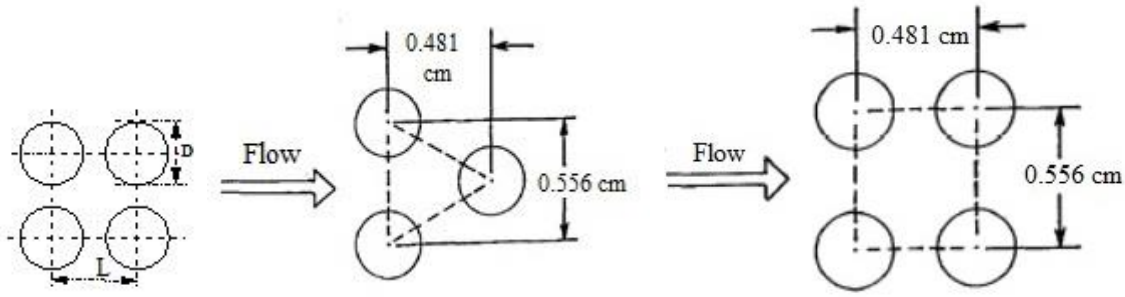

(a) (b) (c)

Figure 2.6: (a) Square pitch array (Martin et al., 1998) (b) triangular pitch array (Chmielewski et al., 1990) and (c) rectangular pitch array (Chmielewski et al., 1990)

Moreover, the above flow geometries apparently cause a different kind of flow phenomena subject to the various parameters such as nature of approaching flow (laminar or turbulent), type of fluids (Newtonian or non-Newtonian) and cross-sectional shape of the body, i.e., circular or non-circular, and the arrangement of cylinders (in-line or staggered), etc. Given all these factors, the flow characteristics are further influenced by the type of fluids and, particularly, in the case of non-Newtonian fluids which characterizes the power-law model exhibiting shear-thickening, shear-thinning and time-independent behavior the influences are observed to be quite significant. The detailed discussion of these fluids is available in the various reference books, text books, etc. (Chhabra and Richardson, 1999, 2008; Bird et al., 2002). However, for the sake of completeness, an overview of these fluids is briefly described in the following section.

2.2 Definition and classifications of fluids

This section briefly describes the different kinds of fluids such as Newtonian, non-Newtonian and viscoelastic along with their classifications and applications, etc.

2.2.1 Newtonian fluids

A Newtonian fluid is one who follows Newton's law of viscosity and expressed as

$$\tau_{yx} = -\mu \frac{dv_x}{dy} \tag{2.3}$$

where, μ is the viscosity and a constant independent of shear rate. The above equation states that the shear force per unit area is proportional to the magnitude of local velocity gradient or shear rate. All gases and most of the simple liquids follow Newton's law of viscosity. A flow diagram between shear stress and shear rate is shown in Fig. 2.7 where the Newtonian fluids yield a

straight line with slope μ which completely characterizes the Newtonian behavior of the fluids. Though no real fluids accommodate the characterization perfectly, many familiar liquids and gases, such as water, air and most low molecular weight substances can be presumed to be Newtonian for practical applications under normal conditions.

2.2.2 Non-Newtonian fluids

Non-Newtonian fluids are those who do not obey Newton's law of viscosity, i.e., whose flow curve between shear stress vs. shear rate curve is non-linear and does not pass through origin. The viscosity of non-Newtonian fluids is not constant at a given temperature and pressure but depends on the other factors such as the rate of shear in the fluid and the duration of shear, or its previous history. Few examples of the fluids which display the non-Newtonian behaviours are solid suspensions, ketchup, toothpaste, human blood, egg whites, drilling muds, molten polymers, mayonnaise, etc. Based the different nature of non-Newtonian fluids, these are classified into three general classes (Bird et al., 2002; Chhabra and Richardson, 1999, 2008) as described below.

2.2.3 Time independent fluids

The fluid in which the rate of shear ($\dot{\gamma}$) at any point in the fluid is a function of the shear stress (τ) at that point are termed as non-Newtonian time independent fluids. These fluids may be described by the rheological equation of the form:

$$\dot{\gamma}_{yx} = f(\tau_{yx}) \tag{2.4}$$

Depending on the form of Eq. (2.4), these fluids are further subdivided into three distinct types as follow.

2.2.3.1 Shear-thinning or Pseudoplastic fluids

These are the most common type of non-Newtonian time-independent fluids which are characterized by an apparent viscosity which constantly reduces with the growth in shear rate. Majority of non-Newtonian fluids are in this category. Fluids such as polymer solutions or melts, greases and multi-phase mixtures such as emulsions, suspensions, foams etc. exhibit the shear-thinning behavior. Other examples of these kind of fluids are the ketchup, whipped cream, paints, nail paints, detergent slurries, biological fluids, etc. The shape of the flow curve is shown in Fig.

2.7, which is generally represented as the power-law equation (sometimes called power-law or Ostwald de Waele model):

$$\tau_{yx} = m\left(\dot{\gamma}_{yx}\right)^{n} \tag{2.5}$$

Where, m is the power-law consistency index and n is the power-law index or flow behavior index. Also, n < 1 represents the shear-thinning fluids. The extent of pseudo-plasticity increases as the values of n decreases.

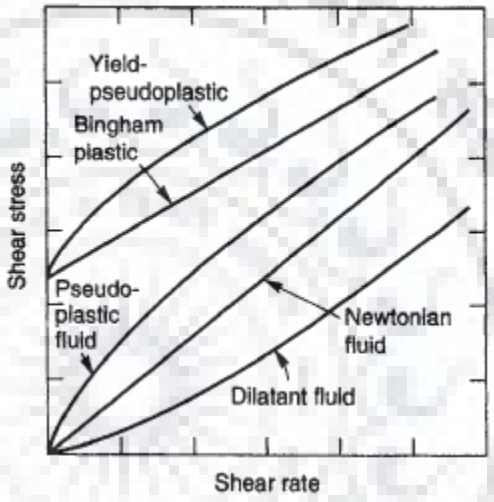

Figure 2.7: Types of time-independent flow behaviour (Chhabra and Richardson, 1999, 2008)

2.2.3.2 Shear-thickening or Dilatant fluids

Similar to shear-thinning fluid, no yield stress is present for the shear-thickening fluid. On the contrary, the apparent viscosity of dilatant fluids increases with the growth in the shear rate. These fluids also obey the power-law equation (i.e., Eq. 2.5) and thus for shear-thickening fluids, n > 1. Examples of dilatant fluids are rare as some highly concentrated suspensions exhibit shear-thickening property, for example, kaolin-water solution, corn flour-water solution, suspensions of titanium.

2.2.3.3 Viscoplastic fluids

The non-Newtonian fluids which are characterized the presence of yield stress (τ_0) (which is a threshold stress) are known as visco-plastic fluids. For flow or deform of such fluids, the stress

must be exceeded. Molten chocolate, yogurt, tomato puree, tomato sauce, blood, cosmetics, nail paints, are some of the examples of yield-stress fluids. When the yield stress is more than the applied stress for such substances, then they behave like elastic solids. Whereas, when the external yield stress surpasses the yield stress, then the fluid may exhibit Newtonian or shear-thinning behavior. There are so many mathematical models available to represent the viscoplastic behavior such as the Bingham plastic model, the Herschel-Bulkley fluid model and the Casson fluid model.

2.2.4 Time-dependent fluids

The apparent viscosity of complex fluids depends not only on the shear rate but also on the time of shear. These fluids are divided into two classes; namely thixotropic and rheopectic.

2.2.4.1 Thixotropic fluids

If a thixotropic fluid is sheared at a constant rate, after a certain period of rest, the structure of the material is progressively broken down and the apparent viscosity decreases with time. The rate of breakdown of the structure during application of shear at a given rate depends on the number of linkages available for breaking and hence decreases with time. The simultaneous rate of reformation of the structure with time as the number of possible new structural linkages increases. A state of dynamic equilibrium is eventually reached when the rate of reformation of structure equals the rate of breakdown. Thixotropy, therefore, is a reversible process and after resting, the structure of the material builds up gradually. A hysteresis loop for a thixotropic fluid is observed on the curve of shear stress vs. shear rate, if the curve is plotted for the rate of shear increasing and decreasing at a constant rate, respectively.

2.2.4.2 Rheopectic fluids

Rheopectic fluids are those in which gradual formation of the structure is observed on application of shear. For example, a 42 percent gypsum paste (1-10μ) in water shaking re-solidifies in 40 minutes if at rest, but in 20 s if the container is gently rolled in the palms of hands, indicating that small shearing motions facilitate structure build-up but large shearing (shaking) destroys it and there is a critical shear rate beyond which breakdown of structure occurs instead of reformation. Vanadium pentoxide and bentonite in dilute aqueous solutions show this type of behaviours.

2.3 Viscoelastic fluids

An important distinction between fluids and solids is the way that these substances dispose of the work upon them in shearing deformations. All the work done on a purely viscous fluid in shear is immediately dissipated as heat, whereas the work done on a perfectly elastic substance in shear, is not dissipated but may be recovered at any time by allowing the elastic material to regain its original configurations.

Further, there exist some materials whose behaviour is partly fluid-like and partly solid-like, the work of shearing deformation in these materials is not completely conserved as in solids, nor completely dissipated as in fluids. These materials are called viscoelastic materials as they possess both of the elastic as well as viscous properties. Although, the various characteristics/properties of these fluids have also been described in terms of the different dimensionless parameters in the literature. Therefore, before presenting the concerned literature on the flow and thermal nature of these fluids through various flow arrangements, it is appropriate now to define these dimensionless parameters which have been used in this study and appeared in literature also.

2.4 Dimensionless parameters

The various pertinent dimensionless parameters which have been used in this work and appear in the literature also are described briefly herein:

- **Reynolds number (Re):** The Reynolds number (Re) for the power-law fluids is defined as:

$$\mathrm{Re} = \frac{\rho D^{n} V^{2-n}}{m} \tag{2.6}$$

  Where, D, ρ and V are the cylinder diameter, density and velocity of the fluids respectively. Reynolds number is the ratio of inertial forces to viscous forces. So, a low Reynolds number means the viscous forces are dominating over inertial forces and vice-versa. Also, for Newtonian fluids (n = 1), Eq. (2.10) reduces to $\mathrm{Re} = DV\rho/\mu$ and with $m = \mu$.

- **Prandtl number (Pr):** The Prandtl number (Pr) for the power-law fluids is defined as:

$$\mathrm{Pr} = \frac{c_p \mu}{k}\left(\frac{V}{D}\right)^{n-1} \tag{2.7}$$

where, c_p and k are the specific heat and thermal conductivity of the fluids, respectively. Prandtl number is the ratio of momentum diffusivity to thermal diffusivity. A small value of Prandtl number (Pr < <1) suggests that the thermal diffusivity dominates over momentum diffusivity and vice-versa. For Newtonian fluids (n = 1), Eq. (2.11) reduces to $\mathrm{Pr} = \mu c_p / k$.

- **Peclet number (Pe):** The Peclet number (Pe) is defined as:

$$\mathrm{Pe} = \mathrm{Re}\,\mathrm{Pr} = \frac{\rho c_p V D}{k} \tag{2.8}$$

The Peclet number is independent of the power-law index and thus offers the possibility of reconciling the results for Newtonian and non-Newtonian power-law fluids both.

- **Richardson number (Ri):** For the case of mixed convection, the buoyancy effects are important which are well described in terms of Richardson number (Ri). The Richardson number (Ri) or buoyancy parameter characterizes the significance of natural convection to that of forced convection (Srinivas et al., 2009) and is defined as follows:

$$\mathrm{Ri} = \frac{\mathrm{Gr}}{\mathrm{Re}^2} = \frac{g\beta(T_w - T_0)D}{V^2} \tag{2.9}$$

where, Gr is the Grashof number describes the relative significance of buoyancy forces to that of viscous forces acting on the fluid. In the case of a power-law fluid, it is defined as below:

$$\mathrm{Gr} = \frac{g\beta\Delta T\rho^2 D^3}{m^2}\left(\frac{V}{D}\right)^{2(1-n)} \tag{2.10}$$

where, g, β and $\Delta T = T_w - T_0$; is the gravitational force, the coefficient of volumetric thermal expansion and temperature difference, respectively. Here, in contrast to Newtonian fluids, Prandtl number and Grashof number for power-law fluids also depend on the velocity and diameter of the cylinder along with the thermo-physical properties. Though, the Richardson number is independent of power-law indices (m, n). The definitions given here are extensively used in the heat transfer literature and are very popular to explain the results of mixed-convection heat transfer. Further, Ri = 0 and $\mathrm{Ri} \to \infty$ represents the cases of forced and free convections respectively, whereas, Ri > 0 and Ri < 0 represents the cases of aiding and opposing buoyancy mixed convections, respectively.

- **Pressure coefficient (C_P):** The pressure coefficient (C_P) on the surfaces of cylinders (solid boundaries) is defined as:

$$C_p = \frac{p(\theta) - p_0}{(1/2)\rho V^2} \tag{2.11}$$

where, p (θ) is the surface pressure at an angle θ and p_0 is the free stream pressure at the exit boundary. The pressure coefficient is the ratio of static pressure to dynamic pressure.

2.5 Literature review

The relevant literature on Newtonian and non-Newtonian fluids to display the forced and mixed convection features across the periodic array of cylinders and/or tube banks is presented and discussed here in this section.

2.5.1 Forced convection features of Newtonian fluids

Extensive research efforts have been devoted to reveal the flow and heat transfer features across the periodic array of cylinders and/or over tube banks in various geometrical configurations (e.g., square, rectangular, triangular and hexagonal arrangements of cylinders, etc.). A sharp inspection of the available literature suggests that the detailed discussion of numerous aspects can be found in many excellent reviews, survey articles, encyclopedia and books (e.g. see Nishimura, 1986; KaKac et al., 1987; Zukaukas, 1987b; Nishimura et al., 1991, 1993; Skartsis et al., 1992a; Ghosh et al., 1994; Perry, 1997; Abrate, 2002, 2011; Ghoshdastidar, 1998, 2012, 2017; Sharma, 2016, etc.) and briefly it is described herein. For instance, the flow through fibrous media and tube bundles has been reviewed by Zukaukas (1987b) and emphasized that the quantitative nature of flow in high porosity cylinder arrays (cylinder arrays are approximated as porous media) is still an infancy area of research. Another review has been presented by Skartsis et al. (1992a) for the Newtonian flow of aligned cylinders in regular arrangements. It encapsulates the relevant literature concerned with fibrous media and cylinder arrays for regular and staggered arrangements. The review includes the theoretical and experimental aspects of determining the permeability through aligned and randomly oriented cylinder arrays. Further review by Ghosh et al. (1994) is concentrated on the flow and heat transfer phenomena over the tube banks etc. Moreover, most of the past studies from these geometries are focused on creeping flow (Sangani and Acrivos, 1982; Drummond and Tahir, 1984; McPhedran, 1986; Bruschke and Advani, 1993; Spelt et al., 2005a) for the various features such as drag coefficients, mobility factor, velocity distribution and Nusselt numbers, etc. Besides, some studies are also based on the energy analysis and thermal modeling of heat transfer

equipment for improving their efficiencies, etc. (Martin et al., 2004; James et al., 2012b). Moreover, numerous studies are focused on the permeability, stability analysis, inelastic instabilities, pressure drop and effective viscosity (μ_{eff}), etc. for both of Newtonian and non-Newtonian fluids using various geometrical configurations of periodic array of cylinder and/or tube banks etc. (Singh et al., 1989; Andjelic and Popp, 1989; Chmielewski et al., 1990; Georgiou et al., 1991; Astrom et al., 1992; Nagelhout et al., 1995; Talwar and Khomami, 1995; Khomami and Moreno, 1997; Alcocer and Singh, 2002; Arora et al., 2002; Abrate 2007; Tamayol and Bahrami, 2009; Geoffrey and Jonathan, 2010; Yazdchi et al., 2011; James et al., 2012a; Nguyen et al., 2013; Gillissen, 2013).

Notwithstanding, in the literature, there are two distinct approaches/schemes available to investigate the flow and thermal problems. In the first scheme, the field equations have been solved for the different geometrical arrangements of a periodic array of cylinders, whereas, in the second scheme, the assemblage of cylinders is modeled by using the approximate cell models where the modeling depends upon the cylinder-cylinder interactions. For instance, the various cell models (zero vorticity or free surface cell models) have been used to approximate the transport properties across an array of cylinders (Happel, 1959; Kuwabara, 1959; Sparrow and Loeffler, 1959; Hashimoto, 1959). These models have returned the satisfactory characteristics of both Newtonian as well as non-Newtonian fluids flow over the collections of spherical, cylindrical and fibrous media. In fact, in either of the cases, whether cell model approximations or the periodic array of cylinders (in-line or staggered), the transport properties of the fluids have been of continuous interest to the researchers over the years. As far as known to us, firstly, Emersleben (1925) investigated the longitudinal flow across the square array of cylinders by using an intricate zeta-function, which yields a good solution for the fluid volume fractions (or porosities) of around 0.8. Further, Launder and Massey (1978) presented the limited analysis of pressure loss and heat transfer for a staggered square array of circular cylinders for the Reynolds number of 50-75 at fixed value of Prandtl number (Pr = 20). A satisfactory agreement with the experimental results of Bergelin et al. (1952) were found. Also, this problem was re-investigated (Wung and Chen, 1989; Chen and Wung, 1989) by solving the steady incompressible form of governing equations for convective flow over staggered and in-line arrangement of cylinders having the pitch (longitudinal/transverse) ratio of 2, Reynolds numbers of 40-800 and Prandtl number of 0.1-10. However, the main emphasis of this study was on the interpretation of the flow fields (streamlines, secondary flow, etc.) with the increasing Reynolds number. They also presented scant results on the mean Nusselt number as a function of the Reynolds number and Prandtl number. Similarly, Edwards et al. (1990) calculated the flow field within spatially

periodic arrays of cylinders arranged in square and hexagonal lattices at higher Reynolds numbers (0 to 200). However, this study was emphasized in the limit of low fluid volume fractions of $\phi_f \leq 0.80$. Further, Hendricks et al. (1991) experimentally investigated the use of brush inserts which can be represented as the cylinder arrays within the complex cooling passage for the mitigation of flow separation and augmentation of local heat transfer. Johnson et al. (1993) examined the unsteady incompressible flow problems consisting periodic arrays of staggered cylinders for the Re = 100. The extensive flow data for drag and lift coefficients etc. were calculated for the uni-periodic and bi-periodic periodicity arising out from such a geometry. Subsequently, Fowler and Bejan (1994) investigated the pressure drop and heat transfer features from the bundles of parallel cylinders for the ranges of Reynolds number; $1 \leq Re \leq 30$; Prandtl number $0.72 \leq Re \leq 100$ and fluid volume fractions; $0.6 \leq \phi_f \leq 0.95$. The study has pointed out the possible errors occurred during the investigation with low Reynolds number, fully developed flow and the cylinders inclinations relative to the flow directions. Im and Ahluwalia (1994) examined highly porous fiber arrays to enhance internal heat transfer. The study suggests that the high porosities are desirable in order to minimize frictional losses. As these situations feature developing or recirculating flows and so there is a need to understand the flow resistance offered by sparse cylinder arrays in the transverse direction. Further, Amiri and Vafai (1994) presented the numerical simulations of forced convective incompressible flow through porous media to investigate the associated transport properties. In all of the above applications, high porosities are desirable in order to minimize frictional losses.

Koch and Ladd (1997) investigated the effect of fluid inertia on the pressure drop required to drive fluid flow through periodic and random arrays of aligned cylinders for the fluid volume fraction of 0.3-0.985 at Re < 180. Their results for creeping flow are consistent with Sangani and Acrivos (1982). The next few studies are either focused on flow and/or heat transfer characteristics in the limited ranges. For instance, Martin et al. (1998) presented numerical analysis of the frictional losses and averaged Nusselt number for convective cross-flow of air over the sparse (square and triangular) periodic arrays ($\phi_f > 0.8$) of cylinders in the laminar regime (Re = 3 to 160) and reported the influence of thermal boundary conditions over the averaged Nusselt number. Subsequently, Beale and Spalding (1998) investigated the fluid flow and heat transfer in tube banks with stream-wise periodic boundary conditions for the in-line square, rotated square and equilateral triangle geometries for the range of $10 \leq Re \leq 1000$; $1 \leq Pe \leq 100$ and pitch to diameter ratio of 1.25-2. The results were compared and found to be satisfactory with the empirical and experimental data within the ranges of conditions covered.

Similarly, Wilson and Bassiouny (2000) numerically explored the heat transfer features for air flow ($Re \leq 50{,}000$) over staggered and the in-line collection of cylinders. A mathematical model was developed to assess the laminar and turbulent flow fields inside tube banks. The governing equations were also solved using finite volume method and observed that the pressure drop and friction factor increased with longitudinal pitches. So, a longitudinal pitch ratio of $\alpha \leq 3$ was recommended to obtain the better performance and to attain a high degree of compactness in an in-line arrangement, whereas $\alpha \leq 1.5$ was required to diminish friction and augment the Nusselt number in the staggered arrangement. Further, Kuwahara et al. (2001) performed the numerical experiment to determine the interfacial convective heat transfer coefficient in porous media. A universal correlation for the Nusselt number was given for the wide ranges of fluid volume fractions, Prandtl and Reynolds numbers. Mandhani et al. (2002) have used stress-free surface cell model for the forced convection characteristics of Newtonian fluids over tube bank within the following ranges of conditions; Reynolds number of 1-500, Prandtl number of 0.71 and 7.7 and fluid volume fractions of 0.4-0.99. The Nusselt number is shown to be strongly dependent on the above dimensionless parameters. An increase in Nusselt number with the increasing value of Reynolds and Prandtl numbers was reported along with the decrease with fluid volume fractions. Their result was found in satisfactory agreement with the previous available numerical and experimental results. Next, Alam and Ghoshdastidar (2002) examined the heat transfer in circular tubes fitted with longitudinal fins for the $Re \leq 1500$. The study displays the velocity profile, friction factor and fin effectiveness under various combinations of parameters for the constant heat flux conditions.

In further works, Hovart et al. (2006) have given an insight into the local flow field and thermal characteristics of cylindrical, ellipsoidal and wing shaped tubes in staggered arrangements by analyzing 100 cases of each tube type. Khan et al. (2006a) presented an analytical study over the tube banks for the heat transfer characteristics in cross-flow. An integral method for boundary layer has been applied for the calculation of average heat transfer from the tube banks. Likewise, Gamrat et al. (2008) numerically examined the thermal equilibrium in a porous medium over an array of square rods in the following ranges: fluid volume fraction from 0.44 to 0.88 and Re from 0.05 to 40 and concluded the insensitiveness of heat transfer for the highest values of Re and Pr. Also, Hantsch et al. (2010) presented an experimental study of fiber array inserts for heat transfer augmentation in an extremely heated duct for the fluid volume fractions up to 0.98 and for very high Reynolds number ranging from 1.75×10^4 to 11.25×10^4. They reported that the array causes a significant pressure drop whereas heat transfer coefficient was also enhanced by 100%.

In the recent studies, Tahseen et al. (2013) used the staggered geometry of circular tube banks to present the heat transfer characteristics for $25 \leq Re \leq 250$, pitch to diameter ratio of 1.25, 1.5, 2 and at a fixed value of Prandtl number (Pr = 0.71). The velocity and temperature fields, Nusselt numbers, etc. have been calculated and compared with the experimental and numerical results displaying good agreement. Fornarelli et al. (2015) used six in-line circular cylinders to examine the flow and heat transfer features at a fixed values of Reynolds and Prandtl numbers of 100 and 0.7(air), respectively and two values of cylinder spacing (L = 3.6D and 4D). A transition was identified for the flow as well as heat both. The stable shear level and shear-level secondary vortices (L = 3.6D) have also been noticed. Subsequently, Crowdy (2016) have studied the uniform flow past a periodic array of cylinders. The problem was solved by a new transform technique and solutions have been given as a set of coefficients of suitable linear systems. A new explicit approximation formula has also been proposed for the blockage coefficients. Afterward, Mangrulkar et al. (2017) have investigated the flow and heat transfer characteristics for cross-flow in the tube banks using splitter plate in the staggered arrangement for the high Reynolds numbers ranging $5500 \leq Re \leq 14500$), splitter plate length to tube diameter ratio of 1 and longitudinal and transverse tube pitch to diameter ratios of 1.75 and 2, respectively. The use of splitter plate enhances the rate of heat transfer and reduces the pressure drop as compared to those of the bare cylinders. The overall increase of 60-82% of heat transfer enhancement has been reported. Additionally, Kumar and Jayadev (2017) have presented the influence of flow shedding frequency on the flow and thermal characteristics over circular tubes under cross-flow. In this investigation, three different flow shedding nature has been observed with the variations in flow inertia and blockage ratios. In the low inertial region, the heat transfer is increased due to the attached flow, whereas increased inertia leads to laminar to turbulent transition causing the heat dissipation.

Besides, past few studies have been reported on developing the various correlations for heat transfer features. For instance, Colburn (1933) proposed an empirical correlation for the Nusselt number for flow through banks of staggered tubes as:

$$Nu = 0.33\,Re^{0.6}\,Pr^{1/3} \tag{2.12}$$

This correlation is valid for 10 or more row of tubes in the staggered arrangement and for Re in the range of $10 < Re < 4 \times 10^4$. Further, the experimental data of Huge (1937) and Pierson (1937) were correlated by Grimison (1937) for both of the in-line and staggered arrangement of cylinders and proposed the following correlation for Nusselt number:

$$Nu = C\,Re^{n} \tag{2.13}$$

where, C and n are the correlation constants. This simple correlation relates to tube banks containing ten or more numbers of rows of tubes. Grimison (1937) also correlated the test measurements of Pierson (1937) and Huge (1937) and derived the following correlation:

$$Nu = 0.32F_a\,Re^{0.61}\,Pr^{0.31} \tag{2.14}$$

where, the arrangement factor F_a has been determined graphically for the different values of Reynolds number based on the transverse and longitudinal pitches. Additionally, Zukauskas (1972) have also developed the following experimental correlation for the average Nusselt number of a tube bank consisting of 16 or more rows:

$$Nu = FC\,Re^{n}\,Pr^{m} \tag{2.15}$$

Where the coefficients C, m and n are given elsewhere (Kreith and Bohn, 1993) along with the correction factor parameter F that accounts for lower than 16 rows in the tube bank.

Therefore, on the basis of above literature review, the following have been observed and noticed:

(i) Many studies/investigations have used the periodic array of cylinder in the different geometries to determine permeability, stability analysis, viscosity and elasticity effects, etc. and these parameters are not being covered in present studies and so are less significant in context of this dissertation

(ii) The studies/investigations which are emphasized on the local and global flow and heat transfer characteristics to reveal the streamlines and isotherms, individual and total drag coefficients, local and average Nusselt numbers, etc. using a periodic array and/or tube banks are the main concern of the present work. These studies are summarized in Table 2.2.

Table 2.2: Summary of literature review for Newtonian fluids

S. No.	Authors/References	Parametric conditions and geometries	Remarks
1	Wung and Chen (1989)	$40 \leq Re \leq 800$; $0.1 \leq Pr \leq 10$ Geometry: Staggered and in-line array of circular cylinders	Convective flow for pitch (longitudinal/transverse) ratio of 2 has been presented. The main objective of this study was the evolution of flow field with increasing Reynolds number.
2	Edwards et al. (1990)	$\phi_f \leq 0.80$; $0 \leq Re \leq 200$ Geometry: Square and Hexagonal lattices	The flow fields were calculated within spatially periodic arrays of cylinders arranged in square and hexagonal lattices. This study is emphasized on low porosity cases less than 0.80.
3	Koch and Ladd (1997)	$Re \leq 180$; $0.38 \leq \phi_f \leq 0.985$ Geometry: Square array of cylinders in periodic and random arrangements	The magnitude of C_D is evaluated over the ranges of Reynolds number and fluid volume fractions through periodic and random arrays of aligned cylinders. The result for $Re \ll 1$ is consistent with Sangani & Acrivos (1982) for the creeping region.
4	Martin et al. (1998)	$0.80 \leq \phi_f \leq 0.99$ $3 \leq Re \leq 160$; $Pr = 0.71$ Geometry: square and triangular array of cylinders	Frictional losses, permeability and convective heat transfer in terms of the Nusselt number have been determined at a fixed value of Prandtl number (i.e. for air).
5	Wilson and Bassiouny (2000)	$Re \leq 50{,}000$ Geometry: in-line and staggered arrays of cylinders	Heat transfer in air flow over a staggered and in-line collection of cylinders has been determined in the fully turbulent regime.
6	Mandhani et al. (2002)	$1 \leq Re \leq 500$; $0.40 \leq \phi_f \leq 0.99$; $Pr = 0.71$ and 7 Geometry: bundle of circular cylinders	Forced convection heat transfer characteristics of cross-flow over tube bank by using the stress-free surface cell model has been determined for air and water.
7	Khan et al. (2006a)	$500 \leq Re \leq 10000$; $Pr = 0.71$; $L/D = 1.25, 2.0, 3.0$ Geometry: in-line and staggered arrangement of circular cylinders	An analytical study of the tube banks for heat transfer characteristics in cross-flow. An integral method for boundary layer has been applied for the calculation of average heat transfer from the tube banks.
8	Hovart et al. (2006)	$Re = 0\text{-}5000$; $L/D = 1.125\text{-}2.0$ Geometry: cylindrical, ellipsoidal and wing shaped tubes in staggered arrangements	Numerical analysis for heat transfer features have been presented. The detailed insight of local heat transfer and fluid flow conditions in a heat exchanger has been obtained.
9	Tahseen et al. (2013)	$25 \leq Re \leq 250$; $L/D = 1.25$, 1.5 and 2 $Pr = 0.71$ Geometry: circular tubes in staggered arrangements	The velocity and temperature fields, Nusselt numbers, etc. have been presented and compared with the experimental and numerical results which show the good agreement.
10	Fornarelli et al. (2015)	$Re = 100$; $Pr = 0.7$; $L = 3.6D$ and $4D$ Geometry: six in-line circular cylinders	The flow and heat transfer features have been examined. A transition was identified for the flow as well as heat both. The stable shear level and shear level secondary vortices for $s = 3.6$ have also been noticed.
11	Mangrulkar et al. (2017)	$5500 \leq Re \leq 14500$; $L/D = 1$; $L_L/D = 1.75$; and $L_T/D = 2$	The flow and heat transfer characteristics for cross flow in tube banks using splitter plate in the staggered arrangement. The use of splitter plate enhances the rate of heat transfer and reduces the pressure drop as compared to those of the bare cylinders. The overall increase of 60-82% of heat transfer enhancement has been reported.

2.5.2 Forced convection features of non-Newtonian fluids

As mentioned in the previous section 2.6.1 that the significant literature is available on the flow and heat transfer characteristics of Newtonian fluids across periodic array of cylinders (Launder and Massey, 1978; Wung and Chen, 1989; Chen and Wung, 1989; Martin et al., 1998; Roychowdhury et al., 2002, etc.). In contrast, scant literature is available to reveal the flow and heat transfer features of non-Newtonian fluids. For instance, the slow and inertial flow of non-Newtonian fluids (Tripathi and Chhabra, 1992, 1996) employed a most common velocity and stress-variational principle (Slattery, 1972) to get frictional pressure gradient over a roll of long circular cylinders. Subsequently, Bruschke and Advani (1993) reported analogous results for hexagonal array of cylinders for the fluid volume fractions of 0.3-0.9 and power-law index; $0.5 \leq n \leq 1$. They employed the lubrication flow approximation for concentrated (strong interactions of cylinders) systems, and the zero vorticity cell model for dilute (weak interactions of cylinders) systems, the intermediate region of concentration was patched up by the weighted average of these two limiting conditions. Similarly, Vijaysri et al. (1999) used the zero vorticity cell models of Kuwabara (1959) to discuss fluid dynamic parameters in terms of drag coefficients in the range of $0.01 \leq Re \leq 10$; $1 \geq n \geq 0.54$ and maximum fluid volume fractions of 0.95. It is shown that the overall drag for pseudo plastic media is seen to decrease below its value for Newtonian fluids. Further, the detailed comparisons between various predictions and limited experimental data reveal that the free surface cell model underpredicts the experimental results whereas the zero vorticity cell-model over-predicts the experimental results, in both cases the discrepancy being of the order of 25-30%. Subsequently, Dhotkar et al. (2000) solved the governing equations for the flow of power-law liquids for the values of Reynolds number up to 10 and for the different values of the voidages. In further works, Shibu et al. (2001) reported the extensive theoretical estimates of pressure, friction and total drag coefficients for the cross-flow of power-law fluids normal to an array of long circular cylinders. The equations of continuity and momentum have been solved numerically for the unknown velocities and pressures. The ranges of parameters studied are; power-law index; $1 \geq n \geq 0.5$; Reynolds number; $1 \leq Re \leq 500$ and fluid volume fractions of 0.4 and 0.5. In general, the lower the value of the flow behaviour index, greater is the divergence between these theoretical predictions and the available experimental results (Chhabra et al., 2000; Prasad and Chhabra, 2001; Malleswara Rao and Chhabra, 2003). In addition to the aforementioned studies based on cell models, Skartsis et al. (1992b) numerically solved for the two-dimensional axisymmetric flow of power-law liquids over a staggered array of cylinders. Similar works used free surface cell models over the range of Re 1-500, porosity 0.4-0.99 and two values of Pr of 0.71 and 7.7 (Mandhani et al., 2002). In subsequent work

(Mangadoddy et al., 2004), the forced convection was investigated across a bundle of circular cylinders in the range of Peclet number 1 to 5000, Re = 1-500 and n = 0.5-1 and fluid volume fractions of 0.4-0.6. The results show that the average Nusselt number displays a strong dependence on these parameters. In fact, the above few studies have been used for the thermal features of non-Newtonian fluids over a bundle of cylinders in which the local or average Nusselt number has been estimated in inertial regions along with the slow flow regime of Ferreira and Chhabra (2004). Further, an experimental study such as Adams and Bell (1968) describes the heat transfer phenomena such as heating and cooling of non-Newtonian kind of fluids using three tube banks for the wide ranges of Re and Pr.

In the recent studies, investigations have been made for the drag coefficients in creeping flow (Spelt et al., 2005a) and inertial flow (Spelt et al., 2005b) regime of non-Newtonian fluids. For creeping flow, the numerical results have been presented along with the lubrication theories for the flow of truncated power-law fluids across square and hexagonal array of cylinders. They suggested that the choice of velocity and length scale in the definition of the drag coefficient is useful, however, in the case of inertial flow, the drag coefficient increases with Reynolds numbers up to 100. In the unsteady state regime, the drag is dominated by the form drag. In the parallel study, the creeping flow of Bingham fluids through periodic square arrays cylinders was also investigated by Spelt et al. (2005c) with the objective to quantify the dependence of the drag coefficient on the Bingham number and the results are further used as a criterion for critical pressure gradient. Subsequently, Soares et al. (2005a) numerically investigated the steady flow of power-law fluids across a bank of long cylinders to determine the drag coefficient in the range of power-law index; $0.3 \leq n \leq 2$, porosity; $0.4 \leq \phi_f \leq 0.9$ and Reynolds number; $0.01 \leq Re$ 500. It has been reported that as the power-law index moves from shear-thinning to shear-thickening, the resulting increase in drag coefficients becomes less pronounced at high porosity values. Further, Khan et al. (2006b) presented the analytical study for the modeling of fluid and heat transfer from infinite circular cylinders to power-law fluids. They have developed closed form solutions for the drag and heat transfer coefficients in terms of generalized Reynolds and Prandtl numbers. Next, Wang and Shao (2012) presented the flow characteristics for time averaged drag coefficient using Lattice Boltzmann Method (LBM) through an infinite array of circular cylinders for the power-law index; $0.4 \leq n \leq 1.8$ and Reynolds number; $50 \leq Re \leq 140$. Subsequently, Singh et al. (2012) have investigated the flow of power-law fluid in fixed beds of cylinders or spheres and solved the ensemble-averaged momentum equation and shown that the drag force acting on the particle/periodic array is a function of the particle-concentration-dependent length scale. Additionally, Quesada and Ellero (2012) have numerically analyzed the viscoelastic fluids

around an array of cylinders confined in a channel for closely as well as widely placed cylinders with fluid volume fractions of 0.68 and 0.86, respectively. The cylinder drag coefficient was observed for the Weissenberg number of ~1.5.

Table 2.3: Summary of literature review for non-Newtonian fluids

S. No.	Authors/References	Parametric conditions and geometries	Remarks
1	Vijaysri et al. (1999)	$0.01 \leq Re \leq 10$; $1 \geq n \geq 0.5$; $0.95 \leq \phi_f \leq 0.4$ Geometry: array of long circular cylinders	Individual and total drag coefficients have been calculated across an array of the long circular cylinder using zero vorticity cell model for the ranges of parameters mentioned.
2	Dhotkar et al. (2000)	$0.01 \leq Re \leq 10$; $0.4 \leq n \leq 1$; $0.40 \leq \phi_f \leq 0.95$ Geometry: assemblage of long circular cylinders	Drag coefficients are reported for the flow of power-law liquids across an assemblage of long cylinders using concentric cylinder cell models. The flow fields in terms of surface vorticity distribution, streamlines, etc. over the surface of cylinders have been presented.
3	Shibu et al. (2001)	$1 \leq Re \leq 500$; $1 \geq n \geq 0.5$; $\phi_f = 0.4, 0.5$ Geometry: array of long circular cylinders	Predictions of drag on the cylinder are predicted over an array of long circular cylinders using both of the zero vorticity and free surface cell models.
4	Mangadoddy et al. (2004)	$1 \leq Pe \leq 5000$; $1 \leq Re \leq 500$; $0.5 \leq n \leq 1$; $0.40 \leq \phi_f \leq 0.60$ Geometry: bundle of long circular cylinders	Forced convection was investigated across a bundle of circular cylinders in the ranges mentioned herein and conveyed that the average Nusselt number displays a strong dependence on these parameters.
5	Prasad and Chhabra (2001)	$0.01 \leq Re \leq 1200$; $0.38 \leq n \leq 1$; $\phi_f = 0.74, 0.78, 0.87$; Geometry: array of long circular cylinders	Steady flow of power-law polymer solutions normal to the array of cylinders and in a bed of screens investigated experimentally. Extensive pressure drop measurements have been done and the drags are reported in terms of loss coefficients.
6	Spelt et al. (2005b)	$0 \leq Re \leq 200$; $0.5 \leq n \leq 1.5$; $0.40 \leq \phi_f \leq 0.99$ Geometry: square array of circular cylinders	Drag coefficients have been determined. At larger Re, the C_D increases with Re at a lower than quadratic rate which is approximately linear for the off axis flow and up to the critical Re. Beyond which, no stable steady state solution is found. In the unsteady state regime, the drag is dominated by form drag.
7	Soares et al. (2005a)	$0.3 \leq n \leq 2$; $0.4 \leq \phi_f \leq 0.9$; $0.01 \leq Re$ 500 Geometry: bank of long circular cylinders.	Drag coefficients have been determined across a bank of long cylinders for power-law fluids displaying shear-thinning and shear-thickening behavior.
8	Wang and Shao (2012)	$0.4 \leq n \leq 1.8$; $50 \leq Re \leq 140$ Geometry: an infinite array of circular cylinders.	Flow characteristics in terms of time averaged drag coefficient are presented using Lattice Boltzmann Method (LBM) through an infinite array of circular cylinders.

Subsequently, no other studies concerned with periodic array of circular cylinders or over tube banks have been reported which could reveal the non-Newtonian characteristics. Besides, many studies are also available on forced convection problem on a single and/or double cylinders to reveal the momentum and thermal features under various ranges of governing parameters (Eckert and Soehngen, 1952; Lange et al., 1998; Soares et al., 2005a, b, 2010; Sharma and Eswaran, 2005a; Dhiman et al., 2006; Sivakumar et al., 2006, 2007; Bharti et al., 2006, 2007a, b, 2008; Patil et al., 2008).

What clearly emerges from the above studies is that there is scant literature available as far as flow and thermal features are concerned across periodic array of cylinders for the non-Newtonian fluids as compared to Newtonian fluids. Further, the flow features have been studied more extensively in contrast to heat transfer characteristics. Based on above discussion, the studies which are mainly concerned with present dissertation are summarized above in Table 2.3.

2.5.3 Mixed convection features of Newtonian and non-Newtonian fluids

As far as the mixed convection flow and heat transfer characteristics of Newtonian and non-Newtonian fluids across periodic array of cylinders and/or over tube banks are concerned, prior works suggest that the mixed convection from these geometries have not been studied extensively. In contrast, numerous studies on forced convection features from such geometries are available as discussed previously (Sections 2.6.1 & 2.6.2). Consequently, the available literature on mixed convection suggest that the most of the works are mainly concentrated on a single cylinder (Sparrow and Lee, 1976; Merkin, 1977; Badr, 1982; Chang and Sa, 1989; Patnaik et al., 1999; Sharma and Eswaran, 2004, 2005b; Sharma et al., 2012; De and Dalal, 2006a, b, 2007; Dhiman et al., 2007, 2008; Soares et al., 2009; Srinivas et al., 2009; Chandra and Chhabra, 2012; Sarkar et al., 2011; Bhowmick et al., 2014, etc.).

So far, scant investigations concerned with mixed convection across a periodic array of cylinders have been reported. For instance, Duli et al. (1995) studied the aiding buoyancy mixed convection over tube banks between two vertical plates for the ranges of Reynolds number (Re $\leq$ 500), Grashof number (Gr $\leq$ 5300) and pitch to diameter ratio (L/D) of 2 and 3 for both of the longitudinal and transverse directions. The result reveals that the flow separation zone is a function of cylinder spacing and so the values of Nusselt numbers are strongly influenced by the interaction between the cylinders. Further, Gowda et al. (1998) examined aiding and opposing mixed convection over tube bundles using finite element method for the range of Reynolds numbers; $50 \leq Re \leq 150$; Richardson number; $-1 \leq Ri \leq +1$ and at a fixed value of Prandtl number

of 0.71 (air). They presented a solution for the 2-D, unsteady Navier-Stokes and thermal equations using an explicit and semi-implicit algorithms for the ranges of parameters studied. The influences of these dimensionless parameters on drag coefficients, Nusselt number, pressure distribution around cylinders, etc. were examined and reported. A significant influence of buoyancy parameter over tube bundles was noticed. An additional study by Haldar (2000) is focused on the combined convection through seven-rod bundles in a circular shell arranged horizontally. The flow and temperature fields were reported and the highest temperature was found at the top of the central rod. The increased buoyancy decreases the flow rate and increases friction and rate of heat transfer. The result has further been compared with the experiments consist of the three identical test sections and found to be satisfactory. Recently, Fornarelli et al. (2016) numerically examined the flow and heat transfer features across an array of six circular cylinders under the aiding and opposing buoyancy conditions ($-1 \leq Ri \leq 1$) at a fixed value of Reynolds and Prandtl number of 100 and 0.7, respectively and for the two values of tube pitches ($L = 3.6D$ and $4D$). Many transitions in the flow fields have been found and dependence of force coefficient and the Nusselt number is reported within the ranges of parameters considered in this study. Further, it is emphasized that the transition occurs due to the rearrangements of the near field flow in a more ordered wake pattern. The above studies are however concerned with the tube bundles but are very limited to particular sets of parameters. In fact, these are the only evidence as far as mixed convection across a periodic array of cylinders and/or over tube banks are concerned.

Scant mixed convection studies are also devoted to double cylinders with the various arrangements such as tandem or pair of side by side cylinder etc. For instance, Chatterjee (2010) investigated the mixed convection across two square cylinders in a tandem arrangement for the Reynolds number; $1 \leq Re \leq 30$. The influence of buoyancy over flow and heat transfer characteristics was reported. Further, Sarkar et al. (2010) have examined the mixed convection problem from two square cylinders in the tandem arrangement at a fixed value of $Pr = 0.7$, $Re = 100$ and buoyancy in the range of $-1 \leq Ri \leq +1$. They observed the vortex shedding for $Ri = 0.25$ for a given cylinder spacing. Similarly, Daniel and Dhiman (2013) investigated the mixed convection from a pair of circular cylinders in the side by side arrangement for the ranges of parameters: Reynolds number; $1 \leq Re \leq 40$ and Richardson number; $0 \leq Ri \leq 1$, flow behaviour index; $0.2 \leq n \leq 1$ and at $Pr = 50$. They concluded that the drag coefficients reduce with decreasing inertial forces and rise with increasing buoyancy effects. The thermal features were noticed to be enhanced with an upturn in both of the inertial and buoyancy forces. Recently, Salcedo et al. (2016) have also examined the mixed convection problem from two isothermal cylinders in a

tandem arrangement for the fixed value of Reynolds and Prandtl numbers of 200 and 7, respectively and blockage ratio of 0.2 along with the range of Richardson number; $-1 \leq Ri \leq 4$. The result reveals how the buoyancy, spacing ratio and wall confinement influences the wakes, vortex dynamics and local and average heat transfer characteristics. Further study is reported by Chatterjee and Raja (2013) for the mixed convection heat transfer past five in-line square cylinders periodically arranged in a vertical duct. The study is focused on a fixed value of Prandtl number of 0.7 and Reynolds number of 100 for both of the confined and unconfined domains with the varying blockage ratios of 0%, 10%, 25% and 50%. The influence of buoyancy parameter has been presented in the range of $-1 \leq Ri \leq 1$. The results have been reported for the individual and total drag coefficients and average Nusselt number, etc.

Table 2.4: Summary of literature review for mixed convection Newtonian and non-Newtonian fluids

S. No.	Authors/References	Parametric conditions and geometries	Remarks
1.	Duli et al. (1995)	$Re \leq 500$; $Gr \leq 5300$ $(L/D) = 2$ and 3. Geometry: tube banks between two vertical plates	Aiding buoyancy mixed convection over tube banks between two vertical plates for both of the longitudinal and transverse directions have been studied. The flow separation zone has been shown to be the function of cylinder spacing. The Nusselt numbers are strongly influenced by the interaction between the cylinders.
2.	Gowda et al. (1998)	$50 \leq Re \leq 150$; $-1 \leq Ri \leq +1$; $Pr = 0.71$ Geometry: in-line circular cylinder	Drag coefficients, Nusselt number and pressure distribution around in-line cylinder were examined. The Strong influence of buoyancy parameter over tube bundles was noticed.
3.	Haldar (2000)	$0 \leq Gr \leq 10^6$; $Pr = 0.71$ Geometry: Combined convection through seven-rod bundles in a circular shell arranged horizontally	The flow and temperature field was reported and the highest temperature was found at the top of the central rod. The increased buoyancy decreases the flow rate and increases friction and rate of heat transfer. The result has been further compared with the experiments and found to be satisfactory.
4.	Fornarelli et al. (2016)	$-1 \leq Ri \leq 1$; $Re = 100$, $Pr = 0.7$; $L = 3.6D$ and $4D$ Geometry: An array of six circular cylinders	Numerically examined the flow and heat transfer features. Many transitions in the flow field are found and dependence of force coefficient and the Nusselt number has been reported. It is emphasized that the transition occurs due to the rearrangements of the near field flow in a more ordered wake pattern.

Overall, the available literature recommends that the mixed convection flow and heat transfer features over a single and/or double cylinders have been studied widely. In contrast, negligible literature is available for mixed convection problems across the periodic array of circular cylinders even with simple Newtonian fluids. The scant mixed convection studies which are

available across a periodic array of circular cylinder and/or over tube banks are summarized above in Table 2.4.

2.6 Summary of literature review

The critical review of available literature on the periodic flow across an array of cylinder and/or over tube banks for Newtonian and non-Newtonian fluids suggests an adequate insights for the global engineering parameters (e.g. drag coefficients, pressure loss, permeability, Nusselt numbers, etc.) mostly by using various cell models. But, these are limited to creeping flow, laminar flow and low porosity or fluid volume fractions of the cylinders. In fact, limited literature is available to reveal the flow and thermal features by using the direct periodic array of cylinders. Additionally, in the case of mixed convection problems, negligible literature/studies are available to these flow geometries. These gaps in the literature motivated us to investigate the problems of forced and mixed convection across an array of circular cylinders to reveal the features of Newtonian and non-Newtonian power-law fluids from such an industrially important flow geometry. So, based on the preceded discussion, the followings are summarized:

1. Scant studies are available by using direct periodic array of cylinders to explore the flow and thermal features.
   (*e.g. Koch and Ladd, (1997), Martin et al. (1998), Spelt et al., (2005b)).*

2. Very limited is known about the individual components of flow and thermal features such as pressure and friction drag coefficients and local Nusselt numbers, etc.
   (e.g. scant studies using cell models by Vijaysri et al. (1999), Shibu et al. (2001)and Soares et al. (2005a) have explored the individual drag coefficients; whereas Mandhani et al. (2002) have explored the local Nusselt number and Tahseen et al. (2013) explored both the features in the limited ranges).

3. The heat transfer characteristics have been studied less in contrast to flow characteristics.
   (e.g., few heat transfer studies in Newtonian flow regime: Chen and Wung (1989), Martin et al. (1998), Wilson and Bassiouny (2000), Mandhani et al. (2002).

4. The flow and heat transfer characteristics of the power-law fluid are starving as compared to Newtonian fluids.
   (e.g. few studies for power-law fluids (i) flow features: Vijaysri et al. (1999), Dhotkar et al. (2000), Shibu et al. (2001), Soares et al. (2005a), Spelt et al. (2005b) and (ii) thermal features: Mangaddody et al. (2004) in the limited ranges.

5. Scant experimental and analytical studied are available for limited ranges of parameters.
   (Experimental: Prasad and Chhabra (2001) and analytical: Khan et al., (2006a, b)).

6. Very few studies are available for mixed convection even with simple Newtonian fluids.
   (e.g. Duli et al. (1995); Gowda et al. (1998), Haldar, (2000) and Fornarelli et al. (2016)).

7. No study is available for mixed convection features to explore the non-Newtonian fluids across periodic array of cylinders.

2.7 Objectives of dissertation

Based on the gap found in the literature review (Sections 2.61-2.6.3), following objectives are set for this dissertation as mentioned in Table 2.5

Table 2.5: Problems studied in this dissertation

S. No.	Problems Studied	Ranges of Physical Parameters
1.	Forced convection flow and heat transfer characteristics of Newtonian fluids across periodic array of circular cylinders	$0.70 \leq \phi_f \leq 0.99$; $1 \leq Re \leq 40$; $0.70 \leq Pr \leq 100$
2.	Forced convection momemtum transfer characteristics of power-law fluids across periodic array of circular cylinders	$0.70 \leq \phi_f \leq 0.99$; $1 \leq Re \leq 40$; $1 \leq Pr \leq 100$; $0.4 \leq n \leq 1.8$
3.	Forced convection heat transfer characteristics of power-law fluids across periodic array of circular cylinders	$0.70 \leq \phi_f \leq 0.99$; $1 \leq Re \leq 40$; $1 \leq Pr \leq 100$; $0.4 \leq n \leq 1.8$
4.	Aiding buoyancy mixed convection characteristics of Newtonian fluids across periodic array of circular cylinders	$0.70 \leq \phi_f \leq 0.99$; $1 \leq Re \leq 40$; $0.70 \leq Pr \leq 50$; $0 \leq Ri \leq 2$
5.	Aiding buoyancy mixed convection characteristics of power-law fluids across periodic array of circular cylinders	$0.70 \leq \phi_f \leq 0.99$; $1 \leq Re \leq 40$; $1 \leq Pr \leq 50$; $0.4 \leq n \leq 1.8$; $0 \leq Ri \leq 2$
(ϕ_f : fluid volume fraction, Pr: Prandtl number, Re: Reynolds number, Ri: Richardson number and n: power-law index)		

Therefore, the aim of this dissertation is to supplement the available knowledge through a CFD investigation for the wide ranges of above pertinent dimensionless parameters to explore the momentum and heat transfer features across the periodic array of circular cylinders in a square configuration. Particularly, this study is focused on both of the forced and mixed (aiding buoyancy) convection features of Newtonian and non-Newtonian power-law fluids for ranges of governing parameters as mentioned in Table 2.5. The dependence of local and global characteristics such as streamline profiles, isotherm contours, pressure coefficient, individual (pressure and friction) and total drag coefficients, local and average Nusselt numbers, etc. over the aforementioned flow governing parameters (ϕ_f , n, Re, Pr and Ri) has been investigated and

explored. In the case of power-law fluids, the shear-thinning and shear-thickening features have been revealed across the periodic array of cylinders. Not to be mentioned, all the above parameters (fluid volume fraction (ϕ_f), inertial (Re), viscous (Pr), buoyancy (Ri) and flow behavior (n) parameters) have shown the strong dependence on the above qualitative and quantitative features. Additionally, the statistical correlations for the drag coefficients and average Nusselt numbers have been developed to gain the further physical insight of the results. Lastly, the present numerical results have been compared with available literature where an excellent agreement was found to exist.

Chapter 3

PHYSICAL AND MATHEMATICAL MODELING

This chapter deals with the problem formulation, details of geometry for the periodic array of circular cylinders in a square arrangement, governing equations and appropriate boundary conditions, etc. Prior to defining the problem formulations and other things, it is appropriate to mention the general assumptions which have been made in this study herein first.

3.1 General assumptions

The following general assumptions have been considered in this work:

1. Two dimensional (2-D) flow
2. Incompressible flow
3. Steady state flow
4. Laminar flow
5. Small temperature difference ($\Delta T = T_w - T_\infty$)
6. In the case of forced convection, the thermophysical properties of the fluids namely density, viscosity, heat capacity and thermal conductivity are assumed to be temperature independent.
7. *Boussinesq approximation (for mixed convection problems):* For small to moderate variations in the density with temperature, it is sufficient and common to use the well-known *Boussinesq approximation* to express its dependence on the temperature as $\rho = \rho_0[1-\beta(T-T_0)]$, where β is the coefficient of volume expansion and T_0 is the reference temperature. This approximation is customarily used to maintain the level of complexity at a tractable level in most of the natural/mixed convection studies (Srinivas et al., 2009). Further, the *Boussinesq approximation* evidently couples the Navier–Stokes equations with the thermal energy equation. Therefore the simultaneous solution of these governing equations is required.
8. Furthermore, viscous heat dissipation, radiation heat transfer and compression work done by pressure are neglected. This approximation restricts the applicability of the present results to the situations where the temperature difference (ΔT) is not too large and/or for moderate viscosity so that the viscous dissipation effects are negligible. Keeping in mind

of Boussinesq approximation, the temperature difference (ΔT) is maintain to be small such that it justifies the unaccountability of the variation of the fluid viscosity with temperature.

In view of all the above assumptions and approximations, the problem statement is now described in the next section.

3.2 Problem formulation

The steady, laminar and incompressible flow of fluids across an array of circular cylinders in the square geometrical arrangement is considered to examine the forced and mixed convection flow and heat transfer features of Newtonian and non-Newtonian power-law fluids. The schematic flow diagram of the problem considered herein is shown in Fig. 3.1(a). The transverse flow of the fluids is occurring in the y-coordinate direction, whereas, the gravity forces are acting in the opposite direction of the flow (i.e., negative y-direction). Further, the variations in fluid density with the temperature yield the buoyancy forces which are acting parallel (vertically upward) to the flow direction and therefore the aiding buoyancy conditions prevail. The end effects (entrance and exit) are neglected due to the assumption that the sufficiently long cylinder's arrays have a large number of rows and this assumption is also sufficient to occur the periodicity across the periodic boundaries. The above square configuration contains equal sized cylinders of diameter D and spacing L which is center to center distance between the two cylinders in proximity and called the tube pitch also. The cylinder spacing is determined using either fluid volume fractions (ϕ_f) and/or solid volume fractions ($\phi_s = 1 - \phi_f$) depending upon what kind of array is used in the investigation. For the case of square array of circular cylinders, it is defined as;

$$\phi_f = 1 - \frac{\pi}{4}\left(\frac{L}{D}\right)^{-2} \tag{3.1}$$

and hydraulic diameter ($D_{h,i}$) is defined as flow area (A_i) per wetted perimeter ($P_{w,i}$) and given by:

$$D_{h,i} = 4A_i/P_{w,i} = D.\,(\phi_f/\phi_s) \qquad \text{where, } A_i = L^2 - \pi D^2/4 \text{ and } P_{w,i} = \pi D \tag{3.2}$$

The numerical computations have been simplified by considering a representative elementary volume as displayed by the solid lines in Fig. 3.1(a). Fig. 3.1(b) represents half of the computational domain due to symmetry conditions for the fluid volume fractions of $\phi_f = 0.70$. The temperatures of flowing fluid and cylinder surfaces are maintained at T_∞ and T_w,

respectively, where $T_w > T_\infty$. Here, the constant wall temperature (CWT) condition has been considered.

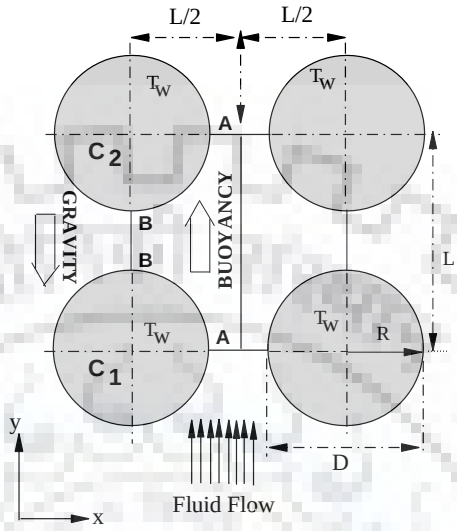

(a)

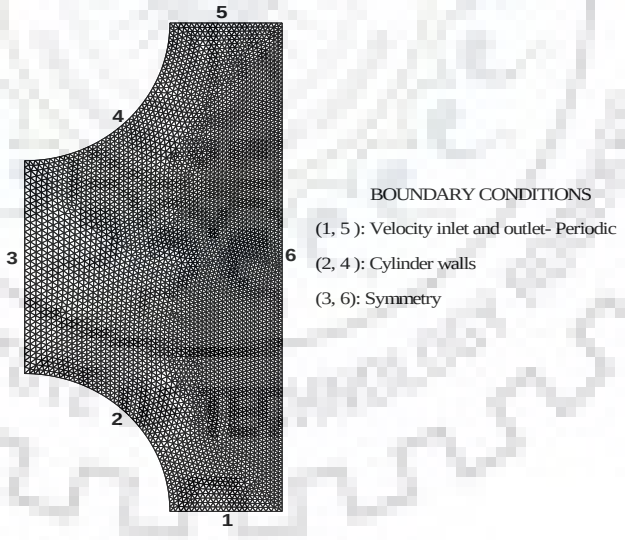

(b)

Figure 3.1: Schematic representation of periodic flow across an array of circular cylinders in a square configuration (a) complete flow domain; here, the points A and B on the surface of the cylinders represent for $\theta = 0^o$ and $\theta = 90^o$, respectively and (b) half of the computational domain

3.3 Governing equations

For an incompressible, 2-D, steady and laminar flow conditions, the flow governing equations and boundary conditions in the Cartesian co-ordinate system are given as follows:

Continuity equation:

$$\frac{\partial V_x}{\partial x} + \frac{\partial V_y}{\partial y} = 0 \tag{3.3}$$

x- Component of momentum equation:

$$\rho\left(V_x \frac{\partial V_x}{\partial x} + V_y \frac{\partial V_x}{\partial y} \right) = -\frac{\partial p}{\partial x} + \left(\frac{\partial \tau_{xx}}{\partial x} + \frac{\partial \tau_{yx}}{\partial y} \right) + \rho g_x \tag{3.4}$$

y- Component of momentum equation:

$$\rho\left(V_x \frac{\partial V_y}{\partial x} + V_y \frac{\partial V_y}{\partial y} \right) = -\frac{\partial p}{\partial y} + \left(\frac{\partial \tau_{xy}}{\partial x} + \frac{\partial \tau_{yy}}{\partial y} \right) + \rho g_y \tag{3.5}$$

where, g_x and g_y are x and y components of gravity forces. For the present case of problem, g_x = 0 and since gravity acts in the negative y-direction (Fig. 3.1a), the y-component of gravity (g_y) is taken as (-g). By using the *Boussinesq approximation* for density (ρ) in the body force term, Eq. (3.5) is rewritten as

$$\rho\left(V_x \frac{\partial V_y}{\partial x} + V_y \frac{\partial V_y}{\partial y} \right) = -\frac{\partial p}{\partial y} + \left(\frac{\partial \tau_{xy}}{\partial x} + \frac{\partial \tau_{yy}}{\partial y} \right) + \rho_0 g\beta(T - T_0) \tag{3.6}$$

In the above equations, V_x and V_y are the x and y components of the velocity vector, ρ and ρ_0 are the fluid densities at temperatures T and T_0, respectively.

Thermal energy equation: The thermal energy equation in terms of the constant transport properties and in the absence of viscous dissipation can be written as

$$V_x \frac{\partial T}{\partial x} + V_y \frac{\partial T}{\partial y} = \alpha\left(\frac{\partial^2 T}{\partial x^2} + \frac{\partial^2 T}{\partial y^2} \right) \qquad \left(\text{where; } \alpha = \frac{k}{\rho c_p}\right) \tag{3.7}$$

where, ρ, c_p and k are fluid density, the specific heat and thermal conductivity, respectively and α is the thermal diffusivity.

If the flow of fluids is non-Newtonian, the rheological equation of state for power-law fluids depends on the rate of stress and rate of strain tensors as

$$\tau_{ij} = 2\eta\varepsilon_{ij} \qquad \text{where; } i, j = x, y \tag{3.8}$$

where, ε_{ij} are the components of the rate of strain tensor and are related to velocity field as follows:

$$\varepsilon_{ij} = \frac{1}{2}\left(\frac{\partial V_i}{\partial j} + \frac{\partial V_j}{\partial i} \right) \tag{3.9}$$

and the viscosity (η) of power-law fluids is defined as

$$\eta = m(I_2 / 2)^{\frac{n-1}{2}} \tag{3.10}$$

where, m is the power-law consistency index, n is the power-law index (n <1: shear-thinning; n = 1: Newtonian and n >1: shear-thickening fluids) and I_2 is the second invariant of rate of strain tensor whose components are given by (Bird et al., 2002):

$$I_2 = 2\sum_i \sum_j \left(\varepsilon_{ij}.\varepsilon_{ij}\right) = 2\left(\varepsilon_{xx}^2 + \varepsilon_{yy}^2\right) + 2\left(\varepsilon_{xy}^2 + \varepsilon_{yx}^2\right) \tag{3.11}$$

In the case of a Newtonian fluids, Eq. (3.10) reduces to $\eta = m = \mu$ and gives the viscosity of Newtonian fluids.

3.4 Boundary conditions

The physically consistent boundary conditions for the problems considered herein across the periodic array of circular cylinders (Patankar et al., 1977) are described as follows:

- On the cylinder's surface: The standard no slip boundary conditions are applied and the cylinders are maintained at constant temperature (T_w) i.e.

$$V_x = 0, \quad V_y = 0 \text{ and } \quad T = T_w \, (>T_0) \tag{3.12}$$

- At the plane of symmetry: There is no flow in the x-direction and the normal gradients of major velocity component and temperature are zero. Therefore;

$$V_x = 0, \ \frac{\partial V_y}{\partial x} = 0 \text{ and } \frac{\partial T}{\partial x} = 0 \tag{3.13}$$

- At inlet and outlet boundaries: The periodically fully developed flow and thermal fields are applied through the periodicity of velocity (i.e. average flow velocity, V) and temperature (bulk fluid temperature, T_∞) at these boundaries;

$$\text{i.e.} \quad V_{x,i} = V_{x,o} = 0 \ ; \ V_y = V \ \text{ and } \ T_i = T_o = T_\infty \tag{3.14}$$

However, the periodic flow conditions in the ANSYS Fluent solver can be imposed in terms of either pressure gradient or the mass flow rate. The present study has used periodic mass flow rate ($\dot{m}$) condition. For a given geometry and fluid, the mass flow rate, in turn, leads to the periodic average velocity. Therefore, the following periodic condition (which are consistent with Eq. 3.14) is imposed at inlet and outlet boundaries,

$$\dot{m}_i = \dot{m}_o \tag{3.15}$$

The numerical simulation of the governing Eqs. (3.3-3.7) along with the above-noted boundary conditions Eqs. (3.12-3.15) maps the flow domain in terms of basic variables i.e. velocity components (V_x and V_y), temperature (T) and pressure fields. These, in turn, are further used to calculate the local and global momentum and heat transport characteristics such as drag coefficients and Nusselt numbers (Bharti et al., 2007a, b; Sivakumar et al., 2006, 2007; Patil et al., 2008), etc., and defined as below:

- **Total drag coefficient (C_D):** The total drag coefficient (C_D) on the surfaces of the cylinder is defined as:

$$C_D = \frac{F_D}{\frac{1}{2}\rho V^2 D} = C_{DP} + C_{DF} \tag{3.16}$$

and the individual drag coefficients such as pressure drag coefficient (C_{DP}) and friction drag coefficient (C_{DF}) are defined as:

$$C_{DP} = \frac{F_{DP}}{(1/2)\rho V^2 D} = \int_S C_p n_y dS \tag{3.17}$$

and

$$C_{DF} = \frac{F_{DF}}{(1/2)\rho V^2 D} = \frac{2^{n+1}}{Re}\int_s (\tau.n_s)dS \tag{3.18}$$

$$= \frac{2^{n+1}}{Re}\int_s (\tau_{yx}.n_x + \tau_{yy}.n_y)dS \tag{3.19}$$

For Newtonian fluids, Eq. (3.18) and (3.19) reduces to Eq. (3.20) and (3.21), respectively:

$$C_{DF} = \frac{F_{DF}}{(1/2)\rho V^2 D} = \frac{4}{Re}\int_s \tau.n_s dS \tag{3.20}$$

$$= \frac{4}{Re}\int_s (\tau_{yx}.n_x + \tau_{yy}.n_y)dS \tag{3.21}$$

where, F_{DP} and F_{DF} are the pressure and frictional components of the drag force per unit length of the cylinder, S is the surface area and n_s are unit vector normal to the cylinder surfaces and defined as:

$$n_s = \frac{xe_x + ye_y}{\sqrt{x^2 + y^2}} = n_x e_x + n_y e_y \tag{3.22}$$

where, e_x and e_y are the x and y components of the unit vectors, respectively and τ the dimensionless shear stress expressed as

$$\tau_{ij} = \eta\left(\frac{\partial V_i}{\partial j} + \frac{\partial V_j}{\partial i}\right) = \left(\frac{I_2}{2}\right)^{\left(\frac{n-1}{2}\right)}\left(\frac{\partial V_i}{\partial j} + \frac{\partial V_j}{\partial i}\right) \tag{3.23}$$

For Newtonian fluids, Eq. (3.23) reduces to Eq. (3.24) with $\eta = \mu$,

$$\tau_{ij} = \mu\left(\frac{\partial V_i}{\partial j} + \frac{\partial V_j}{\partial i}\right) \quad \text{where, } i, j = x, y \tag{3.24}$$

where, η and I_2 are the dynamic viscosity and second invariant of the rate of strain tensor, respectively.

Further, the stream function $\psi(x, y)$ is a convenient parameter by which one can represent two-dimensional, steady, incompressible flow. The stream function, ψ in m^2/s, is related to velocity components V_x and V_y as follows:

$$V_x = \frac{\partial \psi}{\partial y} \quad \text{and} \quad V_y = -\frac{\partial \psi}{\partial x} \tag{3.25}$$

These definition of V_x and V_y can be used in the x and y components of momentum Eqs. (3.4-3.5) to obtain a differential equation for ψ which is equivalent to Navier-Stokes equation. The stream function is very useful because its physical significance is that in steady flow lines defined by ψ = constant, are streamlines which are the actual curves traced out by the particles of the fluid. A stream function exists for all two-dimensional, steady and incompressible flows whether viscous or inviscid, rotational or irrotational (Geankpolis, 1993).

As far as the heat transfer characteristics are concerned, the local Nusselt number is defined as (Bharti et al., 2007a, b):

$$Nu(\theta) = \frac{hD}{k} = -\frac{dT}{dn_s} \tag{3.26}$$

The local Nusselt number is further averaged over the surfaces of periodic cylinders to obtain the surface average Nusselt number as follows:

$$Nu = \int_S Nu(\theta) d\theta \tag{3.27}$$

The average Nusselt number is used in the process engineering design calculations to estimate the rate of heat transfer from isothermal cylinders. Now, after defining the problem statement,

governing equations and boundary conditions, etc., the solution methodology and choices of numerical parameters etc. are described in Chapter 4.

Chapter 4

SOLUTION METHODOLOGY AND CHOICES OF NUMERICAL PARAMETERS

This chapter deals with the solution methodology and choices of numerical parameters for the modeling and simulation of periodic flow problems considered herein this work. The numerical solutions in this work have been obtained by using a computational fluid dynamics (CFD) solver ANSYS FLUENT (2009).

4.1 Solution procedure of periodic problems

The following necessary steps are employed in the modeling and simulation of periodic flow and thermal problems:

(i) CAD modeling using GAMBIT
- creation of computational geometry
- grid generation
- Assignment of boundaries

(ii) CFD modeling using ANSYS Fluent
- Import of the grids/mesh geometry from GAMBIT to ANSYS Fluent
- Defining boundary conditions
- Selection of a solver

(iii) Solution Methodology
- Discretization method
- Pressure velocity coupling
- Relaxation factor
- Solution initialization
- Convergence and analysis of results

All the above steps have been described briefly herein for an overview of solving the periodic flow problems numerically by using the commercial CFD solvers GAMBIT and ANSYS Fluent (2009).

4.2 CAD modeling using GAMBIT

The creation of computational geometry, grid generation and assignment of boundaries, etc. have been done by CAD modeling using GAMBIT. The creation of computational geometry is a two-step process which involves the identification of computational domain and creation of mesh geometry. Once the computational domain has been identified, the mesh geometry can be created by generating the grid points first on the surfaces of solids/cylinders boundaries. Grid generation is a very important step in the solutions of the flow and/or heat transfer problems because the system of grid points used determines the accuracy, efficiency and ease with which these methods generate solutions. This is an essential aspect of computational fluid dynamics that employ finite difference method (FDM), finite volume method (FVM) and finite element method (FEM) for the solution of partial differential equations (PDE). Among these methods, the finite volume method (FVM) is very powerful for obtaining the solutions to PDE's that govern fluid flow and heat transfer problems. However, to use these methods, it is necessary to replace the spatial domain of the problem by a finite number of discrete points or elemental volumes (cells) known as grid points. The process of replacing a spatial domain by a system of grid points is referred as grid generation. In the present work, the grids and mesh geometry have been generated using CFD software called GAMBIT as shown in Figs. 3.1(b).

After creation of mesh geometries, the next step is to define boundary conditions. As mentioned earlier (Chapter 2; Section 2.1.1), there are two types of periodic boundary conditions available in ANSYS Fluent, i.e. rotational and translational. The current problem is concerned with translational periodic boundaries for the fully developed periodic flow. In such a case the pressure drop occurs through the periodic boundary. The periodic boundary conditions are used when the flow across the two opposite planes in the computational domain are identical. Further, the different boundaries of the computational domain is assigned their identity for example in Fig 3.1(b), velocity inlet and outlet, cylinder walls and symmetry conditions have been shown.

4.3 CFD modeling using ANSYS Fluent

Here, after completing mesh generation and assignment of boundaries, the problem is imported in the ANSYS Fluent from the GAMBIT. Further, the grid check and scaling are done along with the creation of periodic zone. Next, the flow and thermal boundary conditions are set up depending upon the problems studied. For instance, the periodic flow condition in ANSYS

Fluent solver can be imposed in terms of either pressure gradient or the mass flow rate. The present study has used periodic mass flow rate conditions. For a given geometry and fluid, the mass flow rate, in turn, leads to the periodic average velocity. Further, for the thermal condition, as the fluid flow through the periodic domain, its temperature approaches that of the wall boundaries. Though, the temperature can be set up in such a way that it behaves periodically. After setting up the flow and thermal conditions, the solver ANSYS Fluent uses the finite volume method (FVM) technique to discretize the governing equations. In this method, the flow/computational domains are distributed into a finite number of control volumes/cells (CVs) of a grid, so that the overlapping of these cells could not happen. The boundaries of the control volumes are defined by the grids, however, the computational nodes are present at the center of the control volumes. The differential equations for mass, momentum and energy, etc., along with the boundary conditions are integrated over these control volumes (CV), each and then the divergence theorem is applied. As a result, a linear algebraic equation, one for each control volume is obtained. This linear algebraic equations set is then computed simultaneously or iteratively. In particular, the 2-D, segregated solver is used to resolve the incompressible laminar flow and heat transfer of the fluid on the non-staggered grid arrangement.

Further, there are two types of solvers found in ANSYS Fluent namely: the density-based solver and the pressure-based solver. The pressure-based solver has been selected as the preferred solver in this thesis. In both the solvers, continuity and momentum equations are used to derive a pressure equation which further is used to deduce the velocity field. For the selected pressure-based coupled algorithm, the continuity and momentum equations are simultaneously solved. The iterations continue until the solution converged. Further, these solvers have three formulation schemes which are coupled-explicit, coupled-implicit and segregated (implicit). Density-based solver works on coupled-explicit or coupled-implicit formulation scheme, whereas the pressure-based solver works on the segregated (implicit) formulation scheme. The segregated (implicit) solver is preferred as it requires less memory than the coupled-implicit solver and flexibility in solution procedure is also provided by the segregated scheme.

4.4 Solution Methodology

This section explains the various steps involved in the simulation of problems such as discretization method, pressure-velocity coupling, relaxation factor, solution initialization, convergence and analysis of results.

4.4.1 Discretization method

The number of different interpolation/discretization schemes are offered by the ANSYS Fluent, which are as follows:

- First-order upwind scheme
- Second-order upwind scheme
- Power-law scheme
- QUICK scheme and others

The present study has used the second order upwind scheme for the discretization of partial differential equations. The second order upwind scheme uses constants and first order derivative but ignores the second order derivative. Moreover, this scheme is necessary when the flow is not aligned to the grid and has a slower convergence. This scheme is more accurate than the first order upwind scheme and having a higher order of stability also.

4.4.2 Pressure-velocity coupling

A pressure-velocity coupling method is used to define the segregated algorithm used by ANSYS Fluent during its calculations. All the momentum equations contain a pressure term in it and the continuity equation has to be satisfied by the velocity field. Therefore, a set of these equations, each for an unknown variable is obtained. Thus, the derivation of the pressure equation from the continuity and momentum equations are possible because of such pressure-velocity coupling algorithms. SIMPLE is the most commonly used algorithm and is used in the present thesis. SIMPLE is based on the presumption that the fluid flows from the region of high pressure to the region of low pressure. There are other improved versions of SIMPLE are also available such as SIMPLEC (Semi-Implicit Method for Pressure-Linked Equations Consistent), SIMPLER (Semi-Implicit Method for Pressure-Linked Equations Revised) and PISO (Pressure Implicit with Splitting of Operators). Although all the above algorithms will converge to the same solution, the use of high under-relaxation factors than SIMPLE accelerates the convergence in the above-improved algorithms. The discrepancy lies in stability and speed. The speed of the functionality of the above algorithms depends on the flow and no single algorithm is said to be faster than other, always.

4.4.3 Relaxation factor

Relaxation factor is introduced to the segregated solver for the stabilization of the iterative process.

- Under-relaxation occurs when relaxation factor < 1. The speed of the convergence may be retarded by the under-relaxation, whereas, an increase in the calculation stability is seen, as the chance of oscillations or divergence in the solutions is decreased.
- No relaxation occurs when relaxation factor = 1. In this, the estimated value of the variable is used.
- Over-relaxation occurs when relaxation factor > 1. The speed of the convergence may be accelerated by the over-relaxation. But it decreases the stability of the calculation.

Further, the numerical errors result in oscillations in the flow solution which are suppressed by the under-relaxation factors. The convergence is significantly retarded by the very small value of under-relaxation factors, even sometimes to the extent that the solution appears to be converged but it actually is not. Hence, it is recommended always to use a high value of under-relaxation factors such that it must not result in divergence or oscillations. Therefore, the default factors in the solver should be used. Also, the momentum and pressure factors can be reduced if the solution is seen to be converged, but the pressure residual is still relatively high as it further refines the solution.

4.4.4 Solution initialization

Solution initialization is vital in ensuring that the initial conditions are similar to the values produced in the converged results. Solution initialization allows a definition of flow variables and therefore the software initializes the flow field to these values. Initial values are the values that are set for the beginning of the flow from that boundary. 'Compute from' allows the user to compute values from a particular zone, in terms of the current project all variables will be calculated from a velocity set at the velocity inlet. A time-step is used to simulate the full flow cycle in the model. Once these settings have been customized, the simulation can begin. After each iteration, ANSYS Fluent reports residuals which are the sum of conserved quantities, back to the user on a window which can also be used to view the convergence history of the model. The graphs can be used to predict how the simulation is converging (or diverging) and can be used to observe initial values of the models.

4.4.5 Convergence of results

A solution is considered to be converged until the change in the value of the variable from one iteration to the next becomes negligible. At convergence, all the distinct conservation

equations such as energy, momentum, etc. are executed in all the CVs to a particularized tolerance and no more change in the solution is observed with further iterations. The error in conservation equations is measured by the residual. Thus, the balances for momentum, energy, mass and scalar are obtained and the solutions are said to be converged when there is no change in the scalar fields and the flow field. A qualitative convergence is generally indicated by the reduction in the residuals by three orders of magnitude. For instance, in this study, the absolute residuals of the continuity, x- and y- velocities and energy are used in the order of 10^{-10}, 10^{-10} and 10^{-14}, respectively. Also, the imbalance in the conservation equations is measured by the residuals. The solution may not be converged if the residuals are still decreasing even if the specified convergence criterion is reached. While, the solution may be converged if the residuals are no longer decreasing, neither there is any change in the other solution monitors, even if the convergence criterion is never met. Lower or higher residuals do not automatically mean a correct or an incorrect solution, respectively. The residuals can also be monitored graphically.

4.5 Choices of numerical parameters

It is well known that the choice of grid sizes exert varying levels of influence on the numerical results. In this work, since the periodic flow has been simulated for the varying level of fluid volume fractions (or porosity) across the periodic array of circular cylinders, therefore, it is necessary to obtain the grids, which on further refinement do not change the numerical results. Further, the numerical parameters which have been used in this dissertation are described briefly herein in terms of their suitability before giving the description of grids and their specifications, etc.

- **Reynolds number (Re):** In this dissertation, the minimum and maximum value of Reynolds number were taken to be Re = 1 and 40, respectively. Over the range Reynolds number being considered herein, the flow is known to be steady, laminar and two-dimensional. It is also well known that the two-dimensional flow around a single circular cylinder is stable in this low range of Re (Gamrat et al., 2008). Further, it is most likely that the case of an array of cylinders is more stable than an isolated single cylinder. Dybbs and Edwards (1984) investigated the flow through the packing of spheres and for complex arrangements of cylinders. They observed the onset instabilities for Re > 150, where, the Reynolds number Re is based on the average pore velocity and an average characteristics length scale for the pores. This critical value corresponds to Re much larger than 40 for the low range of porosity. It was then assumed that instabilities did not occur for the

present low value of Re and that the flow around the solid elements was symmetrical with respect to the x-direction.

Further, in this dissertation, an unsteady behavior was found with Re = 40 for mixed convection Newtonian flow and even with Re = 20 also for non-Newtonian fluid at the higher values of fluid volume fractions of ϕ_f = 0.96, 0.98 and 0.99. Therefore, it is expected that the value of Re above 40 will also display an unsteady behavior. Since, this study is concerned with 2-D, steady and laminar flow, hence the present range of Re was found to be suitable for such an investigation.

- **Prandtl number (Pr):** The range of Prandtl number was taken to be Pr = 0.7 to 100**.** This range covers the behavior of Newtonian and non-Newtonian fluids both**.** This range of Prandtl number is very common in chemical, petroleum and oil related engineering applications. Further, the range of Prandtl number for different fluids such as 0.7-1.0 for air; 7-10 for water/water suspensions and 50-2000 for heavy oils. So, a small value Pr = 0.7 of air which exhibits Newtonian behaviour also suggest that the heat conduction is more significant compared to convection and so the thermal diffusivity is dominating. Further, as the Pr increases, the behaviour is correspondingly reversed. For instance, Pr = 7 (water; Newtonian fluid) means the heat transfer by convection is dominating over conduction i. e. as Pr increases the momentum diffusivity dominates. For example, with butanol (Pr = 50; non-Newtonian fluids), convection dominates. Similarly for engine oils ($Pr \geq 100$; non-Newtonian fluids), convection is very effective in transferring energy from an area in comparison to pure conduction, so in this case, the momentum diffusivity is dominating. So by fixing the above range of Prandtl number, it is possible to display the behaviour of both Newtonian and non-Newtonian fluids.

- **Richardson number (Ri):** The range for the buoyancy parameter or the Richardson number is $0 \leq Ri \leq 2$, where, Ri = 0 is the case of forced convection whereas $Ri \rightarrow \infty$ is the case of free convection. In between 0 to ∞; there is an intermediate region when both of the free and forced convection contributes to the heat transfer. The +ve value of Ri suggests the case of aiding buoyancy mixed convection. In the present investigation, it is found that the increased value of Richardson number causes more turbulence and behavior gradually shifts from steady to unsteady. Due to this reason, an unsteady behavior has been found for Ri = 2 at ϕ_f = 0.96, 0.98, 0.99 and expected to move towards lower fluid volume fractions with further increase in Ri >2. So, for the 2-D, steady and

laminar flow investigation, the maximum value of Ri = 2 was found to be appropriate for most of the results generated in this study except the aforementioned limits.

- **Power-law index (n):** The range of power-law index has been taken to be $0.4 \leq n \leq 1.8$. Further, the non-Newtonian fluids such as dilute polymer solutions with smaller molecules, foams, syrups, starch solutions, high molecular weight polymeric systems (i.e., blends, solutions, melts), emulsions and pulp and paper suspensions, which come across in chemical and related process industries exhibit either shear-thinning (i.e., pseudo-plastic fluids, $n < 1$) and/or shear-thickening (i.e., dilatant fluids, $n > 1$) behavior under suitable flow conditions. The reason behind setting up this range is that it covers a wide range of the shear-thinning, Newtonian and shear-thickening fluid behaviors. In the context of present dissertation, negligible studies are available using a periodic array of circular cylinder to reveal the forced and mixed convection features of the fluids. So the above range of power-law index has been found suitable for present investigation.

- **Fluid volume fraction (ϕ_f):** The range of fluid volume fractions **(ϕ_f)** has been taken to be $0.70 \leq \phi_f \leq 0.99$. The reason behind setting up this range is that it covers a wide range of the porosity of the cylinder arrays. Further, in the context of present dissertation, negligible studies are available with the direct use of periodic array of circular cylinders. The above range of fluid volume fractions is frequently encountered in industrial applications which cover sparse ($\phi_f = 0.99$) to dense ($\phi_f = 0.70$) geometry of cylinder arrangements.

In view of the aforementioned numerical parameters, the grid sensitivity is checked now within the ranges covered herein.

4.5.1 Specification of grids used in grid independence study

The grid independence study has been carried out by using four different kinds of non-uniform unstructured grids represented as G1, G2, G3 and G4 for the lowest fluid volume fractions ($\phi_f = 0.70$) and three different grids G1, G2 and G3 for the highest fluid volume fractions ($\phi_f = 0.99$) with the details given in Table 4.1. Further, in Table 4.1, N_c represents the number of grid points on the quarter surface of the cylinders. A total of 45 grid points has been taken on the quarter surface of the cylinders for each of the grids G1, G2 and G3, whereas 60

grid points were taken for the grid G4. Next, the δ and Δ are the minimum and maximum grid spacing per unit length on the computational boundaries, respectively. In Table 4.1, it can be seen that the maximum grid spacing (Δ) has been fixed to be 0.03 for all the grid types, whereas the minimum spacing is varying from 0.005-0.02. So, the grid refinement from G1 (δ = 0.02) to G2 (δ = 0.01); from G2 to G3 (δ = 0.005); and from G3 to G4 (δ = 0.005), yields the finer grids, respectively. Accordingly, it can be seen that the maximum number of nodes (N = 7715) in computational domain is present for G4 of ϕ_f = 0.70 and N = 146131 for G3 of ϕ_f = 0.99. The influences of these grid sizes on the forced and mixed convection flow and heat transfer characteristics has been examined for the different problems studied as described in the next sections.

Table 4.1: Specifications of grids used for the grid independence study

	Grid specifications				
ϕ_f	Grid	N_c	δ	Δ	N
0.70	G1	45	0.02	0.03	2238
	G2	45	0.01	0.03	3218
	G3	45	0.005	0.03	6620
	G4	60	0.005	0.03	7715
0.99	G1	45	0.02	0.03	61028
	G2	45	0.01	0.03	86714
	G3	45	0.005	0.03	146131

- N_c (number of grid points on the quarter surface of the cylinder), δ and Δ (minimum and maximum grid spacing per unit length on the computational boundaries respectively) and N (total number of nodes in the computational domain).

4.5.2 Grid independence study for the forced convection characteristics of Newtonian and non-Newtonian power-law fluids

The grid independence test was carried out by using above grids (Table 4.1) for the extreme values of flow conditions (ϕ_f = 0.70 and 0.99; Re =1 and 40; Pr = 0.70 and 100; n = 0.4 and 1.8) for Newtonian and non-Newtonian power-law fluids which exhibit shear-thinning and shear-thickening behaviours also. The values of drag coefficient (C_D) and average Nusselt numbers (Nu) for the above grids have been compared in Table 4.2. For Newtonian fluids, it can be seen that the refinement in the grids from G1 to G4 for ϕ_f = 0.70 shows the maximum relative differences in the C_D values of about 0.30%, while it is about 0.11% for ϕ_f = 0.99 in moving from G1 to G3. Similarly, the average Nusselt number was compared in each respective grids,

which shows the maximum relative difference of about 0.23% for ϕ_f = 0.70 and about 0.22% for ϕ_f = 0.99**.**

Table 4.2: Grid independence test for the total drag coefficient (C_D) and average Nusselt number (Nu) for the forced convection characteristics of Newtonian and power-law fluids

ϕ_f	Grid	n = 0.4				n = 1			n = 1.8				
		C_D		ε_r (C_D)		C_D	ε_r (C_D)		C_D		ε_r (C_D)		
		Re→ 1	40	1	40	1	40	1	40	1	40	1	40
0.70	G1	31.7872	0.7609	-	-	144.1932	4.1588	-	-	260.6559	7.7086	-	-
	G2	31.8558	0.7625	0.22	0.21	144.2868	4.1605	0.06	0.04	261.0992	7.7192	0.17	0.14
	G3	31.9253	0.7640	0.22	0.20	144.7263	4.1673	0.30	0.16	261.5043	7.7242	0.16	0.06
	G4	31.9052	0.7635	0.06	0.07	144.7793	4.1682	0.04	0.02	261.2898	7.7193	0.08	0.06
0.99	G1	9.5145	0.3035	-	-	4.6942	0.1805	-	-	1.6748	0.0699	-	-
	G2	9.5319	0.3041	0.18	0.20	4.6985	0.1807	0.09	0.11	1.6768	0.0700	0.12	0.14
	G3	9.5401	0.3044	0.09	0.10	4.7025	0.1809	0.09	0.11	1.6776	0.0701	0.05	0.14

Nu

n	ϕ_f	Grid	Pr = 1		Pr = 100		ε_r (Pr = 1)		ε_r (Pr =100)	
			Re → 1	40	1	40	1	40	1	40
0.4	0.70	G1	2.2018	4.2192	4.2795	6.1551	-	-	-	-
		G2	2.2079	4.2287	4.2884	6.1612	0.28	0.22	0.22	0.10
		G3	2.2128	4.2372	4.2920	6.1657	0.22	0.20	0.20	0.07
		G4	2.2164	4.2324	4.2915	6.1637	0.16	0.11	0.01	0.03
	0.99	G1	1.3196	2.1107	2.1698	2.6542	-	-	-	-
		G2	1.3234	2.1165	2.1741	2.6595	0.28	0.27	0.19	0.20
		G3	1.3256	2.1198	2.1768	2.6606	0.16	0.15	0.12	0.04
1*	0.70	G1	1.9412	3.5714	4.1513	5.2570	-	-	-	-
		G2	1.9456	3.5758	4.1545	5.2710	0.23	0.12	0.08	0.27
		G3	1.9498	3.5824	4.1578	5.2823	0.22	0.18	0.08	0.21
		G4	1.9490	3.5806	4.1527	5.2768	0.04	0.05	0.12	0.10
	0.99	G1	1.1683	1.7812	1.9518	2.4112	-	-	-	-
		G2	1.1679	1.7852	1.9509	2.4126	0.03	0.22	0.05	0.06
		G3	1.1683	1.7892	1.9506	2.4144	0.03	0.22	0.02	0.07
1.8	0.70	G1	1.0918	3.7316	2.7021	4.5014	-	-	-	-
		G2	1.0931	3.7357	2.7048	4.5051	0.12	0.11	0.10	0.08
		G3	1.0941	3.7374	2.7069	4.5061	0.09	0.05	0.07	0.02
		G4	1.0944	3.7462	2.7054	4.5065	0.03	0.07	0.05	0.01
	0.99	G1	0.7162	1.2198	1.4751	1.9945	-	-	-	-
		G2	0.7182	1.2225	1.4789	1.9987	0.27	0.22	0.25	0.21
		G3	0.7195	1.2240	1.4820	2.0012	0.18	0.12	0.20	0.12

- Percent relative change, $\varepsilon_r(X) = 100|(X_i-X_{i+1})/X_i|$ %; where X = C_D or Nu. * For n = 1, Pr = 0.7 instead of Pr = 1

For shear-thinning fluids (n = 0.4) and ϕ_f = 0.70, the grids refinement from G1 to G4, yields a maximum relative differences of about 0.22% and 0.21% at Re = 1 and 40, respectively

in the values of C_D. Further, for ϕ_f = 0.99, the grids refinement from G1 to G3 yields a maximum relative differences of about 0.18% and 0.20% at Re = 1 and 40, respectively. Similarly, for shear-thickening fluid (n = 1.8) at ϕ_f = 0.70, the grid refinement from G1 to G4 yielded the maximum relative differences of 0.17% and 0.14% at Re = 1 and 40, respectively, whereas for ϕ_f = 0.99, grid refinement yielded the maximum relative differences of about 0.12% and 0.14% at Re = 1 and 40, respectively.

The values of average Nusselt number (Nu) has also been compared in Table 4.2 for the power-law fluids. In the shear-thinning region (n = 0.4), when moving from G1 to G4 for ϕ_f = 0.70 and Pr = 1, it was seen that the maximum relative differences in values of Nu are about 0.28% and 0.22% at Re = 1 and 40, respectively. The corresponding maximum differences at Pr = 100 were altered from 0.28 % to 0.22% and 0.22% to 0.10 %, respectively. Under the similar conditions, but for ϕ_f = 0.99 (G1 to G3), the maximum differences in values of Nu were about 0.28% and 0.27% at Re = 1 and 40, respectively and these differences at Pr = 100 were further altered from 0.28 % to 0.19% and 0.27% to 0.20 %, respectively. Likewise, in the shear-thickening region (n = 1.8), at ϕ_f = 0.70 and Pr = 1, the maximum relative differences were about 0.12% and 0.11% at Re = 1 and 40, respectively. At Pr = 100, these differences were changed slightly and altered from 0.12% to 0.10% and 0.11% to 0.08% at Re = 1 and 40, respectively. Similarly, for ϕ_f = 0.99 and Pr = 1, the maximum differences were about 0.27% and 0.22% at Re = 1 and 40, respectively, which again at Pr = 100, altered from 0.27% to 0.25 % and about 0.22% to 0.21%, respectively. The above comparisons suggest that the relative change in the values of C_D and Nu is < 0.5%. Thus, the grid G3 is supposed to be adequately refined to solve the forced convection flow and heat transfer phenomena for Newtonian and power-law fluids and hence was utilized in this study.

4.5.3 Grid independence study for the mixed convection characteristics of Newtonian and non-Newtonian power-law fluids

Here, the grid sensitivity was examined for the mixed convection Newtonian flow for the extreme values of ϕ_f (0.70, 0.99), Re (1, 40), Pr (0.70, 50) at Ri = 2. Table 4.3 compares the value of total drag coefficient (C_D) and average Nusselt number (Nu) obtained for the extreme conditions on the different grid structures. In Table 4.3, it can be seen that the grid refinement from G1 to G4 for ϕ_f = 0.70 and Pr = 0.70 yields the maximum relative differences of about 0.18 % and 0.34% at Re = 1 and Re = 40, respectively. Further, at Pr = 50, the above maximum relative differences were altered from 0.18 % to 0.11% and 0.34% to 0.24 %, respectively.

Similarly, for ϕ_f = 0.70 and Pr = 0.70, the maximum relative differences in the average Nusselt number (Nu) were about 0.21% and 0.19% at Re = 1 and 40, respectively, which were again altered at Pr = 50, from 0.21 % to 0.17% and 0.19% to 0.11 %, respectively. Similarly, for ϕ_f = 0.99 and Pr = 0.70, in the overall grid refinement from G1 to G3, the maximum relative differences in drag coefficient values were found to be 0.30 % and 0.21% at Re = 1 and Re = 40, respectively. Further, at Pr = 50, the above maximum relative differences were altered from 0.30 % to 0.18% and 0.21% to 0.14 %, respectively. Also, at ϕ_f = 0.99 and Pr = 0.70, the grid refinement from G1 to G3 yields the maximum relative differences in average Nusselt number values of about 0.30% and 0.28% at Re = 1 and 40, respectively. These maximum relative differences were further altered from 0.30 % to 0.14% and 0.28% to 0.10 % at Pr=50, respectively.

The grid sensitivity was also examined for the power-law fluids at the extreme values of ϕ_f (0.70, 0.99), Re (1, 40), Pr (1, 50) and fixed values of n = 0.4 and Ri = 2. In Table 4.3, it can be seen that the overall grid refinement from G1 to G4 for ϕ_f = 0.70, yields a maximum relative differences of about 0.43% and 0.24%, in values of drag coefficient, whereas, from G1 to G3 for ϕ_f = 0.99, the maximum relative differences are about 0.49% and 0.27% in the values of drag coefficient at Re = 1 and 40, respectively. Further, the overall grid refinement from G1 to G4 for ϕ_f = 0.70 yields a maximum relative difference of about 0.28% and 0.19% in the values of the average Nusselt number at Re = 1 and 40, respectively. Similarly, the overall grid refinement from G1 to G3 for ϕ_f = 0.99, yields maximum relative differences of about 0.18% and 0.11% in the values of the average Nusselt number at Re = 1 and 40, respectively. Based on the above grids analysis, a relative change in the values of drag coefficient and average Nusselt number (Nu) was found to be < 0.5%. Therefore, the grid G3 was believed to be sufficiently refined in the case of mixed convection to resolve the flow and heat transfer phenomena and hence was utilized in this study.

Table 4.3: Grid independence test for total drag coefficient (C_D) and average Nusselt number (Nu) for the mixed convection flow and thermal features of Newtonian and power-law fluids

n = 1, Ri = 2										
	ϕ_f	Grid	Pr = 0.7		Pr = 50		$\varepsilon_r(X)$			
							Pr = 0.7		Pr = 50	
			Re		Re		Re		Re	
			1	40	1	40	1	40	1	40
C_D	0.70	G1	293.1899	20.4258	319.1044	21.5086	-	-	-	-
		G2	293.7213	20.4954	319.4837	21.5617	0.1812	0.3407	0.1189	0.2469
		G3	293.9354	20.5273	319.6446	21.5914	0.0729	0.1556	0.0504	0.1377
		G4	293.9314	20.5357	319.6561	21.5999	0.0014	0.0409	0.0036	0.0394
	0.99	G1	33.6479	3.5618	39.8972	3.8725	-	-	-	-
		G2	33.7487	3.5692	39.9694	3.8781	0.2996	0.2078	0.1810	0.1446
		G3	33.8036	3.5730	40.0085	3.8827	0.1627	0.1065	0.0978	0.1186
Nu	0.70	G1	0.8883	4.0785	2.7051	10.1608	-	-	-	-
		G2	0.8902	4.0862	2.7096	10.1725	0.2139	0.1888	0.1664	0.1151
		G3	0.8915	4.089	2.7122	10.1772	0.1460	0.0685	0.0960	0.0462
		G4	0.8918	4.0902	2.7128	10.1776	0.0337	0.0293	0.0221	0.0039
	0.99	G1	1.0972	6.178	3.2283	16.1659	-	-	-	-
		G2	1.1005	6.1958	3.2327	16.1822	0.3008	0.2881	0.1363	0.1008
		G3	1.1008	6.2059	3.235	16.1826	0.0273	0.1630	0.0711	0.0025
***n=0.4, Ri=2**										
C_D	0.70	G1	138.6923	7.9856	148.6314	9.2073	-	-	-	-
		G2	139.2941	8.0045	148.9862	9.2182	0.43	0.24	0.24	0.12
		G3	139.5918	8.0199	149.3305	9.2283	0.21	0.19	0.23	0.11
		G4	139.4711	8.0114	149.3705	9.2289	0.09	0.11	0.03	0.01
	0.99	G1	21.7768	2.4048	24.1591	2.7459	-	-	-	-
		G2	21.8846	2.4112	24.2086	2.7498	0.49	0.27	0.20	0.14
		G3	21.9291	2.4153	24.2349	2.7519	0.20	0.17	0.11	0.08
Nu	0.70	G1	0.9921	6.4803	3.2062	22.3992	-	-	-	-
		G2	0.9949	6.4928	3.2098	22.4194	0.28	0.19	0.11	0.09
		G3	0.9972	6.5001	3.2122	22.4355	0.23	0.11	0.07	0.07
		G4	0.9975	6.5015	3.2125	22.4495	0.03	0.02	0.01	0.06
	0.99	G1	1.2496	10.5875	3.9638	26.0542	-	-	-	-
		G2	1.2519	10.5994	3.9687	26.0787	0.18	0.11	0.12	0.09
		G3	1.2528	10.6007	3.9710	26.1003	0.07	0.01	0.06	0.08

- Percent relative change, $\varepsilon_r(X) = 100|(X_i - X_{i+1})/X_i|$ % ; where X = C_D or Nu. * For n = 0.4, Pr = 1 instead of Pr = 0.7

.

.

Chapter 5

FORCED CONVECTION FLOW AND HEAT TRANSFER CHARACTERISTICS OF NEWTONIAN FLUIDS ACROSS PERIODIC ARRAY OF CIRCULAR CYLINDERS

The problem considered herein is the forced convection flow and heat transfer characteristics of Newtonian fluid across a periodic array of circular cylinders in a square configuration. The schematic is shown in Fig. 3.1a. However, for the case of forced convection problem, the buoyancy parameter is Ri = 0 and therefore in Fig. 3.1a, the buoyancy and gravity forces are assumed to be negligible. The problem is well-defined in Chapter-3 and the computational domain for one of the fluid volume fractions (ϕ_f = 0.70) have also been shown in Fig. 3.1b. In this investigation, extensive numerical results have been obtained by systematic variations of Reynolds number as 1, 2, 5, 10, 20 and 40; Prandtl number as 0.7, 1, 5, 10, 20, 50 and 100; and fluid volume fraction as 0.70, 0.75, 0.80, 0.84, 0.86, 0.88, 0.90, 0.92, 0.94, 0.96, 0.98 and 0.99 (Table 2.5). For the present case, the governing Eqs. (3.3-3.7) with the negligible effect of gravity as mentioned in the y-component of momentum equations (Eqs. 3.5-3.6) and boundary conditions (i.e. Eqs. (3.12-3.15)) have been used. Detailed results highlighting the influence of the dimensionless flow governing parameters on the streamlines, pressure and isotherm patterns, individual and total drag coefficients and averaged Nusselt numbers are presented and discussed herein to gain physical insight into the nature of flow and thermal characteristics in this system.

5.1 Validation of numerical solution procedure

Prior to the presentation of new results, the numerical solution procedure used in this work was validated thoroughly against the available literature results. Table 5.1 shows the comparison of the present results of total drag coefficient with the available literature (Singh et al., 1989; Koch and Ladd, 1997; Spelt et al., 2005b) for the extreme values of Reynolds number (Re = 1, 40) and three values of fluid volume fractions (ϕ_f = 0.70, 0.80 and 0.99). The maximum relative deviation (δ_{max}) of present values with literature data has also been included in Table 5.1. An examination of these results shows an excellent agreement (i.e., within ± 2%) with the previous results. Further, the present values of averaged Nusselt number (Nu) have been compared with available literature (Martin et al., 1998; Mangadoddy et al., 2004; Gamrat et al., 2008) in Table

5.1. They also show the excellent agreement of ± 2% with the literature values. The above validations confirm the reliability and accuracy of the numerical solution procedure used herein to obtain the new results. The ensuing sections present the dependence of flow and thermal characteristics on the dimensionless governing parameters**.**

Table 5.1: Comparison of present values of total drag coefficient (C_D) and average Nusselt number (Nu) with available literature

Source	C_D				
	ϕ_f = 0.99		ϕ_f = 0.80	ϕ_f = 0.70	
	Re = 1	Re = 40	Re = 1	Re = 1	Re = 40
Present Results	4.7025	0.1809	52.3347	144.7263	4.1673
Singh et al. (1989)	-	-	51.0700	-	-
Koch and Ladd (1997)	4.5645	0.1815	51.2550	-	-
Spelt et al. (2005b)	4.5884	0.1845	50.9551	142.1367	4.2529
δ_{max} (%)	2.7220	1.9900	2.0631	1.7893	2.0541
	Nu				
	ϕ_f = 0.99			ϕ_f = 0.86	ϕ_f = 0.70
	(Re =5, Pr = 0.7)	(Re = 40, Pr = 0.7)	(Re = 1, Pr = 5)	(Re = 1, Pr = 100)	(Re = 1, Pr = 5)
Present Results	1.3675	1.7892	1.4217	2.8832	2.5295
Martin et al. (1998)	1.3404	1.7933	-	-	-
Mangadoddy et al. (2004)	-	-	1.4015	-	2.6057
Gamrat et al. (2008)	-	-	-	2.8925	-
δ_{max} (%)	1.9817	0.2292	1.4208	0.3226	3.0125

5.2 Fluid flow characteristics

The physical insight into the nature of flow field of the problem under consideration is gained through the streamline and pressure profiles, individual and total drag coefficients and their functional dependence on the dimensionless parameters.

5.2.1 Streamline patterns

The qualitative dependence of the normalized streamline ($\psi^* = (\psi - \psi_{min})/(\psi_{max} - \psi_{min})$) patterns on Reynolds number and fluid volume fraction is shown in Fig.5.1 for the ranges of conditions employed. Qualitatively, the features of the figure reveal a strong dependence of wake size on the fluid volume fraction as well as on the fluid inertia (Re).

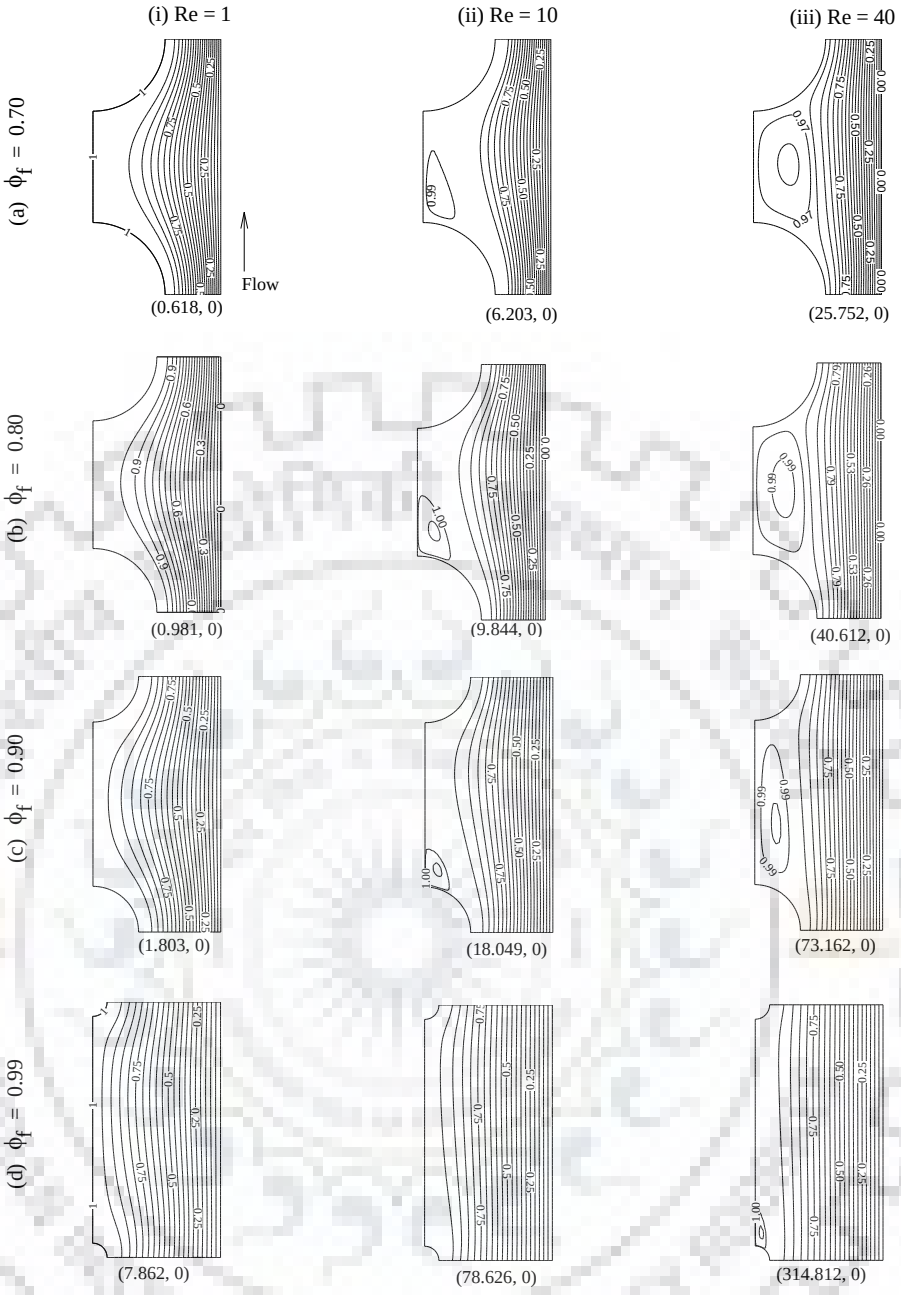

Figure 5.1: Representative variations of normalized streamlines with Reynolds numbers (i) Re = 1 (ii) Re = 10 (iii) Re = 40 and fluid volume fractions (a) ϕ_f = 0.70 (b) ϕ_f = 0.80 (c) ϕ_f = 0.90 (d) ϕ_f = 0.99

The maximum and minimum values of streamlines (ψ_{max} and ψ_{min}) are also shown in Fig. 5.1 for the purposes of comparison. At the lowest value of Reynolds number (Re = 1), flow separation behind the cylinders is not observed over the range of fluid volume fraction $0.70 \leq \phi_f \leq 0.99$. However, the stationary flow (or vacuum) region created in between the cylinders reduces with increasing value of the fluid volume fraction at the lowest Reynolds number. The fluid circulation behind the cylinders is seen to increase with increasing value of the Reynolds number irrespective of the value of the fluid volume fraction. The maximum size of the vortex behind the cylinders

(at ϕ_f = 0.70) gradually decreased with increasing fluid volume fraction over the range of Reynolds number $1 \leq Re \leq 40$. The streamline patterns also show strong interference from the two cylinders at the lower values of ϕ_f which diminishes with increasing value of ϕ_f for all values of Re. The two cylinders act almost like isolated cylinders at the largest value of ϕ_f for all Re. The maximum value of streamline function (ψ_{max}) is observed to be the greatest (ψ_{max} = 314.812) at the greatest values of both Re and ϕ_f (i.e., Re = 40 and ϕ_f = 0.99). The value of streamline function (ψ_{max}) shows a proportional decrease with decreasing values of both Re and ϕ_f. These results clearly indicate that discharges between two consecutive streamlines decrease as the fluid volume fractions and Reynolds number decrease. The streamline pattern is similar to those reported in literature (Edwards et al., 1990; Koch and Ladd, 1997; Spelt et al., 2005b) for square arrays of cylinders and for a single cylinder (Bharti et al., 2006; Soares et al., 2005b), within the ranges covered herein. However, compared to the literature, present flow pattern analysis suggests there is a stronger dependence of flow pattern on the governing parameters than previously thought. The analysis of the pressure profiles in the next section reveals a similar trend.

5.2.2 Pressure profiles

Fig. 5.2 shows the representative variation of the normalized pressure ($p^* = (p-p_{min})/(p_{max}-p_{min})$) with the fluid volume fraction ($0.70 \leq \phi_f \leq 0.99$) and Reynolds number ($1 \leq Re \leq 40$). The dense contours of static pressure seen at the lowest volume fractions (ϕ_f = 0.70), getting sparse with increasing fluid volume fractions. At lower values of fluid volume fraction and Reynolds number, the pressure contours are periodically symmetric in the vicinity of the cylinders. Such feature is clearly due to the no-flow separation under these flow conditions. An increasing value of the Reynolds number or fluid volume fraction shifts the pressure contours away from the cylinders surfaces. The increasing gap between the pressure contours clearly suggests a stronger variation in pressure gradient within the computational domain. For instance, the minimum and maximum values of pressure difference (Δp_{min} = 9.5566 Pa and Δp_{max} = 3270.72 Pa) are observed at Re =1 and ϕ_f = 0.99 and at Re = 40 and ϕ_f = 0.70, respectively.

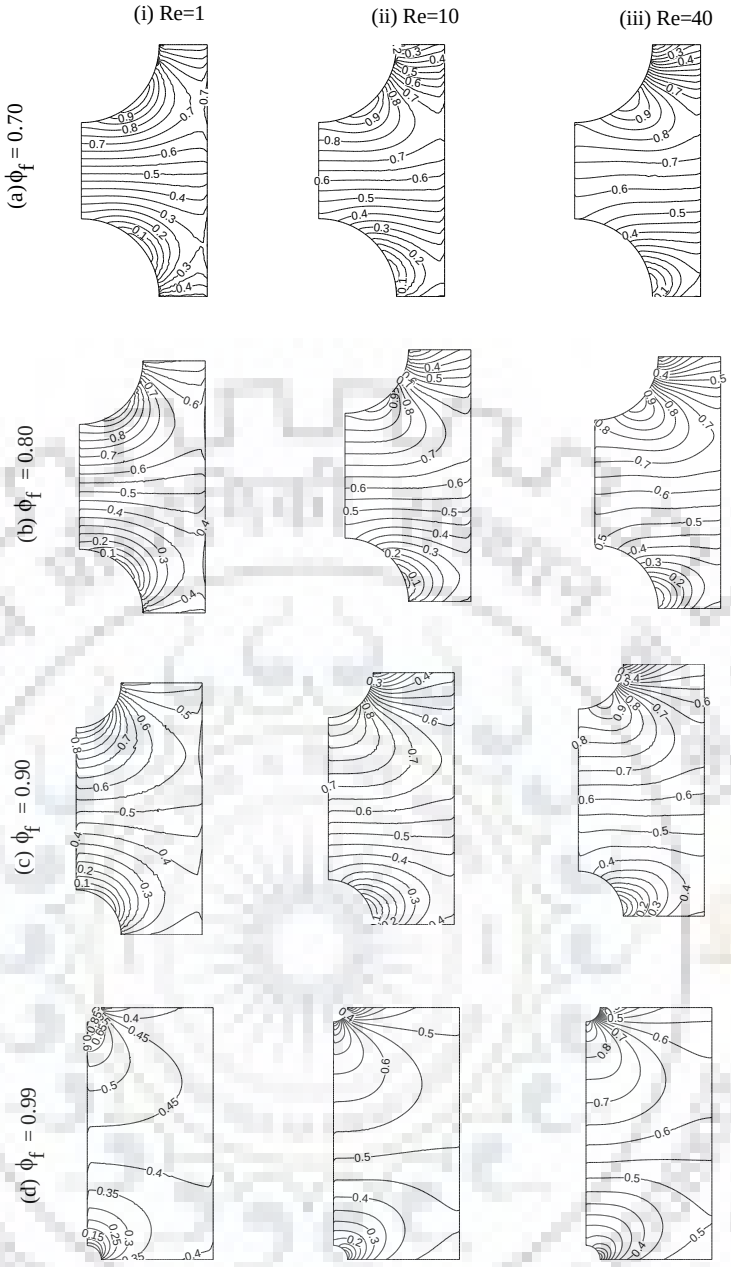

Figure 5.2: Representative variations of normalized static pressure with Reynolds numbers (i) Re = 1 (ii) Re = 10 (iii) Re = 40 and fluid volume fractions (a) ϕ_f = 0.70 (b) ϕ_f = 0.80 (c) ϕ_f = 0.90 (d) ϕ_f = 0.99. (Δp_{min} = 9.5566 Pa at Re = 1 and ϕ_f = 0.99, Δp_{max} = 3278.72 Pa at Re = 40 and ϕ_f = 0.70)

The above noted stronger dependence on flow parameters (ϕ_f, Re) of the local flow patterns (streamline and pressure profiles, for instance), is in turn, expected to alter the global flow and heat transfer characteristics of the problem considered. In the next section, the functional dependence of the global flow characteristics (i.e. individual and total drag coefficients) on Reynolds number and fluid volume fraction have been examined.

5.2.3 Individual and total drag coefficients

Table 5.2 presents the functional dependence of individual and total drag coefficients (C_{DP}, C_{DF} and C_D) on Reynolds number and fluid volume fraction for the range of conditions studied. Irrespective of the fluid volume fraction (ϕ_f), as expected, the pressure drag coefficient (C_{DP}) was seen to decrease with increasing value of the Reynolds number. As observed in Fig. 5.2, the clustering of pressure contours is dense in the whole computational domain at lower values of Reynolds number and fluid volume fraction. The pressure drag coefficient was consequently large under these conditions. It was also seen to decrease with increasing value of the fluid volume fraction for all values of Reynolds number. An increasing value of the fluid volume fraction allows the fluid to occupy most of the region in between the cylinders due to the sufficiently large gap between the cylinders. The minimum interference effects observed in local flow field (Figs. 5.1 and 5.2) at large values of Reynolds number and/or fluid volume fractions, in turn, yield the minimum value of pressure drag coefficient. For instance, as the Reynolds number is increased from 1 to 40, C_{DP} values reduced from 73.0562 to 2.4904 and from 2.3332 to 0.1148 at fluid volume fractions of 0.70 and 0.99, respectively.

Table 5.2 also depicts the dependence of the friction drag coefficient (C_{DF}) on Reynolds number and fluid volume fraction. Qualitatively similar to C_{DP} (Re, ϕ_f), friction drag coefficient also reduced with increasing values of Reynolds number and/or fluid volume fraction. At low values of Re, viscous effects dominate over the inertial effects which result in a large value of friction drag coefficient, under otherwise identical conditions. The viscous effects weaken with increasing Re and thus C_{DF} values are also reduced. On the other hand, the smallest fluid volume fraction provides minimum flow area for the fluid to penetrate through the arrays of cylinders, and therefore the friction effects become stronger under such conditions, as observed through the dense clustering of streamline and pressure contours (Figs.5.1 and 5.2). The minimum value of C_{DF} was observed at the largest values of both Re and ϕ_f . For instance, as Re increased from 1 to 40, C_{DF} values altered from 71.670 to 1.6769 and from 2.3693 to 0.0661 at ϕ_f of 0.70 and 0.99, respectively.

The total drag coefficient ($C_D = C_{DP} + C_{DF}$) was seen to have qualitatively similar dependence as that of C_{DP} and C_{DF} on Reynolds number and fluid volume fraction. The total drag coefficient decreases with increasing values of both Reynolds number and/or fluid volume fraction over the ranges of conditions explored (see Table 5.2). For instance, as the fluid volume fraction increased from 0.70 to 0.99, C_D changed from 144.7263 to 4.7025 and from 4.1673 to 0.1809 at Reynolds numbers of 1 and 40, respectively.

Table 5.2: Variations of individual (C_{DP} and C_{DF}) and total drag (C_D) coefficients with fluid volume fractions and Reynolds number

Re	ϕ_f = 0.70	0.75	0.80	0.84	0.86	0.88	0.90	0.92	0.94	0.96	0.98	0.99
	C_{DP}											
1	71.0562	43.4821	25.5881	16.4529	12.9038	9.9281	7.5446	5.7412	4.8105	3.8755	2.8971	2.3332
2	35.6386	22.0360	13.0071	8.2438	6.5553	5.0672	3.8252	2.9731	2.5163	2.0616	1.5693	1.2822
5	14.9532	9.1417	5.4966	3.5525	2.8293	2.2097	1.6854	1.3250	1.1358	0.9375	0.7261	0.6015
10	7.9041	4.9473	3.0451	2.0541	1.5790	1.2363	0.9459	0.7546	0.6408	0.5334	0.4136	0.3453
20	4.3985	2.7792	1.7264	1.1188	0.8918	0.7009	0.5383	0.4257	0.3665	0.3068	0.2407	0.1995
40	2.4904	1.5468	0.9533	0.6284	0.4990	0.3924	0.3020	0.2398	0.2019	0.1747	0.1380	0.1148
	C_{DF}											
1	73.6701	44.1688	26.4367	17.0605	13.3938	10.3209	7.7389	5.9606	4.9723	3.9821	2.9296	2.3693
2	36.8435	22.0939	13.2774	8.5102	6.7195	5.1871	3.8983	3.0134	2.5195	2.0448	1.5168	1.2428
5	14.3575	8.8812	5.3578	3.4527	2.7270	2.1132	1.5945	1.2392	1.0447	0.8498	0.6407	0.5298
10	7.1772	4.4665	2.7085	1.7745	1.3787	1.0685	0.8067	0.6272	0.5297	0.4329	0.3277	0.2726
20	3.5236	2.1309	1.3348	0.8569	0.6758	0.5251	0.3972	0.3094	0.2615	0.2148	0.1652	0.1365
40	1.6769	1.0309	0.6241	0.4045	0.3182	0.2472	0.1874	0.1463	0.1244	0.1025	0.0792	0.0661
	C_D											
1	144.7263	87.6509	52.0248	33.5134	26.2976	20.2490	15.2835	11.7018	9.7828	7.8576	5.8267	4.7025
2	72.4821	44.1299	26.2845	16.7540	13.2748	10.2543	7.7235	5.9865	5.0358	4.1064	3.0861	2.5250
5	29.3107	18.0229	10.8544	7.0052	5.5563	4.3229	3.2799	2.5642	2.1805	1.7873	1.3668	1.1313
10	15.0813	9.4138	5.7536	3.8286	2.9577	2.3048	1.7526	1.3818	1.1705	0.9663	0.7413	0.6179
20	7.9221	4.9101	3.0612	1.9757	1.5676	1.2260	0.9355	0.7351	0.6280	0.5216	0.4059	0.3360
40	4.1673	2.5777	1.5774	1.0329	0.8172	0.6396	0.4894	0.3861	0.3263	0.2772	0.2172	0.1809
	$C_{DR}=C_{DP}/C_{DF}$											
1	1.0193	0.9845	0.9679	0.9644	0.9634	0.9619	0.9749	0.9632	0.9675	0.9732	0.9889	0.9899
2	1.0222	0.9974	0.9796	0.9687	0.9756	0.9769	0.9812	0.9866	0.9987	1.0082	1.0346	1.0317
5	1.0415	1.0293	1.0259	1.0289	1.0375	1.0457	1.0570	1.0692	1.0872	1.1032	1.1333	1.1353
10	1.1013	1.1076	1.1243	1.1576	1.1453	1.1570	1.1726	1.2031	1.2097	1.2322	1.2621	1.2667
20	1.2483	1.3042	1.2934	1.3056	1.3196	1.3348	1.3552	1.3759	1.4015	1.4283	1.4570	1.4615
40	1.4851	1.5004	1.5275	1.5535	1.5682	1.5874	1.6115	1.6391	1.6230	1.7044	1.7424	1.7368

The role of fluid volume fraction on the global flow characteristics was examined by normalizing the drag coefficients as $X^N = X(Re, \phi_f)/X(Re, \phi_{f,max})$, where X represents the individual and total drag coefficients (C_{DP}, C_{DF} and C_D), under otherwise identical conditions. In the present work, $\phi_{f,max} = 0.99$. Fig. 5.3 presents the dependence of normalized drag coefficients (C_{DP}^N, C_{DF}^N and C_D^N) on fluid volume fraction and Reynolds number. The normalized values are always seen to be greater than one over the ranges of conditions, which indicates a significant role of the fluid volume fraction on the drag characteristics. This figure clearly shows that the normalized drag values increase when the cylinders are brought closer together. For a fixed value of Re, the normalized drag values are seen to decrease monotonically with increasing value of fluid volume fraction. For a fixed value of ϕ_f, the normalized drag values decrease as Re

increases. However, this dependence is more significant at lower Re which diminishes at higher Re. Overall, over the ranges of conditions examined, the drag coefficients were observed to vary by as much as 30-fold.

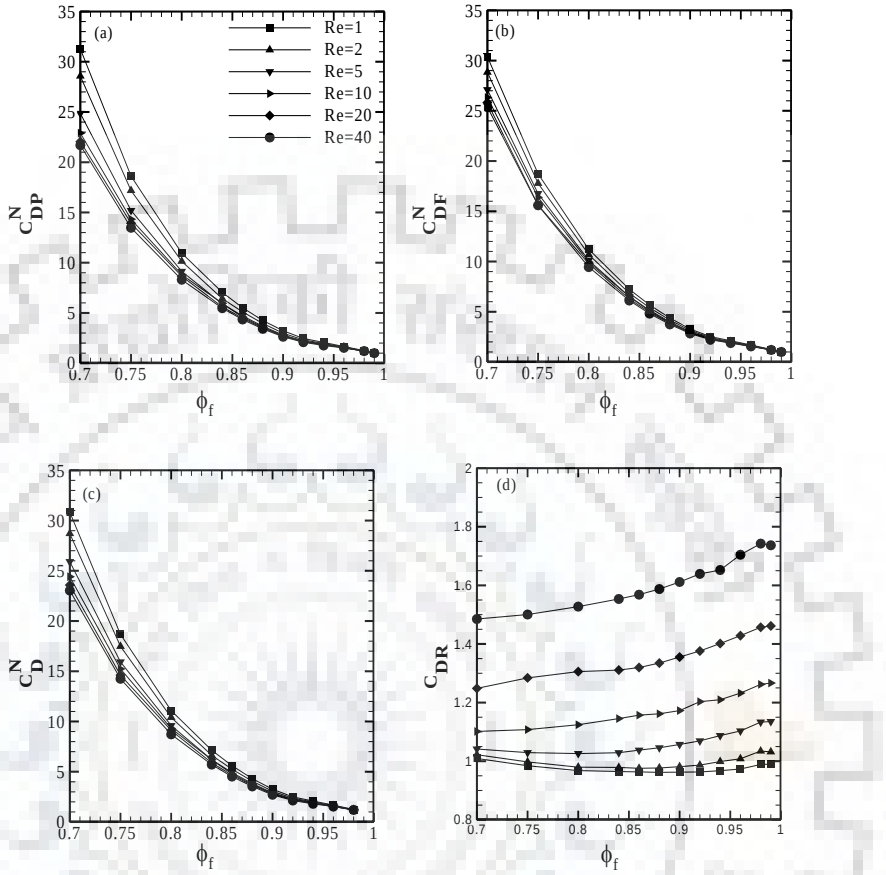

Figure 5.3: Dependence of normalized drag coefficients on fluid volume fractions (ϕ_f) and Reynolds number (Re) (a) pressure drag coefficient (b) friction drag coefficient (c) total drag coefficient and (d) drag ratio ($C_{DR} = C_{DP}/C_{DF}$)

To understand the relative contribution of pressure force over the viscous force, the drag ratio (C_{DR}) was examined, defined as $C_{DR} = C_{DP}/C_{DF}$, under otherwise identical conditions. Fig. 5.3(d) shows the complex dependence of drag ratio on both Reynolds number and fluid volume fraction. A $C_{DR} > 1$ suggests the dominance of pressure force over viscous force. A C_{DR} value increases with increasing value of Reynolds number ($Re \geq 5$) for all values of fluid volume fractions. However, for the lower values of Reynolds number ($Re < 5$), C_{DR} values show complex variation with both Reynolds number and fluid volume fraction. Such complexities are inherent due to varying influence of periodic boundary conditions on the flow field. For instance, at low Re, the fluid is not stratified in the whole computational domain due to small (or negligible) pressure in the vicinity of cylinders (see Figs. 5.2 and 5.3) and correspondingly, the friction drag dominates over the pressure drag under these conditions. However, more resistance to flow is

observed due to the pressure than due to friction at large values of Re. The maximum C_{DR} obtained is equal to 1.7368 at Re = 40 for ϕ_f = 0.99.

Additionally, statistical analysis of the present numerical values of individual and total drag coefficients has been carried out to develop an empirical relation which gives the functional dependence of drag coefficients (C_{DP}, C_{DF}, C_D) on Reynolds number and fluid volume fraction. This functional dependence is expressed by Eq. (5.1) as

$$X = \alpha Re^{\beta} \qquad \text{where} \qquad \alpha = a\phi_f^2 - b\phi_f + c \quad \text{and} \quad \beta = d\phi_f^2 - e\phi_f - g \tag{5.1}$$

Here, X is C_{DP}, C_{DF} or C_D. The best fit correlation coefficients of Eq. (5.1) along with their statistical analysis (based on 72 data points for each C_{DP}, C_{DF} and C_D) are shown in Table 5.3. The present numerical values show an excellent correspondence with the values predicted (using Eq. 5.1) in Fig. 5.4. For instance, this correlation for C_D has average and maximum deviations of ~1.5 % and ~3%, respectively. The predictions of Eq. 5.1 was compared with the different cell models available in the literature (Bruschke and Advani, 1993; Vijaysri et al., 1999 and Tripathi and Chhabra, 1992, 1996). For instance, Bruschke and Advani (1993) presented a numerical solution for the creeping flow of power law fluids over an array of cylinders, modeled via the use of zero vorticity cell models. They presented their results in terms of mobility factor M' which can be shown to be equal to $(\phi_{max}/\phi)^{1+n}/C_D$. For Newtonian fluids, their results are in good agreement with present results e.g. at ϕ_f = 0.70, Re = 1; their C_D = 194.10 against the present value of 144.7263. Similarly, Tripathi and Chhabra (1992, 1996) applied the well-known concentric cylinders free surface cell models (Happel, 1959) to approximate the porosity among the cylinder. The drag on the cylinder was reported to decrease below the corresponding value of Newtonian fluids. In this investigation also, an excellent agreement was found for the drag values i.e. C_D = 136.19 at ϕ_f = 0.70, Re = 1 while the corresponding present value of C_D = 144.7263. Further, Vijaysri et al. (1999) used zero vorticity cell models of Kuwabara (1959) to discuss fluid dynamic parameters in terms of drag coefficients. Again, in the case of Newtonian fluids an excellent correspondence was found (C_D = 193.99 against the present value of C_D = 144.7263). Among all the above comparisons, the maximum discrepancies were of the order of 6-25%.

The preceding discussion has shown the pronounced effect of Reynolds number and fluid volume fraction on the qualitative and quantitative nature of periodic flow across a bank of tubes. By analogy, these governing parameters would be expected to strongly influence heat transfer characteristics.

Table 5.3: Correlation coefficients appearing in the functional dependence of drag coefficients (δ: relative r.m.s deviations from the numerical data; Total # of data points: 72 for each of the C_{DP}, C_{DF} and C_D)

Correlation Constants	C_{DP}	C_{DF}	C_D
a	980.23	990.58	1965.2
b	1872	1902.6	3763.3
c	896.82	916.94	1808
d	0.6999	1.0348	0.8676
e	0.8585	1.6045	1.2201
g	0.6552	0.3962	0.5293
R^2	0.9988	0.9996	0.9998
δ_{max} (%)	4.9636	4.6498	3.0548
δ_{avg} (%)	2.4851	2.3989	1.5359

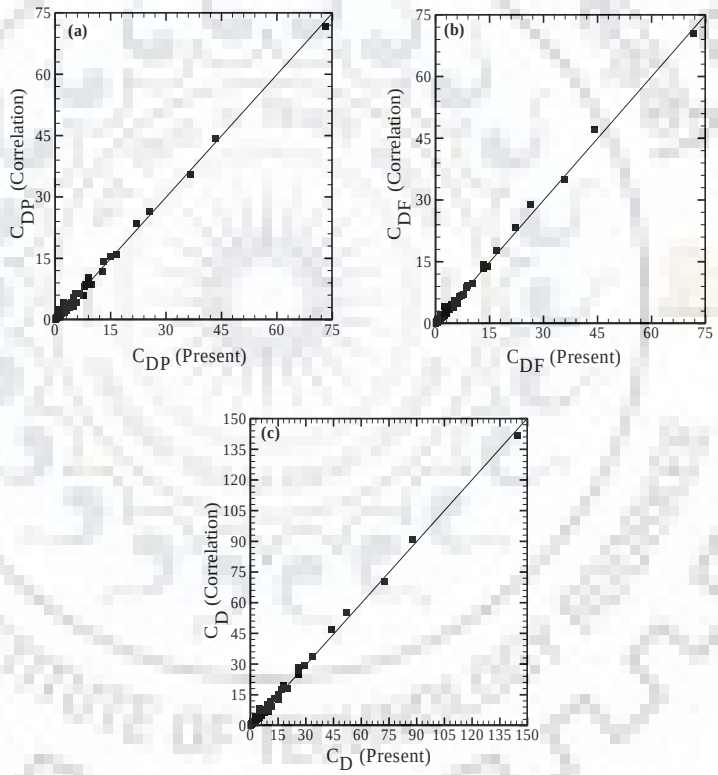

Figure 5.4: Best fit comparisons of present numerical versus predicted values of (a) pressure drag coefficient (b) friction drag coefficient and (c) total drag coefficient

5.3 Heat transfer characteristics

The dependence of forced convection heat transfer characteristics (i.e., isotherm patterns and average Nusselt number) on Reynolds number ($1 \leq Re \leq 40$), Prandtl number ($0.7 \leq Pr \leq 100$) and fluid volume fraction ($0.70 \leq \phi_f \leq 0.99$) is presented and discussed in the ensuing section.

An empirical relation which gives the functional dependence of average Nusselt number (Nu) on Re, Pr and ϕ_f is also obtained.

5.3.1 Isotherm patterns

Figs. 5.5 and 5.6 show the variation of isotherms with Reynolds number and fluid volume fraction for two values of Prandtl number (Pr=1 and 100), respectively. Specifically, Figs. 5.5 and 5.6 plot normalized values of temperature ($T^* = (T-T_{min})/(T_{max}-T_{min})$), which allows easier comparison of the different plots. The maximum temperatures are seen on the surfaces of the cylinders, which are isothermally heated. As expected, the isotherm patterns show a strong dependence on the governing parameters (Re, Pr and ϕ_f) over the ranges examined. For a fixed value of fluid volume fraction, the crowding of isotherms in the flow direction (bottom to top) increases with increasing value of Reynolds number, irrespective of the value of Prandtl number. At high Reynolds number, isotherms were seen to cluster in the vicinity of cylinders as well as in the core region of the computational domain. An increasing value of fluid volume fraction also shows similar influences on the heat transfer patterns, i.e., clustering of isotherms was more pronounced when cylinders were brought closer together. At large values of ϕ_f , the downstream cylinder displays very dense clustering in comparison of the upstream cylinder. This suggests that, at this spacing, cylinders are largely independent and that much of the heat transfer is from the forward face of the cylinder. It can also be observed that the symmetric isotherm patterns for the low Reynolds number flows suggest the dominance of conduction over convection; however, at high Reynolds numbers, isotherms in open flow areas are aligned parallel to the y-axis and more complicated patterns appear in the wake. Also, much sharper temperature gradients appear closer to the cylinders as the Reynolds number increases. Thus, the resulting temperature gradients, and hence the heat transfer rate increases with increasing Re and/or Pr. The influence of the volume fraction on isotherm patterns is, however, seen to be more pronounced at high Reynolds and/or Prandtl numbers. It can also be seen in Figs. 5.5 and 5.6, as the Reynolds number increases, the clustering of the isotherms became dense and confined in the vicinity of the cylinders. The density of isotherm lines indicates the magnitude of the thermal gradients; that is, clustered lines indicate a steep gradient, while sparse lines indicate a weak gradient. Thermal gradients, in turn, indicate the magnitude of heat transfer rates. The above qualitative feature is similar to Martin et al. (1998) for the square array of cylinder at Pr = 0.7. These patterns are also consistent with the single cylinder (Bharti et al., 2007b, 2008) under the limiting conditions. This complex dependence of local heat transfer (Figs. 5.5 and 5.6) on the pertinent dimensionless parameters (Re, Pr and ϕ_f) is expected to alter the global heat transfer characteristics. The

ensuing section explores the functional dependence of average Nusselt number on dimensionless flow governing parameters.

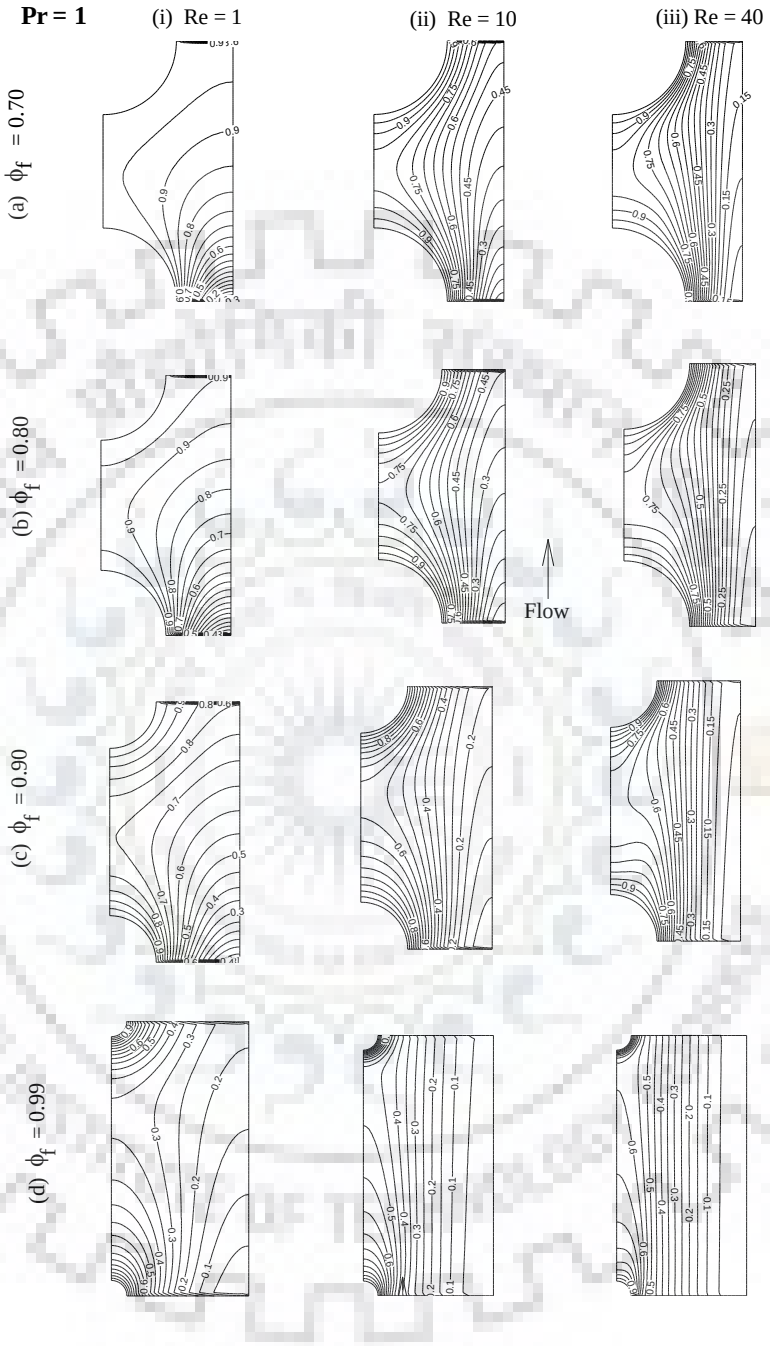

Figure 5.5: Representative variations of normalized isotherms at Pr = 1 with Reynolds numbers (i) Re = 1 (ii) Re = 10 (iii) Re = 40 and fluid volume fractions (a) ϕ_f = 0.70 (b) ϕ_f = 0.80 (c) ϕ_f = 0.90 (d) ϕ_f = 0.99

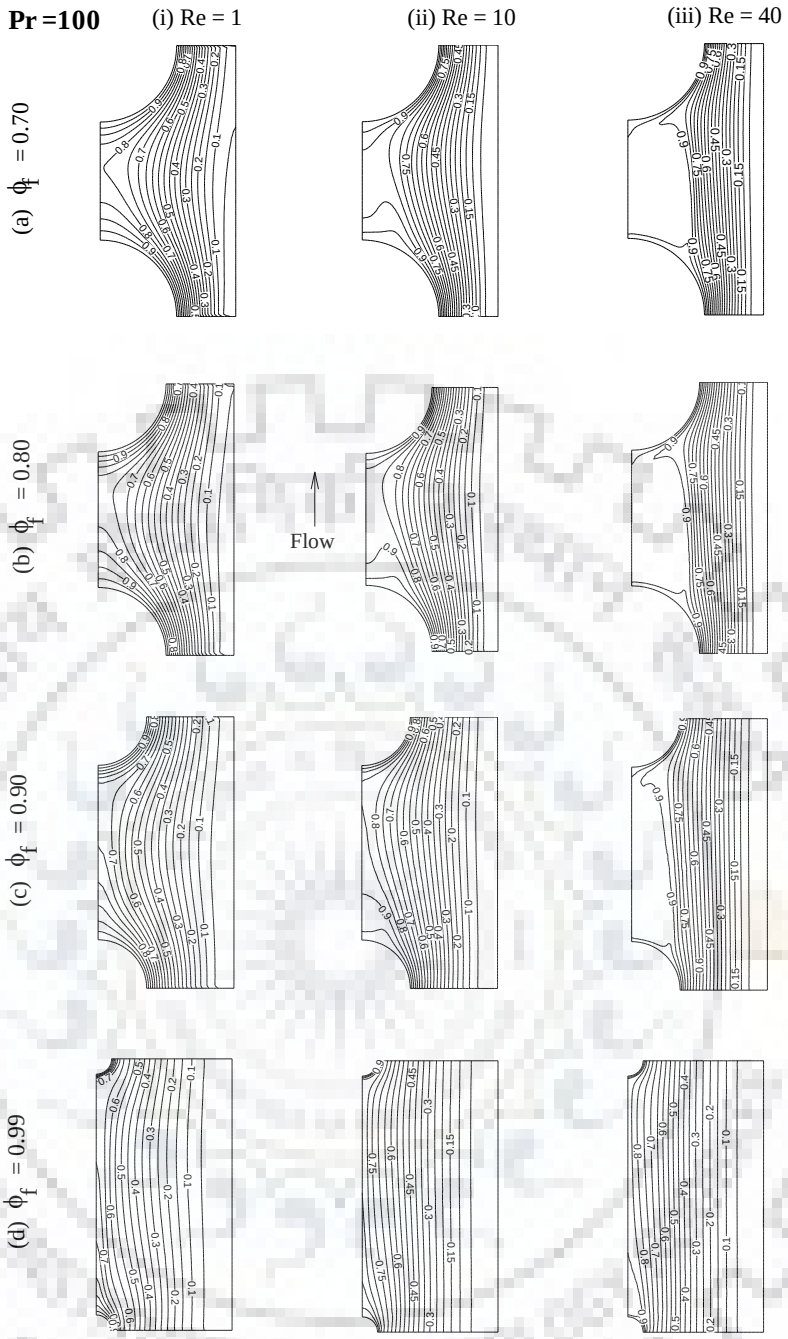

Figure 5.6: Representative variations of normalized isotherms at Pr = 100 with Reynolds numbers (i) Re = 1 (ii) Re = 10 (iii) Re = 40 and fluid volume fractions (a) ϕ_f = 0.70 (b) ϕ_f = 0.80 (c) ϕ_f = 0.90 (d) ϕ_f = 0.99

5.3.2 Average Nusselt number

Table 5.4 presents the functional dependence of average Nusselt number (Nu) on the governing dimensionless parameter (Re, Pr, ϕ_f). As expected, for a fixed value of fluid volume fraction, the average Nusselt number increased with increasing value of Reynolds number or Prandtl

number. However, an opposite dependence of Nu on ϕ_f was observed; i.e., Nu decreases with increasing ϕ_f, irrespective of the values of Re and Pr. In other words, heat transfer improved when the cylinders were brought closer together. In fact, the effect of con Nu is more pronounced than either of Re or Pr. The maximum value of the average Nusselt number was found to be about 5.2823 for ϕ_f = 0.70 at Re = 40 and Pr = 100, whereas the minimum value was about 1.1683 for ϕ_f = 0.99 at Re = 1 and Pr = 0.7.

Table 5.4: Variation of surface average Nusselt number (Nu) with fluid volume fractions (ϕ_f), Reynolds (Re) and Prandtl (Pr) numbers

Pr	Re	ϕ_f											
		0.70	0.75	0.80	0.84	0.86	0.88	0.90	0.92	0.94	0.96	0.98	0.99
0.7	1	1.9498	1.8726	1.7264	1.6513	1.6065	1.5562	1.5295	1.4596	1.3926	1.2542	1.2272	1.1683
	2	2.2667	1.9998	1.8965	1.8291	1.7319	1.6623	1.5909	1.4836	1.4124	1.3927	1.3598	1.2998
	5	2.5839	2.3614	2.2823	2.1839	2.0838	1.9524	1.8820	1.8178	1.7367	1.6331	1.4740	1.3675
	10	2.7749	2.5542	2.4594	2.3096	2.2584	2.1964	2.1205	2.0363	1.9171	1.7812	1.6010	1.5878
	20	3.0022	2.9266	2.7817	2.6241	2.5326	2.4302	2.3191	2.2032	2.0612	1.9073	1.7185	1.6992
	40	3.5824	3.3594	3.0996	2.8722	2.7534	2.6250	2.4904	2.3512	2.1912	2.0222	1.8738	1.7892
1	1	2.1025	1.9249	1.8572	1.7764	1.6768	1.6635	1.6131	1.5537	1.4656	1.4008	1.3610	1.2346
	2	2.3845	2.1856	1.9183	1.8852	1.8126	1.7558	1.6982	1.6241	1.5490	1.4858	1.4560	1.3637
	5	2.6714	2.4398	2.3477	2.2812	2.2129	2.1567	2.0048	1.9326	1.8384	1.7152	1.5423	1.4331
	10	2.8668	2.6735	2.5987	2.4868	2.4138	2.3282	2.2316	2.1222	1.9972	1.8511	1.6650	1.6520
	20	3.3300	3.1680	2.9609	2.7535	2.6457	2.5283	2.4049	2.2728	2.1295	1.9703	1.7795	1.7607
	40	3.8215	3.5363	3.2362	2.9778	2.8490	2.7107	2.5675	2.4142	2.2558	2.0830	1.9028	1.8404
5	1	2.5295	2.3372	2.2162	2.1118	2.0940	2.0579	2.0048	1.9320	1.8361	1.7085	1.5333	1.4217
	2	2.7727	2.6829	2.6106	2.4953	2.4285	2.3348	2.2357	2.1237	1.9960	1.8481	1.6612	1.5476
	5	3.5332	3.3109	3.0433	2.8092	2.6883	2.5612	2.4322	2.2951	2.1494	1.9954	1.8098	1.7047
	10	3.8257	3.5797	3.2378	2.9570	2.8199	2.6808	2.5409	2.3977	2.2487	2.0901	1.9118	1.8067
	20	4.1817	3.7879	3.4287	3.1156	2.9673	2.8184	2.6691	2.5160	2.3574	2.1883	2.0022	1.8974
	40	4.4702	4.0475	3.6459	3.3356	3.1825	3.0218	2.8577	2.6840	2.5040	2.3148	2.1043	1.9878
10	1	2.8626	2.6827	2.6100	2.4963	2.4225	2.3342	2.2345	2.1220	1.9935	1.8463	1.6510	1.5440
	2	3.3595	3.1912	2.9640	2.7499	2.6394	2.5180	2.3920	2.2586	2.1159	1.9608	1.7720	1.6657
	5	3.9332	3.5822	3.2250	2.9440	2.8052	2.6650	2.5269	2.3827	2.2354	2.0812	1.9095	1.8122
	10	4.1530	3.7382	3.3435	3.0490	2.9016	2.7563	2.6121	2.4663	2.3178	2.1634	1.9960	1.9032
	20	4.3382	3.9128	3.5131	3.2063	3.0563	2.9020	2.7482	2.5903	2.4286	2.2579	2.0786	1.9848
	40	4.6298	4.1817	3.7648	3.4474	3.2935	3.1284	2.9607	2.7792	2.5926	2.3958	2.1840	2.0730
20	1	3.3597	3.1914	2.9634	2.7523	2.6395	2.5181	2.3915	2.2583	2.1154	1.9610	1.7658	1.6671
	2	3.8308	3.4143	3.1794	2.9072	2.7754	2.6374	2.4988	2.3579	2.2123	2.0590	1.8861	1.7826
	5	4.1545	3.7302	3.3286	3.0242	2.8787	2.7335	2.5911	2.4490	2.3053	2.1600	1.9993	1.9160
	10	4.2770	3.8287	3.4148	3.1082	2.9587	2.8106	2.6654	2.5201	2.3754	2.2277	2.0747	1.9944
	20	4.4495	4.0086	3.5977	3.2846	3.1342	2.9751	2.8185	2.6548	2.4942	2.3207	2.1536	2.0699
	40	4.7707	4.3012	3.8712	3.5469	3.3962	3.2248	3.0554	2.8658	2.6712	2.4670	2.2562	2.1550
50	1	3.9370	3.5856	3.2269	2.9460	2.8078	2.6677	2.5284	2.3883	2.2440	2.0958	1.9299	1.8295
	2	4.0574	3.7320	3.3265	3.0230	2.8812	2.7375	2.5967	2.4578	2.3190	2.1765	2.0224	1.9336
	5	4.2964	3.8275	3.4052	3.0878	2.9428	2.7977	2.6579	2.5210	2.3880	2.2518	2.1139	2.0492
	10	4.3750	3.9021	3.4782	3.1686	3.0194	2.8687	2.7245	2.5820	2.4452	2.3061	2.1738	2.1172
	20	4.6867	4.2228	3.6982	3.3790	3.2336	3.0644	2.9047	2.7420	2.5771	2.3969	2.2506	2.1926
	40	5.1021	4.4846	4.0178	3.6980	3.5521	3.3650	3.1921	2.9819	2.7780	2.5534	2.3520	2.2710
100	1	4.1578	3.7324	3.3287	3.0272	2.8832	2.7404	2.6014	2.4645	2.3284	2.1890	2.0388	1.9506
	2	4.2733	3.8095	3.3842	3.0766	2.9345	2.7925	2.6556	2.5220	2.3913	2.2595	2.1195	2.0479
	5	4.3582	3.8710	3.4452	3.1267	2.9839	2.8399	2.7050	2.5719	2.4462	2.3212	2.1999	2.1506
	10	4.6912	4.1535	3.5262	3.2051	3.0684	2.9140	2.7721	2.6299	2.4997	2.3649	2.2527	2.2157
	20	4.9966	4.4325	3.7848	3.4583	3.3268	3.1409	2.9776	2.7978	2.6408	2.4695	2.3324	2.2914
	40	5.2823	4.6884	4.1682	3.8283	3.7270	3.5160	3.3557	3.0934	2.8840	2.6428	2.4318	2.4144

Further efforts were made to present the functional dependence of average Nusselt number on Re, Pr, ϕ_f as a closure relationship. The statistical analysis (based on 504 data points) of the present numerical values (Table 5.4) yielded the following correlation;

$$Nu = \alpha Re^{b} Pr^{c} \quad \text{where} \quad \alpha = [a + d\phi_f^{e}(RePr)^{g}] \tag{5.2}$$

The best-fit correlation coefficients (a, b, c, d, e and g) appearing in Eq. (5.2) along with their minimum, maximum and average deviations are summarized in Table 5.5. An excellent agreement can be seen in Fig. 5.7(a) between the present numerical data and the predictions of Eq. (5.2). The average and maximum deviations are within 2% and 5% respectively for 97% of the data points. Only 3% of data points have deviations >5% with a maximum deviation of 11.36%. Notwithstanding numerous analytical studies based on periodic arrays are available in the literature, out of these studies, no one is the same, which could be compared directly with the present study, for instance, Sangani and Acrivos (1982) relate to low Reynolds number and Peclet number, while in many other cases, different geometrical configuration and different parameters are employed (e.g. Launder and Massey, 1978; Wilson and Bassiouny, 2000, etc.). However, it is possible to contrast the present predictions with the results of Chen and Wung (1989); Martin et al. (1998); Gamrat et al. (2008); Mangadoddy et al. (2004); Mandhani et al. (2002), etc. For instance, Chen and Wung (1989) have presented the mean values of Nusselt number for one value of fluid volume fraction, namely, ϕ_f = 0.8; Re = 40, 120, 400 and 800 and for Pr = 0.1, 1 and 10. They correlated their results using the following empirical expression

$$\text{For in-line arrays:} \quad Nu = 0.8Re^{0.4}Pr^{0.37} \tag{5.3}$$

Table 5.5: Correlation coefficients appearing in the functional dependence of Nusselt number and j_H factor (δ: relative r.m.s deviations from the numerical data; Total # of data points: 504 for each of the Nu and j_H)

Correlation Constants	a	b	c	d	e	g	R^2	δ_{max} (%)	δ_{avg} (%)
Nu	17.1857	0.1608	0.1599	-15.7552	0.1669	0.0061	0.9665	11.3671	5.6958
j_H	1.279	0.6703	1.2718	-0.2178	0.0304	-2.1283	0.9937	5.3272	2.7014

The above correlation (Eq. 5.3) is similar to the present correlation (Eq.5.2) for the average Nusselt number. Using the above correlation (Eq. 5.3), a value of Nu = 3.4987 at ϕ_f = 0.8, Pr = 1 and Re = 40 was obtained against the present value of Nu = 3.2362 under the identical conditions. An inspection of these results shows that while the present result is slightly lower than the predictions of Eq. (5.3), generally by 7.5%, still, a good correspondence is seen to exist with the predictions. Similarly, a good correspondence was seen between the present and power-law correlation of Martin et al. (1998) for the average Nusselt number which compares well for Prandtl number.

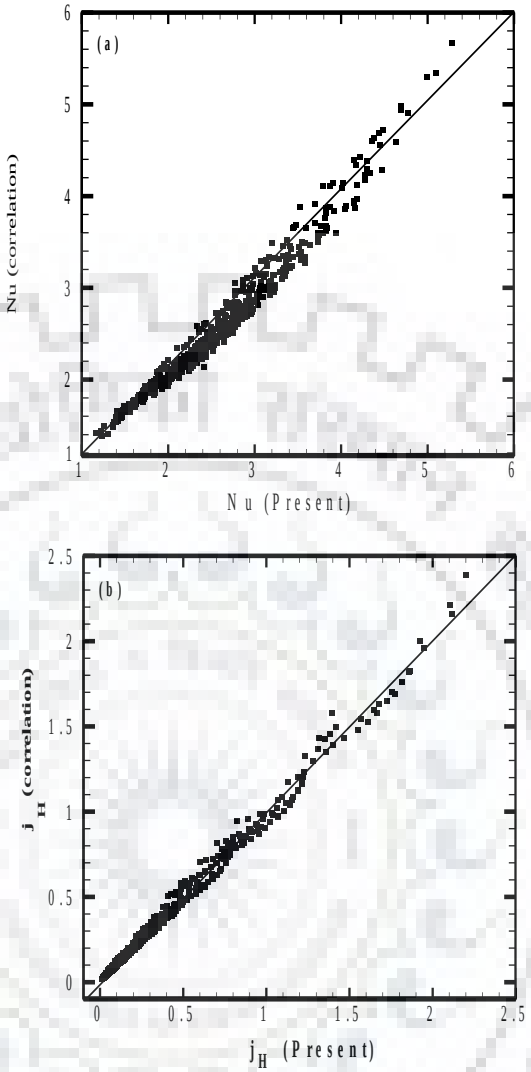

Figure 5.7: The best fit analysis of present numerical values versus predicted values of (a) average Nusselt number and (b) the Colburn j_H factor

(Pr = 0.70) and fluid volume fraction ($0.80 \leq \phi_f \leq 0.99$) with maximum discrepancies within 2% (Table 5.1). Next, correspondence was found with results of Gamrat et al. (2008) as shown in Table 5.1 at ϕ_f = 0.86, Re = 1, Pr = 100. As compared to Nu = 2.8925 of Gamrat et al. (2008), the present value was found to be Nu = 2.8832 which shows an excellent agreement with a deviation of only 0.32 %. However, not listed in Table 5.1, but an agreement at higher fluid volume fraction of ϕ_f = 0.98 was also seen with the results of Gamrat et al. (2008), e.g. at ϕ_f = 0.98, Pr = 100 and Re = 40, there is a deviation of only 5.45 % in the present (Nu = 2.4318) and their result (Nu = 2.5722). Analogously, the results of Mangadoddy et al. (2004) as shown in Table 5.1 show an excellent agreement at Pr = 5 and Re = 1 with two extremes of fluid volume

fractions. These values of Nu show a deviations of 3.01% and 1.42% for ϕ_f = 0.70 and 0.99, respectively. After above comparisons, an endeavor was further made to compare with the experimental results of literature. However, there is no direct experimental study on heat transfer for periodic flow across tube bank is available, albeit, very few experimental studies are available.

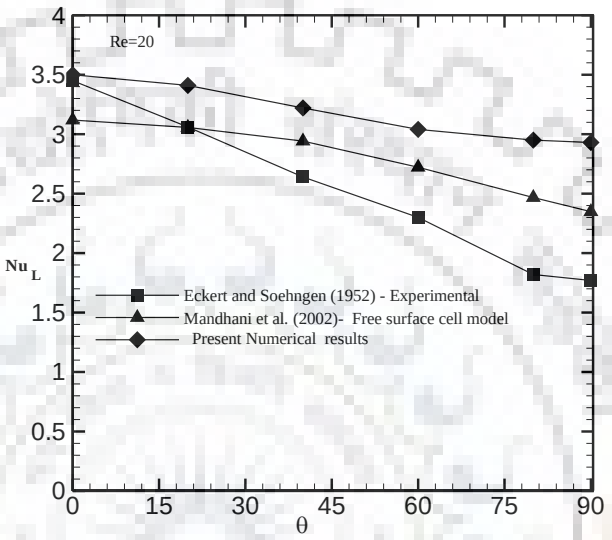

Figure 5.8: Comparison of local Nusselt number with present, free surface cell model of Mandhani et al. (2002) and experimental results of Eckert and Soehngen (1952) at ϕ_f = 0.99, 0.999 and 1, respectively

For instance, Eckert and Soehngen (1952) reported the values of the local Nusselt number for the flow of air over a heated cylinder. A comparison between the present values, free surface cell model of Mandhani et al. (2002) and experimental study of Eckert and Soehngen (1952) is shown in Fig. 5.8, where a good agreement can be seen to exist. The discrepancy seen in Fig. 5.8 can be attributed in part at least to the finite values of L/D ratio and the wall effects encountered in such experimental studies and to the fact that the predictions relate to ϕ_f = 0.99, ϕ_f = 0.999 and ϕ_f = 1, respectively.

Furthermore, to delineate the role of Reynolds and Prandtl numbers, the average Nusselt number is generally presented in terms of the Colburn heat transfer factor (or j_H factor) defined as

$$j_H = \frac{Nu}{RePr^{1/3}} \tag{5.4}$$

The j_H factors have a feature to accord the results of various Reynolds number and Prandtl number on a single curve. The variation of the Colburn factor with fluid volume fraction, Reynolds number and Prandtl number is shown in Fig. 5.9. This Figure shows that the Colburn factor has a linear dependence on the flow governing parameters. The j_H factor decreases with increasing Re and/or Pr for a given fluid volume fraction. A proportional decrease in j_H factor was also seen with increasing value of ϕ_f , irrespective of the values of Re and Pr.

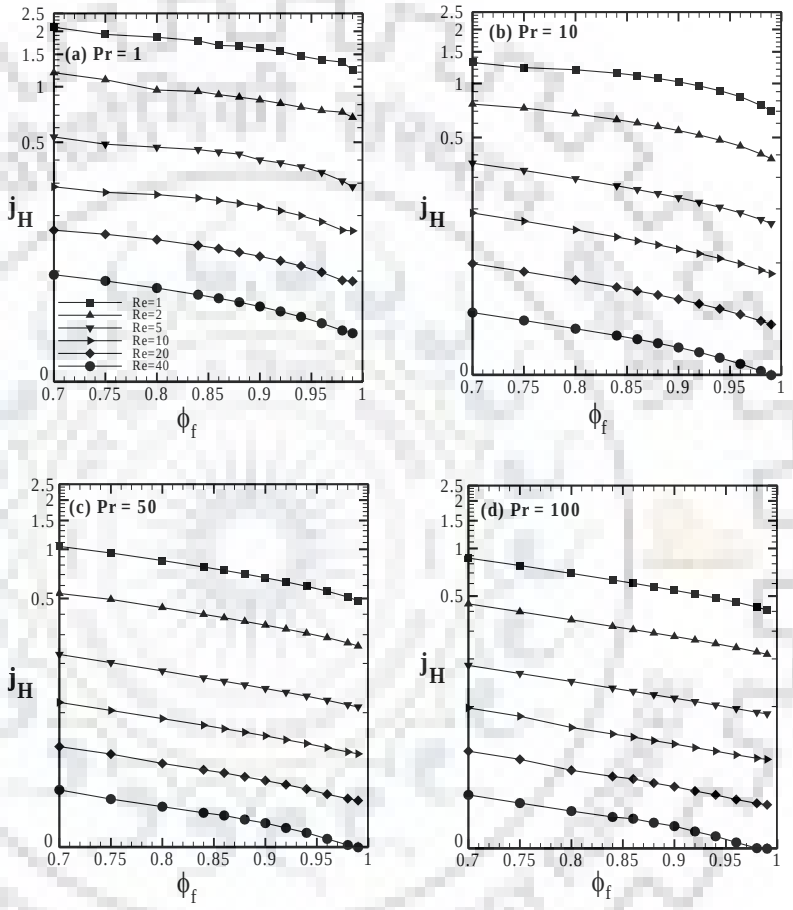

Figure 5.9: The Colburn j_H factor variation with Reynolds number and fluid volume fraction for (a) Pr = 1 (b) Pr = 10 (c) Pr = 50 and (d) Pr = 100

The j_H factor is a maximum for the smallest values of ϕ_f , Re and Pr examined and a minimum for the largest values examined. A statistical analysis of the present data yielded the following correlation

$$j_H = \alpha(\phi Re)^g \qquad \text{where } \alpha = [a\phi_f^b Re^c Pr^d + e] \tag{5.5}$$

The values of empirically fitted constants (a, b, c, d, e and g) appearing in Eq. (5.5) along with the minimum, maximum and average deviations are also summarized in Table 5.5. An excellent

agreement can be seen in Fig. 5.7(b) between the present numerical data and the predictions of Eq. (5.5). The average and maximum deviations are within 2% and 5% respectively for the entire range of data points. The predictions of above correlation were also compared with the literature (Mandhani et al., 2002), again an excellent correspondence was seen. Fig. 5.10 shows a comparison between the predictions of Eq. (5.5) and that of free surface cell model of Mandhani et al. (2002) at Pr = 0.7 and ϕ_f = 0.70-0.99. It can be clearly seen that the agreement is consistent with maximum discrepancies of 3-10%.

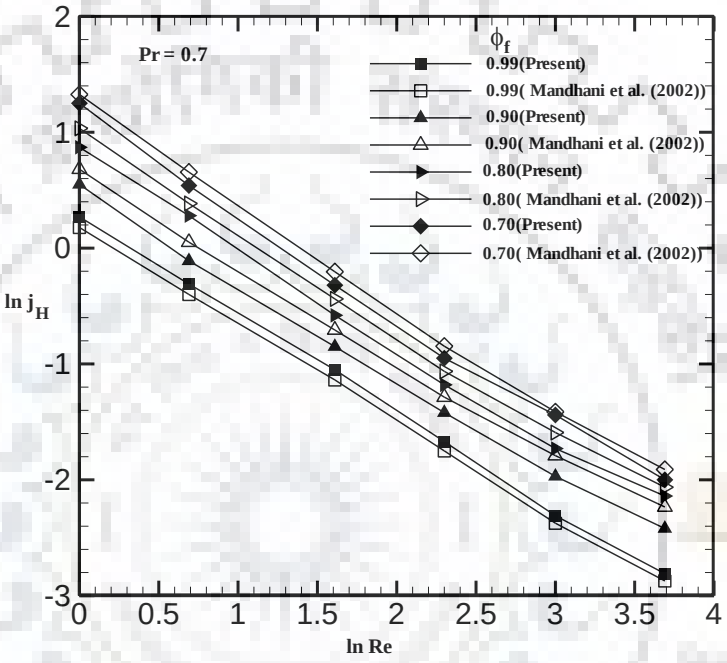

Figure 5.10: Comparison of average Nusselt number with free surface cell models of Mandhani et al. (2002)

In summary, the momentum and heat transfer characteristics of periodic flow across an array of circular cylinders are significantly varied over the ranges of governing parameters. Most significant was the effect of fluid volume fraction: as cylinders were brought closer together, drag increased and Nusselt number significantly improved; between ϕ_f = 0.99 and 0.70, Nusselt number roughly doubled, irrespective of Re and Pr. Notwithstanding, the forced convection feature of Newtonian fluid has been described herein, on the contrary, the non-Newtonian behavior for the same has been described in the next Chapter 6.

Chapter 6

FORCED CONVECTION MOMENTUM TRANSFER CHARACTERISTICS OF POWER-LAW FLUIDS ACROSS PERIODIC ARRAY OF CIRCULAR CYLINDERS

The forced convection flow characteristics of non-Newtonian power-law fluids across the periodic array of circular cylinders have been investigated and presented in this chapter. Extensive study on the flow characteristics of power-law fluids have been carried out for the following range of pertinent dimensionless parameters: Reynolds number (Re) = 1, 2, 5, 10, 20 and 40; power-law indices (n) = 0.4, 0.6, 0.8, 1, 1.4 and 1.8 and an extensive variations of fluid volume fractions of ϕ_f = 0.70, 0.75, 0.80, 0.84, 0.86, 0.88, 0.90, 0.92, 0.94, 0.96, 0.98 and 0.99. The governing equations (as described in chapter 3) i. e. Eqs. (3.3)-(3.11) (except the energy Eq. 3.7) are applied with the negligible effect of gravity as mentioned in the y-component of momentum equations (Eqs. 3.5-3.6) and boundary conditions, i. e. Eqs. (3.12)- (3.15) have been used. Within the ranges above, extensive numerical results have been obtained by systematic variations of above flow governing parameters and the influences of these parameters over the streamlines, pressure coefficients, individual (pressure and friction) and total drag coefficients are presented and discussed in the following sections. Particularly, the shear-thinning and shear-thickening behavior across a periodic array of cylinder have been explored. Before the presentation and discussion of the new results, the present numerical approach has been validated with the available literature in the next section.

6.1 Validation of numerical solution procedure

The numerical solution procedure was validated by comparing the present results of C_D with the available literature as shown in Table 6.1. For instance, at ϕ_f = 0.70 and Re = 1, the value of C_D for shear-thinning (n = 0.6) and shear-thickening (n = 1.4) fluids, display an excellent agreement with the results of Vijaysri et al. (1999) and Spelt et al. (2005b) showing a maximum deviations of 1.63% and 1.5%, respectively. Likewise, at ϕ_f = 0.70, the value of C_D for Newtonian fluids (n = 1), display a good correspondence with the results of Vijaysri et al. (1999), Spelt et al. (2005b) and Soares et al. (2005a) with a maximum deviation of 5.90% for Re = 1 and 2.05% for

Re = 40 with the results of Spelt et al. (2005b). Further, at ϕ_f = 0.99, a deviation of 2.42% and 1.99% was found between the present results and Spelt et al. (2005b) for Re = 1 and 40, respectively.

Further, for Re = 0.01 (creeping flow) and ϕ_f = 0.80 and 0.99, the present results of shear-thinning (n=0.5) and shear-thickening (n = 1.5) fluids were found to be in excellent agreement with the results of Spelt et al. (2005a) and Bruschke and Advani (1993), showing a maximum deviation of 2.31%. Also, for Newtonian fluids, the present results were in excellent agreement (maximum discrepancy 2.70%) with the numerical results of Spelt et al. (2005a), Bruschke and Advani (1993) and Edwards et al. (1990). In view of above comparisons with literature, the current findings are believed to be correct within ±1-3%. After gaining the confidence over the numerical solution approach, the new results of flow characteristics are presented and discussed in the next section.

Table 6.1: Comparison of present values of total drag coefficient (C_D) with literature values

	Source	n = 0.6	n = 1				n = 1.4
		ϕ_f = 0.70	ϕ_f = 0.99		ϕ_f = 0.70		ϕ_f = 0.70
		Re = 1	Re = 1	Re = 40	Re = 1	Re = 40	Re = 1
C_D	Present Results	61.7689	4.7025	0.1809	144.7263	4.1673	202.8281
	Vijaysri et al. (1999)	60.7600	-	-	136.1900	-	-
	Spelt et al. (2005b)	-	4.5884	0.1845	142.1367	4.2529	205.8700
	Soares et al. (2005a)	-	-		136.1800	-	-
	δ_{max} (%)	1.63	2.42	1.99	5.90	2.05	1.50

		ϕ_f = 0.99			ϕ_f = 0.80		
		n = 0.5	n = 1	n = 1.5	n = 0.5	n = 1	n = 1.5
C_D (Creeping flow)	Present Results	17.1810	8.6094	3.9798	29.8023	50.8600	84.5617
	Edwards et al. (1990)	-	-	-	-	51.7343	-
	Bruschke and Advani (1993)	-	-	-	29.2504	52.177	-
	Spelt et al. (2005a)	17.0125	8.3767	4.0600	30.4920	50.4051	82.8614
	δ_{max} (%)	0.98	2.70	2.02	2.31	2.52	2.01

6.2 Fluid flow characteristics

The qualitative (streamline profiles) and quantitative (pressure coefficient, pressure, friction and total drag coefficients, etc.) feature of power-law fluid flow has been presented and discussed in this section.

6.2.1 Streamline profiles

The dependence of the normalized streamline (as defined in Chapter 5, Section 5.2.1) patterns has been shown in Figs. 6.1-6.3 with the systematic variations of dimensionless parameters such as Reynolds number (Re), power-law index (n) and fluid volume fractions (ϕ_f). An inspection of these plots (Figs. 6.1-6.3) reveals a strong dependence of normalized streamlines over the above parameters (Re, n and ϕ_f). For instance, at lowest value of fluid volume fraction and Reynolds number (ϕ_f = 0.70 and Re = 1), a curved streamlines can be seen nearer to the cylinders for all of the shear-thinning (n < 1), Newtonian (n = 1) and shear-thickening (n >1) fluids (Fig. 6.1). Such streamlines were appeared because of the strong interference between the two periodic cylinders at the lowest value of fluid volume fraction (ϕ_f = 0.70). Further, dense streamlines can be seen for shear-thinning fluids over the surface of cylinders in contrast to Newtonian and shear-thickening fluid (Fig. 6.1). Moreover, as the fluid behavior changes from shear-thinning to Newtonian and Newtonian to shear-thickening, a small wake can also be seen in the vicinity of two cylinders at n = 1 and 1.8 (Fig. 6.1). The impact of increased fluid volume fractions is also displayed in Fig. 6.1. As the fluid volume fractions increase from ϕ_f = 0.70 to 0.90 and 0.90 to 0.99, the interference between the two cylinders is getting weak, resulting, the streamlines are less curved and dense for ϕ_f = 0.90 and 0.99 as compared to ϕ_f = 0.70. However, straight streamlines can also be seen in the core region of computational domain in Fig. 6.1 for all of the fluid volume fractions (ϕ_f = 0.70, 0.90 and 0.99) and fluid behavior index (n = 0.4, 1 and 1.8). The influence of increased Reynolds number is revealed in Figs. 6.2-6.3 at Re = 10 and 40, respectively. The fluid circulation behind the cylinder is seen to increase with increasing values of Reynolds number for both of the power-law index (n) and fluid volume fractions (ϕ_f) (Figs. 6.2-6.3). For instance, at Re = 10 (Fig. 6.2), the streamlines are observed to be denser and less swirled as compared to Re = 1 (Fig. 6.2) for all the values of fluid volume fractions (ϕ_f) and power-law index (n). Further, due to the increased fluid inertia, the wakes can be seen for ϕ_f = 0.90 along with ϕ_f = 0.70 in Fig. 6.2, but it doesn't appear for ϕ_f = 0.99, except a very small traces of wakes at n = 1.8 (Figs. 6.2-6.3). Similarly, at Re = 40 (Fig. 6.3), a strong influence of increased Reynolds number yields almost denser and straight streamlines in the vicinity of two cylinders for all the value of ϕ_f and n along with the vortex formation for ϕ_f = 0.70 and 0.90.

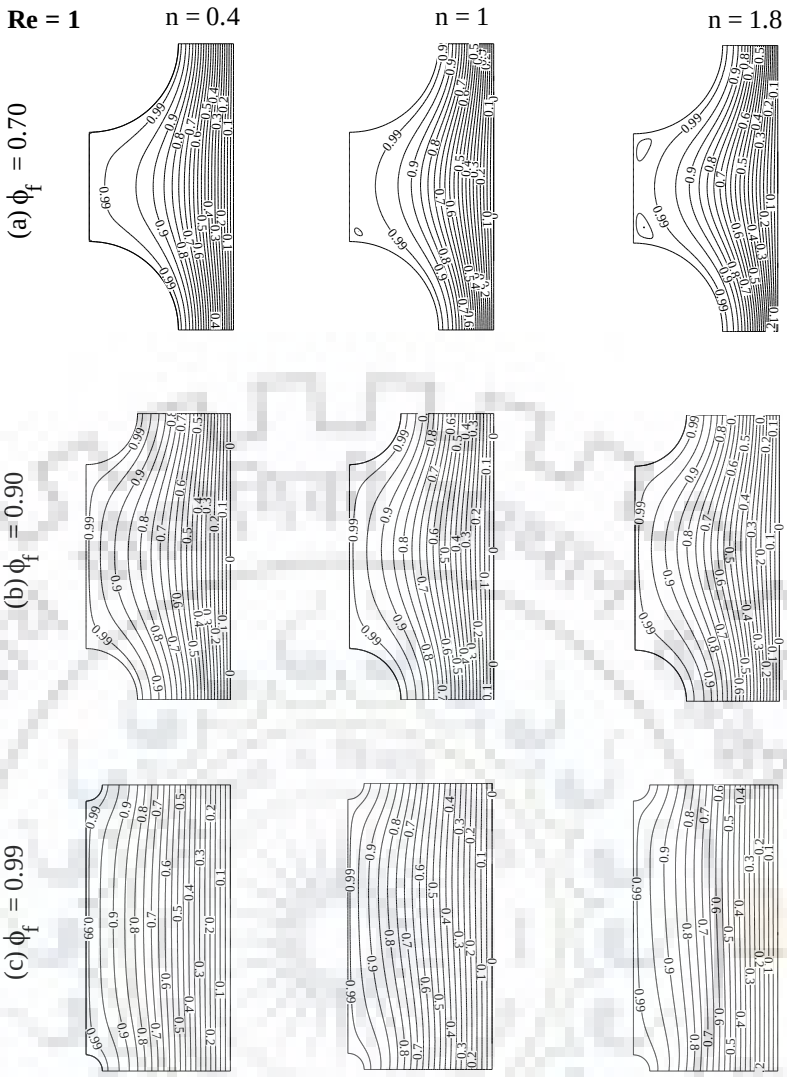

Figure 6.1: Normalized streamline profile at Re = 1 with systematic variation of power-law index n = 0.4, 1 and 1.8 and fluid volume fractions (a) ϕ_f = 0.70 (b) ϕ_f = 0.90 and (c) ϕ_f = 0.99

Moreover, the denser streamlines for Re=10 and 40 (Figs 6.2-6.3) suggest that the discharges between the two consecutive streamlines are increasing with the increasing value of Reynolds number irrespective of the value of the power-law index and fluid volume fraction. Additionally, the density of streamlines and vortex is more prominent for ϕ_f = 0.70 as compared to ϕ_f = 0.90 and 0.99 (Fig. 6.3). This again indicates the stronger interference between the two cylinders at ϕ_f = 0.70, which diminishes with the increasing value of fluid volume fractions. As a consequence, at the maximum value of fluid volume fraction (ϕ_f = 0.99), the interference between the two cylinders is nearly negligible, and both the cylinders behave almost like a single isolated cylinders. Next, the influences of the power-law index can also be seen clearly over the streamline patterns in Figs. 6.2-6.3. For instance, as the fluid behavior changes from Newtonian to shear-thinning and shear-thickening, the density of streamlines increases and decreases,

respectively for all the value of ϕ_f and Re. So, a stronger dependence of streamline patterns was seen for shear-thinning fluids in contrast to shear-thickening fluids for all of the n, ϕ_f and Re in Figs. 6.1-6.3.

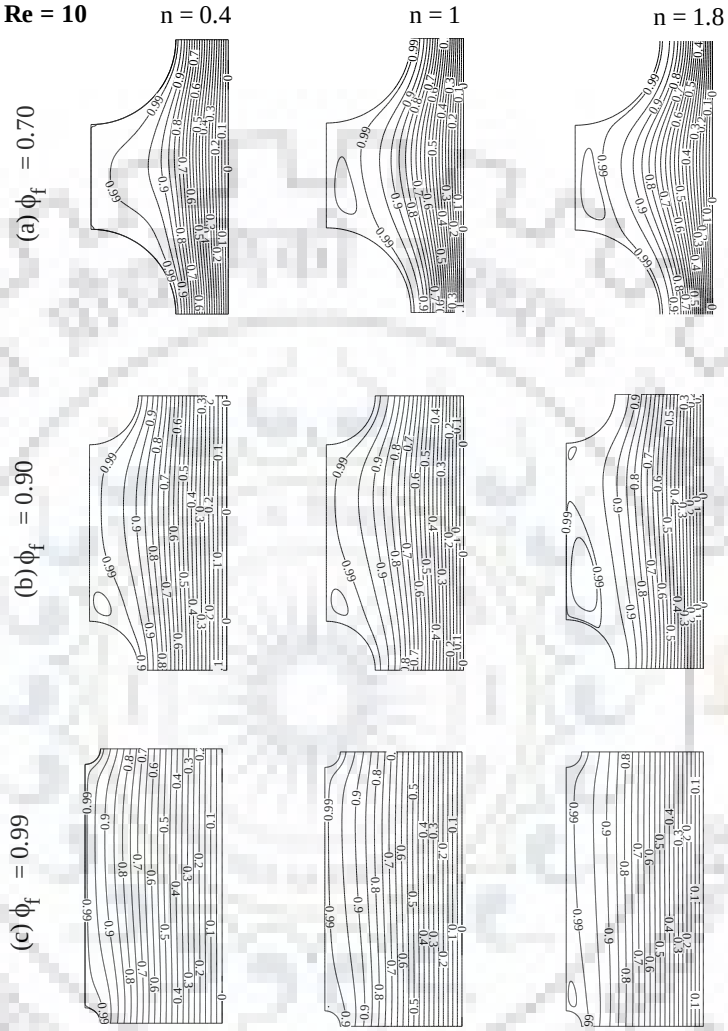

Figure 6.2: Normalized streamline profile at Re=10 with systematic variation of power-law index n= 0.4, 1 and 1.8 and fluid volume fractions (a) ϕ_f = 0.70 (b) ϕ_f = 0.90 and (c) ϕ_f = 0.99

Overall, a complex streamline pattern has been observed for the power-law fluids owing to shear-thinning and shear-thickening fluids behavior across the periodic array of cylinders. These qualitative features were found to be the similar with literature for the square array of cylinders (Edwards et al., 1990; Koch and Ladd, 1997, Spelt et al., 2005b) and in the limit of single cylinders (Bharti et al., 2006; Soares et al., 2005a) within the ranges of conditions covered herein.

The dependence of normalized streamline patterns explained above are however further examined in terms of the pressure coefficient as discussed in the subsequent section.

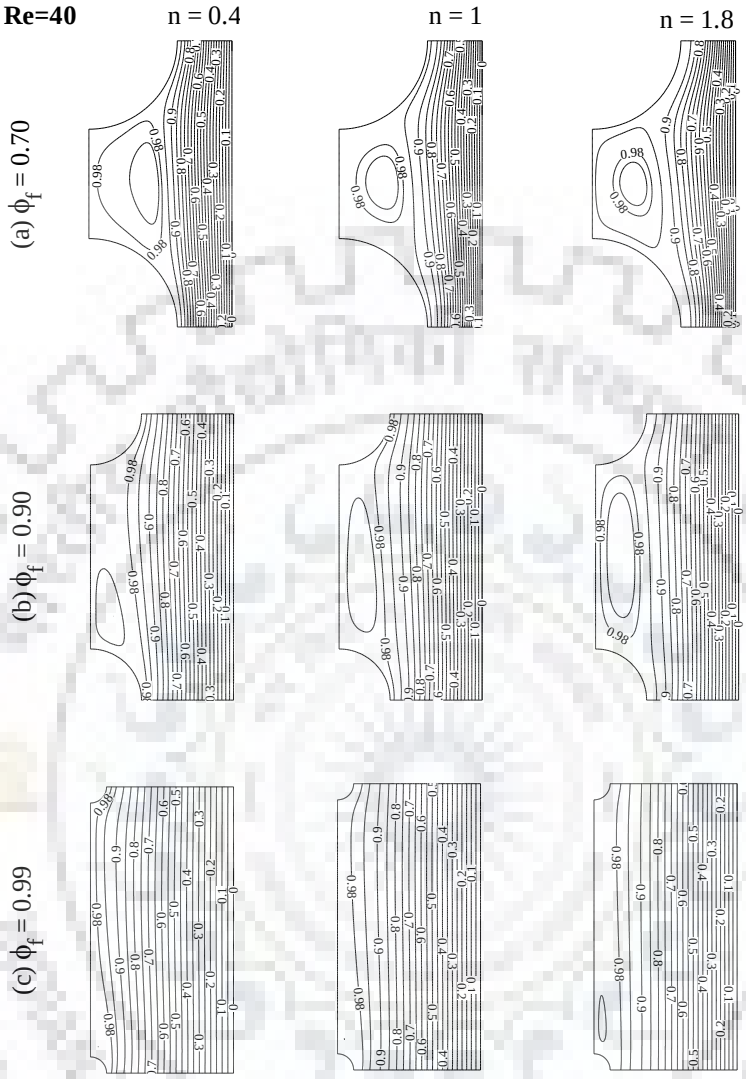

Figure 6.3: Normalized streamline profile at Re = 40 with systematic variations of power-law index (n) = 0.4, 1 and 1.8 and fluid volume fractions (a) ϕ_f = 0.70 (b) ϕ_f = 0.90 and (c) ϕ_f = 0.99

6.2.2 Distribution of the pressure coefficient (C_P) on the surfaces of the cylinders

The distribution of pressure coefficient over the surface of periodic cylinders (C_1 and C_2) is shown in Fig. 6.4 with the systematic variations of Reynolds number (Re = 1 and 40), power-law index (n = 0.4, 1 and 1.8) and fluid volume fraction (ϕ_f = 0.70, 0.90 and 0.99). At Re = 1 and ϕ_f = 0.70 (Fig.6.4a (i)), the pressure coefficient for upstream cylinder C_1 is seen to decrease from its maximum value at the front stagnation point ($\theta = 0°$) along the surface towards the rear

followed by an increase due to the recirculation of the fluid in the rear side of the cylinder C_1. For instance, the minimum value of C_P occurs at $\theta = 45°$ and then it starts increasing and converging till $\theta = 90°$. The above behavior has been observed for all the values of the power-law index. The pressure coefficient over the surface of the cylinder C_1 is seen to be higher for shear-thinning fluids than Newtonian and shear-thickening fluids in the upstream side of the cylinder C_1.

For downstream cylinder C_2 and at Re = 1 and ϕ_f =0.70 (Fig. 6.4 a(i)), the behavior is seen to flip over to the downstream side of the cylinder C_2. For instance, the pressure coefficient is seen to increase from its minimum value at $\theta = 0°$ for along the surface towards the rear followed by an increase due to the recirculation of the fluid in the rear side of the C_2. The maximum value of C_P occurs at $\theta = 45°$ and then there is a gradual decrease till $\theta = 90°$. The above behavior has been observed for all of the shear-thinning, Newtonian and shear-thickening fluids. Further, as contrast to cylinder C_1, the pressure coefficient over the surface of the cylinder C_2 is higher for shear-thickening fluids than the Newtonian and shear-thinning fluids.

The influence of increasing fluid volume fractions (ϕ_f) over the pressure coefficient is displayed in Figs. 6.4(b-c) at ϕ_f = 0.90 and 0.99, respectively. It can be observed that as the fluid volume fraction is increased from ϕ_f = 0.70 to ϕ_f = 0.90 and from ϕ_f = 0.90 to ϕ_f = 0.99, a corresponding decrease in pressure coefficient is seen for both the value of Reynolds number 1 and 40. So, the minimum value of pressure coefficient is seen at ϕ_f = 0.99 in Figs. 6.4(c). Further, an opposite trend is seen herein as compared to ϕ_f = 0.70 (Fig. 6.4(a-i)). For instance, the maximum value of Cp shifts from shear-thinning to shear-thickening for upstream cylinder C_1 and from shear-thickening to shear-thinning fluids for downstream cylinder C_2. Moreover, the maximum and minimum C_P in these fluid volume fractions (ϕ_f = 0.90 and 0.99) occur at $\theta = 90°$ (Fig. 6.4b-c (i)) in contrast to $\theta = 45°$ in lower fluid volume fraction of ϕ_f = 0.70.

Further, a strong dependence of pressure coefficient is seen with the increase in Reynolds number (Fig 6.4(ii)). For instance, at higher Reynolds number and lower fluid volume fraction (Re = 40 and ϕ_f = 0.70), the point of minimum C_P on the surface of the cylinder C_1 shifts towards the front stagnation point in the range of $\theta = 0°$-15^0 (Fig. 6.4 a (ii)) irrespective of fluid behavior. Out of these, the lowest C_P is observed for shear-thickening fluid at about $\theta = 15^0$ and then there is a recovery due to better circulation in the rear side of the cylinder C_2 and approaches the maximum C_P at $\theta = 90°$. Similarly, the maximum C_P for the shear-thinning and Newtonian fluids

is observed at θ = 90°. Further, for downstream cylinder C_2, at Re = 40, ϕ_f = 0.70, the behavior is almost consistent to that of Re = 1, and therefore, the maximum C_P can be observed at θ = 45°.

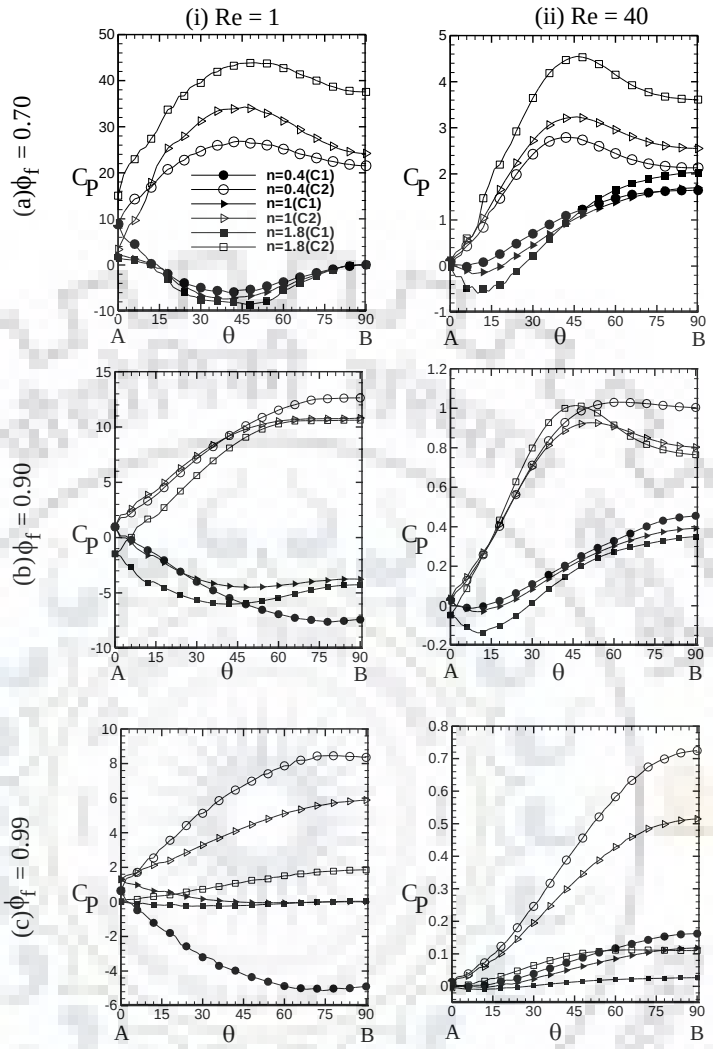

Figure 6.4: Effect of Re and n with the variation of pressure coefficient (Cp) on the surfaces of cylinders C_1 and C_2 for (a) ϕ_f = 0.70 (b) ϕ_f = 0.90 and (c) ϕ_f = 0.99

The dependence of C_P with increased fluid volume fraction can be observed in Figs. (6.4b (ii)-6.4c (ii)). For instance, at Re = 40 and ϕ_f = 0.90 and 0.99, similar to Re = 1, the maximum value of C_P shifts from shear-thickening to shear-thinning fluids for both of the cylinder C_1 and C_2 which is observed at θ = 90°. In fact, the effect of increased inertia in terms of Reynolds number has the reduced pressure coefficients across all the fluid volume fractions and therefore, the difference between the maximum and minimum C_P is also lowest at Re = 40 (Fig. 6.4(ii)) as compared to Re = 1 (Fig. 6.4(i)). Overall, the pressure coefficient on the surface of the cylinder C_2 was observed to be higher for shear-thickening fluids in lower fluid volume fraction (ϕ_f = 0.70) for the extreme values of Reynolds number (Re = 1 and 40), whereas a reverse trend was

observed for higher fluid volume fractions (ϕ_f = 0.90 and 0.99) in which higher values of pressure coefficient for shear-thinning fluids were observed. The above trend is similar to Vijaysri et al. (1999) and Shibu et al. (2001) for the flow over tube banks and also found similar to a single cylinder of Bharti et al. (2006).

6.3 Drag coefficients

In this section, the dependence of individual (pressure and friction) and overall drag coefficients over the governing parameters (ϕ_f , Re and n) is discussed for the entire ranges of conditions covered herein.

6.3.1 Dependence of pressure drag coefficient (C_{DP}) on ϕ_f , Re and n

The dependence of individual and total drag coefficients (C_{DP}, C_{DF} and C_D) on the fluid volume fraction (ϕ_f), Reynolds number (Re) and power-law index (n) and is shown in Table A1 (Appendix-A). The pressure drag coefficient (C_{DP}) is seen to decrease with increasing value of the Reynolds number irrespective of the fluid volume fraction (ϕ_f) and power-law index (n). However, for a fixed value of Re, the value of C_{DP} increases and/or decreases significantly as the fluid behaviour changes from shear-thinning to shear-thickening. This behavior can be clearly seen in Table A1. For instance, at ϕ_f = 0.70 and Re = 1, the values of C_{DP} are 19. 1597, 71.0562 and 116.8942 for n= 0.4, 1 and 1.8, respectively. Similarly, at ϕ_f = 0.70 and Re = 40, the values of C_{DP} are 0.5122, 2.4904 and 3.9972 for n = 0.4, 1 and 1.8, respectively. The above changes in C_D value occur primarily because of the dominance of viscous forces at the lower values of Reynolds number in contrast to the dominance of pressure forces at higher Reynolds number. Further, the strong influence of fluid volume fraction (ϕ_f) over the pressure drag coefficient can be seen in Table A1. For instance, it is observed that the value of C_{DP} is increasing for the fluid volume fractions in the range of $0.70 \leq \phi_f \leq 0.90$ for all the values of power-law index and Reynolds number, whereas, a reverse trend is seen in the range of $0.92 \leq \phi_f \leq 0.99$ under the identical conditions of Re and n. Therefore, for the range of fluid volume fraction $0.70 \leq \phi_f \leq 0.90$, the values of C_{DP} drop below Newtonian in the shear thinning region (n < 1), while it grows up above the Newtonian in the shear-thickening region (n > 1). However, these behaviors are opposite over the ranges of fluid volume fraction $0.92 \leq \phi_f \leq 0.99$. For instance, at ϕ_f = 0.75 and Re = 1, the values of C_{DP} are 13.8266, 43.4821 and 57.1925 for n = 0.4, 1 and 1.8,

respectively, whereas, at ϕ_f = 0.99 and Re = 1, the values of C_{DP} are 5.7355, 2.3435 and 0.7267 for n = 0.4, 1 and 1.8, respectively (Table A1). In fact, these behaviors are the consequences of the stronger and lower velocity gradients in the lower and higher fluid volume fractions respectively and as a result, the interference between the two cylinders is stronger at lower values of ϕ_f, which diminishes with the increasing value of ϕ_f and the two cylinders approach almost the single cylinder limit. Additionally, the changes in the pressure drag coefficient with the power-law index is linked with the varying levels of viscosity as encountered by the periodic cylinders in the shear-thinning and shear-thickening fluids region. Overall, a non-monotonous behavior of pressure drag coefficient was observed with the ϕ_f, n and Re. The flow dynamics described herein are further described in terms of friction drag coefficient in the following section.

6.3.2 Dependence of friction drag coefficient (C_{DF}) on ϕ_f, Re and n

Table A1 (Appendix-A) also represents the dependence of the friction drag coefficient (C_{DF}) on Reynolds number, power-law index and the fluid volume fraction. Qualitatively, similar to C_{DP} (ϕ_f, Re and n), the C_{DF} reduces with increasing values of Reynolds number and/or fluid volume fractions irrespective of the values of the power-law index (Table A1). On the other hand, the smallest fluid volume fraction provides minimum flow area for the fluids to penetrate through the arrays of cylinders and, therefore, the friction effects become stronger under such conditions, as observed through the dense clustering of streamlines (Figs. 6.2-6.3) and higher values of C_{DF} in Table A1. The dependence of C_{DF} on power-law index shows a complex behaviour in both of the shear-thinning and shear-thickening fluids. For instance, the pressure drag coefficient (C_{DP}) is dominating over friction drag coefficient (C_{DF}) for the shear-thinning fluids, whereas, an opposite behaviour can be seen for the shear-thickening fluids except at Re = 40. These trends can be observed across all the values of fluid volume fractions. The minimum value of C_{DF} is observed at the largest values of both Re as well as ϕ_f and the smallest value of n. For instance, at n = 0.4, as Re increased from 1 to 40, C_{DF} values altered from 12.7656 to 0.2518 and from 3.8046 to 0.0944 at ϕ_f = 0.70 and 0.99, respectively (Table A1). In contrast, the maximum value of C_{DF} is observed at the smallest values of both Re as well as ϕ_f and the largest value of n. The above decrease or increase in C_{DP} or C_{DF} value is, however, small for the range $20 \leq Re \leq 40$. Therefore, small values of Re and increasing level of shear thickening behaviour always yield the higher values of friction drag coefficients as compared to pressure drag coefficients.

6.3.3 Dependence of total drag coefficient (C_D) on ϕ_f, Re and n

The dependence of total drag coefficient over the governing parameters (ϕ_f, Re and n) has been shown in Fig. 6.5 and the results are also summarized in Table A1. The total drag coefficient has virtually similar dependence of C_{DP} and C_{DF} on fluid volume fractions, power-law index and Reynolds number. In Fig. 6.5, it can be observed that as the fluid behavior changes from shear-thinning to shear-thickening, the total drag coefficient increases for the fluid volume fraction in the ranges of $0.70 \leq \phi_f \leq 0.90$ and decreases for the ranges of $0.92 \leq \phi_f$ n ≤ 0.99. This behavior is caused due to the varying fluid volume fractions or the porosity of the cylinders. Further, the role of power-law index diminishes with the increasing value of fluid volume fractions and thereby a shift in the behaviour of the shear-thinning and shear-thickening fluids is observed. Thus, in Fig. 6.5 and Table A1, adequate changes in the values of total drag coefficient can be seen among the shear-thinning, Newtonian and shear-thickening fluids. These trends are consistent with the results of Spelt et al. (2005b) and Soares et al. (2005a).

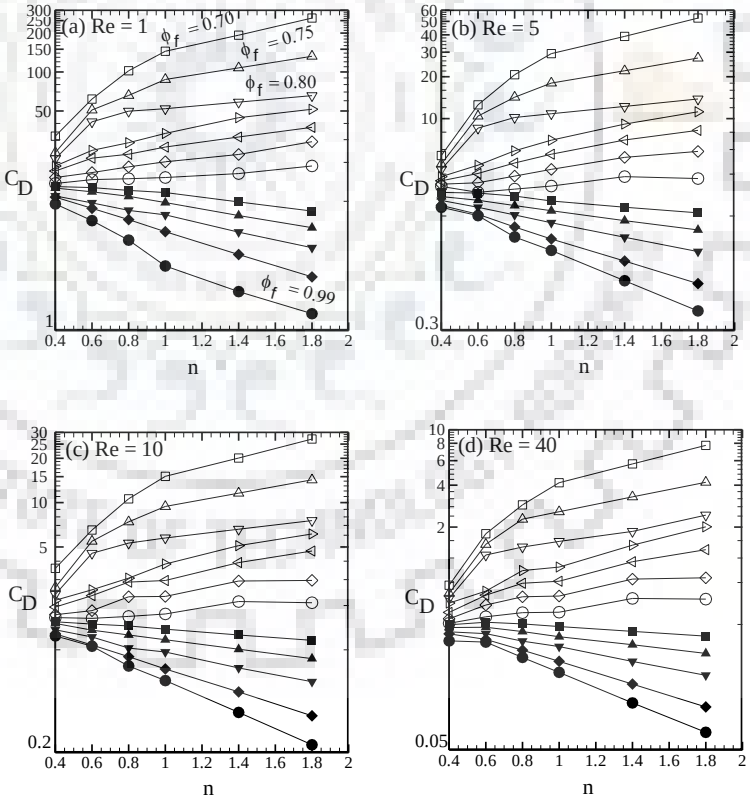

Figure 6.5: Power-law index (n) vs. log C_D with the systematic variation of fluid volume fractions (ϕ_f = 0.70-0.99)

The above flow characteristics are further analyzed by normalizing the drag coefficient with the maximum fluid volume fractions ($\phi_{f,max}$) as follows, $X^N = X(Re, \phi_f)/X(Re, \phi_{f,max})$, where X represents the individual and total drag coefficients (C_{DP}, C_{DF} and C_D), and $\phi_{f,max} = 0.99$. Figs. 6.6-6.8 present the dependence of normalized drag coefficients (C_{DP}^N, C_{DF}^N and C_D^N) over the fluid volume fraction ($0.70 \leq \phi_f \leq 0.90$), power-law index ($0.40 \leq n \leq 1.8$) and Reynolds number ($1 \leq Re \leq 40$). As expected, the normalized values of drag coefficients are seen to be always greater than 1, i.e., $X^N > 1$ in Figs. 6.6-6.8. Further, the values of normalized drag values are found to be the largest at the smallest value of fluid volume fraction ($\phi_f = 0.70$) for all of the Re and n. For a fixed value of Re, the normalized drag values are seen to decrease monotonically with increasing value of fluid volume fraction. For a fixed value of ϕ_f, the normalized drag values are decreasing with increasing Re which can be seen in Fig. 6.6a-6.6d for C_{DP}^N or Fig. 6.7a-6.7d for C_{DF}^N and Fig. 6.8a-6.8d for C_D^N. In these figures, it can also be observed that the normalized drag coefficients (C_{DP}^N, C_{DF}^N and C_D^N) of shear-thickening fluids are dominating over shear-thickening fluids for all the values of Re. However, significant dependence of normalized drag values is observed at lower Re which reduces correspondingly at higher Re.

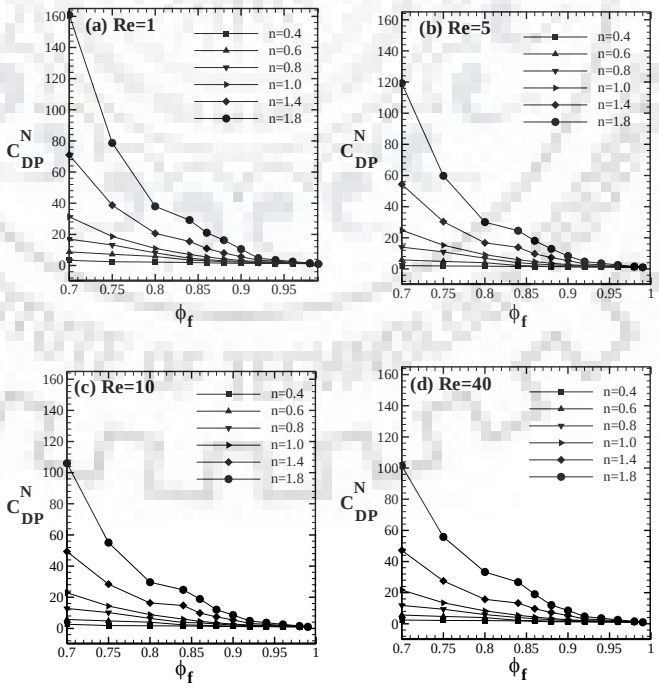

Figure 6.6: Variation of normalized pressure drag coefficient (C_{DP}^N) with fluid volume fraction (ϕ_f) and power-law index (n) for (a) Re = 1 (b) Re = 5 (c) Re = 10 and (d) Re = 40

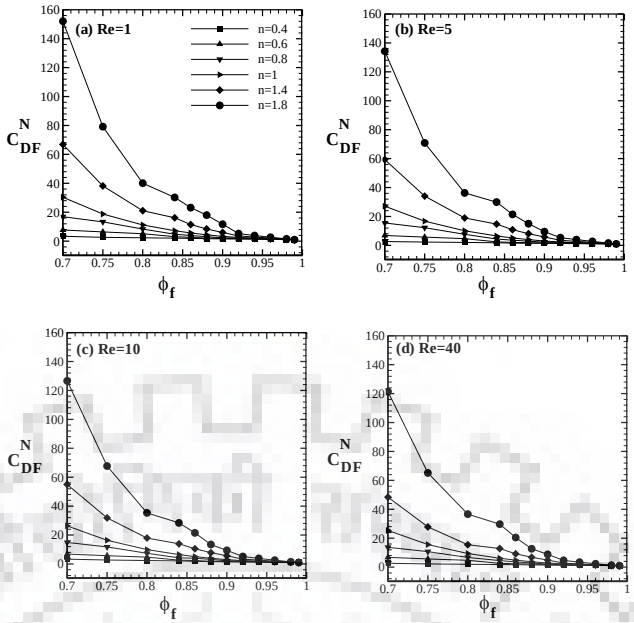

Figure 6.7: Variation of normalized friction drag coefficient (C_{DF}^{N}) with fluid volume fraction (ϕ_f) and power-law index (n) for (a) Re = 1 (b) Re = 5 (c) Re = 10 and (d) Re = 40

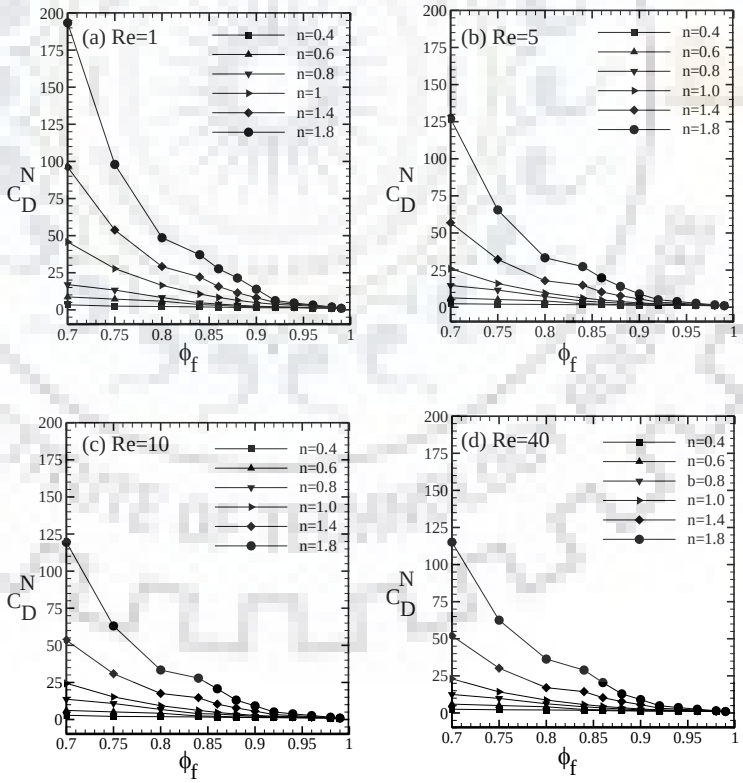

Figure 6.8: Variation of normalized total drag coefficient (C_D^N) with fluid volume fraction (ϕ_f) and power-law index (n) for (a) Re = 1 (b) Re = 5 (c) Re = 10 and (d) Re = 40

To understand the relative contribution of pressure drag coefficient and the friction drag coefficient, the drag ratio (C_{DR}) has been defined as $C_{DR} = C_{DP}/C_{DF}$ and shown in Fig. 6.9 for the extreme values of Reynolds number (Re = 1 and 40). Fig. 6.9 shows the complex dependence of drag ratio on both Reynolds number and fluid volume fraction over the ranges of the power-law index ($0.40 \leq n \leq 1.8$) studied herein. For instance, in Fig. 6.9(a), the $C_{DR} > 1$ suggests the dominance of pressure forces over the viscous component of forces. Further, this ratio is seen to be < 1 for shear-thickening fluids (n > 1) in Fig. 6.9(a), which suggests that the flow is dominated by the viscous forces rather than the pressure forces in this region at low Reynolds number. However, at high Reynolds number (Re = 40), the C_{DR} always seems to be the greater than one in Fig. 6.9(b), and therefore the pressure force is always dominating over viscous forces irrespective of the shear-thinning and/or shear-thickening fluid behavior. Additionally, the C_{DR} is increasing correspondingly with the increasing value of fluid volume fractions in Fig. 6.9(b), which once again indicates that the pressure forces are dominating at higher Re with the increasing value of fluid volume fractions. These typical behaviors are due to the influence of varying periodic boundary conditions over the flow field. For instance, at low Re, the fluid is not stratified in the whole computational domain due to small (or negligible) pressure in the vicinity of the cylinder (see Figs. 6.1 and 6.2) and correspondingly, the friction drag is dominating over the pressure drag under these conditions. However, more resistance to flow is observed due to the pressure in comparison of the friction at large values of Re.

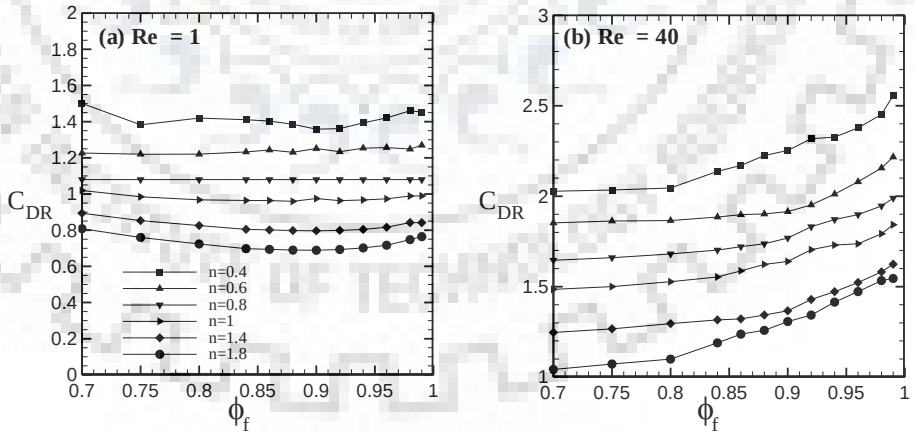

Figure 6.9: Dependence of drag ratio ($C_{DR} = C_{DP}/C_{DF}$) on Reynolds number (Re), power-law index (n) and fluid volume fraction (ϕ_f) for (a) Re = 1 and (b) Re = 40

To encapsulate the numerical results obtained in this work, a statistical analysis of the present numerical results has been carried out to develop a closure relationship. The following correlation best represents the functional dependence of drag coefficients (based on 432 data

points for each of the C_{DP}, C_{DF} and C_D) over the power-law index (n), Reynolds number (Re) and the fluid volume fraction (ϕ_f):

$$X = an^b \phi_f^c \, Re^d + e(n\,Re)^g \tag{6.1}$$

Here, X being C_{DP}, C_{DF} and C_D. The empirically fitted constants (a, b, c, d, e and g) appeared in Eq. (6.1) along with their statistical parameters are listed in Table 6.2. The present numerical values show an excellent correspondence with the values predicted using Eq. (6.1) as shown in Fig. 6.10. For instance, the above correlation for C_D has the average and maximum deviations of ~3.29 % and ~8.48% for the 90 % of data points, respectively. Other deviations lie within 9-20% for 6 % of the data points and only 4% of the data points show a deviation within 21-35%. Further, the present results were compared with the available literature for the shear-thinning and Newtonian fluids as shown in Fig. 6.11. For instance, a good correspondence can be seen in Fig. 6.11 of the present results with the predictions of zero vorticity cell model of Vijaysri et al. (1999), free surface cell model of Tripathi and Chhabra (1992) and approximation of the Bruschke and Advani (1993). The minimum discrepancies in the above comparison are within 1.64-11.12%. Additionally, the present results have been compared with the experimental results of Prasad and Chhabra (2001) within the ranges of parameters studied herein. For instance, they have presented their experimental results in terms of loss coefficients (Λ) defined as $\Lambda = C_D \, Re_p$, where C_D is the total drag coefficient and Re_p is the modified Reynolds number. They have used Re_p = 1 as the limiting value for the creeping flow region and also pointed out that in the concentrated systems, i.e., the low value of fluid volume fractions, the creeping flow occurs up to about Re_p 5-10. So for Re_p = 1, the loss coefficient is equal to drag coefficient (Λ = C_D). In the view of these, the present result shows a good contrast with this experimental results. For instance, at Re = 1, the present value of C_D is 14.30 (n = 0.4, ϕ_f = 0.88) against the experimental result of 12.37 (n = 0.38, ϕ_f = 0.87) with a discrepancy of 13.65%. Similarly, at ϕ_f = 0.88, the present value of C_D is 15.6917 (n = 0.6) against the experimental value of 14.84 (n = 0.62) with a discrepancy of 5.43%. Notwithstanding, these comparisons are not at the exact values of parameters, perhaps, a good correspondence is seen to exist between the present numerical and the experimental results. However, this level of discrepancies is acceptable between the numerical and experimental comparison. Overall, the detailed flow dynamics across the periodic array of cylinders are influenced intricately by the values of the Reynolds number, fluid volume fraction and the power-law index.

Table 6.2: Functional parameters for the dependence of the individual (C_{DP} and C_{DF}) and total drag (C_D) coefficients on power-law index, Reynolds number and fluid volume fractions

Correlation Constants	C_{DP}	C_{DF}	C_D
a	2.0284	2.4374	4.3362
b	0.9731	1.2960	1.1712
c	-9.7203	-9.2856	-9.5368
d	-0.9730	-0.9943	-0.9736
e	2.2382	1.3414	4.2218
f	-0.9332	-0.9903	-1.2954
R^2	0.9738	0.9824	0.9617
*%δ_{max}	7.2439	5.4483	8.4785
*% δ_{avg}	5.5674	3.2963	4.3215
* 90% of data points have the above deviations are within 3-8%; 6% of data points have deviations within 9-20% and remaining 4% have deviations within 21-35%.			

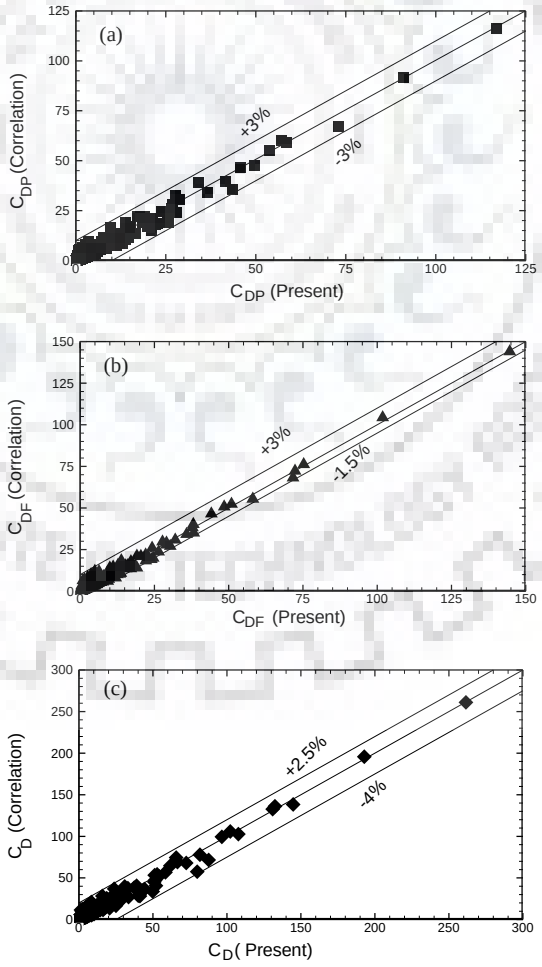

Figure 6.10: Best fit of present numerical results vs. correlation values of (a) C_{DP} (b) C_{DF} and (c) C_D

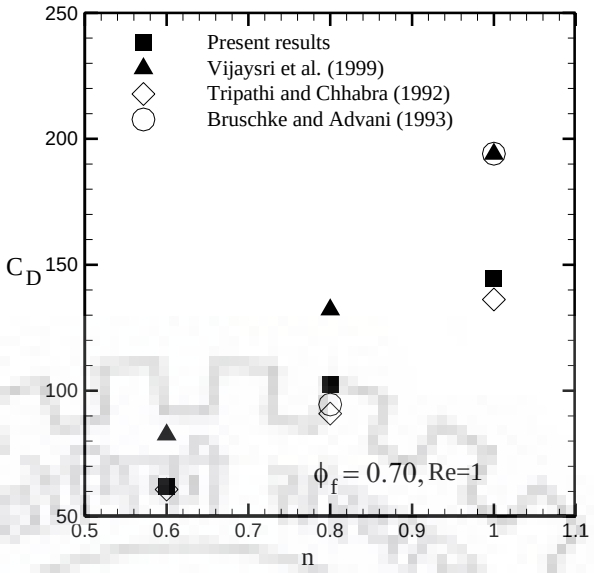

Figure 6.11: Comparison between present results of total drag coefficient (C_D) and that of literature for the shear-thinning and Newtonian fluids

Chapter 7

FORCED CONVECTION HEAT TRANSFER CHARACTERISTICS OF POWER-LAW FLUIDS ACROSS PERIODIC ARRAY OF CIRCULAR CYLINDERS

The forced convection heat transfer characteristics of non-Newtonian power-law fluids have been investigated herein across the periodic array of circular cylinders. The local and global characteristics of heat transfer have been examined for the following ranges of governing parameters: Re = 1, 2, 5, 10, 20 and 40; Pr = 1, 5, 10, 20, 50 and 100; n = 0.4, 0.6, 0.8, 1, 1.4 and 1.8 and ϕ_f = 0.70, 0.75, 0.80, 0.84, 0.86, 0.88, 0.90, 0.92, 0.94, 0.96, 0.98 and 0.99. The governing equations (as described in Chapter 3), i. e. Eqs. (3.3)-(3.11) are applied with the negligible effect of gravity as mentioned in the y-component of momentum equations (Eqs. 3.5-3.6) and boundary conditions, i. e. Eqs. (3.12)-(3.15) have been used. Within the ranges above, extensive numerical results have been obtained by systematic variations of above flow governing parameters and the influences of these parameters over the isotherm patterns, local and averaged Nusselt numbers, the Colburn j_H factor, etc. are presented and discussed to explore the shear-thinning and shear-thickening behaviors across the periodic array of cylinders. Though, before presenting and discussing the new results, the present numerical approach has been validated with the available literature.

7.1 Validation of numerical solution procedure

The relevant comparison of present numerical results and that of literature is shown in Table 7.1. It is also essential to point out the fact that there are scant studies available for the forced convection heat transfer across the periodic array of cylinders even with the simple Newtonian fluids. However, negligible literature is available for the direct comparison of the present results within the ranges of parameters studied herein. Perhaps, an endeavor was made to validate the results within the framework of the available literature. Also, in the case of higher fluid volume fraction such as ϕ_f = 0.99, the periodic cylinders behave as an isolated single cylinders and so it is comparable with a single cylinder (Bharti et al., 2007a). Similarly, a good comparison could be made with the tandem arrangements of cylinders with different gap ratio (Patil et al., 2008). In view of these, the current numerical solution procedure has been validated. So, for Newtonian fluids, the current results obtained for the average Nusselt number under

steady flow conditions, show a good correspondence with the results of Gamrat et al. (2008) for ϕ_f = 0.86, Pr = 100 and Re = 1 with a maximum deviation of about 0.3%. Similarly, at Pr = 5, Re = 1 and the extreme fluid volume fractions of 0.70 and 0.99, the results display the good correspondence with the results of Mangadoddy et al. (2004) showing a maximum deviation of about 3%.

Table 7.1: Comparison of present numerical results of average Nusselt number (Nu) with available literature

Source	n = 1					
	Nu (ϕ_f = 0.70)		Nu (ϕ_f = 0.86)		Nu (ϕ_f = 0.99)	
	Re = 1, Pr = 5		Re = 1, Pr = 100		Re = 1, Pr = 5	
Present results	2.5295		2.8832		1.4217	
Gamrat et al. (2008)#	-		2.8925		-	
Mangadoddy et al. (2004)##	2.6057		-		1.4015	
δ_{max} (%)	3.01		0.32		1.42	
	n ≠ 1					
Source	Nu (ϕ_f = 0.99)			Nu (ϕ_f = 0.80)		
	n = 0.4 (Pr = 1, Re = 5)	n = 1.8 (Pr = 1, Re = 1)	n = 1.4 (Pr = 100, Re = 5)	n = 0.4 (Pr = 100, Re = 1)	n = 1.8 (Pr = 100, Re = 1)	n = 1.8 (Pr = 1, Re = 40)
Present results	1.6454	0.7195	1.7188	3.3138	2.2825	2.0769
Soares et al. (2005b)*	1.6210	-	1.7542	-	-	-
Patil et al. (2008)**		0.7314		3.2230	2.2174	2.0456
Bharti et al. (2007a)*	1.6840	-	-			
δ_{max} (%)	2.30	1.65	2.05	2.74	2.85	1.51
# periodic array of cylinders, ## free surface cell model * single cylinder; ** two tandem cylinders						

For power-law fluids, the current results of Nu were compared with the prior studies (Soares et al., 2005b; Patil et al., 2008; Bharti et al., 2007a) in the range of $0.4 \le n \le 1.8$; $0.70 \le \phi_f \le 0.99$ and $1 \le Re \le 40$. Within the ranges mentioned herein, the current numerical results of shear-thinning and shear-thickening fluids are in good agreement with previous results of Soares et al. (2005b), Patil et al. (2008) and Bharti et al. (2007a), showing a maximum deviation of less than 3%. For instance, at ϕ_f = 0.99, Pr = 1 and Re = 5, the shear-thinning fluid (n = 0.4) shows the maximum discrepancy within 2.3% with Soares et al. (2005b) and Bharti et al. (2007a). Likewise, for the same fluid volume fraction of 0.99, but in the region of shear-thickening flow (n = 1.4 and 1.8), the agreement was again found good with the Soares et al. (2005b) and Patil et al. (2008) at Pr = 100, Re = 5 and Pr = 1, Re = 1, respectively, with a maximum discrepancy of about 2.1%. Further, for ϕ_f = 0.80 (Pr = 100, Re = 1 and Pr = 1, Re = 40), the numerical results were found to be the consistent (maximum discrepancy of less than 3%) with the results of Patil

et al. (2008) for both of the shear-thinning as well as shear-thickening fluids. In view of above comparisons with literature, the current findings are believed to be the correct within ±2-3%. After gaining the confidence over the numerical solution approach, the new results of heat transfer characteristics are presented and discussed in the next section.

7.2 Thermal patterns

Representative isotherm patterns are shown in Figs. 7.1-7.4 with the systematic variations of Re, Pr, n, and ϕ_f . Specifically, Figs 7.1-7.4 display the normalized values of temperature (as defined in Chapter 5, Section 5.3.1). As anticipated, the isotherm patterns were found to be strongly dependent on the ranges of engineering parameters (Re, Pr, n and ϕ_f) studied herein. For a given fluid volume fraction (ϕ_f), the clustering of isotherms in the flow domain is growing up with the increased inertial and/or viscous diffusion rate. It can be seen that as the viscous diffusivity increases (increased Prandtl number), more dense streamlines appear in the vicinity of periodic cylinders (Figs. 7.1b-7.4b), which qualitatively enhances the rate of heat transfer. An increasing value of ϕ_f shows somewhat slightly different behavior on the isotherm patterns. The clustering of isotherms is more prominent (Fig. 7.1) when cylinders come closer to each other (e. g. ϕ_f = 0.70). Further, as the fluid volume fractions increase, the isotherms are getting closer to cylinders and straighter streamlines appear in the wake (Figs. 7.2-7.3). At the maximum value of fluid volume fraction (ϕ_f = 0.99), the upstream cylinder displays strongly sharper gradients in comparison of downstream cylinder (Fig. 7.4) and therefore in such a case (ϕ_f = 0.99), the cylinders are generally independent and most of the heat transfer is due to the upstream cylinder (Fig. 7.4). Overall, the impact of fluid volume fraction on isotherm is appreciated to be more prominent at higher Re and/or Pr. For instance, at high Re, isotherms were seen to be denser in the neighborhood of cylinders and also in the whole computational domain for all the values of the n, ϕ_f and Pr. In such a case of high Re, isotherms in open flow regions are observed to be parallel to flow direction and added intricate patterns display in the wake (Figs. 7.1-7.4). Further, much steeper temperature gradients are seen nearer to cylinders as Re increases. A steep or weak temperature gradient accounts a rise or fall in the rate of heat transfer, respectively. These behaviors are observed in Figs. 7.1-7.4 for Re = 10, 20 and particularly at Re = 40 for both of the shear-thinning as well as shear-thickening fluids. Indeed, this is because in such a case, the heat transfer takes place primarily by convection with the increasing values of Re. However, it can

also be observed that the symmetrical isotherm patterns at the small Re indicate that the conduction is dominating over convection.

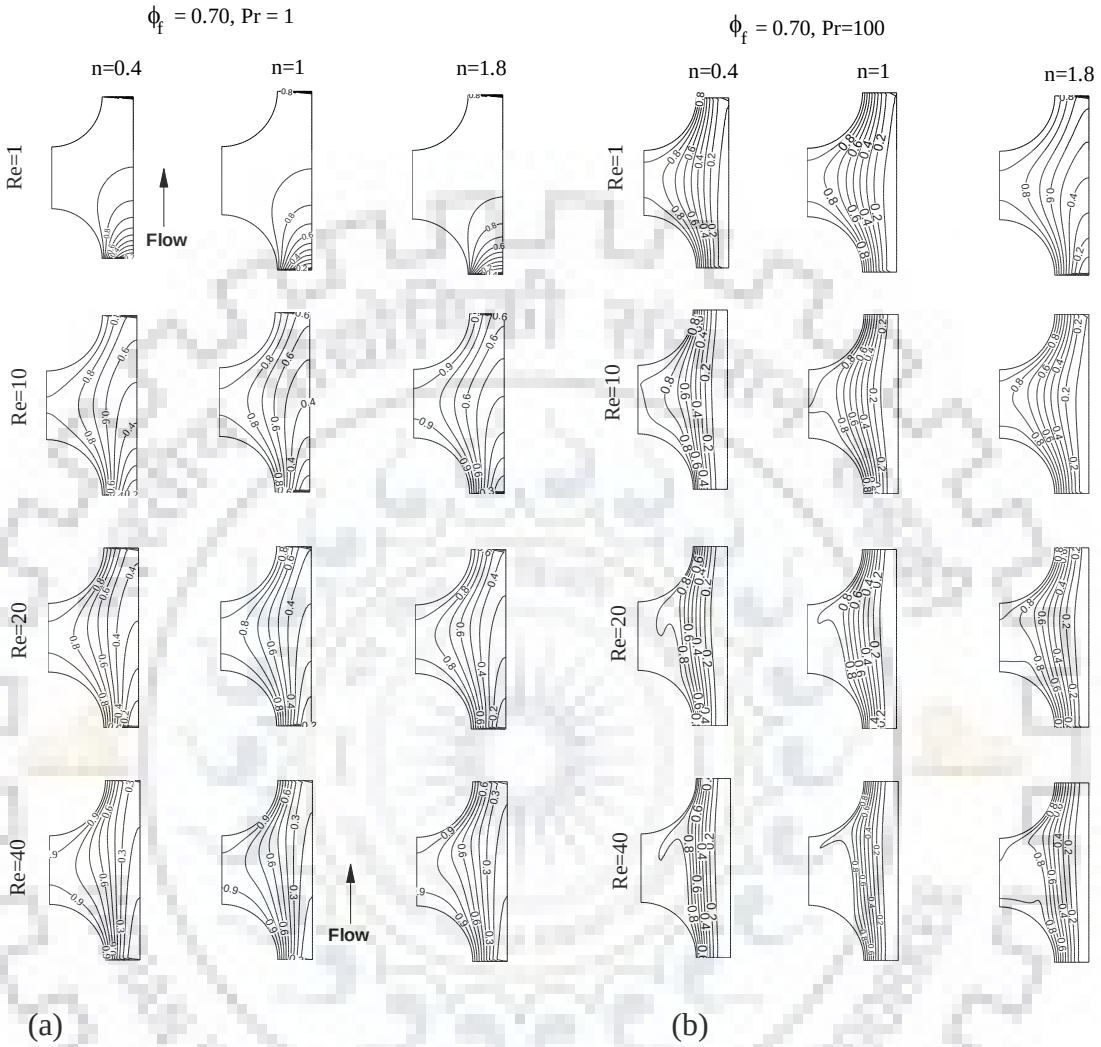

Figure 7.1: Typical variations of normalized isotherms with n=0.4, 1, 1.8 and Re = 1, 10, 20, 40 at ϕ_f = 0.70 (a) Pr = 1 and (b) Pr =100

The impact of flow behavior index (n) on isotherms is observed to be additionally noticeable at higher Re and/or Pr, irrespective of fluid volume fraction (ϕ_f). Moreover, when the fluid flow nature shifts from shear-thickening to shear-thinning, a growing density of isotherms gives a complete upturn in the temperature gradients. This behavior can be clearly observed in Figs. 7.1 and 7.2 for ϕ_f = 0.70 and 0.99, respectively. This happens because of the occurrence of the thinner thermal boundary layer in shear-thinning fluids as compared to corresponding Newtonian or shear-thickening fluids. A similar qualitative feature has been reported for the single cylinder (Patil et al., 2008; Bharti et al., 2007a). This intricate behavior of

isotherms on Re, Pr, n and ϕ_f is further investigated by means of local Nusselt number as described in the subsequent Section 7.2.1.

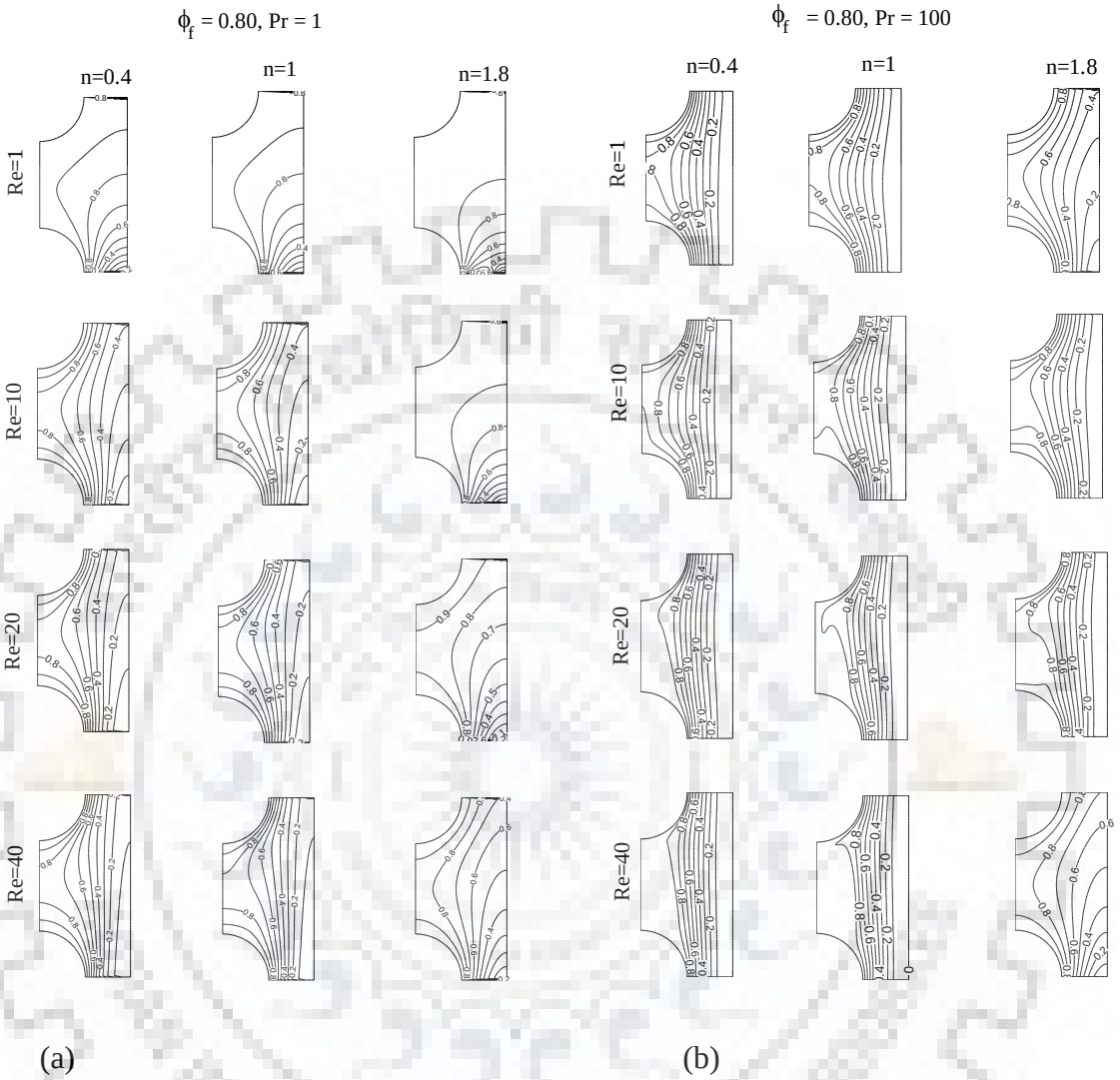

Figure 7.2: Typical variations of normalized isotherms with n = 0.4, 1, 1.8 and Re = 1, 10, 20, 40 at ϕ_f = 0.80 (a) Pr = 1 and (b) Pr = 100

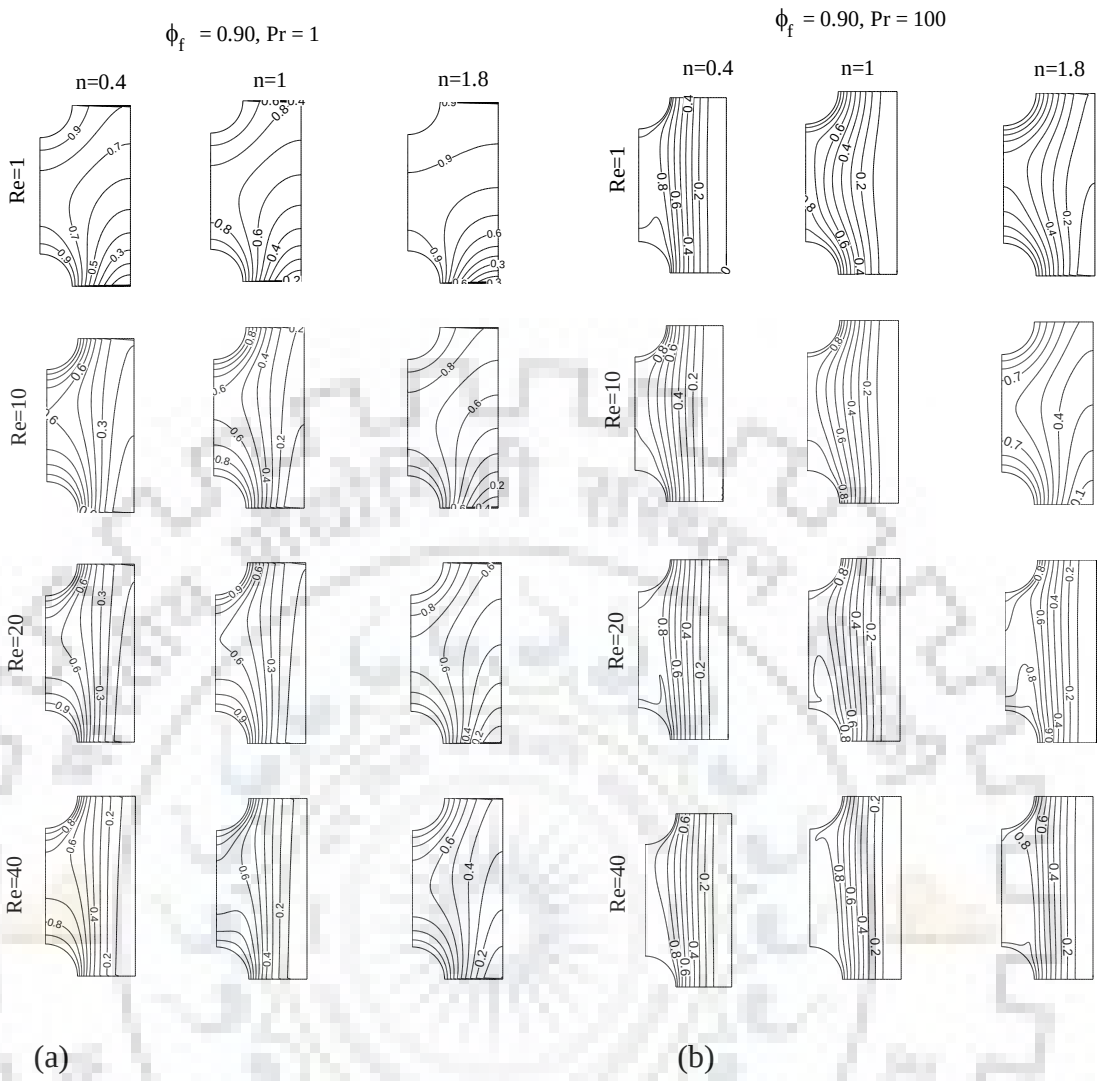

Figure 7.3: Typical variations of normalized isotherms with n = 0.4, 1, 1.8 and Re = 1, 10, 20, 40 at ϕ_f = 0.90 (a) Pr = 1 and (b) Pr =100

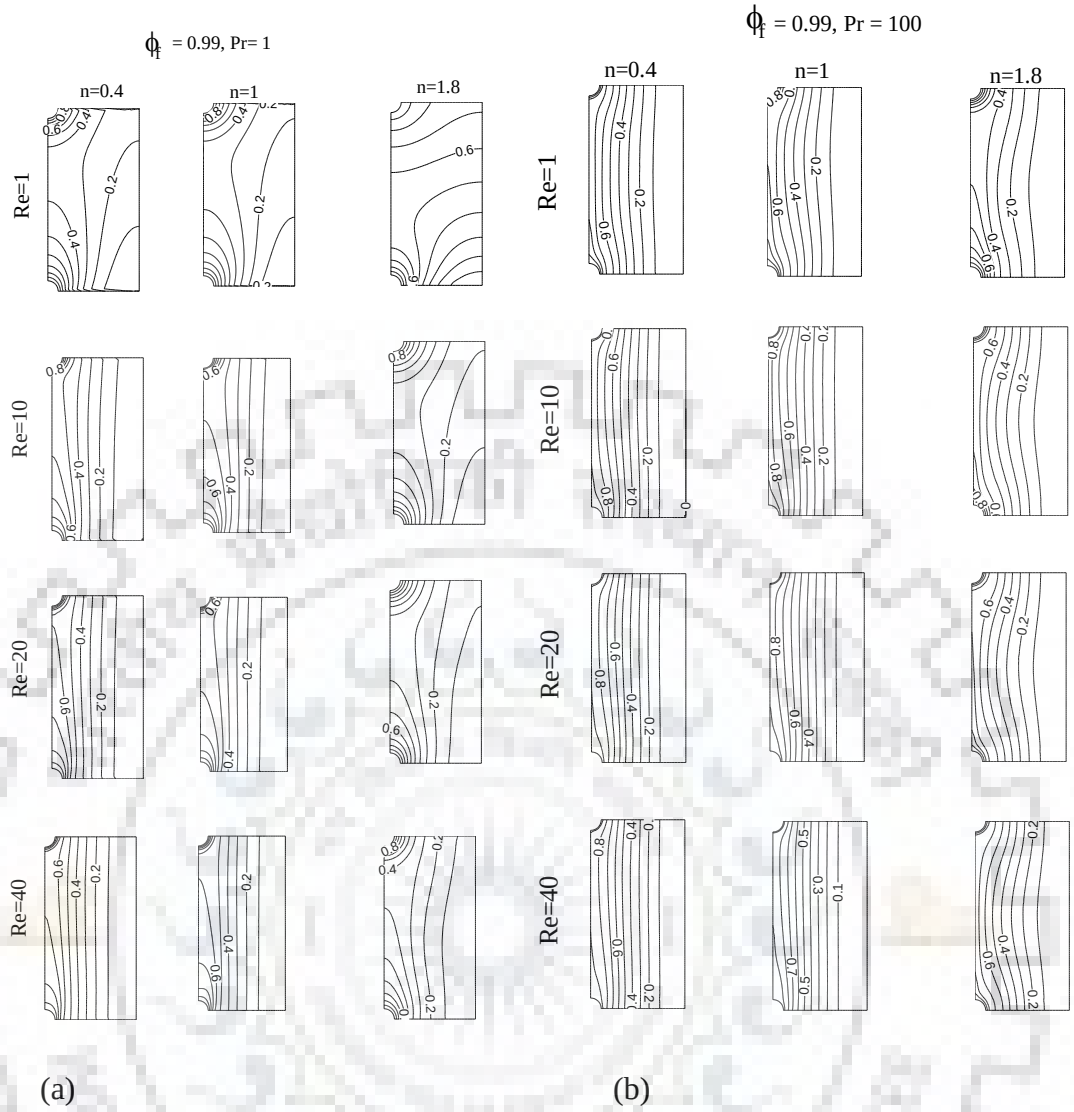

Figure 7.4: Representative variations of normalized isotherms with n = 0.4, 1, 1.8 and Re = 1, 10, 20, 40 at ϕ_f = 0.99 (a) Pr = 1and (b) Pr = 100

7.3 Local Nusselt number

The local Nusselt number (Nu_L) for upstream cylinder (C_1) is shown in Figs. 7.5 and 7.6 with the systematic variations of n, ϕ_f and Pr at Re = 1 and 40, respectively. The corresponding Nu_L for the downstream cylinder (C_2) is displayed in Figs. 7.7 and 7.8 under the identical conditions. The Nu_L values for cylinder C_1 are greater than that for cylinder C_2, i.e., $Nu_L(C_1) > Nu_L(C_2)$, although both of these values are lower than that of a single cylinder (Bharti et al., 2007a) under otherwise similar conditions. Further, the changes in Nu_L for the cylinder C_1 are qualitatively identical to a single cylinder (Bharti et al., 2007a). For a given Re and Pr (e.g. at Re = 1 and Pr = 1), it can be seen in Figs. 7.5-7.6 that the values of local Nusselt numbers are maximum at lower fluid volume fraction (ϕ_f = 0.70) at $\theta = 0^o$. In contrast, with an increase in fluid volume fractions from 0.70

to 0.99, a corresponding decrease in Nu_L was noticed at $\theta = 90^o$. Also, at small values of Re or Pr, as expected, the value of Nu_L shows virtually no changes as the surfaces of the cylinder is transverse from the front ($\theta = 0^o$) to the rear ($\theta = 90^o$) stagnation points (Figs. 7.5a and 7.6a). This is because, at a low value of Re and/or Pr, heat transfer occurs mainly by conduction as compared to convection. Further, there is an increase in Nu_L with increased value of Re and/or Pr across all the fluid volume fractions. The maximum value of Nu_L can be seen in Fig. 7.5 at Pr = 100, Re = 40 and ϕ_f = 0.70. The above local thermal features from the downstream cylinder (C_2) (Figs. 7.7 and 7.8) are prejudiced with Re or Pr in a manner analogous to that of the upstream cylinder (C_1) except at Re = 1, Pr = 1 for ϕ_f = 0.70, where heat transfer happens mostly by conduction as compared to convection.

The power-law index also displays a great impact on the values of Nu_L. For the shear-thinning fluids with a given values of Re, Pr and ϕ_f , both cylinders show an improvement of heat transfer for the reducing value of n (or rising shear-thinning behavior) and as a result, an increasing value of Nu_L can be seen in Figs. 7.5-7.8. However, the shear-thickening fluids display the reverse trend in contrast to shear-thinning fluids, i.e., the Nu_L reduces with an increasing value of n. This examination also reveals that the influence of flow behavior index is greater in the shear-thinning as contrast to shear-thickening fluids. Such features are also noted on a single cylinder (Bharti et al., 2007a).

Moreover, the Nu_L for the periodic cylinders (C_1 and C_2) strongly depends on fluid volume fractions and displays the subsequent special characteristics. The opposite behavior can be seen in Figs. 7.6 and 7.8 at the maximum fluid volume fractions of 0.99 for Re = 40 with respect to the lower fluid volume fractions and lower Reynolds numbers. Such a feature once again reveals that both cylinders act as an isolated cylinder under the maximum fluid volume fractions and high Re and/or Pr. The above typical variations of isotherm pattern and local Nusselt number with the Re, Pr and ϕ_f observed herein, in turn, will alter with average or overall heat transfer. It is explored in subsequent sections with the help of global behaviours such as the average Nusselt number and the Colburn j_H factor and their dependence on the flow governing parameters (n, Re, Pr and ϕ_f).

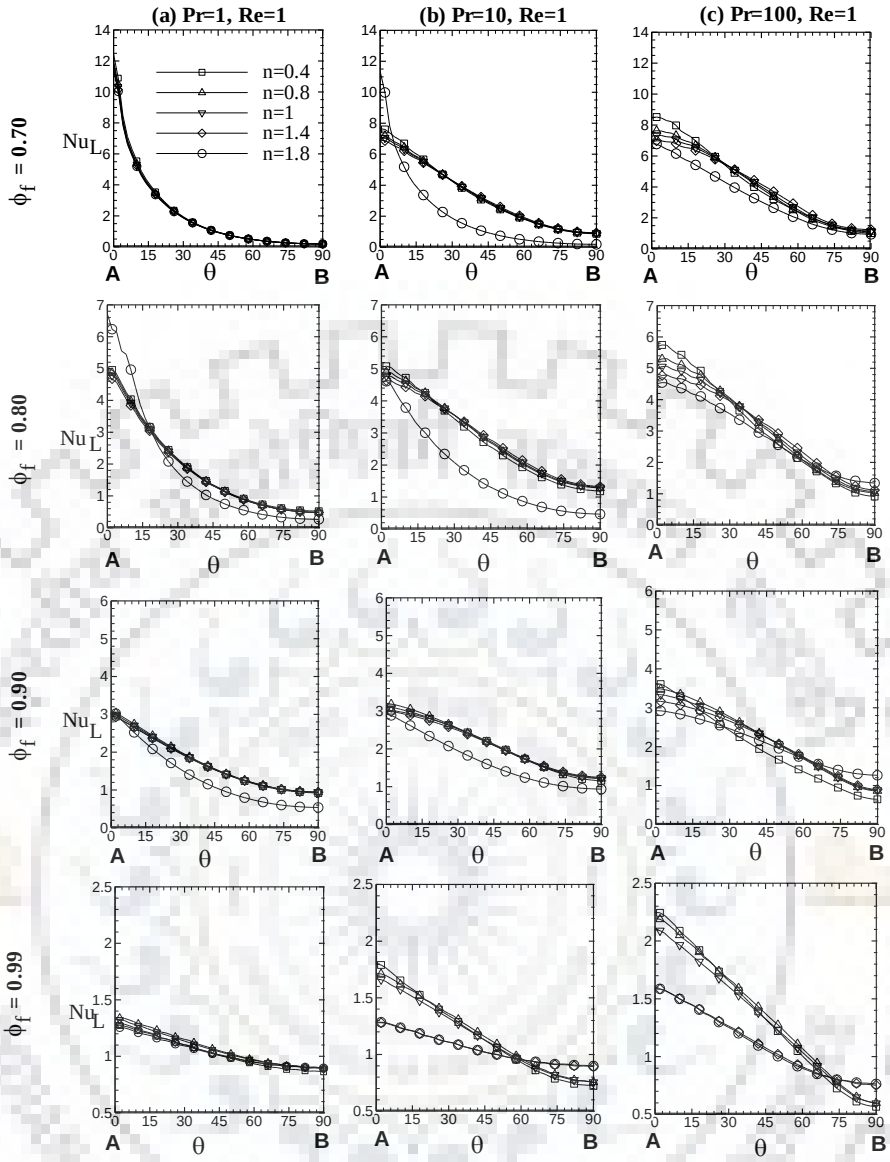

Figure 7.5: Dependence of local Nusselt number (Nu_L) on fluid volume fraction and power-law index at Re = 1 and Pr = 1, 10 and 100 over the surfaces of upstream cylinder 1 (C_1)

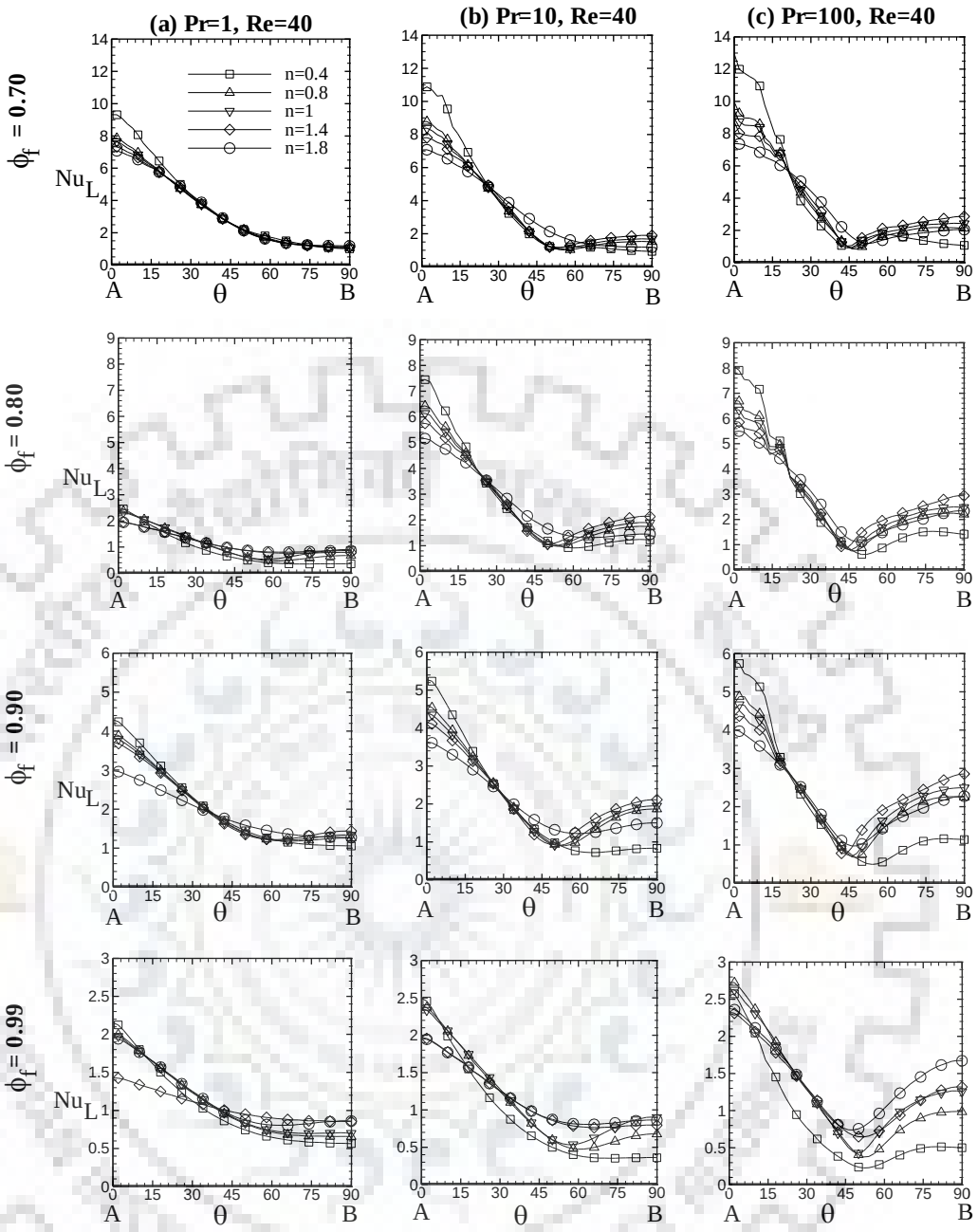

Figure 7.6: Dependence of local Nusselt number (Nu_L) on fluid volume fraction and power-law index at Re = 40 and Pr = 1, 10 and 100 over the surfaces of upstream cylinder 1 (C_1)

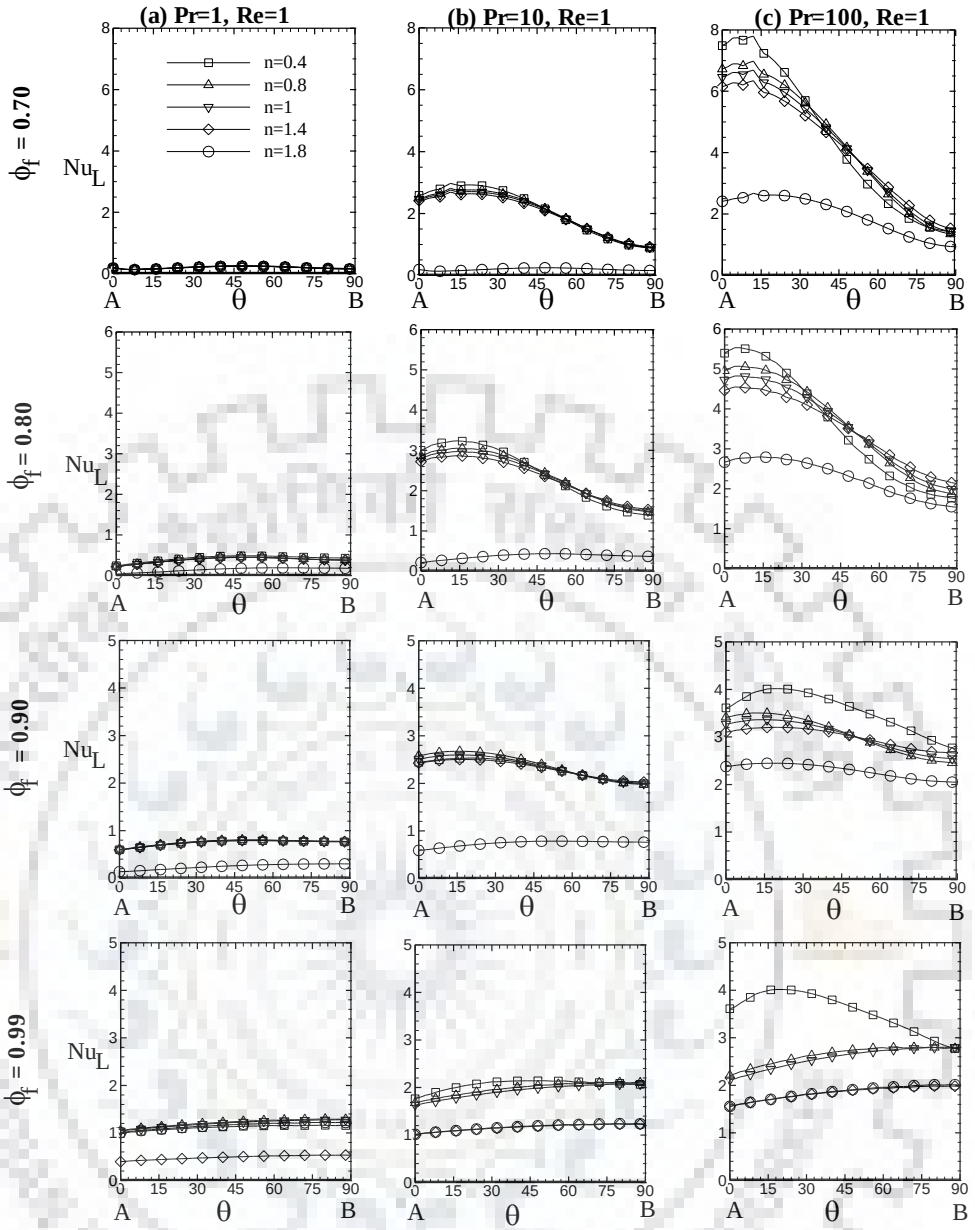

Figure 7.7: Dependence of local Nusselt number (Nu_L) on fluid volume fraction and power-law index at Re = 1 and Pr = 1, 10 and 100 over the surfaces of downstream cylinder 2 (C_2)

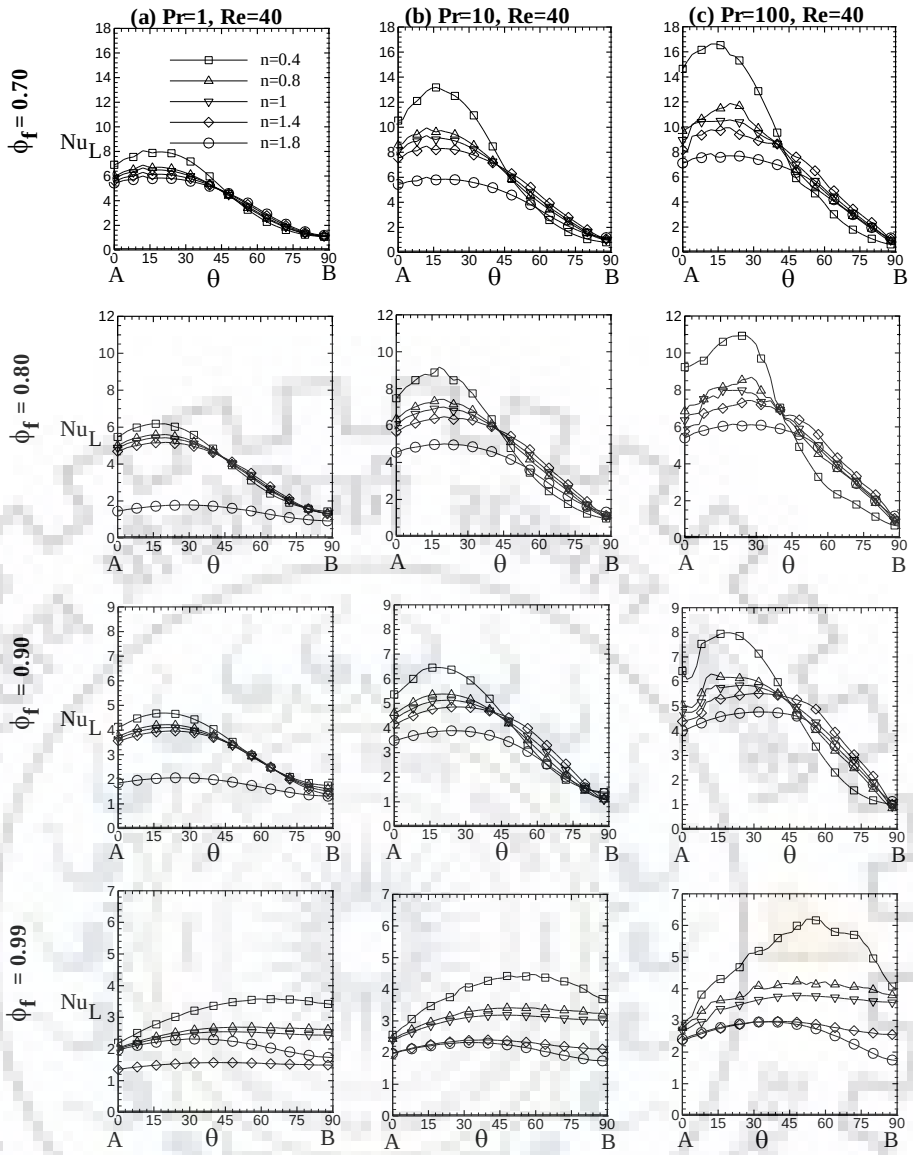

Figure 7.8: Dependence of local Nusselt number (Nu_L) on fluid volume fraction and power-law index at Re = 40 and Pr = 1, 10 and 100 over the surfaces of downstream cylinder 2 (C_2)

7.4 Average Nusselt number

The variation in average Nusselt number (Nu) is strongly dependent over Re, Pr, n and ϕ_f as shown in Tables B1-B3 (Appendix-B). From an inspection of these results, the general trends emerged are as follows:

As the value of n reduces (increasing shear-thinning nature), the surface average Nusselt number increases and accordingly an upturn in heat transfer has been noticed. Particularly, in the shear-thinning regions, the fluid particles follow an additional flow oriented path due to which the comparative significance of the diffusion transport rises. It explicates a cause of enhancement in the Nu with shear-thinning nature (Daniel and Dhiman, 2013).

The average Nusselt number reduces gradually with the rise in ϕ_f, which reveals the point that the resultant velocity and temperature gradients reduce with a rise in fluid volume fractions. This is linked to the strong dependence of Nu on ϕ_f, which yields sparse and steeper velocity and temperature gradients in smaller and higher fluid volume fractions, respectively. For instance, at Re = 1, Pr = 100, n = 0.4, ϕ_f = 0.70, the Nu value is 4.2920 which altered to a value of 2.7015 for ϕ_f =0.90 and to 2.1768 for ϕ_f = 0.99 (Table B3). Thus, an enhancement in the Nu is found to be approximately 97% in the shear-thinning region between the minimum (ϕ_f = 0.70) and maximum (ϕ_f = 0.99) values of fluid volume fractions for the highest value of Pr and the lowest values of Re and n. The corresponding Nu values for Re = 40 are 6.1657, 3.4670 and 2.6606 at ϕ_f = 0.70, 0.90 and 0.99, respectively. Here, an enhancement of 131% is observed under the identical conditions. This again suggests a stronger influence of Re in a dense medium than that in a sparse medium.

However, the reverse patterns are obtained for the shear-thickening fluids (increasing value of n). The increasing level of shear-thickening behavior decreases the average Nusselt number and showing a varying diminishment in heat transfer. For example, at Re = 1, Pr = 100, n = 1.8, ϕ_f = 0.70, the Nu value is 2.7069 which altered to a value of 2.1854 for ϕ_f = 0.90 and to 1.4820 for ϕ_f = 0.99 (Table B3). Again, an enhancement of about 83% has been observed in the shear-thickening region. The corresponding Nu values for Re = 40 are 4.5061, 2.9828 and 2.0012 at ϕ_f = 0.70, 0.90 and 0.99, respectively. In general, a different level of variations in average Nusselt number has been seen owing to shear-thinning and shear-thickening behaviors. Further, at low Re, the change in Nu is small as compared to high Re and it is related to the point that in such situations the heat transfer is mostly by conduction and it is free of the fluid viscosity. It, therefore, does not matter whether the type of fluid is Newtonian or non-Newtonian (Mangadoddy et al., 2004). This again is similar with the features found in the mass transfer in non-Newtonian fluids for the spherical particles (Chhabra et al., 2001) and a bundle of cylinders (Ferreira and Chhabra, 2004). Yet, with a gradual increase in Re, the Nu starts to increase steadily. For instance, at Re = 1, Pr = 10, n = 0.4 and ϕ_f = 0.70, the Nu value is 3.1265, while the corresponding values of Nu are 4.6045 and 5.2934 at Re = 10 and 40, respectively (Table B2). Similarly, for Re = 1, Pr = 10, n = 1.8 and ϕ_f = 0.70, the Nu value is 1.5951, while the corresponding values of Nu are 2.7817 and 3.7374 at Re = 10 and 40, respectively (Table B2). The above rise in Nu occurs because of the higher fluid velocity with increasing value of Re,

which eventually provides quick movement of the fluids and increased rate of convection and thus leads to improved heat transfer from the cylinder surfaces.

Further, for a given Re, n and ϕ_f , the Nu increases with an increase in Pr, but at different rates subject to the various values of Re, n and ϕ_f . As an illustration, in the shear-thinning region (n = 0.4), at ϕ_f = 0.70, Re = 1, the values of Nu are 2.2128 and 4.2920 corresponding to Pr = 1 and 100, respectively. Almost similar behavior can be observed for Newtonian as well as shear-thickening fluids for the analogous conditions. It is convenient to mention herein that the aforesaid inter-dependencies of n, ϕ_f , Re and Pr are very similar and consistent with the results reported in the literature (Kawase and Ulbrecht, 1981a, b; Zhu, 1995; Satish and Zhu, 1992).

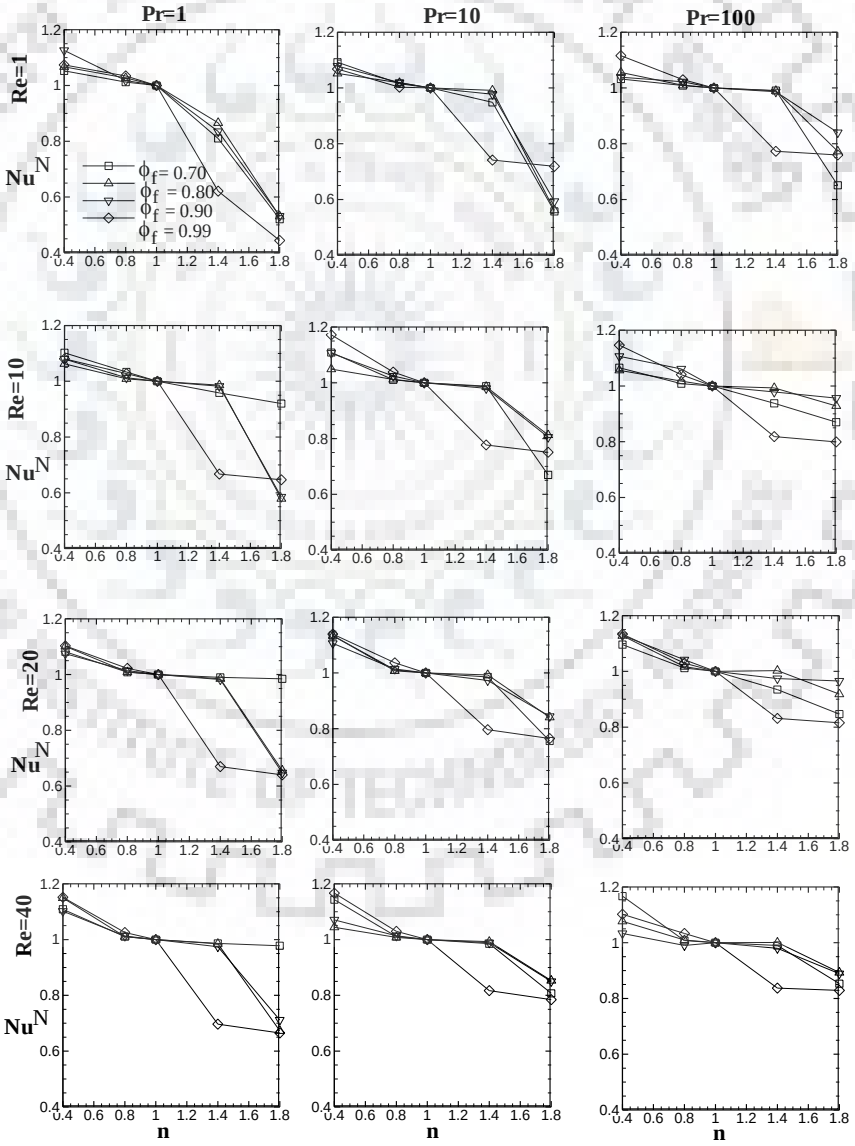

Figure 7.9: Dependence of normalized average Nusselt number (Nu^N) vs. power-law index (n) on fluid volume fraction, Reynolds number and Prandtl numbers (Nu is normalized with Newtonian value)

The above thermal characteristics were further examined by normalizing the Nu with different parameters. For instance, the influence of flow behavior index on thermal features was examined by normalizing the averaged Nusselt numbers with their corresponding Newtonian values:

$$X^N = \frac{X(n)}{X(n=1)}; \qquad \text{where,} \quad X=Nu \tag{7.1}$$

Fig. 7.9 depicts the variations of normalized averaged Nusselt number (Nu^N) over the Re, Pr, n and ϕ_f . For a fixed Re, Pr and ϕ_f , an improvement of heat transfer with the reducing n can be seen; so the normalized Nusselt numbers X^N are observed to be greater than 1 for shear-thinning nature; whereas, a reverse trend has been seen to the shear-thickening nature, i.e., $X^N < 1$. Thus, the effect of n is greater in shear-thinning nature than the shear-thickening nature.

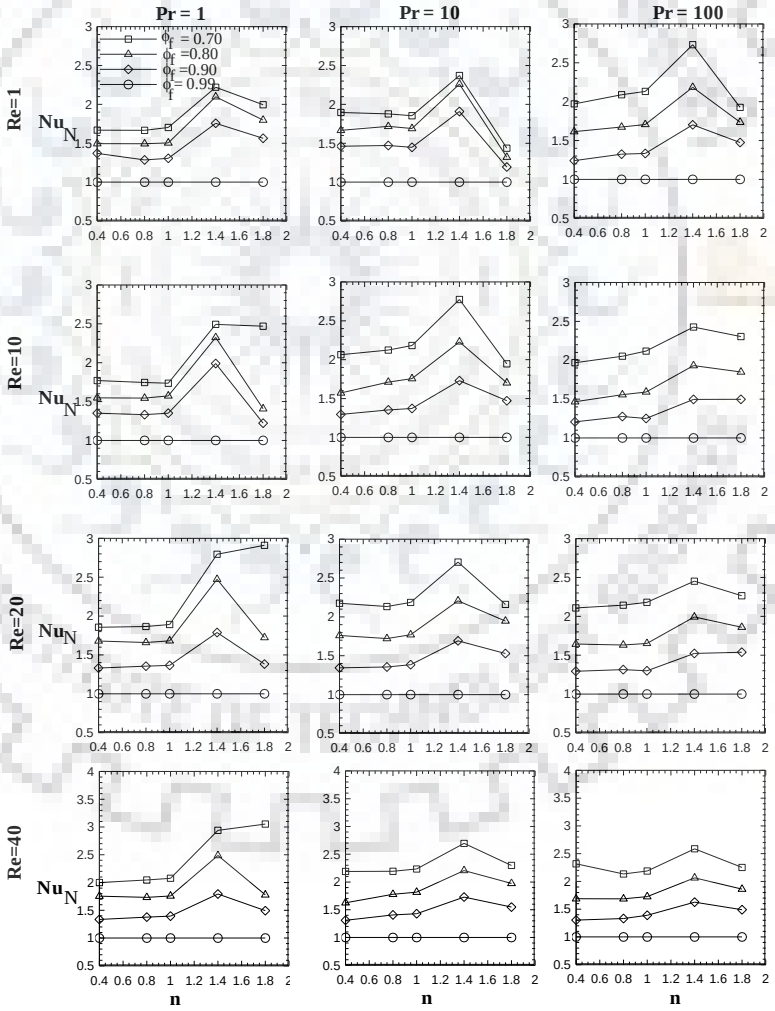

Figure 7.10: Dependence of normalized average Nusselt number (Nu_N) vs. power-law index (n) on fluid volume fraction, Reynolds and Prandtl numbers (Nu is normalized with maximum fluid volume fraction $\phi_{f,max}$ = 0.99)

Moreover, to measure the level of interaction between both of periodic cylinders, the Nu values were further normalized using the maximum fluid volume fraction ($\phi_{f,max} = 0.99$) as:

$$X_N = \frac{X(\phi_f)}{X(\phi_{f,max})} \tag{7.2}$$

Fig. 7.10 displays the variations of Nu_N with Re, Pr, n and ϕ_f. As the fluid volume fraction increases, the Nu_N decreases and approaches unity and thereby both cylinders display the feature of an isolated single cylinder. For example, at Re = Pr = 1, as the fluid volume fraction increases from 0.70 to 0.99, the normalized value of average Nusselt number changes from 1.6 to 1, 1.7 to 1, and 2 to 1 at n = 0.4, 1, and 1.8, respectively. At smaller fluid volume fractions and Re, greater values of Nu at $\phi_f = 0.70$ in contrast to $\phi_f = 0.99$, specify a substantial influence in the Nu for the upstream cylinder (C_1) because of the existence of the downstream cylinder (C_2). An increasing Re and/or Pr increases the Nu_N under similar situations. It happens apparently because of the growing wake region in the vicinity of cylinders.

Additional endeavor has been done to represent the functional dependence of Nu over the parameters above (Re, Pr, ϕ_f and n) in terms of suitable correlations. The statistical analysis (based on 432 data points for each n) of the current numerical results conceded the following correlations:

$$Nu = an^b \phi_f^c Re^d Pr^e + f \exp(\phi_f) \qquad \text{for } n < 1 \text{ and } n > 1 \tag{7.3a}$$

$$Nu = \alpha Re^b Pr^c \quad \text{where,} \quad \alpha = [a + d\phi_f^e (RePr)^f] \qquad \text{for } n = 1 \tag{7.3b}$$

The correlation coefficients and exponents (a, b, c, d, e and f) along with their statistical parameters have been given in Table 7.2. These correlations have been developed by the non-linear regression of the numerical data. The best fit for the extreme values of n between present numerical data and the predictions of Eq. 7.3(a) is displayed in Fig. 7.11, where an excellent correspondence can be observed. An average deviation within 2% was noticed for the 97% data points, whereas the maximum deviation was within the 5% under the identical conditions. The above deviations are lie within 5-12% for the 3% of data points. Notwithstanding, many studies across periodic array of circular cylinders and/or over tube banks are reported in the literature (Spelt et al., 2005a, b; Dhotkar et al., 2000; Vijaysri et al., 1999; Shibu et al., 2001; Malleswara Rao and Chhabra, 2003; Chhabra et al., 2000; Ferreira and Chhabra, 2004). Among these studies, no one is exactly the same which could be compared directly with the present study of power-law fluids.

Table 7.2: Correlation constants yielded in functional dependence of average Nusselt number (Nu) (Eq. 7.3) and the Colburn j_H factor (Eq. 7.4) (δ: relative r.m.s deviations from the numerical data; number of data points: 432 for each of Nu and j_H)

Correlation constants	Nu						j_H					
	n → 0.4	0.6	0.8	1	1.4	1.8	0.4	0.6	0.8	1	1.4	1.8
a	1.1845	0.8432	0.7965	17.1857	0.8278	0.5346	-0.5026	-0.1171	-1.8530	1.2790	-0.6092	-0.9784
b	-0.7083	-2.1270	-5.1552	0.1608	5.3894	2.2251	-3.3772	-8.7029	-7.5658	1	4.6437	2.2272
c	-1.3918	-1.2290	-1.2138	0.1599	-0.4722	-0.9767	-0.7595	-0.7384	-0.7247	0.6703	-0.4701	-0.5312
d	0.0725	0.0603	0.0594	-15.7552	0.03679	0.0892	-0.8123	-0.7983	-0.7878	1.2718	-0.7020	-0.6072
e	0.0573	0.0526	0.0522	0.1669	0.03282	0.0829	0.0193	0.0203	0.0192	-0.2178	0.0495	0.0212
f	-0.3164	-0.431	-0.459	0.0061	-1.5470	-0.5197	5.9188	7.5264	9.5056	0.0304	5.1440	6.2874
g	-	-	-	-	-	-	-0.8179	-0.8057	-0.7959	-2.1283	-0.7335	-0.6281
R^2	0.9374	0.9480	0.9469	0.9665	0.9085	0.9112	0.99	0.9920	0.9928	0.9937	0.9845	0.9865
δ_{max} (%)	12.58	11.87	11.97	11.37	12.98	12.97	5.37	5.33	5.33	5.33	5.86	5.68
δ_{avg} (%)	5.70	5.06	5.10	5.69	5.88	5.84	2.75	2.70	2.70	2.70	2.89	2.86

For instance, Spelt et al. (2005a, b) are concerned with flow characteristics of power-law fluids such as drag coefficients, velocity variances, etc. Similarly, Dhotkar et al. (2000), Vijaysri et al. (1999) and Shibu et al. (2001) have explored the flow features of non-Newtonian fluids for various porosities of cylinders using different cell models, etc. However, a good correspondence has been found with the Newtonian fluids (Gamrat et al., 2008; Chen and Wung, 1989; Martin et al., 1998; Mandhani et al., 2002; Mangododdy et al., 2004) within the ranges of conditions covered herein. For instance, Martin et al. (1998) examined the averaged Nusselt number for convective cross-flow of air (Pr = 0.7) across the sparse periodic arrays (ϕ_f > 0.8) of cylinders in laminar region. A good agreement can be seen in Figure 7.12(a) between the present results and that of Martin et al. (1998), where an improved convergence can be seen with increasing values of fluid volume fractions (ϕ_f) with maximum deviations of 6.5%. Further, Gamrat et al. (2008) presented the thermal features across an array of square rods for the fluid volume fractions of 0.44 to 0.88 and inertial effects (Re) up to 40. Their result for Nu is 2.8925 against the present results of 2.8832 at ϕ_f = 0.86, Pr = 100 and Re = 1, shows an excellent agreement in Fig. 7.12(b) with a variance of 0.32 % only. Additional consistency was found with the free surface cell model of Mangadoddy et al. (2004). A good analogy can also be seen in Fig. 7.12(b) for Pr = 5 and Re = 1 at the extreme conditions of fluid volume fractions. It can be seen that the convergence is again improving as the fluid volume fraction is increasing from ϕ_f = 0.70 to 0.99. The maximum deviation was found to be in the order of 3%. In spite of the above good agreement, the additional endeavor has been made to delimit the role of governing parameters (n, ϕ_f , Re, Pr) by expressing the Nu in terms of the Colburn heat transfer factor (j_H) as described in the next section.

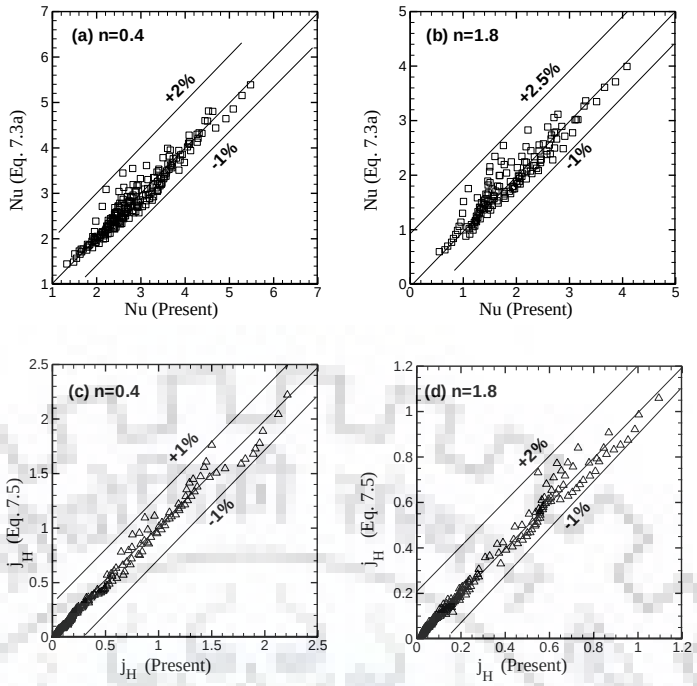

Figure 7.11: Best fit of present numerical vs. correlation values of Nu and j_H for the extreme values of power-law index (a, c) n = 0.4 and (b, d) n = 1.8

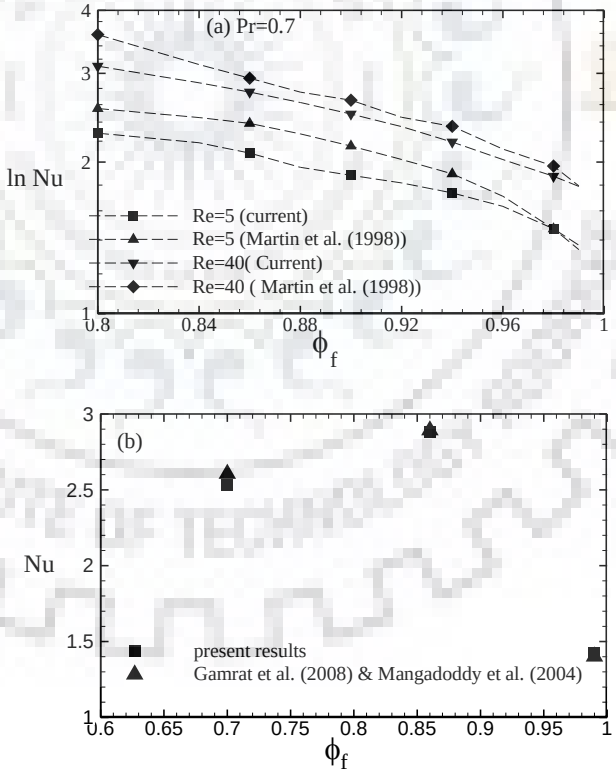

Figure 7.12: Contrast between present results of the average Nusselt number (Nu) with (a) periodic array of circular cylinders of Martin et al. (1998) and (b) free surface cell models of Mangadoddy et al. (2004) and with the results of Gamrat et al. (2008) in the Newtonian flow regime

7.5 The Colburn heat transfer factor (j_H)

The functional dependence of current numerical results on Re, Pr, n and ϕ_f using the j_H factor (as defined in chapter 5, Eq. 5.4) is best represented by a correlation given by Eq. (7.4):

$$j_H = an^b \phi_f^c Re^d Pr^e + f (n \phi_f Re)^g \quad (7.4)$$

The correlation coefficients and exponents (a, b, c, d, e and g) along with their statistical parameters to the current data are also included in Table 7.2. This correlation has been developed by the non-linear regression of the data. The best fit for the extreme values of flow behavior index between current numerical data and the predictions of Eq. (7.4) is also displayed in Fig. 7.11 where a good agreement is seen to exist. The average and maximum deviations are within 2% and 5%, respectively for complete ranges of data points. Although this method not only merges data for a broad range of Pr, but the causing deviations are too rather lower as compared to Eq. (7.3).

Overall, the heat transfer and/or thermal features of power-law fluids across a periodic array of cylinders in cross-flow are observed to be prejudiced in a complicated manner with the Re, Pr, n and ϕ_f . At high Re, the wake interventions are more noticeable when the fluid volume fractions are lower. Additionally, while the cylinders are far away as in the case of maximum fluid volume fraction (ϕ_f = 0.99), no wake interference happens and both cylinders behave as a single isolated cylinder. Further, the shear-thinning and shear-thickening fluid behaviors which have been elucidated from present periodic geometry have also displayed the distinguished thermal features with the varying porosity and/or fluid volume fractions of the cylinders. It is assumed that the addictions above on the power-law index and porosity are accountable too for the non-monotonous behavior as appreciated in this investigation. Lastly, it is essential to point out that the forced convection features of Newtonian fluids (Chapter 5) and non-Newtonian fluids (Chapters 6 and 7) have been elaborated widely, but the mixed convection features of these fluids are also equally important and therefore are discussed in next two Chapters 8 and 9 to know the more physical insights of these fluids.

Chapter 8

AIDING BUOYANCY MIXED CONVECTION CHARACTERISTICS OF NEWTONIAN FLUIDS ACROSS PERIODIC ARRAY OF CIRCULAR CYLINDERS

This chapter deals with the mixed-convection flow across a periodic array of circular cylinders to reveal the flow and heat transfer features of Newtonian fluids under the aiding buoyancy condition. The schematic and mess geometries are shown in Figs. 3a and 3b of Chapter-3. The governing equations (as mentioned in Chapter-3) are applied with the n = 1 for the case of Newtonian fluids. The study examines the dependence of local and global characteristics for the following ranges of governing parameters: Re = 1, 2, 5, 10, 20, 40; Pr = 0.7, 1, 10, 50 and Ri = 0, 1and 2 and with a wide variation of fluid volume fractions of ϕ_f = 0.70, 0.75, 0.80, 0.84, 0.86, 0.88, 0.90, 0.92, 0.94, 0.96, 0.98 and 0.99. In the mixed convection problem, the gravity and buoyancy forces are acting in opposite directions of each other which can be seen in Fig. 3(a) and so the role of buoyancy parameter in terms of Richardson number (Ri) has been investigated within the ranges of conditions. The influences of these dimensionless flow governing parameters on the streamlines and isotherm patterns, pressure coefficient, individual and total drag coefficients and local and averaged Nusselt numbers are presented and discussed to gain physical insights from such an industrially important system. However, prior to presenting the detailed new results, the numerical solution procedure has been validated first in the next section.

8.1 Validation of numerical solution procedure

It is to be imperative to point out the fact that there is no direct study available to contrast the mixed convection flow and heat transfer of Newtonian fluids across the periodic array of cylinders. Perhaps, an endeavor has been made to contrast the present results with the available literature on single cylinder because at the maximum fluid volume fraction of ϕ_f = 0.99 both the periodic cylinders acts as a single isolated cylinders. For instance, in the case of forced convection (Ri = 0), Mandhani et al. (2002) compared the heat transfer (local Nusselt number) for ϕ_f = 0.99 with a single cylinder of Eckert and Soehngen (1952) and Lange et al. (1998). A good agreement was found. Similarly, the flow and heat transfer characteristics of Soares et al.

(2005b) and Bharti et al. (2007a) the single circular cylinder was found to be consistent with the maximum fluid volume fraction of $\phi_f = 0.99$ for the forced convection cases.

In view of above, the relevant comparison for mixed convection has been summarized in Table 8.1. The present numerical results obtained for drag coefficient (C_D) under steady flow conditions (Pr = 1, Ri = 2), were found to be consistent with the numerical results of Srinivas et al. (2009) at Re = 1, showing a maximum discrepancy of 2.82%. Further, under the identical conditions, a good agreement (maximum discrepancy of 3.36%) was found with the results of Srinivas et al. (2009) and Chandra and Chhabra (2012) at Re = 40. Likewise, at Pr = 1 and Ri = 1, the values of drag coefficient again display a good correspondence with the results of Srinivas et al. (2009) at Re = 1 and 40, showing maximum discrepancies of 2.29% and 0.76%, respectively.

Table 8.1: Comparison of present results of total drag coefficient (C_D) and average Nusselt number (Nu) with literature values for the mixed convection Newtonian flows across the periodic array of cylinders at the maximum fluid volume fractions of $\phi_f = 0.99$

Source	Ri=2, Pr=1			Ri=1, Pr=1		
	C_D (Re=1)	C_D (Re=40)		C_D (Re=1)	C_D (Re=40)	
Present Results	37.8053	3.6980		27.9522	2.9814	
Srinivas et al. (2009)*	38.8716	3.8225		28.5949	2.9586	
Chandra and Chhabra** (2012)	-	3.796		-	-	
% deviations	2.82	3.36		2.30	0.76	
	Ri=2			Ri=1		
	Pr=1	Pr=50		Pr=1	Pr=50	
	Nu (Re=1)	Nu (Re=1)	Nu (Re=40)	Nu (Re=1)	Nu (Re=1)	Nu (Re=40)
Present Results	1.2108	3.2350	16.1826	1.0504	3.0529	14.8162
Srinivas et al. (2009)*	1.1816	3.1662	16.1785		2.9976	15.1594
Soares et al. (2009)*	-	-	-	1.0300	-	-
Daniel and Dhiman (2013)***	-	-	-	-	2.9978	15.1479
% deviations	2.41	2.12	0.03	1.94	1.81	2.31

Single cylinder; ** semi-circular cylinder; *** two tandem cylinders

Moreover, an excellent agreement was found for the average Nusselt number with the results of Srinivas et al. (2009), Soares et al. (2009) and Daniel and Dhiman (2013) in Table 8.1. For instance, at Pr = 1 and Ri = 2, the present result was in good agreement with Srinivas et al. (2009) with a maximum deviation of 2.41%. Next, at Pr = 50 and Ri = 2, these deviations were found to be 2.12% and 0.025% at Re = 1 and 40, respectively. Similarly, at Pr = 1, Ri = 1, an excellent agreement was found with the result of Soares et al. (2009) with a maximum discrepancy of 1.94% at Re = 1. For Pr = 50 and Ri = 1, a very good agreement was seen with the results of

Srinivas et al. (2009) and Daniel and Dhiman (2013) with maximum deviations of 1.81% and 2.31% at Re = 1 and 40, respectively. Given above excellent agreement with the literature, the present results were generated for the complete range of parameters studied herein.

8.2 Fluid flow and heat transfer characteristics

The microscopic features of flow and heat transfer for the mixed convection under aiding buoyancy conditions have been discussed in this section.

8.2.1 Streamline profiles

The qualitative dependence of normalized streamline (as defined in Chapter 5, Section 5.2.1) patterns have been shown in Figs. 8.1-8.3 at Pr = 1, 10 and 50, respectively with the systematic variations of fluid volume fractions (ϕ_f = 0.70, 0.90 and 0.99), Reynolds (Re = 1, 10 and 40) and Richardson (Ri = 1 and 2) numbers. The wake size displays a complex behavior over the above governing parameters (ϕ_f , Re and Ri). It can be seen in Figs. 8.1-8.3, as the fluid volume fraction increases from ϕ_f = 0.70 to 0.99, the recirculation zone also increases correspondingly, results in the streamlines gradually shift towards the surface of the cylinders.

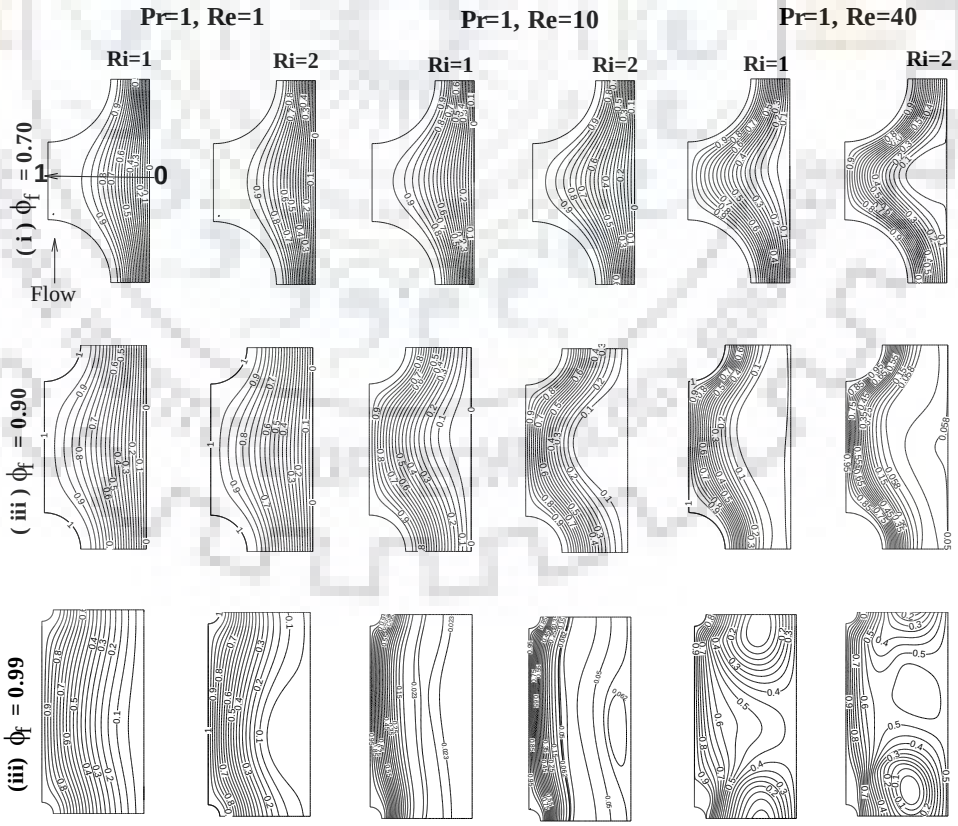

Figure 8.1: Representative variations of normalized streamlines at Pr = 1, Reynolds number (Re = 1 and 40), Richardson number (Ri = 1 and 2) and fluid volume fractions of (i) ϕ_f = 0.70 (ii) ϕ_f = 0.90 and (iii) ϕ_f = 0.99

For instance, at ϕ_f = 0.70 and Re = 1(Fig 8.1(i)), the streamlines are far from the cylinders, but as ϕ_f increases from ϕ_f = 0.70 to 0.90 and 0.90 to 0.99, a corresponding shift in streamlines towards cylinders can be seen clearly irrespective of Prandtl number. So, the crowding of isotherms is seen to be more over the surface of the cylinders for ϕ_f = 0.99 in Fig. 8.1(iii) for all the values of Reynolds and Richardson numbers. The same feature is observed at Pr = 10 and 50 in Figs. 8.2 and 8.3 respectively under the identical conditions.

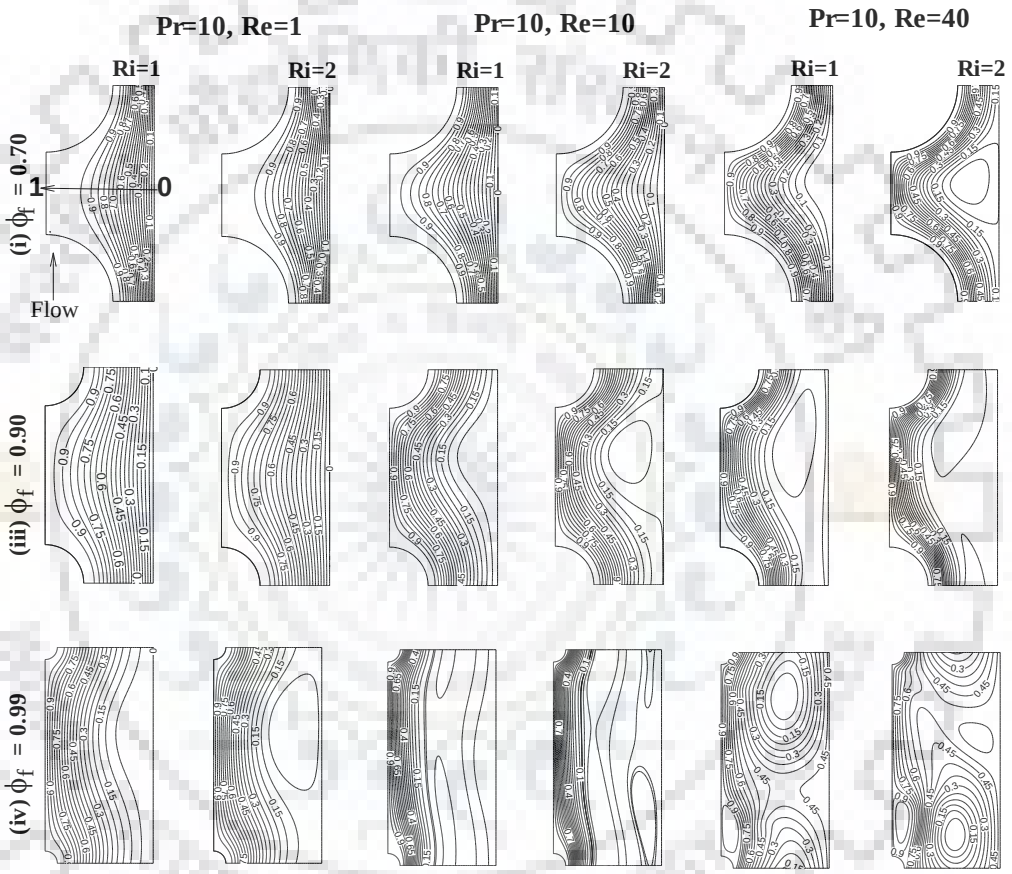

Figure 8.2: Representative variations of normalized streamlines at Pr = 10, Reynolds number (Re = 1 and 40), Richardson number (Ri = 1 and 2) and fluid volume fractions of (i) ϕ_f = 0.70 (ii) ϕ_f = 0.90 and (iii) ϕ_f = 0.99

The impact of increased Reynolds number can be appreciated over the streamlines. As the Reynolds number increases from Re = 1 to 10 or 10 to 40 (Figs. 8.2-8.3), the fluid circulation in the vicinity of cylinders is seen to increase which further shifts the streamlines towards cylinders and therefore, more curved and dense streamlines can be seen in the vicinity of periodic cylinders. This behavior reflects that the discharges between two consecutive streamlines increase as the

Reynolds number and fluid volume fractions increase. An influence of buoyancy parameter (Ri) was also observed strongly over the streamlines. In Figs. 8.1-8.3, more pronounced streamlines can be seen at Ri = 2 in contrast to Ri = 1, for all the values of fluid volume fraction (ϕ_f). Hence, an increase in Ri yields denser and swirled streamlines which indicate the magnitude of increased buoyancy/mixing in Figs. 8.1-8.3. Further, for a given value of Ri, as Reynolds number increases, the recirculation improves in size and so the streamlines are clustered over the surface of the cylinders. Almost analogous patterns have been observed for all the fluid volume fractions, but the influence and visibility are more prominent at higher fluid volume fractions and Reynolds numbers. As opposed to the forced convection, the influence of Prandtl number over the flow field is also significant in mixed convection because of the linkage between flow and energy equations. As the Prandtl number increases from Pr = 1 to 10 and 10 to 50 (Figs. 8.2 and 8.3), the size of wake decreases which gives rise to more swirl and vortex formation. These effects can be visualized more at higher fluid volume fractions and Reynolds numbers in Fig. 8.3 at Re = 40 and ϕ_f = 0.90 and 0.99.

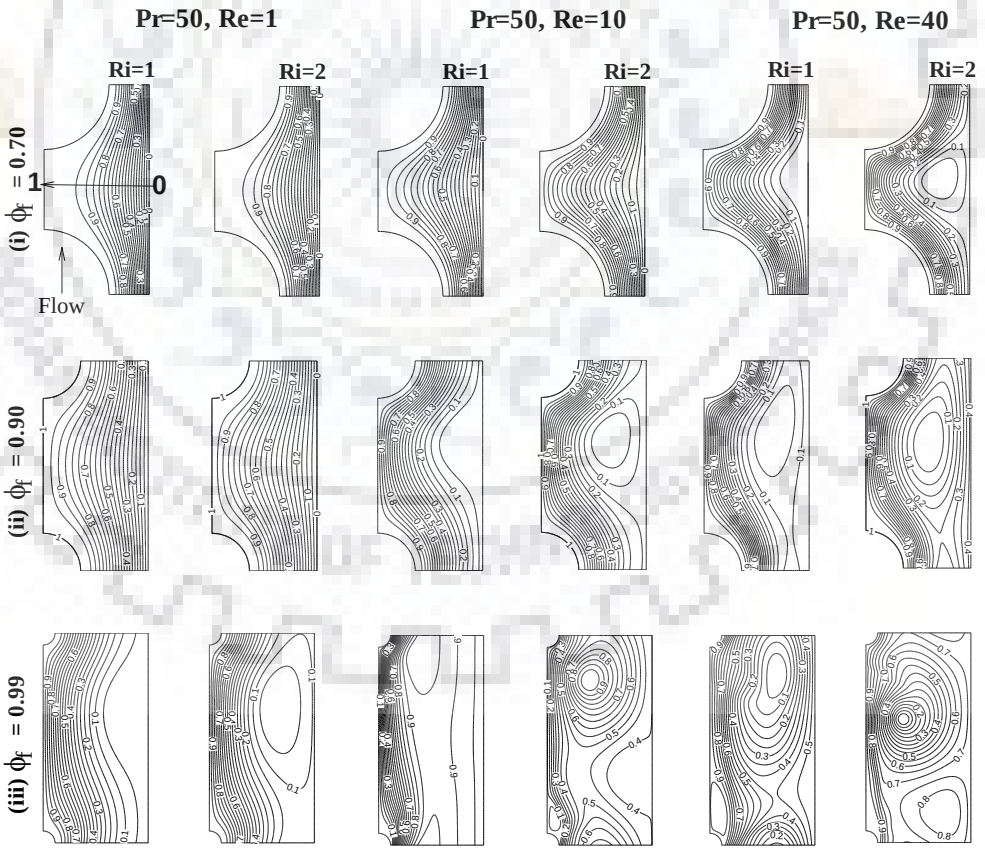

Figure 8.3: Representative variations of normalized streamlines at Pr = 50, Reynolds number (Re = 1 and 40), Richardson number (Ri = 1 and 2) and fluid volume fractions of (i) ϕ_f = 0.70 (ii) ϕ_f = 0.90 and (iii) ϕ_f = 0.99

Moreover, the streamlines display strong dependence at the low values of ϕ_f, as compared to the high value of ϕ_f. These streamline patterns are similar for mixed convection across a single cylinder and/or tandem cylinders (Badr, 1982, 1984; Soares et al., 2009; Daniel and Dhiman, 2013) or periodic array of cylinders (Gowda et al., 1998). Further, the above strong dependence of streamline patterns over ϕ_f, Re, Pr and Ri is additionally examined in terms of isotherm patterns over the surfaces of cylinders as described in the next Section.

8.2.2 Isotherm profiles

Figs. 8.4-8.6 illustrate the representative variations of the normalized isotherm patterns over the fluid volume fraction (ϕ_f), Reynolds (Re), Prandtl (Pr) and Richardson (Ri) numbers. In facts, these plots are the normalized values of temperature (as defined in Chapter 5, section 5.3.1). An examination of Figs. 8.4-8.6, clearly display a complex dependence of isotherm patterns over the above governing parameters. For a fixed value of ϕ_f (Figs. 8.4-8.6), the gathering of isotherms in the transverse direction has been grown up with an increase in Re and/or Pr. An increase in ϕ_f yields more clustered isotherms over the surfaces of the cylinders. However, the influence of the fluid volume fractions on isotherms is seen to be more prominent at higher Re and/or Pr. Further, the symmetric isotherm patterns at the low Re (e.g., Re = 1 in Figs. 8.4-8.6) suggest that the heat transfer is mainly by conduction in contrast to convection. At high Re (e.g., Re = 10 and 40) for ϕ_f = 0.70 and 0.90, isotherms are still symmetric, but these are denser and clustered as compared to Re=1. Moreover, the different behavior of isotherms are seen at Re = 40 and ϕ_f = 0.99 for both of the Pr and Ri. Also, steeper temperature gradients appear nearer to cylinders as Re increases. Furthermore, the impact of Richardson number (Ri) on the isotherm patterns is appreciable. It can be seen in Figs. 8.4-8.6, more pronounced isotherms appear for Ri=2 in contrast to Ri = 1, because as the Richardson number increases the level of buoyancy/mixing increases due to the more interactions among the fluid particle at the molecular level which results in an improvement in heat transfer. This effect is less visible at Re = 1 and Pr = 1, but as the Re and Pr increase, the influence of Ri is visible in the above figures. The above qualitative feature is similar to those found in the literature for mixed convection (Gowda et al., 1998) and under the limiting cases of a single cylinder (Soares et al., 2009; Daniel and Dhiman, 2013). This complex dependence of isotherm patterns has been further elaborated using pressure coefficient over the surfaces of periodic cylinders as described in the following section.

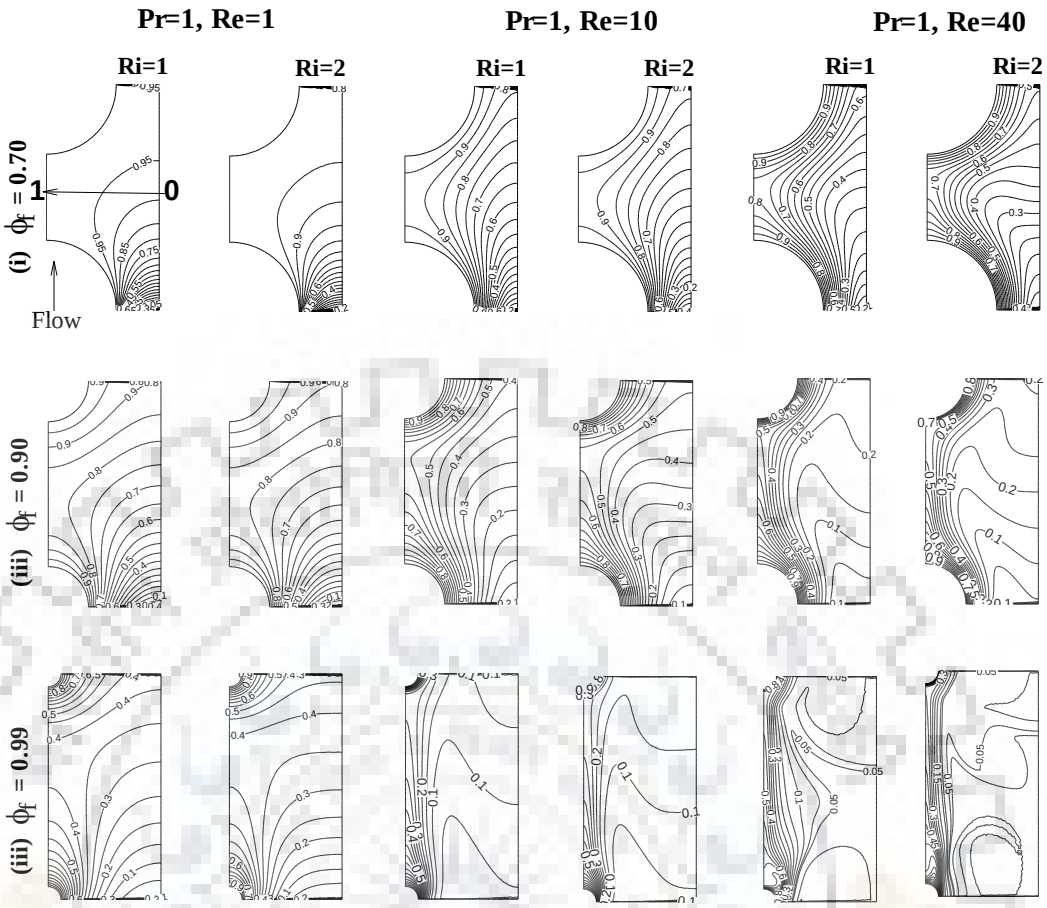

Figure 8.4: Representative variations of normalized isotherms at Pr = 1; Re = 1, 10 and 40; Ri = 1 and 2 and fluid volume fractions of (i) ϕ_f = 0.70 (ii) ϕ_f = 0.90 and (iii) ϕ_f = 0.99

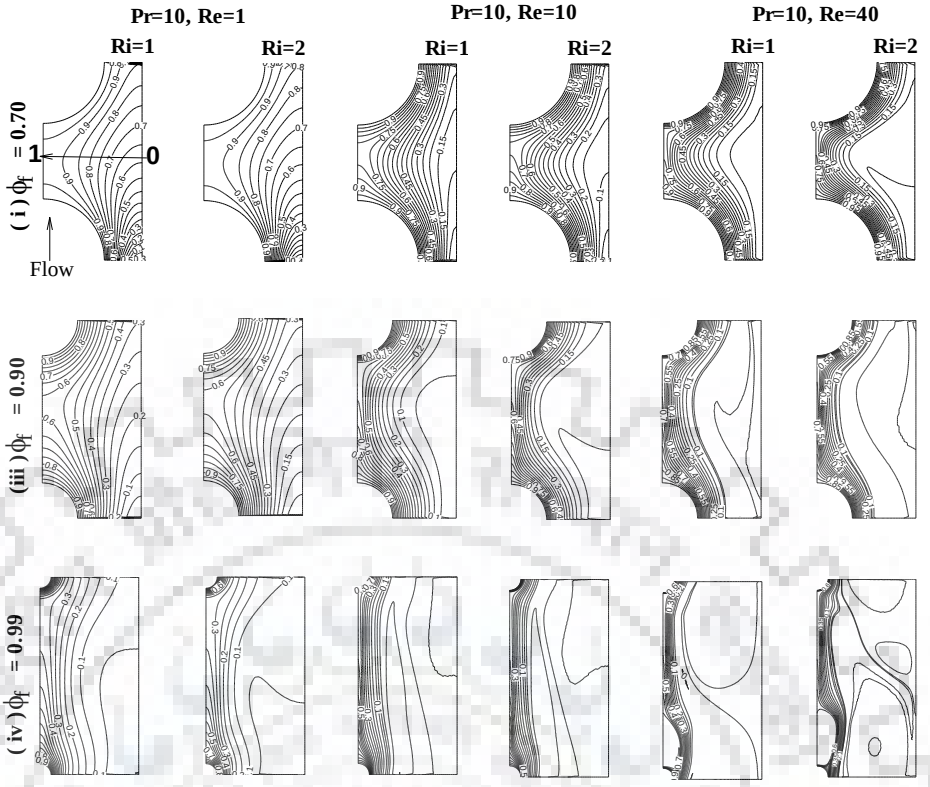

Figure 8.5: Representative variations of normalized isotherms at Pr = 10; Re = 1, 10 and 40; Ri = 1 and 2 and fluid volume fractions of (i) ϕ_f = 0.70 (ii) ϕ_f = 0.90 and (iii) ϕ_f = 0.99

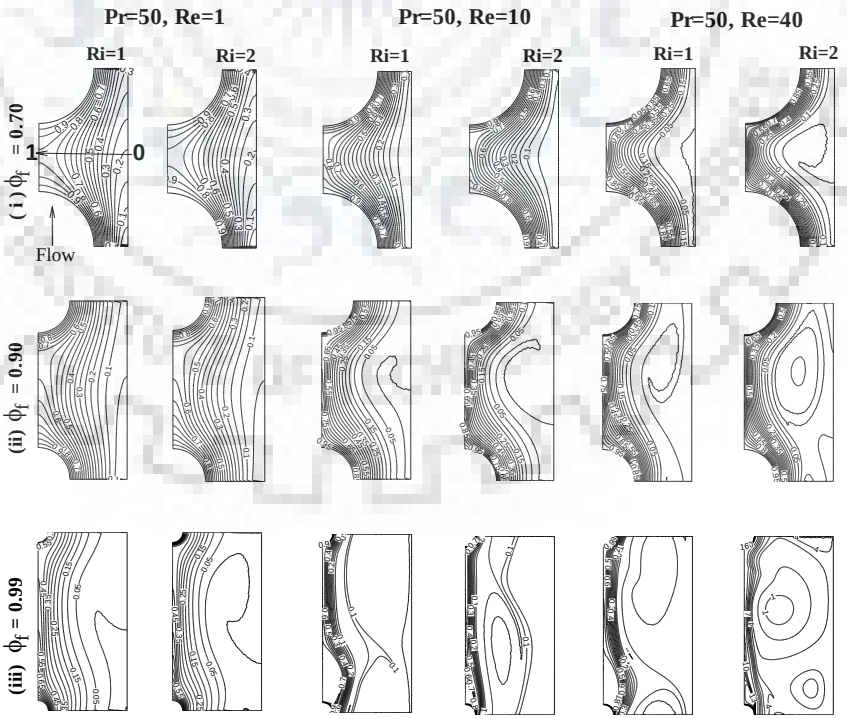

Figure 8.6: Representative variations of normalized isotherms at Pr = 50; Re = 1, 10 and 40; Ri = 1 and 2 and fluid volume fractions of (i) ϕ_f = 0.70 (ii) ϕ_f = 0.90 and (iii) ϕ_f = 0.99

8.2.3 Pressure coefficient (C_P) on the surfaces of the cylinders

The distribution of pressure coefficient over the periodic cylinders is displayed in Figs. 8.7 and 8.8 at Pr = 1 and 50, respectively with the systematic variations of Reynolds number (Re = 1 and 40), fluid volume fraction (ϕ_f = 0.70, 0.90 and 0.99) and buoyancy parameter (Ri = 1 and 2). At Pr = 1, Ri = 1, Re = 1 and ϕ_f = 0.70 (Fig. 8.7a (i)), the C_P for upstream cylinder (C_1) is observed to be dropped rapidly from its maximum value at the front stagnation point (θ = 5-10°) for along the surfaces followed by an increase due to the recirculation of the fluid in the rear side of the cylinder C_1

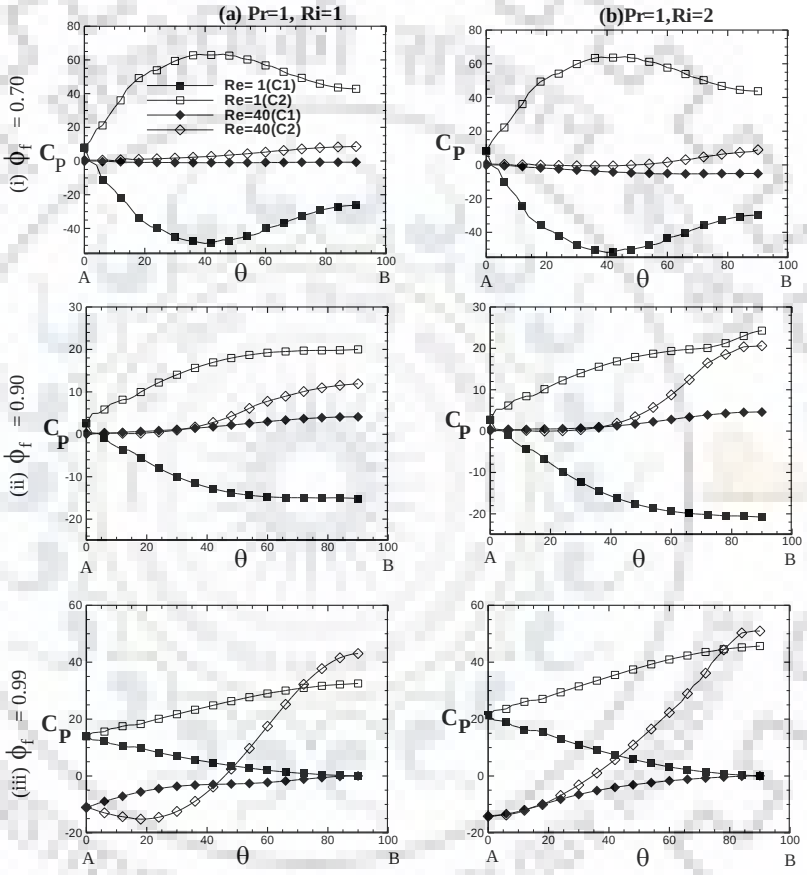

Figure 8.7: Dependence of pressure coefficient (C_P) over the surfaces of cylinders (C_1 and C_2) at Pr = 1 with the systematic variations of Richardson number (Ri = 1 and 2), fluid volume fractions (ϕ_f = 0.70, 0.90 and 0.99) and Reynolds number (Re = 1 and 40)

For instance, the minimum value of C_P occurs between θ = 35^0 to 45°, afterward, it starts increasing till θ = 90°. The above behavior was observed for both the value of Re 1 and 40, but the change in Re = 40 is very gradual as compared to Re = 1. Also, an increase in the Re tends to decrease the C_P over the surface of both the cylinders. Therefore, the minimum and maximum C_P were seen at Re = 1 for upstream cylinder (C_1) and downstream cylinder (C_2), respectively for both of the Ri = 1 and 2 (Figs. 8.7i a-b). Next, the effect of buoyancy parameter (Ri) was

observed in Figs. 8.7i-iii (a and b). An increased value of C_P was observed for Ri = 2 in contrast to Ri = 1 for all the value of fluid volume fractions and Reynolds numbers. The reason behind such behavior is that in the case of increased buoyancy, the magnitude of inertial effects increases which gives rise to pressure coefficient whereas the potential energy of the molecules also increases which again exerts more pressure over the surface of cylinders.

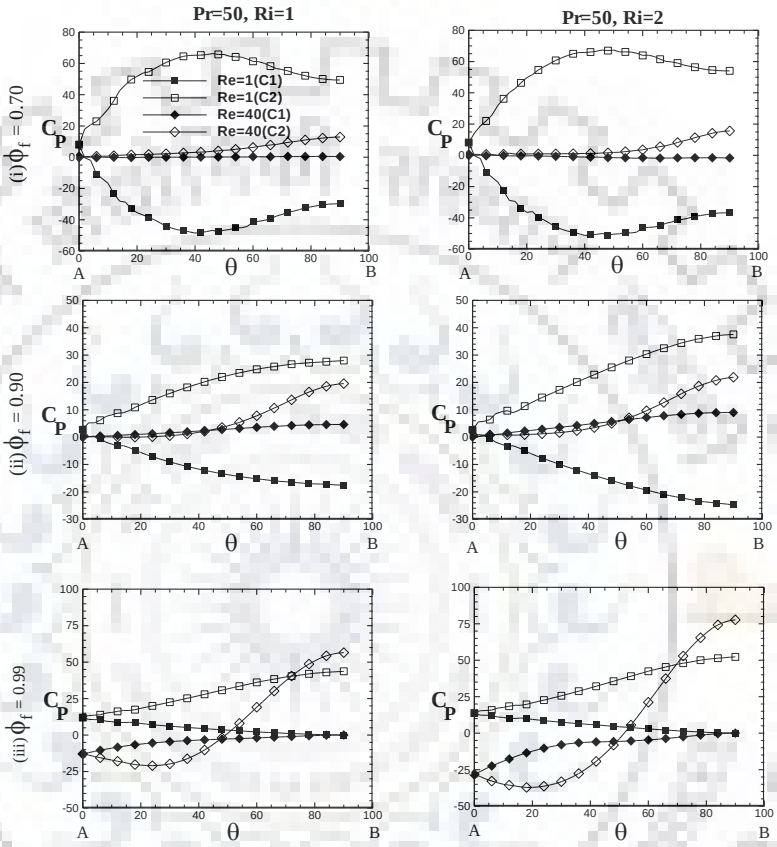

Figure 8.8: Dependence of pressure coefficient (C_P) over the surfaces of cylinders (C_1 and C_2) at Pr = 50 with the systematic variations of Richardson number (Ri = 1 and 2), fluid volume fractions (ϕ_f = 0.70, 0.90 and 0.99) and Reynolds number (Re = 1 and 40)

Further, the dependence of pressure coefficient on fluid volume fraction can be seen in Fig. 8.7(i-iii) for both of the Ri values. As the fluid volume fraction increases from ϕ_f = 0.70 to 0.90 and 0.90 to 0.99, the inertial effects dominating and the C_P values tend to increase with Re. Therefore, as expected, the maximum value of C_P can be observed in ϕ_f = 0.99 at Re=40 for cylinder C_2 (Fig. 8.7iiia-b). The above behavior happens because as one move from the lower fluid volume fraction to higher fluid volume fraction, the cylinder interactions are getting weak and at the highest fluid volume fraction, both of the cylinders act almost like an isolated single cylinders. However, within any fluid volume fraction, the C_P value is always higher for cylinder C_2 irrespective of the value of Re, Pr and Ri. Other influence includes the impact of increased Prandtl

number as shown in Fig. 8.8. Almost similar behaviors were seen with increased Prandtl number (Pr=50) under the ranges of identical conditions. As expected, an increase in pressure coefficient with an increase in Prandtl number was seen across all the fluid volume fractions. Further, the pressure coefficient was observed to be greatly influenced by the Richardson number at lower Re as compared to higher Re. This is primarily because of the point that the impact of free convection weakens with the increasing inertial forces at higher Re. The above dependence of pressure coefficient (Cp) is identical to that mentioned for the limiting cases of single cylinders (Srinivas et al., 2009; Chandra and Chhabra, 2012).

8.2.4 Local Nusselt number (Nu_L)

Typical variations of local Nusselt number (Nu_L) over the periodic cylinders (C_1 and C_2) are presented in Figs. 8.9-8.12. Fig. 8.9 displays the changes of local Nusselt number (Nu_{L1}) over the surface of periodic cylinder (C_1) for Ri = 1 and 2, ϕ_f = 0.70, 0.90, 0.99, Re = 1, 10, 40 and at a fixed value of Pr = 1. The local Nusselt number (Nu_{L1}) decreases as the fluid volume fraction (ϕ_f) increases from ϕ_f = 0.70-0.99 for all the values of Ri = 1, 2 and Re = 1, 10, 40. Further, for ϕ_f = 0.70 and 0.90, the maximum value of local Nusselt number was observed at the $\theta = 0^o$ (front of the cylinder C_1) for all of the Ri = 1, 2 and Re = 1, 10, 40. The local Nusselt number starts gradually decreasing as the θ increases from $\theta = 0^0$ to 90^0. Therefore, the minimum value was seen at $\theta = 90^0$ (rear of the cylinder C_1) under the identical conditions. The above behavior is slightly changed in maximum fluid volume fraction (ϕ_f = 0.99). Notwithstanding, for Re = 1 and 10, the behavior is similar to ϕ_f = 0.70 and 0.90, but a different trend was observed at Re = 40 for both of the Ri = 1 and 2. In Fig. 8.9 a(iii), the maximum value of Nu_{L1} is again seen at $\theta = 0^o$, but the minimum value occurred between $\theta = 30^o$ to 45^0 for Re = 40 in contrast to $\theta = 90^o$ for Re = 1 and 10. From $\theta = 45^o$ onward, a recovery was seen till $\theta = 90^o$. Similarly, in Fig. 8.9 b (iii), for Re = 40, all else remaining same except the minimum Nu_{L1} occurred between $\theta = 60^o$ to 75^0 and then recovery takes place till $\theta = 90^o$. Additionally, a significant influence of the buoyancy parameter (Ri) was seen over the local Nusselt numbers. In Fig. 8.9, an increased value of Nu_{L1} can be seen for Ri = 2 in contrast to Ri = 1 under the range of conditions covered herein. Because of the more distortion with increased buoyancy, the steep thermal gradients appear nearer to the periodic cylinders with an increase in Ri and therefore heat transfer rises.

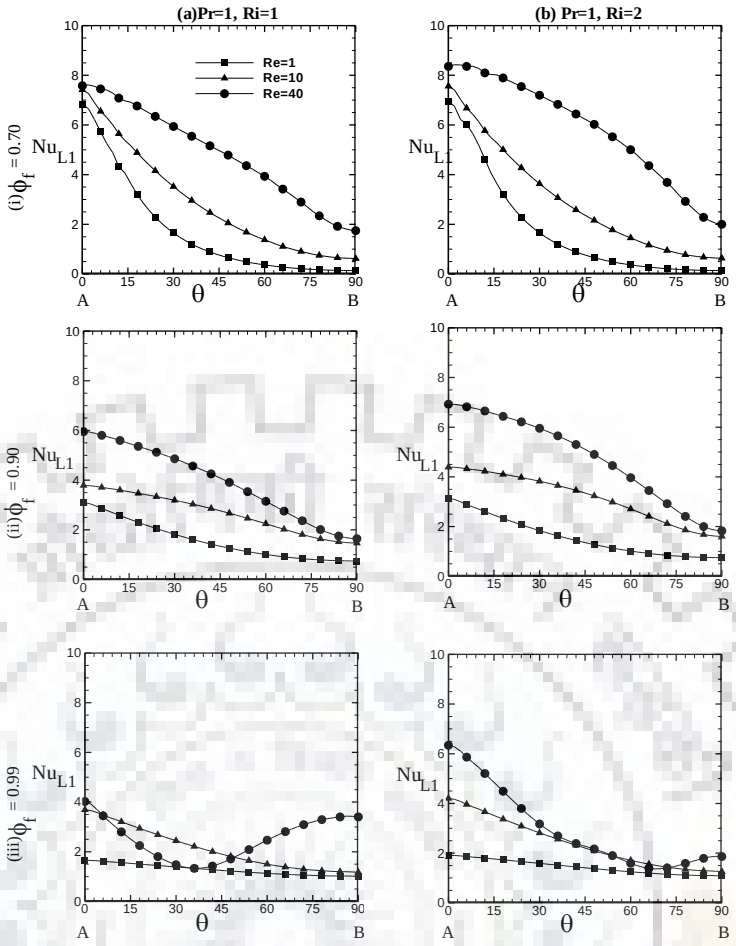

Figure 8.9: Representative variations of local Nusselt number (Nu_{L1}) over the surface of upstream cylinder (C_1) at Prandtl number (Pr = 1) and Richardson number (Ri = 1 and 2), fluid volume fractions (ϕ_f = 0.70, 0.90 and 0.99) and Reynolds number (Re = 1, 10 and 40)

On the other hand, Fig. 8.10 depicts the dependence of local Nusselt number (Nu_{L2}) over the surface of the periodic cylinder (C_2) under the identical conditions of the cylinder (C_1). As expected, the variation in local Nusselt number (Nu_{L2}) is quite different as compared to the local Nusselt number (Nu_{L1}). For a given fluid volume fraction of ϕ_f = 0.70 and Pr = 1, Ri = 1, (Fig. 8.10 a(i)), a very gradual change is occurring and therefore the maximum value of local Nusselt number (Nu_{L2}) was seen between $\theta = 30^0$ to 45^0 and minimum at $\theta = 90^0$ for all the values of Reynolds number. Similarly, for Pr = 1, Ri = 2 (Fig. 8.10 b (i)), the variations are identical except the maximum Nu_{L2} occurs between $\theta = 75^0$ to 90^0 at Re = 40. Since, at small values of Re and/or Pr, the local Nusselt number display virtually little variations because in this case, the heat transfer takes place mainly by conduction in contrast to convection. Further, for the fluid volume fraction of ϕ_f = 0.90 and 0.99 (Figs. 8.10(ii-iii)), an opposite trend is seen in contrast to the upstream cylinder (C_1) for both of the Ri = 1 and 2. Therefore, the minimum and maximum values of Nu_{L2} are seen at $\theta = 0^o$ and $\theta = 90^o$, respectively for all of the Re and Ri. Next, the

influence of buoyancy parameter (Ri) can be observed herein again, and so an increased value of Nu_{L2} can be seen for Ri = 2 in contrast to Ri = 1 across all the fluid volume fractions (ϕ_f).

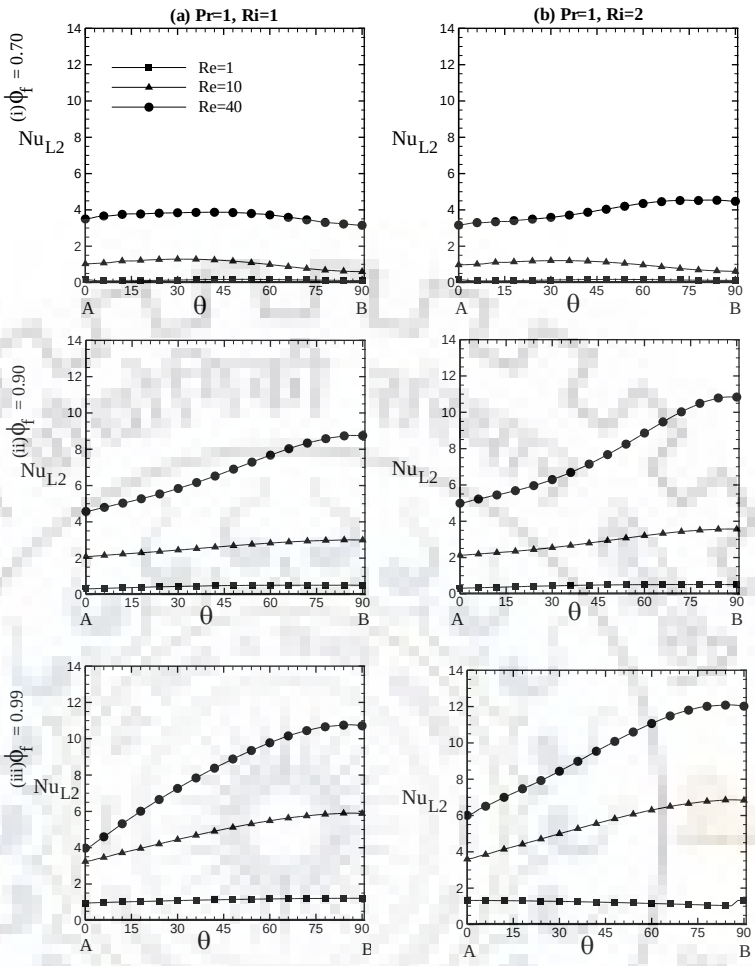

Figure 8.10: Representative variations of local Nusselt number (Nu_{L2}) over the surface of downstream cylinder (C_2) at Prandtl number (Pr = 1) and Richardson number (Ri = 1 and 2), fluid volume fractions (ϕ_f = 0.70, 0.90 and 0.99) and Reynolds number (Re = 1, 10 and 40)

Further, as expected, an increase in local Nusselt numbers (Nu_{L1} and Nu_{L2}) can be seen with increasing value of Reynolds number (Figs. 8.9-8.10). Thus, the maximum value of Nu_{L2} can be seen at ϕ_f = 0.99, Pr = 1, Ri = 2 and Re = 40 in contrast to Nu_{L1} at ϕ_f = 0.70, Pr = 1, Ri = 2 and Re = 40 (Figs. 8.9(b-i)).

The influence of increased Prandtl number on local Nusselt numbers is shown in Figs. 8.11 and 8.12 for the upstream cylinder (C_1) and downstream cylinder (C_2), respectively under the identical conditions, except Pr = 50 instead of Pr = 1. As expected, an increase in local Nusselt number with increasing value of Prandtl number is seen across all the fluid volume fractions. Further, the variation in local Nusselt numbers (Nu_{L1} and Nu_{L2}) at Pr = 50 was found to be similar to Pr = 1, but with the increased value of Nu_{L1} and Nu_{L2}. In addition, both of the periodic cylinders

(C_1 and C_2) strongly dependent on fluid volume fractions and shows the following peculiar features. The opposite behavior can be seen at a maximum fluid volume fraction of ϕ_f =0.99 at Re = 40. Such a feature, reveal that both cylinders act as an isolated cylinder under the maximum fluid volume fraction and high Reynolds and/or Prandtl numbers. The aforementioned local flow and heat transfer features are however further examined in terms of global characteristics (drag coefficients and average Nusselt number) in the subsequent sections.

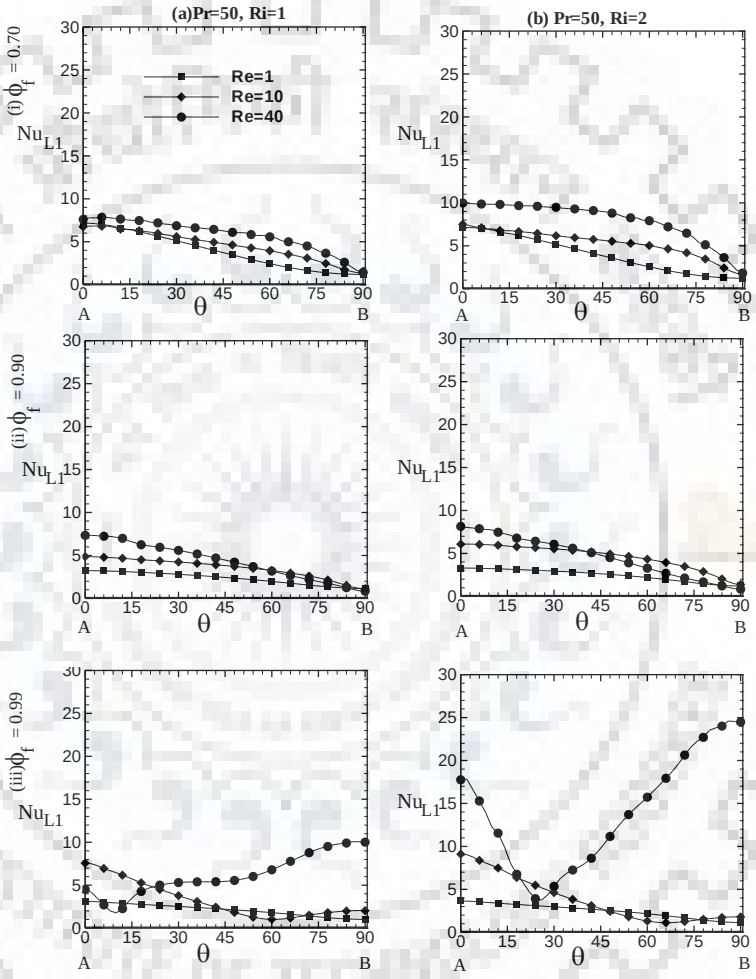

Figure 8.11: Representative variations of local Nusselt number (Nu_{L1}) over the surface of cylinder (C_1) at Prandtl number (Pr = 50), Richardson number (Ri = 1 and 2), fluid volume fractions (ϕ_f = 0.70, 0.90 and 0.99) and Reynolds number (Re = 1, 10 and 40)

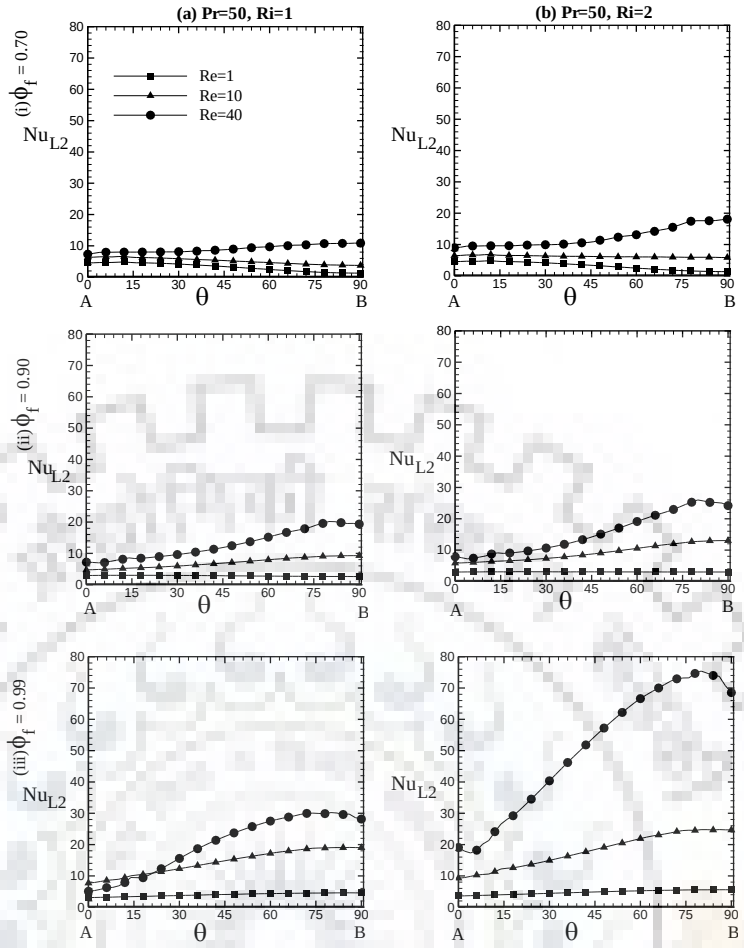

Figure 8.12: Representative variation of local Nusselt number (Nu_{L2}) over the surface of cylinder (C_2) at Prandtl number (Pr = 50), Richardson number (Ri = 1 and 2), fluid volume fractions (ϕ_f = 0.70, 0.90 and 0.99) and Reynolds number (Re = 1, 10 and 40)

8.3 Macroscopic characteristics

Here, the various quantitative flow and thermal features such as pressure, friction and total drag coefficients and average Nusselt number, etc., are described in this section. The influences of governing parameters studied have been elaborated over the above characteristics.

8.3.1 Pressure drag coefficient (C_{DP})

The dependence of pressure drag coefficient has been displayed in Table C1 (Appendix-C) over governing dimensionless parameters (ϕ_f , Re, Pr and Ri). Out of these pertinent parameters, the dependence on fluid volume fraction (ϕ_f) is more prominent than the other parameters. For instance, for the fixed values of Re, Pr and Ri, the C_{DP} values decrease as the fluid volume fraction gradually increases from 0.70 to 0.99, resulting the influences are greater in the region

of lower fluid volume fraction as compared to higher fluid volume fraction. For instance, for a fixed value of Re = 1, Pr = 0.7 and Ri = 1, the C_{DP} value is 147.0031 for ϕ_f = 0.70 against the C_{DP} value of 88.3842 of ϕ_f = 0.75 and 11.7483 of ϕ_f = 0.99, etc. (Table C1).

Further, an increase in C_{DP} can be observed with increasing value of Ri. Also, at higher Prandtl number, the effect of buoyancy parameter is found to be more prominent. For instance, for a fixed value of Pr = 0.70, ϕ_f = 0.70 and Re = 1, the C_{DP} value is 147.0031 for Ri = 1 and 150.6507 for Ri = 2 (Table C1). These C_{DP} values were seen to be improved at higher Prandtl number such as at Pr = 50; the above C_{DP} value is altered from 147.0031 to 154.7525 for Ri = 1 and 150.6507 to 166.0560 for Ri = 2. Similarly, at maximum fluid volume fraction of ϕ_f = 0.99 and at Pr = 0.70, Re = 1, the C_{DP} value is 11.7483 for Ri = 1 and 17.5621 for Ri = 2. These value again altered at higher Prandtl number of Pr = 50, as such, the C_{DP} value is altered from 11.7483 to 13.9318 for Ri = 1 and from 17.5621 to 20.5888 for Ri = 2 under the identical conditions. The above enhancement in C_{DP} value revealed that as the buoyancy parameter increases, the more mixing takes place in the vicinity of periodic cylinders which further improves with the increased Prandtl number. Additionally, when compared with forced convection (Ri = 0), the mixed convection provides more distortion to flow and therefore a sharper velocity gradient appears which gives rise to pressure drag coefficient (C_{DP}).

The impact of Reynolds and Prandtl numbers on C_{DP} is also revealed in Table C1. As the Reynolds number increases, the pressure drag coefficient (C_{DP}) correspondingly decreases, irrespective of the other parameters (ϕ_f, Pr and Ri). A higher value of C_{DP} can be seen at lower Reynolds number for any of the fluid volume fractions for a given Pr and Ri. For instance, for a fixed value of ϕ_f = 0.70, Pr = 0.7 and Ri = 1, the C_{DP} value is 147.0031 for Re = 1 and 75.5807 and 33.3814 for Re = 2 and 5, respectively. This feature reveals that as the Reynolds number increases, the inertial forces are dominating over friction forces and so the pressure drag coefficient reduces. Further, in contrast to forced convection (Ri = 0), where Prandtl number does not influence the drag coefficients, a significant influence of Prandtl number is observed in the mixed convection case (Ri >0). It can be seen that the value of C_{DP} varies with the variations in Prandtl number (Table C1). For instance, for a fixed value of ϕ_f = 0.70, Re = 1 and Ri = 1, the C_{DP} value is 147.0720 for Pr = 1, 149.9247 for Pr = 10 and 154.7525 for Pr = 50, etc. Noticeably, the influence of Prandtl number is found to be lesser as compared to the fluid volume fraction, Reynolds and/or Richardson numbers. Overall, an intricate pattern of governing parameters was

seen on pressure drag coefficient (C_{DP}) and expected to contrast well with friction drag coefficient (C_{DF}) also as described in the next section.

8.3.2 Friction drag coefficient (C_{DF})

Typical variations of friction drag coefficient (C_{DF}) with the dimensionless parameters (ϕ_f , Re, Pr and Ri) are listed in Table C2 (Appendix C). Similar to C_{DP}, the C_{DF} displays a strong dependence on above parameters. Again, the dependence on fluid volume fraction is more prominent as compared to the Reynolds, Prandtl and or Richardson numbers. Thus, at a fixed values of Re, Pr and Ri, the C_{DF} values always decrease as the value of fluid volume fraction is progressively increase from ϕ_f = 0.70 to 0.99. As a consequence, the influences are greater in the region of lower fluid volume fraction as compared to higher fluid volume fraction. Further, a significant role of buoyancy effect in terms of Richardson number is seen here in the case of friction drag coefficient (C_{DF}). An increasing value of C_{DF} can be observed in Table C2 as the Richardson number is increasing. Further, at higher Prandtl number, the impact of Richardson number is more prominent, e.g., for a fixed value of Pr = 0.70, ϕ_f = 0.70 and Re = 1, the C_{DF} value is 142.1439 for Ri = 1 and 143.2847 for Ri = 2. These C_{DF} values are improved at higher Prandtl number as such for instance, at Pr = 50, the above C_{DF} value is altered from 142.1439 to 147.2794 for Ri = 1 and from 143.2847 to 153.5886 for Ri = 2 under the identical conditions. Additionally, the dependence of C_{DF} on Re and Pr have been shown in Table C2. Analogous to C_{DP}, the C_{DF} is decreasing as the Reynolds number is increasing. Thus, a higher value of C_{DF} can be seen at lower Reynolds number in any of the fluid volume fractions for a given Pr and Ri. As far as the influence of Prandtl number is concerned, a similar trend to pressure drag coefficient (C_{DP}) can be seen in Table C2. Further, as can be observed in Tables C1 and C2, the pressure drag coefficient is always dominating over friction drag coefficient within the ranges of conditions studied herein. In fact, a complex dependence of pressure drag coefficient (C_{DP}) and friction drag coefficient (C_{DF}) was seen over the governing parameters (n, ϕ_f , Re and Ri). The influences of these parameters are further examined over the total drag coefficient (C_D).

8.3.3 Total drag coefficient (C_D)

Typical variations of total drag coefficient (C_D) on governing parameters (ϕ_f , Re, Pr and Ri) are displayed in Table C3 of Appendix-C. As can be observed in Table C3, the C_D discloses the similar kind of dependence as that of C_{DP} and C_{DF}. So, a strong dependence of C_D on above

dimensionless parameters can be seen in Table C3. Further, as discussed earlier, the dependence on fluid volume fraction (ϕ_f) is more prominent than the other parameters.

The additional endeavor was made to develop a simple statistical correlation of the total drag coefficient (C_D) in terms of governing parameters (ϕ_f , Re, Pr, Ri). The developed correlation was expressed by Eq. (8.1) as follows:

$$C_D = a_1 \phi_f^{b_1} \, Re^{c_1} \, Pr^{d_1} \, Ri^{e_1} + \exp(Ri) \tag{8.1}$$

The correlation coefficients and exponents appeared in the Eq. (8.1) are listed in Table 8.2. The above correlation is developed by the linear regression based on 576 data points having a regression coefficient of R^2 = 0.9936. The best fit of the present numerical values versus the correlation values of Eq. (8.1) has been shown in Fig. 8.13(a). An excellent agreement was found between the present results and predictions of Eq. (8.1). For instance, Eq. (8.1) has an average and maximum deviations of ~3.75 % and ~9.15%, respectively for the 91% of the data points whereas the 6% of the data points have the average and maximum deviations of ~10.61 % and ~20.15%, respectively, only 3% of the data points have the discrepancies within 20 to 30%. The behavior above is once again well described by Eq. (8.1). For instance, a strong dependence of C_D on ϕ_f can be seen in Table C3, and therefore as the ϕ_f increases, the C_D decreases rapidly since ϕ_f is raised by a power of 7.4970. Similarly, an increase in Re tend to decrease C_D significantly, but as compared to ϕ_f , the influence is less pronounced because Re is raised to the power of 0.8564. Besides, an increase in Pr and Ri accounts an increase in C_D. It can also be seen that the exponents of Pr and Ri are 0.0271 and 0.0539, respectively, i.e. the influence of Ri is more pronounced than Pr on C_D. An exponential increase in the C_D value with Ri can also be seen in above correlation.

Table 8.2: Correlation coefficients and exponents appeared in Eq. (8.1) and Eq. (8.3) for the total drag coefficient (C_D) and average Nusselt number (Nu), respectively

C_D		Nu			
-	-	α	α_i	α_j	α_k
a_1	18.8790	a	7.0377	-20.6330	17.1860
b_1	7.4970	b	-0.1279	0.4398	0.1608
c_1	0.8564	c	-0.0750	0.2716	0.1599
d_1	0.0271	d	-6.8756	20.1450	-15.7550
e_1	0.0539	e	-0.1329	0.4560	0.1669
-	-	g	-0.0929	0.3227	0.1660
-	-	h	0.2322	-0.6101	0.1669
R^2	0.9936	R^2	0.9954		

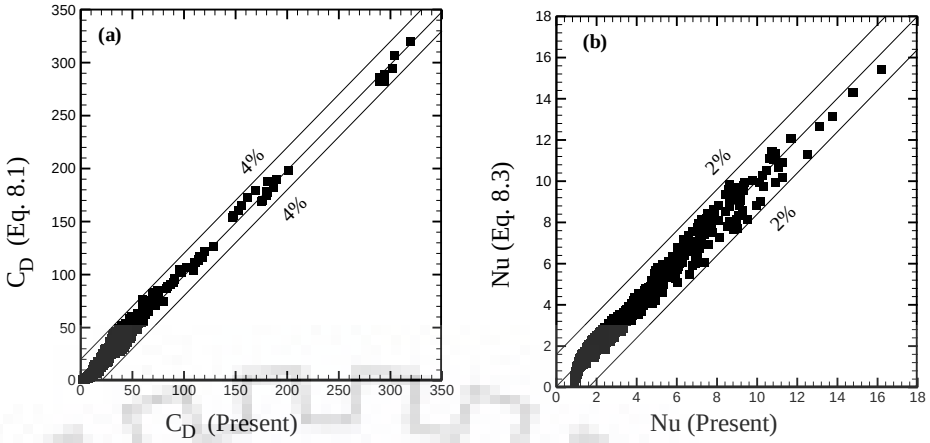

Figure 8.13: Best fit of present numerical vs. correlation values of (a) total drag coefficient (C_D) and (b) average Nusselt number (Nu)

As mentioned earlier, many studies are available related to mixed convection over single and/or two tandem cylinders, in contrast, only a few studies (Duli et al., 1995; Gowda et al., 1998) are available for mixed convection across an array of cylinders over the limited ranges of parameters. Therefore, the direct comparison of the present result is not possible, however within the limit of a single cylinder, a good agreement can be seen in Fig. 8.14 between the present results and that of Srinivas et al. (2009) and Chandra and Chhabra (2012) with an average and maximum deviations of 1-4%, respectively. The flow characteristics described above are further delineated in terms of normalized parameters in the following section.

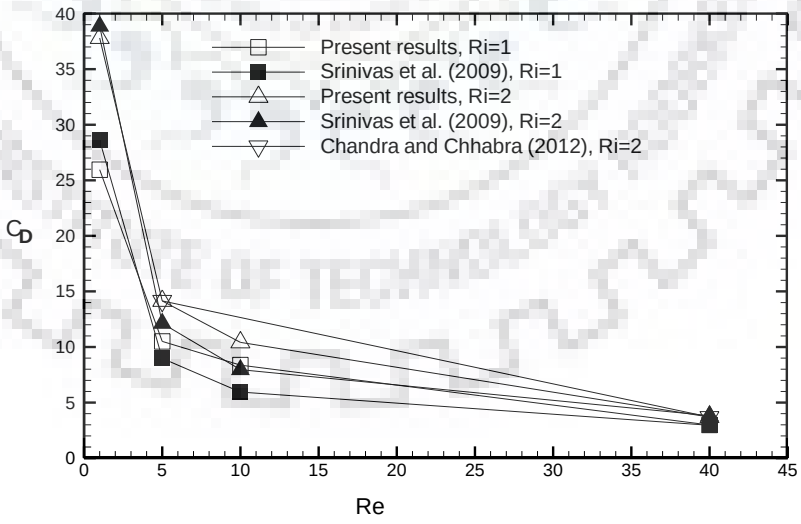

Figure 8.14: Comparison of total drag coefficient (C_D) for maximum fluid volume fraction of ϕ_f = 0.99 with the single cylinder of Srinivas et al. (2009), Chandra and Chhabra (2012) at Pr = 1 and Ri = 1 and 2

8.3.4 Influence of buoyancy parameter (Ri)

Notwithstanding, the influence of buoyancy parameter (Ri) on the drag coefficients has been discussed briefly earlier, perhaps, it is also useful to describe the influence of this parameter over the individual and total drag coefficients in terms of normalized parameters. In view of above, the mixed convection values of drag coefficients were normalized using their corresponding forced convection values (Ri = 0) as follows:

$$Y^N = \frac{Y(Ri)}{Y(Ri=0)}; \quad \text{where } Y = C_{DP,}\ C_{DF,}\ C_D \text{ and/or Nu} \tag{8.2}$$

The normalized plots of pressure, friction and total drag coefficients vs. fluid volume fractions are shown in Figs. 8.15(I-II) and 8.16 (I), respectively with the variations of Reynolds, Prandtl and Richardson numbers. An inspection of these plots reveals that the similar pattern is being followed by each of the C_{DP}^N, C_{DF}^N and/or C_D^N. As expected, an opposite trend is seen in these plots in contrast to the aforementioned behavior of C_{DP}, C_{DF} and/or C_D. i. e. the normalized values (Y^N) go up with the increase in the fluid volume fractions (ϕ_f). The above upturn is more significant at Re = 10 and 40 as compared to Re = 1 (Figs. 8.15 (I & II) and Fig 8.16(I)). Furthermore, the influence of buoyancy parameter is clearly visible in these plots. The solid and dashed lines represent the behavior at Ri = 1and 2, respectively. A higher normalized values (Y^N) can be seen at Ri = 2 as compared to Ri = 1 for all the values of Reynolds as well as Prandtl numbers. This behavior can generally be attributed to higher stresses owing to aiding buoyancy. Additional information includes the unsteady behavior at a higher fluid volume fraction of ϕ_f = 0.99. For instance, the behavior was observed to be unsteady at Re = 20 and 40 at ϕ_f = 0.99 for all the values of Prandtl number and Richardson number (Figs. 8.15 I-II (a & b)). Further, the unsteady behavior was seen to be increased with the Prandtl number. For instance, at Pr = 50, Figs. 8.15 (I-II(c)), an unsteady behavior at ϕ_f = 0.98 was also observed for Re = 40 along with ϕ_f = 0.99. Overall, the normalized values of drag coefficients have shown the non-monotonous behavior with the fluid volume fraction, Reynolds, Prandtl and Richardson numbers.

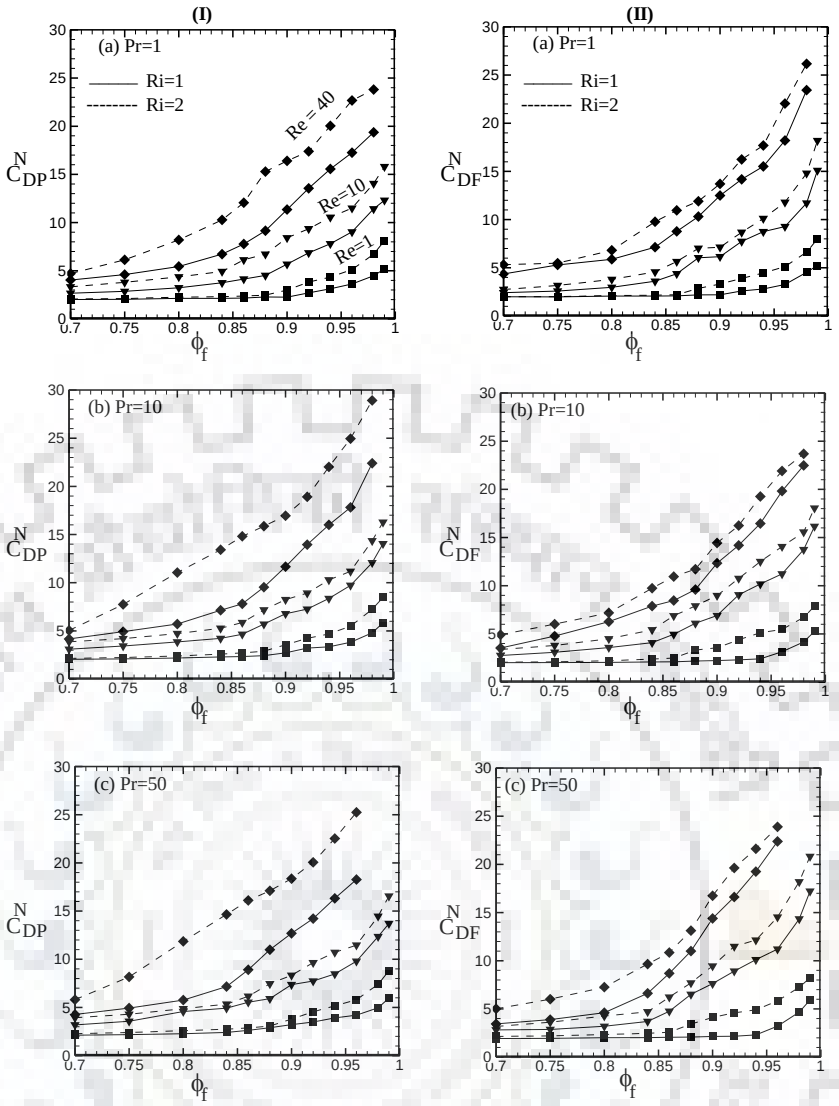

Figure 8.15: Dependence of normalized pressure and friction drag coefficients on fluid volume fractions (ϕ_f), Reynolds number (Re) and Richardson number (Ri) for (a) Pr = 1; (b) Pr = 10 and (c) Pr = 50 (normalized with Ri = 0)

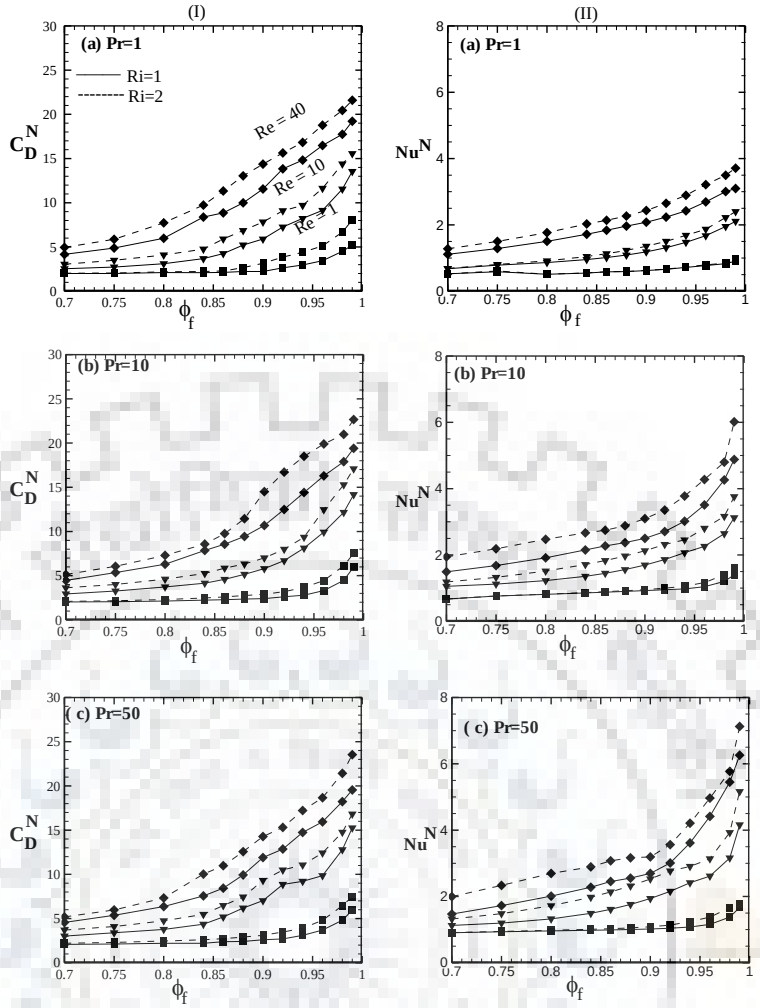

Figure 8.16: Dependence of normalized drag coefficients and average Nusselt number on fluid volume fractions (ϕ_f), Reynolds number (Re) and Richardson number (Ri) for (a) Pr = 1; (b) Pr = 10 and (c) Pr = 50 (normalized with Ri=0)

8.3.5 Average Nusselt number

The dependence of surface average Nusselt number (Nu) on the governing parameters (ϕ_f , Pr, Re and Ri) is displayed in Table C4 (Appendix-C). An enhancement in Nu values was seen with an increase in Re and/or Pr for a given value of ϕ_f (Table C4). Further, in the present case of mixed convection (Ri > 0), a reverse trend of Nu on ϕ_f was seen in contrast to forced convection (Ri = 0) case, i.e., Nu increases with increasing ϕ_f for a given Re and Pr and thereby the rate of heat transfer was improved as the fluid volume fractions were upturn. Further, the influence of ϕ_f on Nu was found to be stronger than either of the Re, Pr or Ri. Additional enhancement in heat transfer was observed because of the buoyancy parameter (Ri). An increased value of Nu can be seen in Table C4 for Ri = 2 as compared to Ri = 1. The reason for above enhancement is

that as the Ri rises, the potential energy of the molecules increases which gives rise to more mixing and returns the improved heat transfer. This can be observed in isotherms also where the sharp and dense thermal gradients appear with increased Ri. Thus, the maximum value of the Nu obtained is 16.1826 for ϕ_f = 0.99 at Pr = 50, Re = 40 and Ri = 2, while the minimum value is 0.8862 for ϕ_f = 0.70 at Pr = 0.7, Re = 1 and Ri = 1.

The normalized value of average Nusselt number (Nu) is plotted in Fig 8.16(II) versus the fluid volume fractions (ϕ_f). The Nu values have also been normalized similar to drag coefficients as defined in Eq. (8.2) corresponding to their forced convection values (Ri = 0). An examination of these plots (Figs. 8.16(IIa-c)) discloses that the normalized values (Nu^N) are increasing as the fluid volume fractions (ϕ_f) are increasing. The above increase is more significant for Re = 10 and 40 as compared to Re = 1. Additionally, the effect of Ri is clearly visible in these plots. The solid and dashed lines represent the behavior at Ri = 1 and 2, respectively. A greater normalized value (Nu^N) can be seen at Ri = 2 in contrast to Ri = 1 for all the values of Re and/or Pr. Furthermore, for ϕ_f = 0.99, an unsteady behavior was observed at Re = 40, Pr = 50 and Ri = 1 and 2. This behavior can generally be ascribed to higher stresses owing to aiding buoyancy and/or mixing.

Additional efforts were made to develop a correlation for the average Nusselt number in terms of governing parameters (Re, Pr, ϕ_f and Ri). The statistical analysis of the results returned the following correlations for Nu:

$$Nu = a\,Re^{b}\,Pr^{c} + d\,Re^{e}\,Pr^{g}\,\phi_f^{h} \tag{8.3}$$

where, the correlation constants a, b, c, d, e, g and h are related as

$$\alpha = \alpha_i Ri^2 + \alpha_j Ri + \alpha_k \quad (\text{where } i, j, k = 1,2,3\ ;\ \alpha = a, b, c, d, e, g, h) \tag{8.4}$$

The correlation coefficients and exponents (a, b, c, d, e, g and h) together with their statistical parameters are also summarized in Table 8.2. The best fit of the present numerical versus the correlation values of Eqs. (8.3-8.4) has also been shown in Fig. 8.13(b). An excellent agreement was found between the present numerical results and the predictions of Eqs. (8.3-8.4). For instance, these correlations have shown the average and maximum deviations of 2% and 5% respectively for 96% of the data points, whereas the deviations were within 5-15% for rest 4% of the data points. As mentioned above (Section 8.3.3) that the direct contrast of present findings is not possible due to the negligible literature. Moreover, other mixed convection studies are either focused on single or double cylinders (Chatterjee and Raja, 2013; Sparrow and Lee, 1976; Badr, 1982; Srinivas et al., 2009; Daniel and Dhiman, 2013). Though, within the single cylinder

limit, the present results have been compared with the available literature for the maximum fluid volume fraction (ϕ_f = 0.99) in Fig. 8.17. A good agreement can be seen for both of the Ri =1 and 2 in Figs. (8.17a and 8.17b), respectively at Pr = 1, 10 and 50. The average and maximum deviations lie within 1-2%, respectively.

Broadly speaking, an enhancement in Prandtl and/or Reynolds numbers enhances the rate of heat transfer as reported by many researchers. The scant available study by Duli et al. 1995 and Gowda et al. (1998) for mixed convection over in line tube bundles affirms the above characteristics. Further, for the forced convection across a periodic array of cylinders, the above features are reported (Mandhani et al., 2002; Zukauskas 1972; Martin et al., 1998; Gamrat et al., 2008, etc.). Also, some different characteristics which were found in this investigation are the influence of fluid volume fractions (ϕ_f) and Prandtl number over the Nusselt numbers and drag coefficients. Firstly, as discussed above, an increase in Nusselt number was observed with the increasing values of fluid volume fractions (ϕ_f) for the case of mixed convection. This is in contrast to forced convection where the opposite trend has been found. This might be happening because as the fluid volume fractions (ϕ_f) increases, the fluids get more time to distort and swirl in the increased vicinity of periodic cylinders due to buoyancy effects, results the more heat transfer takes place. Secondly, an increase in individual and total drag coefficients was also observed with increased Prandtl number. This is again opposite to forced convection where the Prandtl number does not influence the flow characteristics.

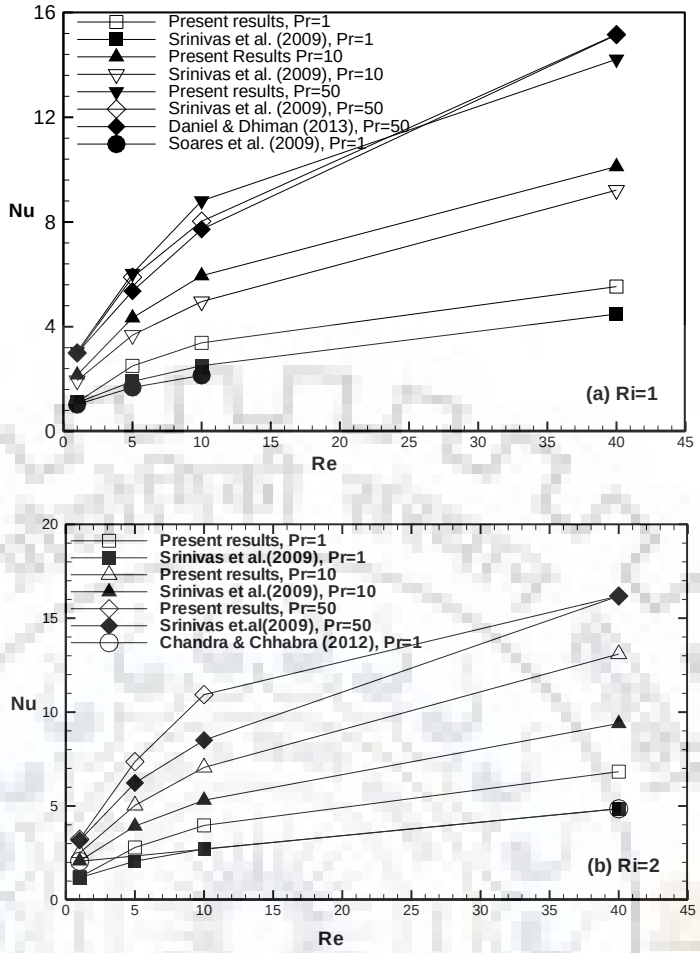

Figure 8.17: Comparison of average Nusselt number (Nu) for the maximum fluid volume fraction of $\phi_f = 0.99$ with the single cylinder of Srinivas et al. (2009), Soares et al. (2009), Chandra and Chhabra (2012) and tandem cylinder of Daniel and Dhiman (2013) for (a) Ri = 1 and (b) Ri = 2

Overall, the flow and thermal features of Newtonian fluids across an array of circular cylinders in cross-flow were found to be prejudiced in a complex manner with the fluid volume fractions (ϕ_f), Reynolds (Re), Prandtl (Pr) and Richardson (Ri) numbers. At higher Re, the wake interferences were found to be stronger when the fluid volume fractions (ϕ_f) were small. Further, at maximum fluid volume fraction ($\phi_f = 0.99$), interferences between both the periodic cylinders were weakened and both cylinders were acting almost like a single isolated cylinders. It is convenient to point out here that, however, the periodic array of cylinders in square geometry have been examined herein, but other types of arrangements like triangular, rectangular, hexagonal with in line or staggered configurations are also equally significant based on the fluid volume fractions or porosity of the cylinders.

Chapter 9

AIDING BUOYANCY MIXED CONVECTION CHARACTERISTICS OF POWER-LAW FLUIDS ACROSS PERIODIC ARRAY OF CIRCULAR CYLINDERS

Mixed-convection flow and thermal features across the periodic array of circular cylinders with aiding buoyancy conditions have been studied for non-Newtonian power-law fluids. The problem is well-described in Chapter 3 and the schematics and computational domain for one of the fluid volume fraction (ϕ_f = 0.70) are also shown in Figs. 3a and 3b, respectively. The study examines the dependence of local and global characteristics of mixed convection for the following ranges of governing parameters: Re = 1, 2, 5, 10, 20 and 40; Pr = 1, 10 and 50; Ri = 0, 1 and 2; n = 0.4, 0.6, 0.8, 1, 1.4 and 1.8 and ϕ_f = 0.70, 0.75, 0.80, 0.84, 0.86, 0.88, 0.90, 0.92, 0.94, 0.96, 0.98 and 0.99. For the mixed convection of non-Newtonian fluids, the governing equations (Eqs. 3.3-3.11) are applied with the buoyancy and gravity effect as mentioned in the y-component of momentum equations (Eqs. 3.6-3.7) and boundary conditions, i. e. Eqs. (3.12) - (3.15) have been used. The systematic variations of the above parameters yielded the numerical results which are explained in the following sections. However, prior to presenting and discussing the new results, the present numerical approach has been validated with the available literature in the subsequent section.

9.1 Validation of numerical solution procedure

For mixed convection of non-Newtonian fluids, the present results have been compared in Table 9.1 with the available literature. For instance, at n = 0.4, Pr = 50, Ri = 1, the value of $C_{D,}$ shows a good agreement with the result of Daniel and Dhiman (2013) with a relative difference of 1.36%. Likewise, at n = 0.6, Pr =1 and Ri = 2, the C_D values again display a good correspondence with the result of Srinivas et al. (2009) with relative discrepancies of 0.71% and 0.74%, at Re = 1 and 40, respectively and also with Chandra and Chhabra (2012) at Re = 40 with relative deviations of 1.23%. Moreover, an excellent agreement was found for the average Nusselt number (Nu) with the results of Srinivas et al. (2009) and Daniel and Dhiman (2013) in Table 9.1. For instance, at n = 0.4, Pr = 50 and Ri = 1, the maximum deviations were found to be 1.03% and 0.48% in the values of Nu at Re = 1 and 40, respectively with results of Daniel and Dhiman

(2013). Next, at n = 0.4, Pr = 50, Ri = 2 and Re = 40, the present result was in good agreement with Srinivas et al. (2009) with relative deviations of 2.27%. Further, at n = 0.6, Pr = 1 and Ri = 2, the maximum deviations were found to be 0.24% in the value of Nu at Re = 1 with results of Srinivas et al. (2009). In view of the above excellent agreement with the available literature, the present results was believed to be the accurate and hence generated for the complete range of parameters studied herein.

Table 9.1: Comparison of present values of total drag coefficient (C_D) and average Nusselt number (Nu) with available literature for non-Newtonian mixed convection flow at ϕ_f = 0.99

	n	Pr	Ri	Re	Present work	Literature value	% deviation
C_D	0.4	1	2	40	2.4153	2.4200[a]	0.19
		50	1	1	23.2447	23.5660[b]	1.36
	0.6	1	2	1	36.8176	37.0797[a]	0.71
		1	2	40	2.9145	2.893[a]	0.74
		1	2	40	2.9145	2.879[c]	1.23
Nu	0.4	50	1	1	3.0710	3.0397[b]	1.03
		50	1	40	22.6795	22.7901[b]	0.48
		50	2	40	26.1003	25.5206[a]	2.27
	0.6	1	2	1	1.2382	1.2340[a]	0.24

a; Srinivas et al. 2009 (single cylinder), b; Daniel and Dhiman, 2013(two tandem cylinders), c; Chandra and Chhabra, 2012 (semi-circular cylinder)

9.2 Fluid flow and heat transfer characteristics

In this section, the influence of governing parameters (n, ϕ_f , Re, Pr and Ri) on the streamline profiles, isotherm patterns and pressure coefficients, etc. have been presented and discussed.

9.2.1 Streamline profiles

The qualitative dependence of the normalized streamline (as defined in Chapter 5; Section 5.2.1) patterns are shown in Figs. 9.1-9.6 with the systematic variations of power-law index (0.4, 1 and 1.8), fluid volume fractions (ϕ_f = 0.70, 0.80, 0.90 and 0.99), Richardson numbers (1 and 2) and at extreme values of Reynolds number (1 and 40) and Prandtl number (1 and 50). The contours and wake sizes display a complex dependence on the above pertinent dimensionless parameters

(n, ϕ_f , Re, Pr and Ri) for the ranges of conditions covered herein. It can be seen in Figs. 9.1-9.6 that as the fluid volume fraction (ϕ_f) increases from ϕ_f = 0.70 to 0.99, the recirculation zone increases in size, both in terms of the length and width of the wakes, results in streamlines gradually shift towards the surfaces of the cylinders for all of the shear-thinning (n < 1), Newtonian (n = 1) and shear-thickening (n > 1) fluids. For instance, at ϕ_f = 0.70, Pr = 1 and Re = 1 (Fig 9.1a (i)), the streamlines are far from the cylinders, but as ϕ_f increases from ϕ_f = 0.70 to 0.80, 0.80 to 0.90 and 0.90 to 0.99 (Fig. 9.1), a corresponding shift in streamlines towards cylinders is seen and particularly at ϕ_f = 0.99, where these are gathered over the surfaces of cylinders. Further, as the fluid behavior changes from Newtonian to shear-thinning and/or shear-thickening, the re-circulatory region shrinks and/or expands, respectively due to the density changes, result in the straight and dense streamlines are seen for the shear-thinning (Figs. 9.1 a(i-iv)) as compared to shear-thickening fluids (Figs. 9.1 c (i-iv)).

Further, the strong influence of increased Reynolds number from Re=1 to 10 and 10 to 40 can be seen in Figs. 9.2-9.3 for Pr = 1 and Figs. 9.5-9.6 for Pr = 50, respectively over the streamlines. As the Reynolds number increases from Re = 1 to 10 and 10 to 40, the fluid circulation behind the cylinders is seen to increased due to the increasing inertial effects, and therefore, more curved, swirled and clustered streamlines can be seen in the vicinity of periodic cylinders. The inertial effects are more pronounced for the shear-thinning fluids as compared to shear-thickening fluids (Figs. 9.2-9.3, 9.5-9.6) and especially at the maximum fluid volume fractions of ϕ_f = 0.99. For instance, the wakes and vortex formations are seen for all the fluid volume fractions in shear-thinning region (Fig. 9.3a (i-iv)), whereas only one wake is seen in the Newtonian region (Fig. 9.3b (ii)) at ϕ_f = 0.80 and Ri = 2 and in shear-thickening region at ϕ_f = 0.90 and Ri = 2 (Fig. 9.3c (iii)), except at ϕ_f = 0.99. This is because as the fluid volume fraction increases, the role of power-law index diminishes correspondingly and therefore, at the maximum fluid volume fractions of ϕ_f = 0.99, the vortex formation and wakes can be seen in Fig. 9.3 (iv) for all of the shear-thinning, Newtonian and shear-thickening fluids.

A significant influence of buoyancy parameter (Ri) is also observed over the streamline profiles in Figs. 9.1-9.6. In fact, Ri affects the size of the recirculatory region between the cylinders. More pronounced streamlines can be seen aft the cylinders at Ri = 2 in contrast to Ri = 1, irrespective of the other parameters (ϕ_f , n, Re, Pr). Hence, an increasing value of the Ri reflects the magnitude of increased buoyancy/mixing, results more clustered, swirled streamlines and vortex formations in the vicinity of periodic cylinders. Qualitatively, similar patterns are seen throughout all the fluid volume fractions from ϕ_f = 0.70 to 0.99, but the influence and visibility

are more pronounced at higher values of fluid volume fractions and Reynolds numbers. Moreover, in contrast to forced convection, due to the linkage between the flow and thermal equations via the body force term, the flow field is greatly influenced by Prandtl number (Pr) too in the case of mixed convection. The influences of increased Prandtl number (Pr = 50) can be seen in Figs. 9.4-9.6 at Re = 1, 10 and 40, respectively. At Pr = 50, the patterns are almost similar to Pr = 1 for all of the Re = 1, 10 and 40, but due to the decrease in wake sizes, more swirled, clustered streamlines, wakes and vortexes are seen in the domain of the periodic cylinders. These effects can be visualized more at higher fluid volume fractions and Reynolds numbers for both of the shear-thinning as well as shear-thickening fluids. Moreover, the streamline patterns also show strong interference from the two cylinders at the lower values of ϕ_f which diminishes with increasing value of ϕ_f for all values of Re. The two cylinders act almost like isolated single cylinders at the largest value of ϕ_f for all of the Re, Pr, Ri and n. The above streamline patterns are similar to those reported in the literature for mixed convection across a single cylinder and or periodic array of cylinders (Badr, 1982, 1984; Gowda et al., 1998; Soares et al., 2009; Daniel and Dhiman, 2013, etc.). The wake patterns described herein are also consistent with the literature in the limit of forced convection across a periodic array of cylinder (Martin et al., 1998).

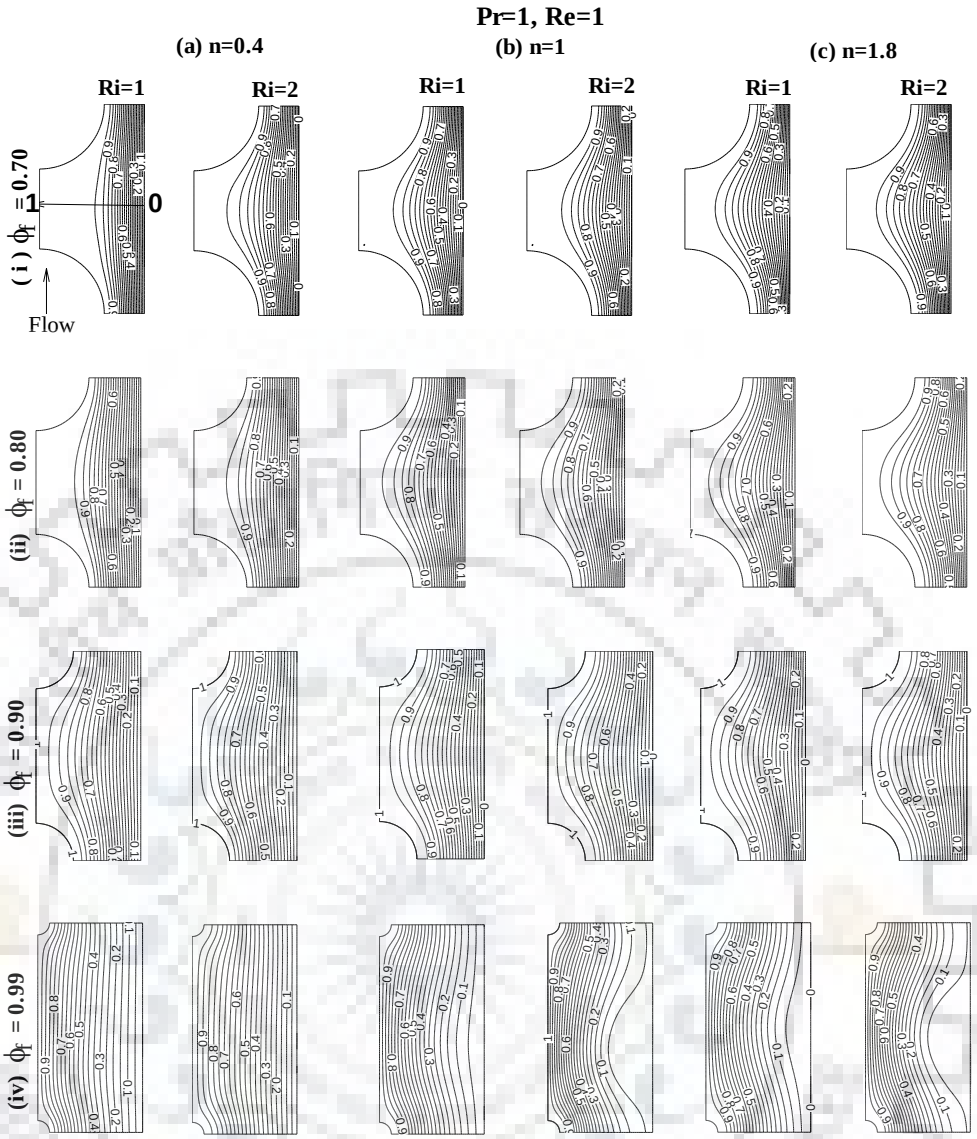

Figure 9.1: Dependence of normalized streamlines over the power-law index (n = 0.4, 1, 1.8), fluid volume fractions (ϕ_f = 0.70, 0.80, 0.90, 0.99) and Richardson number (Ri = 1 and 2) at a fixed values of Pr = 1 and Re = 1

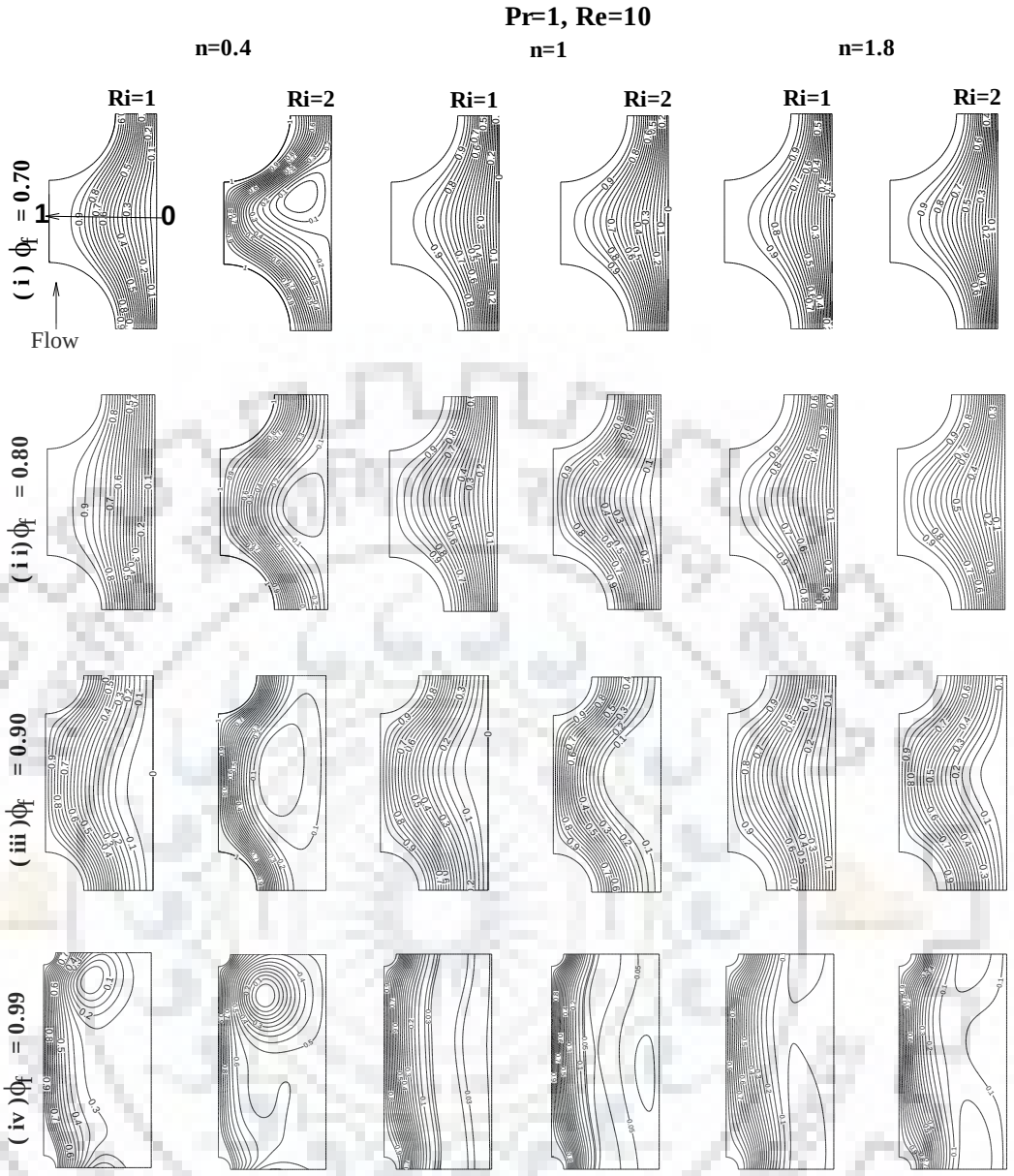

Figure 9.2: Dependence of normalized streamlines over the power-law index (n = 0.4, 1, 1.8), fluid volume fractions (ϕ_f = 0.70, 0.80, 0.90, 0.99) and Richardson number (Ri = 1 and 2) at a fixed values of Pr =1 and Re = 10

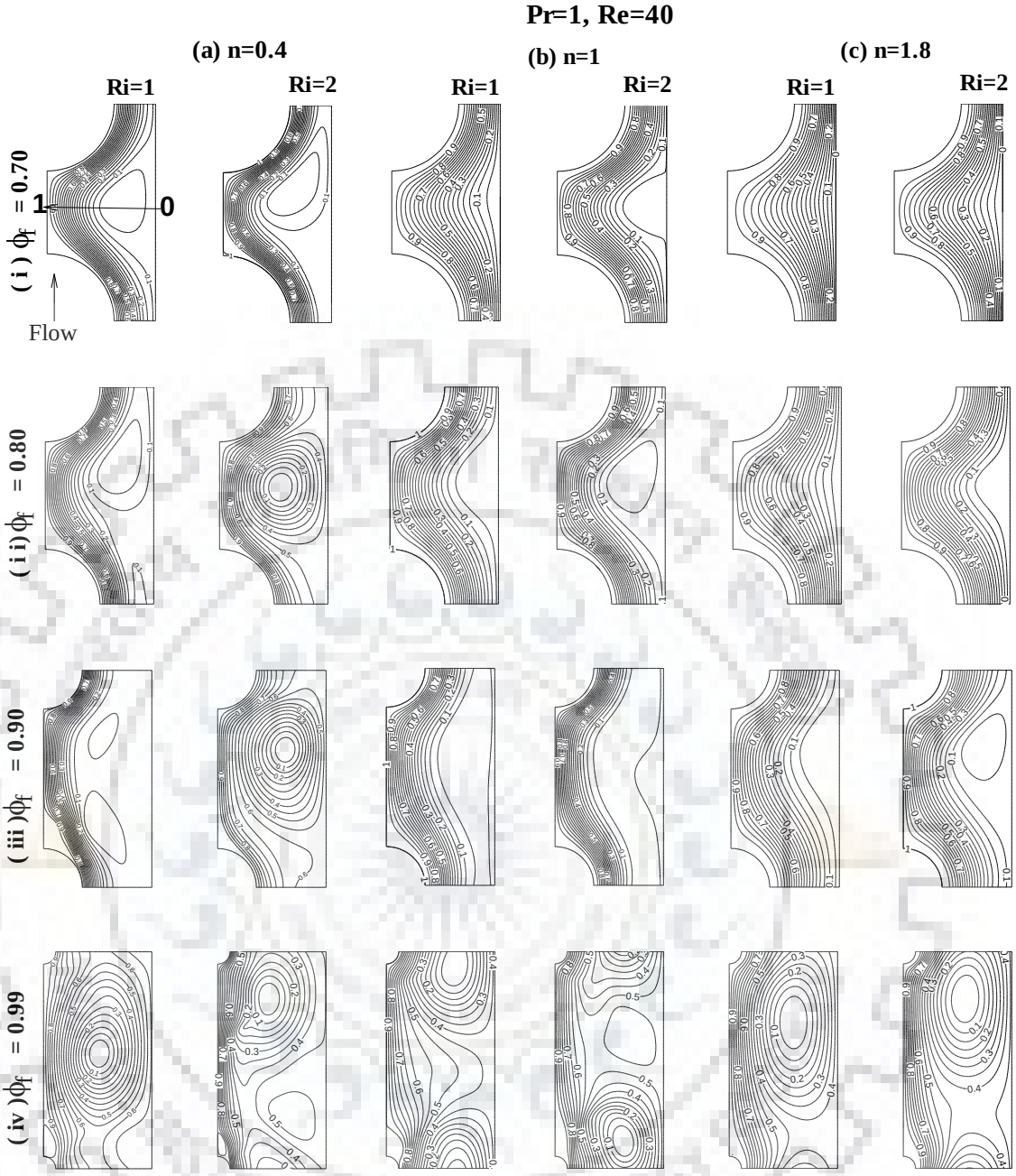

Figure 9.3: Dependence of normalized streamlines over the power-law index (n = 0.4, 1, 1.8), fluid volume fractions (ϕ_f = 0.70, 0.80, 0.90, 0.99) and Richardson number (Ri = 1 and 2) at a fixed value of Pr = 1 and Re = 40

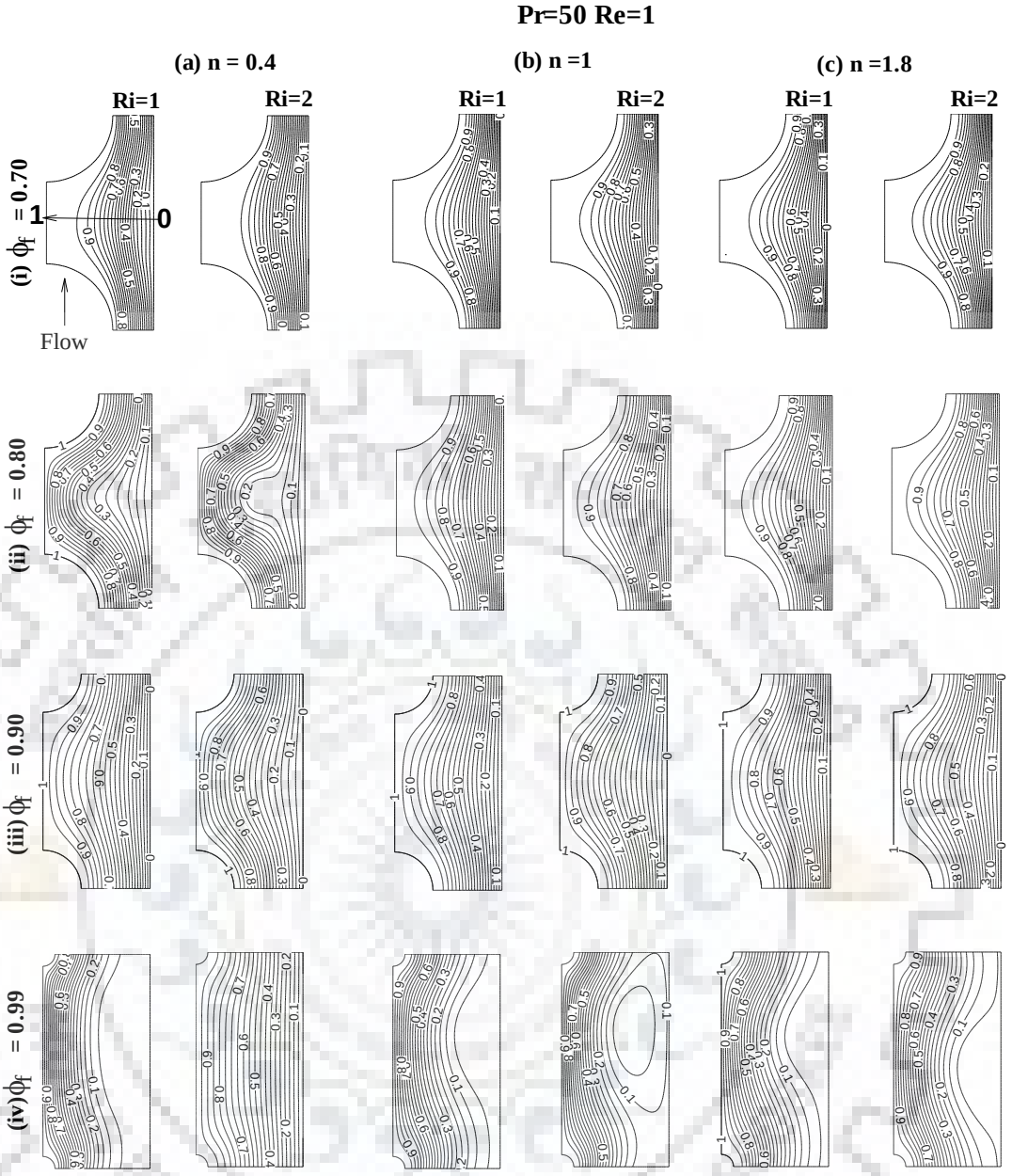

Figure 9.4: Dependence of normalized streamlines over the power-law index (n = 0.4, 1, 1.8), fluid volume fractions (ϕ_f = 0.70, 0.80, 0.90, 0.99) and Richardson number (Ri = 1 and 2) at a fixed value of Pr = 50 and Re = 1

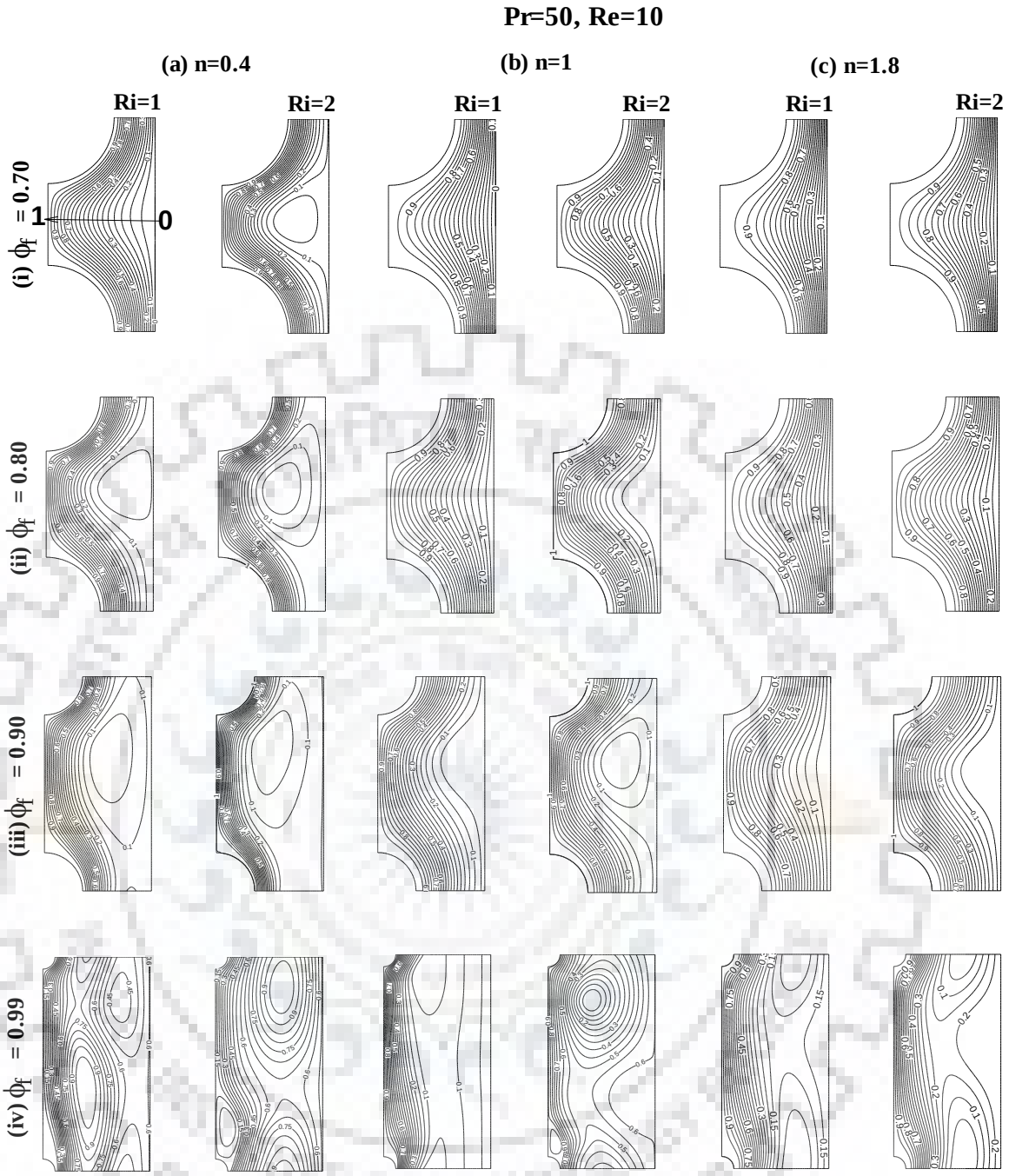

Figure 9.5: Dependence of normalized streamlines over the power-law index (n = 0.4, 1, 1.8), fluid volume fractions (ϕ_f = 0.70, 0.80, 0.90, 0.99) and Richardson number (Ri = 1 and 2) at a fixed values of Pr = 50 and Re = 10

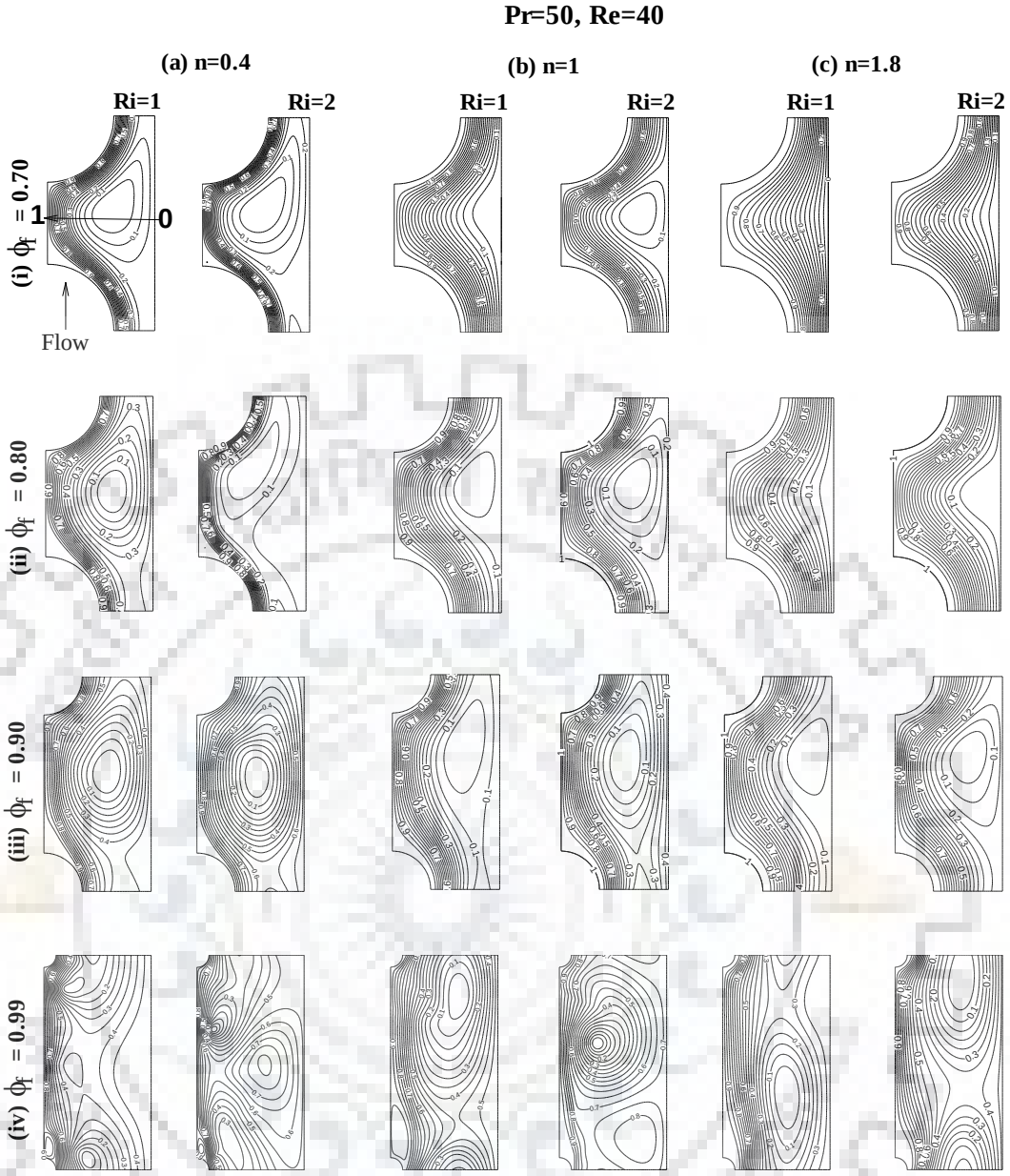

Figure 9.6: Dependence of normalized streamlines over the power-law index (n = 0.4, 1, 1.8), fluid volume fractions (ϕ_f = 0.70, 0.80, 0.90, 0.99) and Richardson number (Ri = 1 and 2) at a fixed values of Pr = 50 and Re = 40

9.2.2 Isotherm profiles

Figs. 9.7-9.12 display the dependence of normalized isotherms (as defined in Chapter 5; Section 5.3.1) patterns over the power-law index (n), fluid volume fractions (ϕ_f), Reynolds (Re), Prandtl (Pr) and Richardson (Ri) numbers. An examination of these figures reveals that the isotherm patterns display the complex dependence on the above dimensionless parameters. For instance, at low value of Pr = 1 and Re = 1 in Fig. 9.7(i); the isotherms are seemed to be almost symmetrical

and far from the surfaces of the cylinders at ϕ_f = 0.70, irrespective of the power-law index (n) Richardson number (Ri), but, as ϕ_f increases from 0.70 to 0.80, 0.80 to 0.90 and 0.90 to 0.99 (Figs. 9.7ii-iv), the recirculation/flow domain improves and therefore, a corresponding shifts of isotherms towards cylinder surfaces is seen and more pronounced isotherms in the vicinity of cylinders. Further, at large values of fluid volume fraction (ϕ_f = 0.99), the dense clustering is seen over the surfaces of periodic cylinders (Figs. 9.7-9.12). In fact, at maximum fluid volume fraction (ϕ_f = 0.99) and/or porosity, the cylinders interactions are almost negligible and most of the heat transfer is due to the upstream cylinder. Further, the symmetric isotherm patterns for the low Reynolds number flows (Re=1) suggest the dominance of conduction over convection.

As the fluid behaviour altered from shear-thickening to shear-thinning, an enhancement in the compactness of the isotherms results in an overall increase in the temperature gradients. This happens because of the thinner thermal boundary layer in shear-thinning fluids than that of Newtonian and shear-thickening fluids under otherwise identical conditions. Further, for a fixed value of fluid volume fraction, the crowding of isotherms in the flow direction rises with an upturn in Reynolds and Prandtl numbers (Figs. 9.8-9.12). With increasing inertial effects i.e. as the Reynolds number increases, the clustering of the isotherms became dense and confined in the vicinity of the cylinders. The density of isotherm lines indicates the magnitude of the thermal gradients; that is, clustered lines indicate a steep gradient, while sparse lines indicate a weak gradient. Thermal gradients, in turn, indicate the magnitude of heat transfer rates. Further, the influence of buoyancy parameter on the isotherm patterns is appreciable. It can be seen in Figs. 9.7-9.12, more pronounced isotherms appear for Ri = 2 in contrast to Ri = 1 because as the Richardson number increases, the level of buoyancy in terms of mixing increases and hence an enhancement in heat transfer takes place. This effect is less visible at low Re and Pr = 1 (Fig. 9.7), but as the Reynolds number and Prandtl number increase, the influences of Ri is clearly visible in the Figs. 9.8-9.12. The above qualitative feature is similar to those found in the literature for mixed convection (Gowda et al., 1998) and under the limiting cases of a single cylinder (Soares et al., 2009; Daniel and Dhiman, 2013, etc.). These patterns are also consistent within the range of forced convection (Martin et al., 1998; Mandhani et al., 2002, etc.). This complex dependence of isotherm patterns on the pertinent dimensionless parameters (n, Re, Pr, Ri and ϕ_f) is further examined in terms of pressure coefficients over the cylinder surfaces as described in the next section.

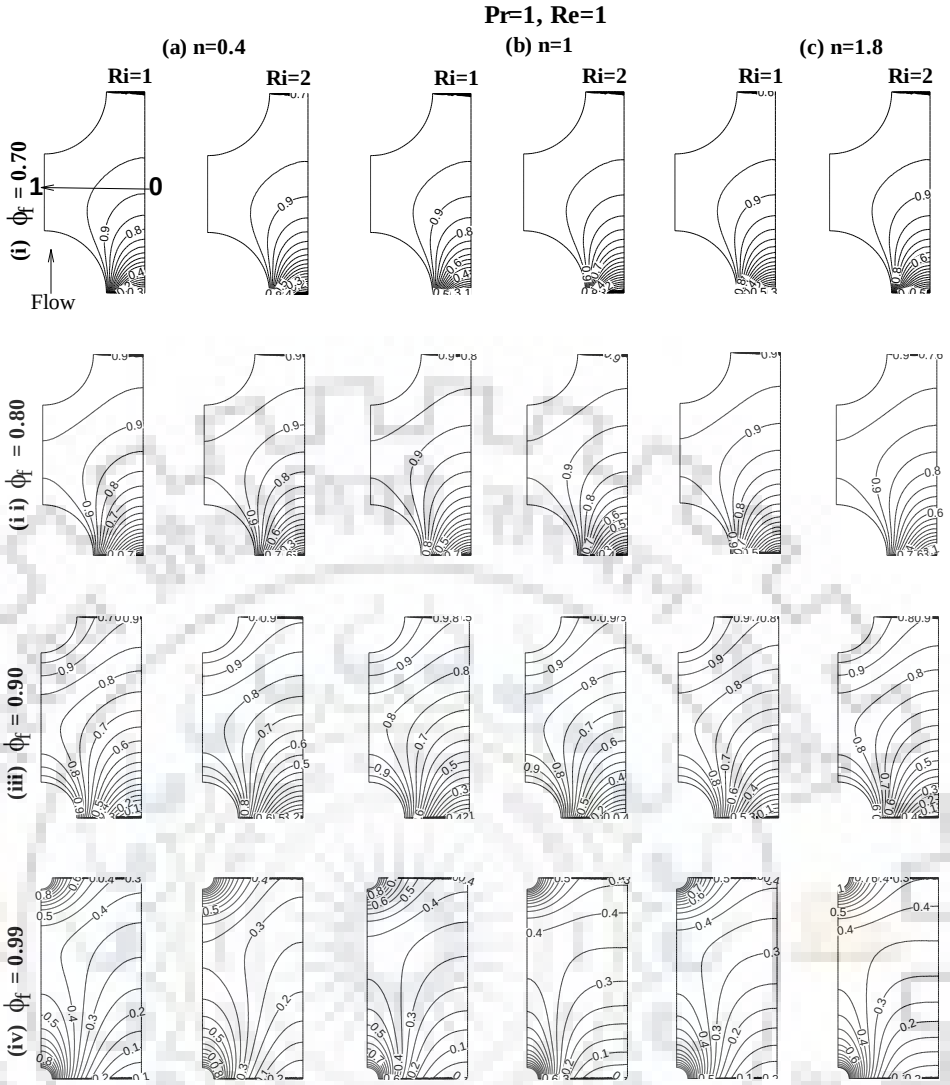

Figure 9.7: Dependence of normalized isotherm patterns over the power-law index (n = 0.4, 1, 1.8), fluid volume fractions (ϕ_f = 0.70, 0.80, 0.90, 0.99) and Richardson number (Ri = 1 and 2) at a fixed values of Prandtl number (Pr = 1) and Reynolds number (Re = 1)

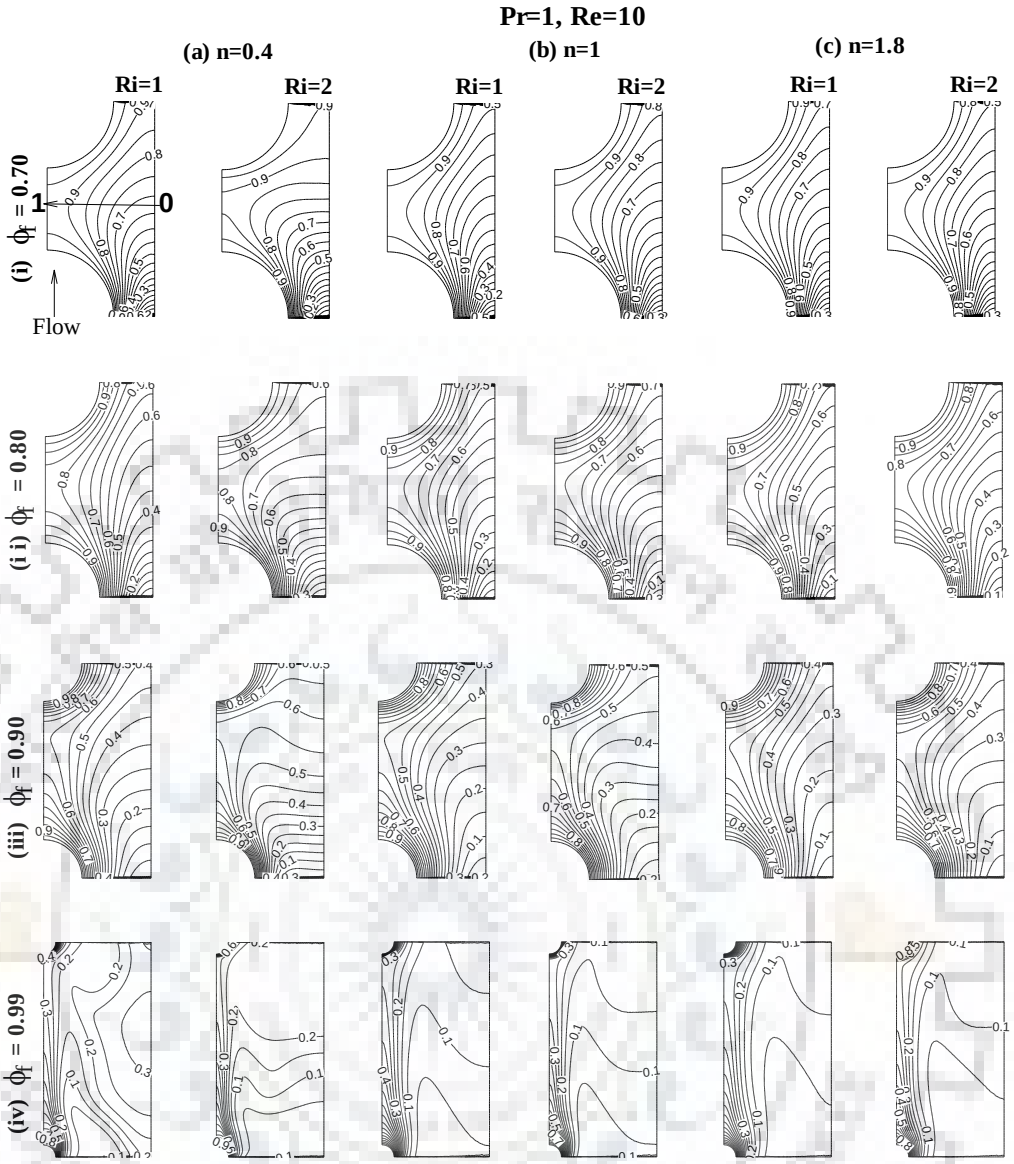

Figure 9.8: Dependence of normalized isotherm patterns over the power-law index (n = 0.4, 1, 1.8), fluid volume fractions (ϕ_f = 0.70, 0.80, 0.90, 0.99) and Richardson number (Ri = 1 and 2) at a fixed values of Prandtl number (Pr = 1) and Reynolds number (Re = 10)

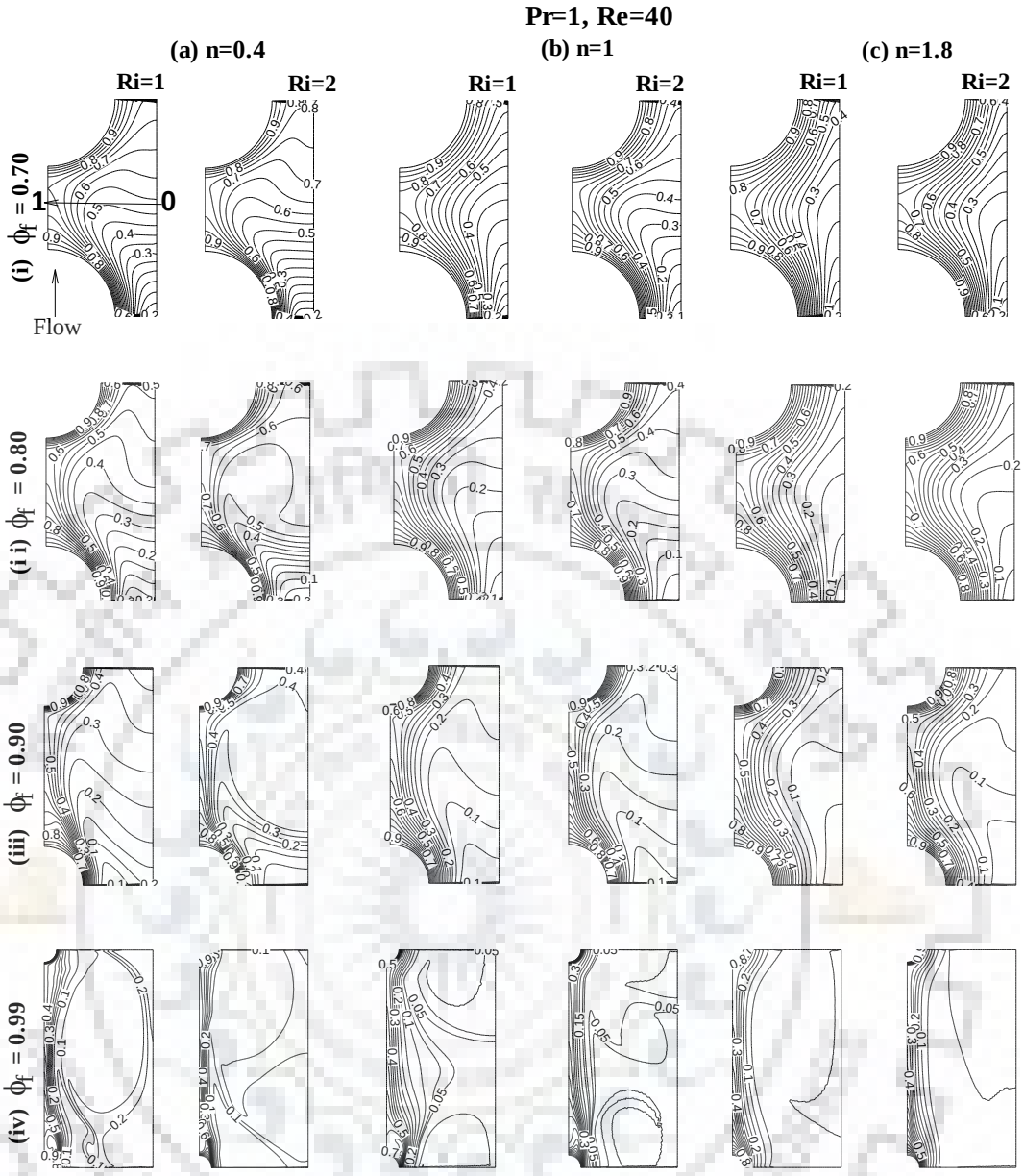

Figure 9.9: Dependence of normalized isotherm patterns over the power-law index (n = 0.4, 1, 1.8), fluid volume fractions (ϕ_f = 0.70, 0.80, 0.90, 0.99) and Richardson number (Ri = 1 and 2) at a fixed values of Prandtl number (Pr = 1) and Reynolds number (Re = 40)

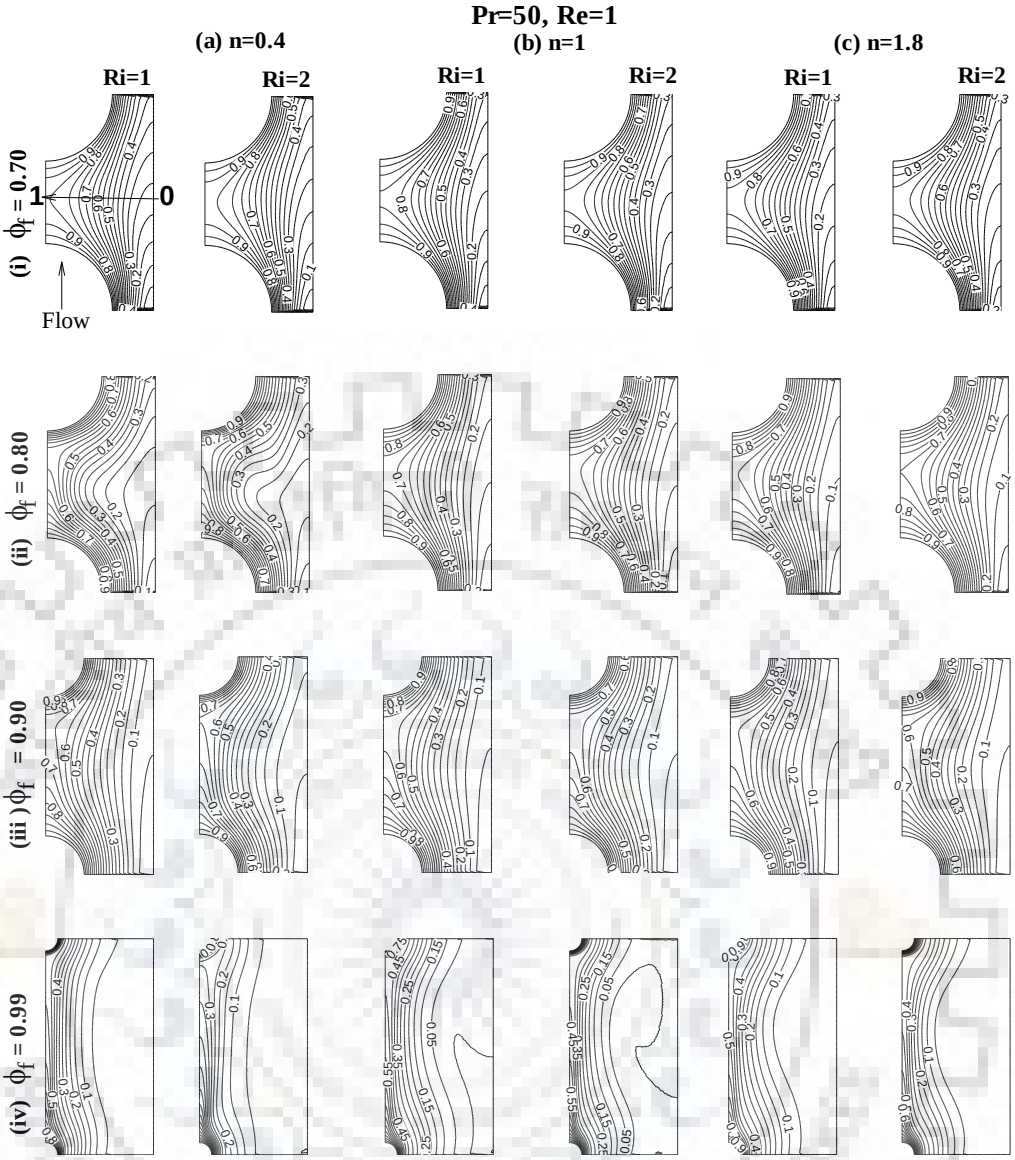

Figure 9.10: Dependence of normalized isotherm patterns over the power-law index (n = 0.4, 1, 1.8), fluid volume fractions (ϕ_f = 0.70, 0.80, 0.90, 0.99) and Richardson number (Ri = 1 and 2) at a fixed values of Prandtl number (Pr = 50) and Reynolds number (Re = 1)

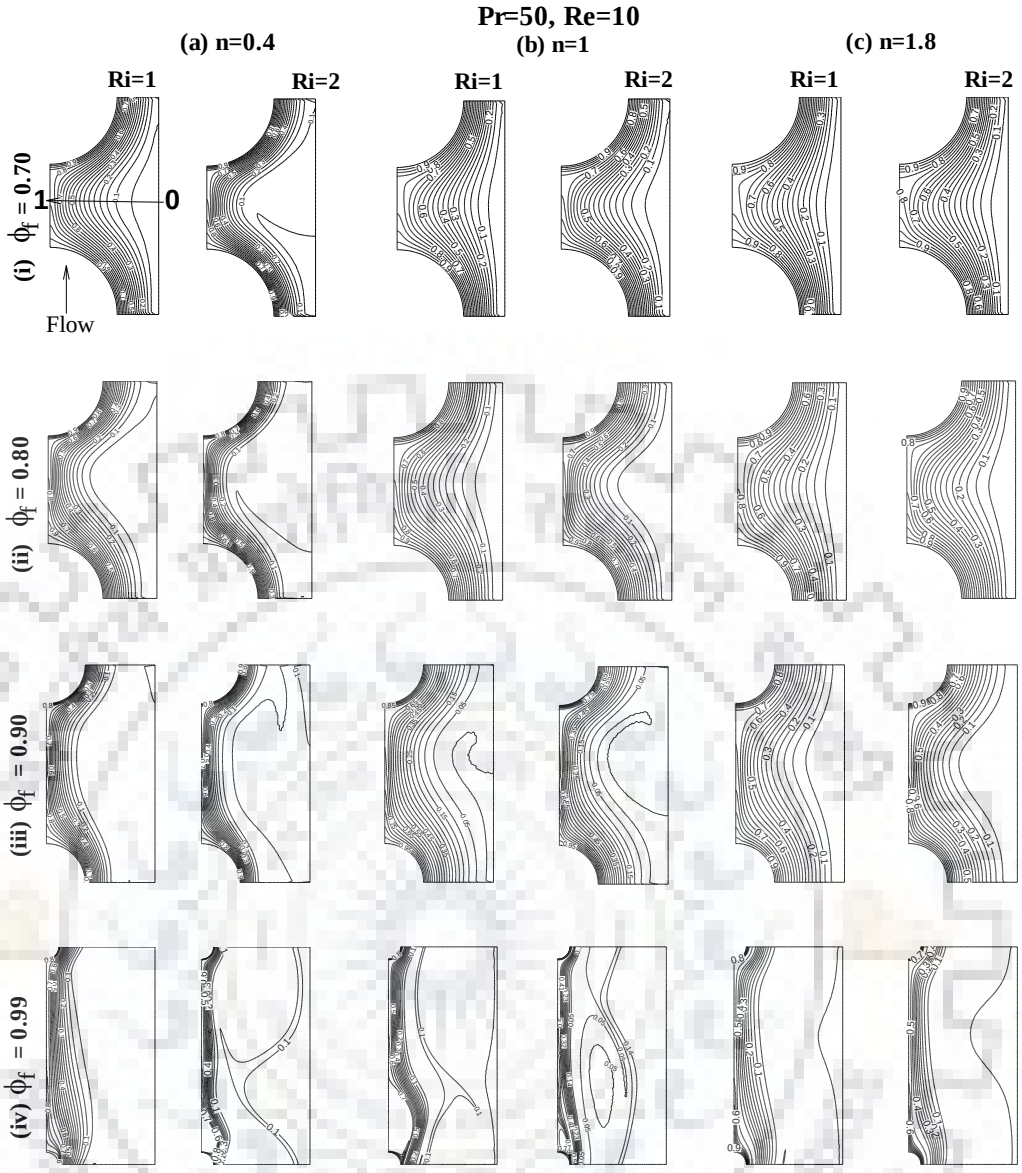

Figure 9.11: Dependence of normalized isotherm patterns over the power-law index (n = 0.4, 1, 1.8), fluid volume fractions (ϕ_f = 0.70, 0.80, 0.90, 0.99) and Richardson number (Ri = 1 and 2) at a fixed values of Prandtl number (Pr = 50) and Reynolds number (Re = 10)

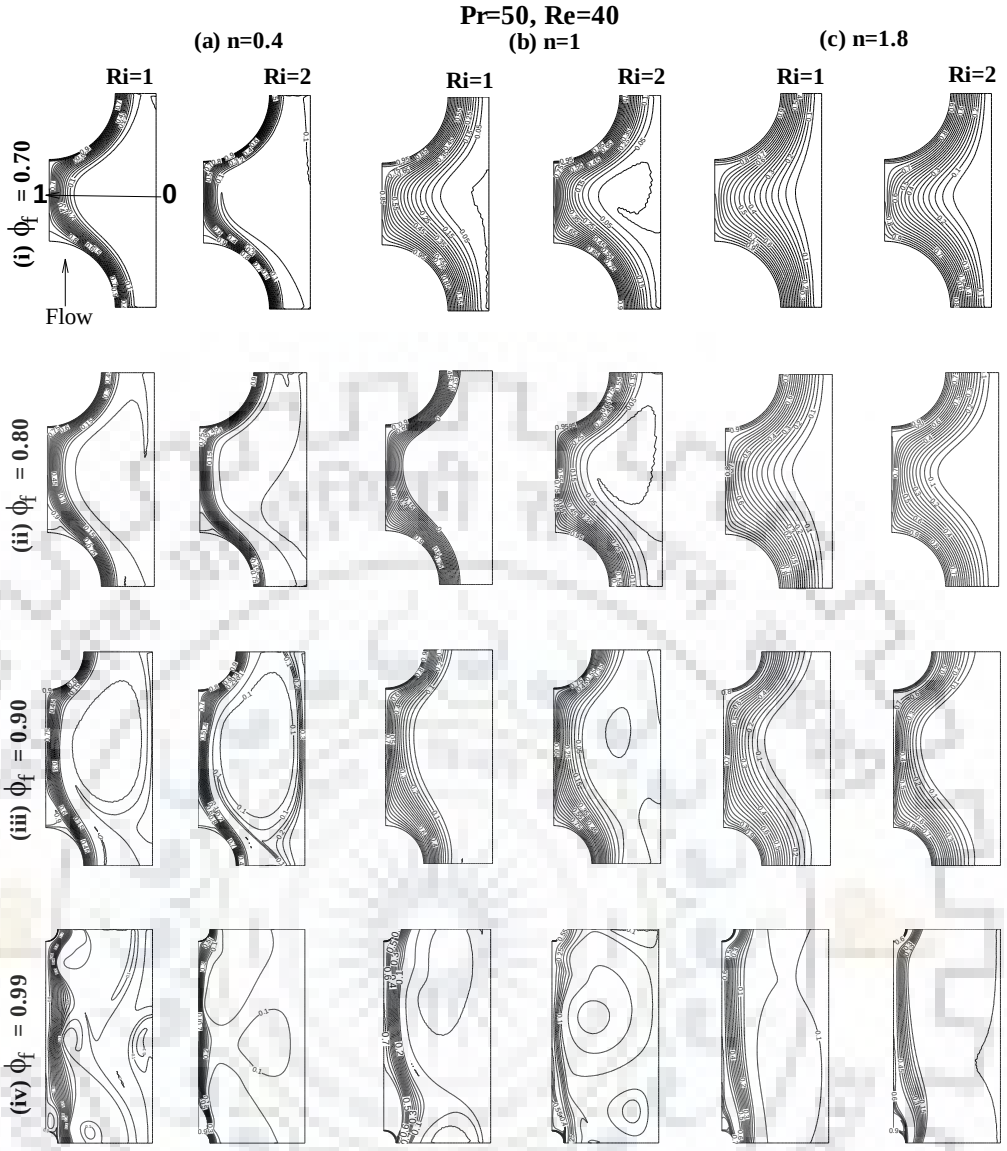

Figure 9.12: Dependence of normalized isotherm patterns over the power-law index (n = 0.4, 1, 1.8), fluid volume fractions (ϕ_f = 0.70, 0.80, 0.90, 0.99) and Richardson number (Ri = 1 and 2) at a fixed values of Prandtl number (Pr = 50) and Reynolds number (Re = 40)

9.2.3 Pressure coefficient (C_P) on the surfaces of the cylinders

The distribution of pressure coefficient over the surfaces of the periodic cylinders is shown in Figs. 9.13 and 9.14 with the systematic variations of fluid volume fractions (ϕ_f = 0.70, 0.90, 0.99), power-law index (n = 0.4, 1, 1.8), Reynolds (Re = 1, 10, 40) and Prandtl (Pr = 1 and 50) numbers and at the maximum values of Richardson number (Ri = 2). For shear-thinning fluids (n = 0.4) at Pr = 1, Re = 40 and ϕ_f = 0.70 (Fig. 9.13 a(i)), the pressure coefficient (C_P) for upstream cylinder (C_1) is seen to decrease gradually from its maximum value at the front stagnation point ($\theta = 5°$) for along the surface of the cylinder (C_1). For instance, the minimum value of C_P occurs at $\theta = 90^0$. The above behavior was observed to be slightly different for Re =

1 and 10 under the similar conditions. The pressure coefficient for upstream cylinder (C_1) is seen to decrease gradually from its maximum value at the front stagnation point ($\theta = 0°$) for along the surface of the cylinder (C_1) followed by an increase between the $\theta = 40^0$ to 60^0. For instance, the minimum value of C_P occurs at $\theta = 50^0$ and afterward, it starts increasing gradually till $\theta = 90^0$. Also, an increase in the Reynolds number tends to increase the pressure coefficient over the surface of the cylinder (C_1). Therefore, the larger interval was seen at Re = 40 for the minimum and maximum C_P for upstream cylinder (C_1) and downstream cylinder (C_2), respectively. However, the behavior of downstream cylinder (C_2) was observed to be quite different in contrast to the upstream cylinder (C_1). For instance, for the above shear-thinning fluid (n = 0.4) and at Pr = 1, Re = 40 and ϕ_f = 0.70 (Fig. 9.13a (i)), the pressure coefficient was seen to rise from its minimum value at $\theta = 5°$ for along the surface towards the rear and reaches it's maximum at $\theta = 90°$. Further, a gradual decrease in the C_P value was observed which starts from $\theta = 0^0$ for Re = 1 and 10 till $\theta = 45^0$ and then starts recovery and reaches it's maximum at $\theta = 90°$. The above increase is more prominent at Re = 40 as can be seen clearly whose maximum value was again at $\theta = 90°$. Moreover, as compared to cylinder C_1, the pressure coefficient over the surface of the cylinder C_2 was noticed higher for all the values of fluid volume fractions and Reynolds numbers. Also, as the fluid behaviour changes from shear-thinning to Newtonian and Newtonian to shear-thickening, the pressure coefficient was seen to be increasing (Fig. 9.13i (a-c)). For instance, the pressure coefficient of Newtonian fluid was observed to be higher than shear-thinning and lower than the shear-thickening fluids. Furthermore, the above behaviour is quite different for the maximum fluid volume fractions (ϕ_f = 0.99). An opposite trend was observed for ϕ_f =0.99 as compared to ϕ_f =0.70 and 0.90. The pressure coefficient is seen to be higher in shear-thinning fluids than that for Newtonian and shear-thickening fluids. This is because, at higher fluid volume fractions (ϕ_f = 0.99), the two cylinders act almost like isolated single cylinders (Figs. 9.13 and 9.14). These figures show a stronger influence of the power-law index (n) on the pressure coefficient for both of the shear-thinning as well as shear-thickening fluids. Other influence includes the impact of increased Prandtl number (Pr) as shown in Fig. 9.14. Almost similar behavior was seen with increased Prandtl number (Pr=50) under the ranges of identical conditions. As expected, an increase in pressure coefficient with increasing value of Prandtl number was seen across all the fluid volume fractions. Further, the value of pressure coefficient at the front and rear stagnation points was seen to be more strongly influenced by the value of the Richardson number (Ri) at low Reynolds numbers than that at higher values of Reynolds numbers. This was simply because the role of free convection diminishes with increasing Reynolds number. The variation of the pressure coefficient described above is similar to those

reported in the literature (Srinivas et al., 2009; Chandra and Chhabra, 2012) for the limiting cases of single cylinders. The other local behaviors have been examined in terms of heat transfer parameter (local Nusselt number) as discussed in the subsequent section.

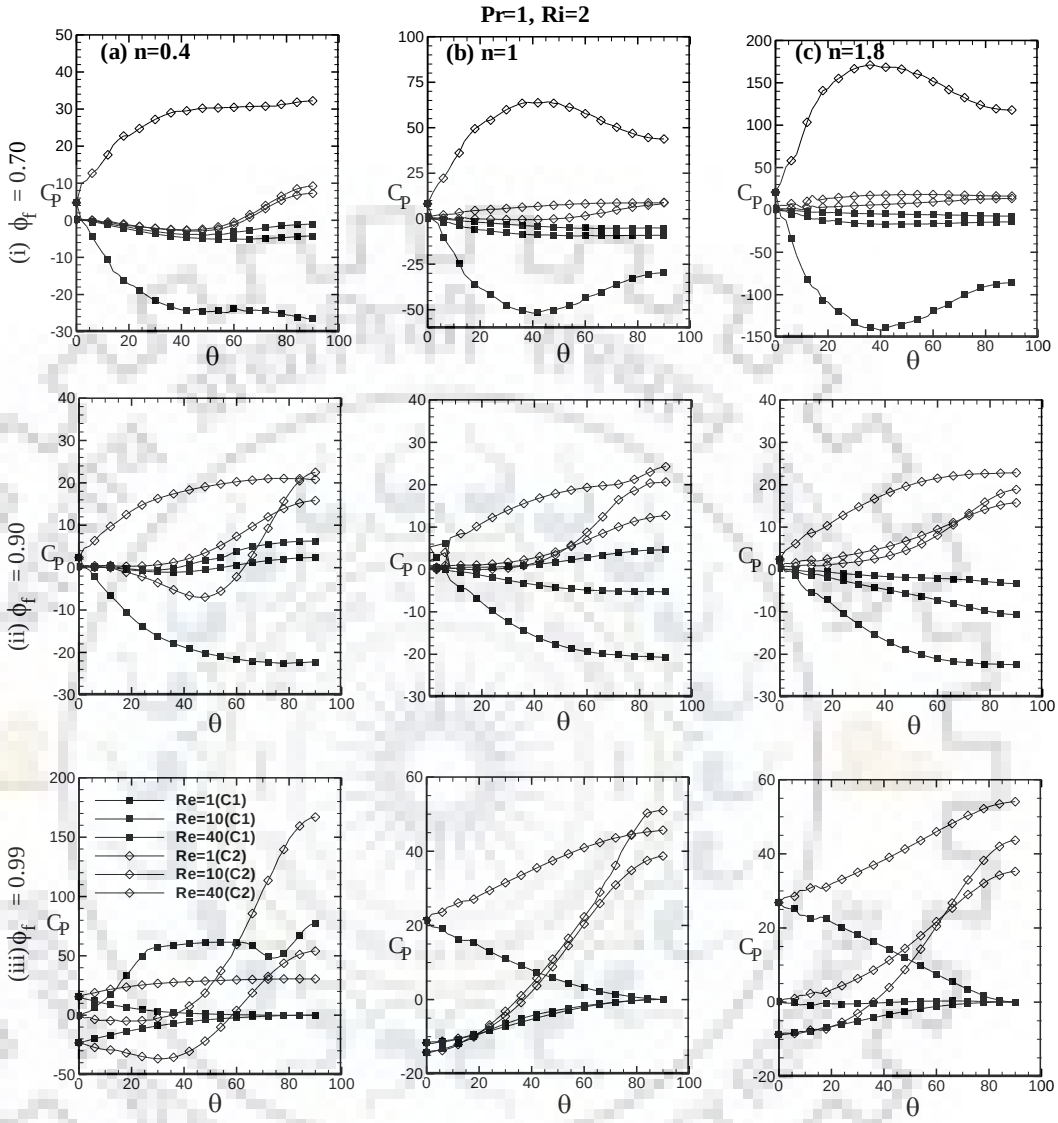

Figure 9.13: Distribution of pressure coefficient (C_P) over the surfaces of cylinders ($C_1$and C_2) with the systematic variations of power-law index (n = 0.4, 1and 1.8), fluid volume fractions (ϕ_f = 0.70, 0.90 and 0.99), Reynolds number (Re = 1, 10 and 40) at a fixed values of Pr =1 and Ri = 2

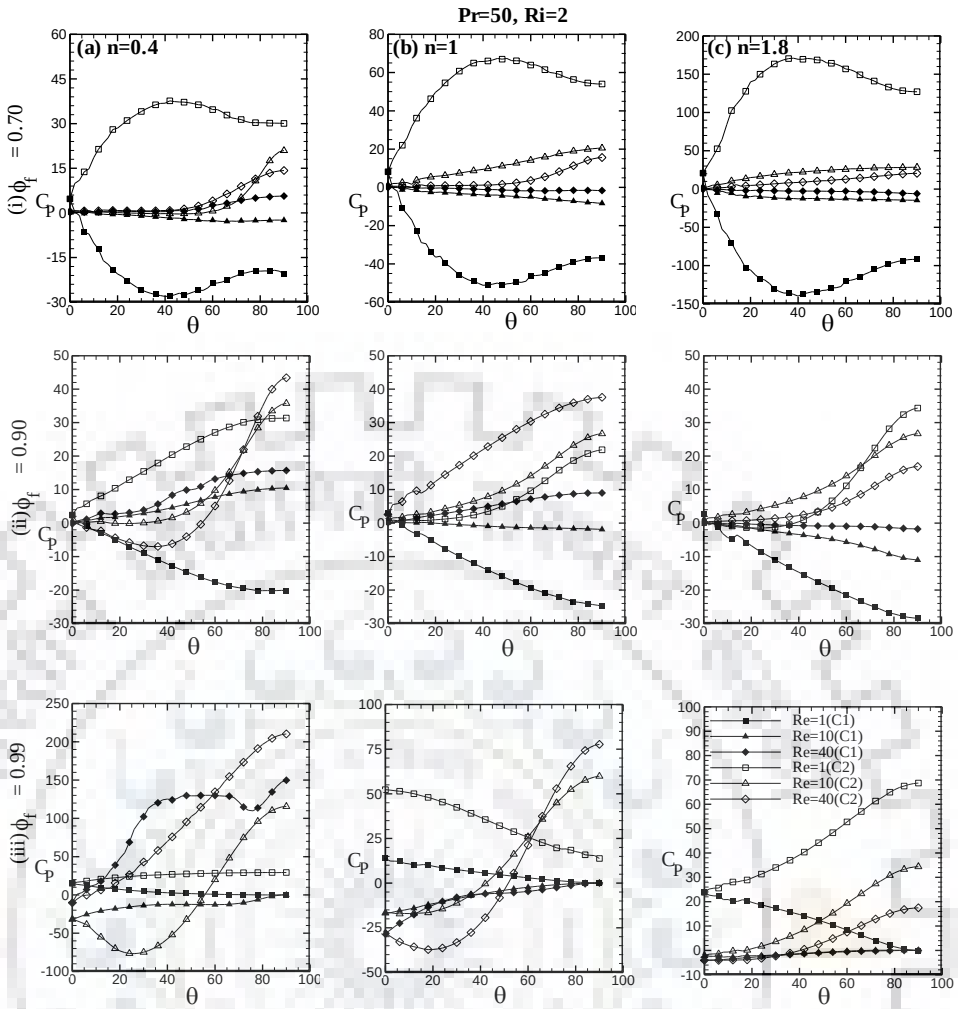

Figure 9.14: Distribution of pressure coefficient (C_P) over the surfaces of cylinders ($C_1$and C_2) with the systemic variations of power-law index (n = 0.4, 1and 1.8), fluid volume fractions (ϕ_f = 0.70, 0.90 and 0.99) and Reynolds number (Re = 1, 10 and 40) at a fixed values of Pr = 50 and Ri = 2

9.2.4 Local Nusselt number (Nu_L)

Representative variations of the local Nusselt number (Nu_L) over the upstream cylinder (C_1) and downstream cylinder (C_2) with the power-law index(n), fluid volume fraction (ϕ_f), Reynolds number (Re), Prandtl number (Pr) and Richardson number (Ri) are shown in Figs. 9.15-9.18. Broadly, an examination of these plots (Figs. 9.15-9.18) reveals that the local Nusselt number is found to be maximum and minimum for shear-thinning and shear-thickening fluids than their corresponding Newtonian fluids, respectively under otherwise identical conditions. Fig. 9.15 shows the variation of local Nusselt number (Nu_{L1}) over the surface of cylinder C_1 for the range of Richardson number (Ri = 1 and 2), fluid volume fraction (ϕ_f = 0.7, 0.90 and 0.99) and Reynolds number (Re = 1, 10 and 40) at a fixed value of Prandtl number (Pr = 1). It can be seen that the local Nusselt number (Nu_{L1}) is decreasing as the fluid volume fraction (ϕ_f) is increasing

from 0.70 to 0.90 for all the values of Richardson and Reynolds numbers. The same pattern is followed in maximum fluid volume fraction of ϕ_f = 0.99 except Re = 40 (Fig. 9.15(iii a-b)). Further, it can be seen that the maximum local Nusselt number (Nu_{L1}) was observed at the $\theta = 0^o$ (front of the cylinder C_1) for all of the dimensionless parameters (n, ϕ_f , Re and Ri) at Pr = 1 (Fig. 9.15). The local Nusselt number (Nu_{L1}) starts gradually decreasing as the θ increasing from 0^0 to 90^0. Therefore, the minimum value was seen at $\theta = 90^0$ (rear of the cylinder C_1) under the identical conditions. The above behavior is slightly changed in maximum fluid volume fraction (ϕ_f = 0.99). Notwithstanding, for Re = 1 and 10, the behavior is similar to ϕ_f = 0.70 and 0.90, but a different trend was observed at Re = 40 for shear-thinning and Newtonian fluids for both of the Ri = 1 and 2. In Fig. 9.15(a-iii), the maximum value of Nu_{L1} is again seen at $\theta = 0^o$, but the minimum value occurred between $\theta = 45^o$ to 60^0 for Re = 40 in contrast to $\theta = 90^o$ for Re = 1 and 10. From $\theta = 60^o$ onward, a recovery was seen till $\theta = 90^o$. Similarly, in Fig. 8.15(b-iii), for Re = 40, all else remaining same except the minimum Nu_{L1} occurred between $\theta = 30^o$ to 45^0 for Ri = 1 and $\theta = 60^o$ to 75^0 for Ri = 2, then recovery takes place till $\theta = 90^o$. Additionally, a significant influence of the Ri was seen over the local Nusselt numbers. In Fig. 9.11, an increased value of Nu_{L1} can be seen for Ri = 2 in contrast to Ri = 1 under the range of conditions covered herein. Because of the more distortion with increased buoyancy, the steep thermal gradients appear in the vicinity of cylinders and hence heat transfer enhances with increasing Ri.

Fig. 9.16 depicts the variation of local Nusselt number (Nu_{L2}) over the surface of the downstream cylinder (C_2) under the identical conditions to the upstream cylinder (C_1). As expected, the variation in local Nusselt number (Nu_{L2}) is quite different herein as compared to the local Nusselt number (Nu_{L1}) i.e. almost an opposite trend is seen. Thus, at the lower Reynolds number (Re = 1), for any of the fluid volume fraction (ϕ_f) and at Pr = 1, Ri = 1 and 2, a very gradual change is occurring for all of the shear-thinning, Newtonian and shear-thickening fluids. The maximum value of local Nusselt number (Nu_{L2}) was seen between $\theta = 40^0$ to 50^0 and minimum at $\theta = 90^0$ for ϕ_f = 70. Similarly, for ϕ_f = 0.90 and 0.99, the minimum and maximum Nu_{L2} was seen at $\theta = 0^0$ and $\theta = 90^0$, respectively under the identical conditions. Further, at higher Reynolds numbers (Re = 10 and 40), the minimum and maximum Nu_{L2} was seen at $\theta = 0^0$ and 90^0, respectively for all the values of n, ϕ_f and Ri except n = 1.8 (Fig 9.16c (i)), where the maximum and minimum Nu_{L2} occurs at $\theta = 0^0$ and $\theta = 90^0$ for Re = 40 and at $\theta = 25^0$ to 35^0 and $\theta = 0^0$ for Re = 10. Thus, the maximum value of Nu_{L2} can be seen at ϕ_f = 0.99, n = 0.4, Pr = 1, Ri = 2 and Re = 40 and minimum at ϕ_f = 0.70, n = 1.8, Pr = 1, Ri = 1 and Re = 1 (Figs. 9.16(a-iii and c-i)). The above changes in the local Nusselt number happen because, at small value of

Re or Pr, one would intuitively expect the value of Nu_L to show virtually no or small variations due to the fact that at low value of Re and/or Pr, heat transfer occurs primarily by conduction with a very small contribution from convection. Next, the influence of Ri can also be observed herein once again and thereby an increased value of Nu_{L2} can be seen for Ri=2 in contrast to Ri=1 for all the values of fluid volume fractions, power-law index and Reynolds numbers.

The influence of increased Prandtl number on local Nusselt numbers is shown in Figs. 9.17 and 9.18 for upstream cylinder (C_1) and downstream cylinder (C_2), respectively at Pr = 50. As expected, an increase in local Nusselt number with increasing value of Prandtl number is seen for all the value of the power-law index (n) and fluid volume fractions (ϕ_f). Further, the variation in local Nusselt numbers (Nu_{L3} and Nu_{L4}) at Pr = 50 was found to be almost similar to Pr = 1, except few cases. The main discrepancies were noticed for the value of higher Reynolds number (Re = 40) and fluid volume fraction (ϕ_f = 0.99) for all of the shear-thinning, Newtonian and shear-thickening fluids (Figs. 9.17-9.18). Also, both of the periodic cylinders (C_1 and C_2) strongly dependent on fluid volume fractions and show the following peculiar features. The opposite behavior can be seen at maximum fluid volume fractions of ϕ_f = 0.99 and Re = 40. Such a feature reveals that both cylinders act as an isolated cylinder under the maximum fluid volume fractions and high Reynolds number and/or Prandtl number. Because of the wake interference, the local Nusselt number at the front stagnation point of the downstream cylinder is quite different from that seen for the upstream cylinder in a periodic arrangement. The behavior above is similar to Gowda et al. (1998) for mixed convection and under the limiting cases of a single cylinder (Soares et al., 2009; Daniel and Dhiman et al., 2013). The above typical variations of streamlines, isotherm pattern, pressure coefficients and local Nusselt number with Re, Pr, Ri, n and ϕ_f observed herein, in turn, will alter with drag coefficients and average or overall heat transfer. It is explored in subsequent sections with the help of global behavior such as individual and total drag coefficients and average Nusselt number.

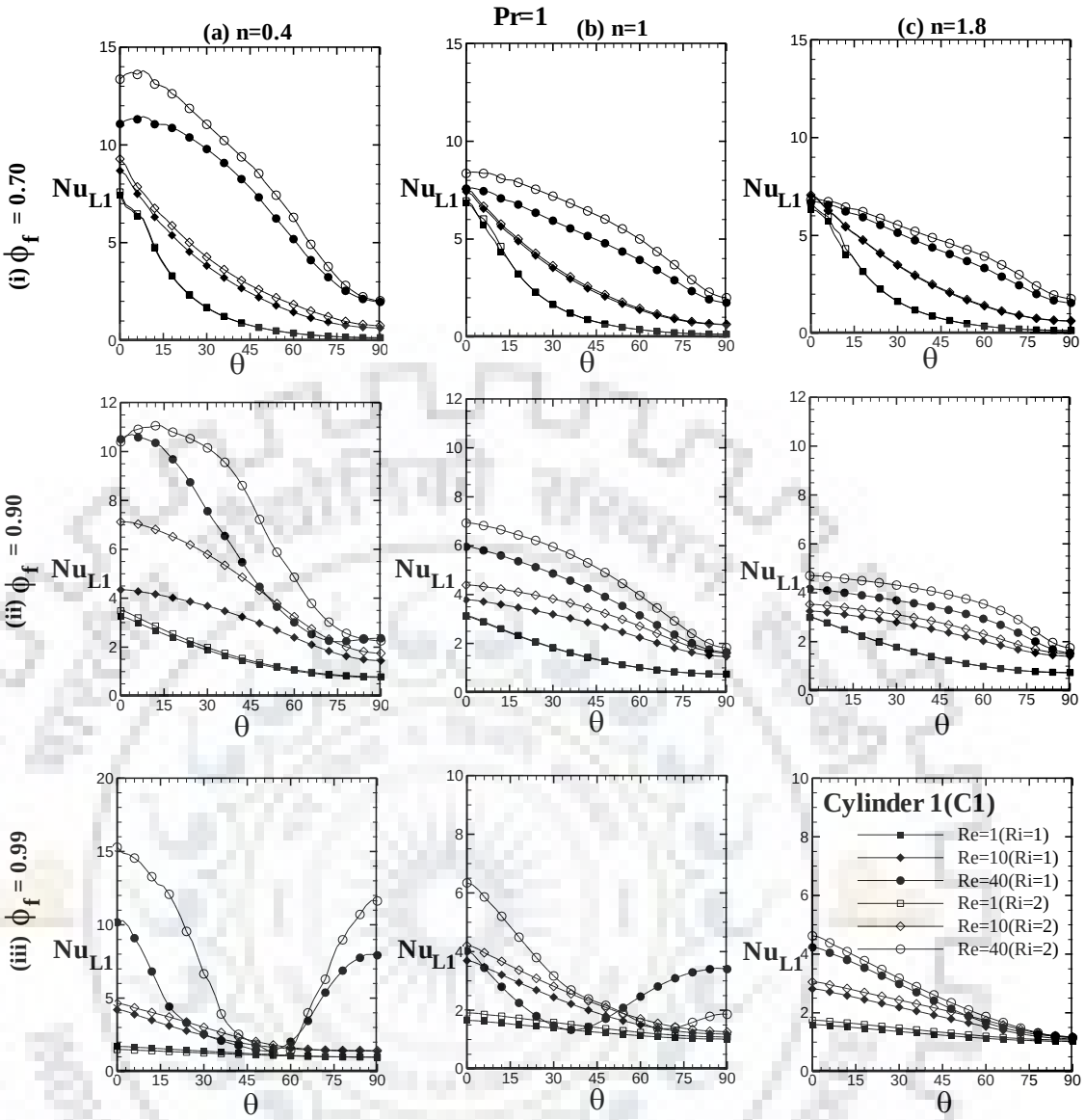

Figure 9.15: Variation of local Nusselt number (Nu_{L1}) over the surface of upstream cylinder (C_1) for power-law index (n = 0.4, 1 and 1.8), fluid volume fractions (ϕ_f = 0.70, 0.90 and 0.99), Reynolds number (Re = 1, 10 and 40), Richardson number (Ri = 1 and 2) at a fixed Prandtl number (Pr = 1)

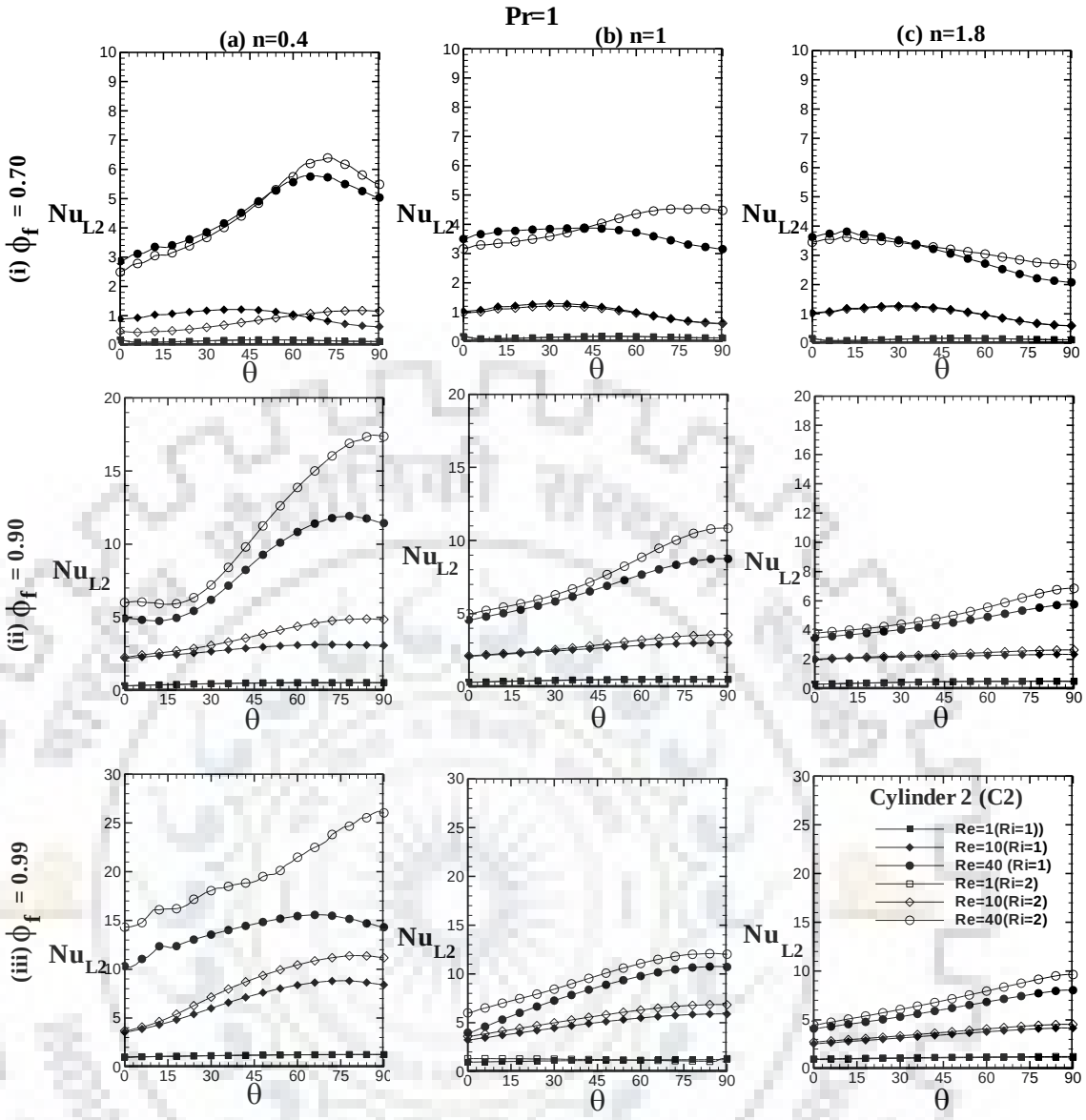

Figure 9.16: Variation of local Nusselt number (Nu_{L2}) over the surface of downstream cylinder (C_2) for power-law index (n = 0.4, 1and 1.8), fluid volume fractions (ϕ_f = 0.70, 0.90 and 0.99), Reynolds number (Re = 1, 10 and 40), Richardson number (Ri = 1 and 2) at a fixed Prandtl number (Pr = 1)

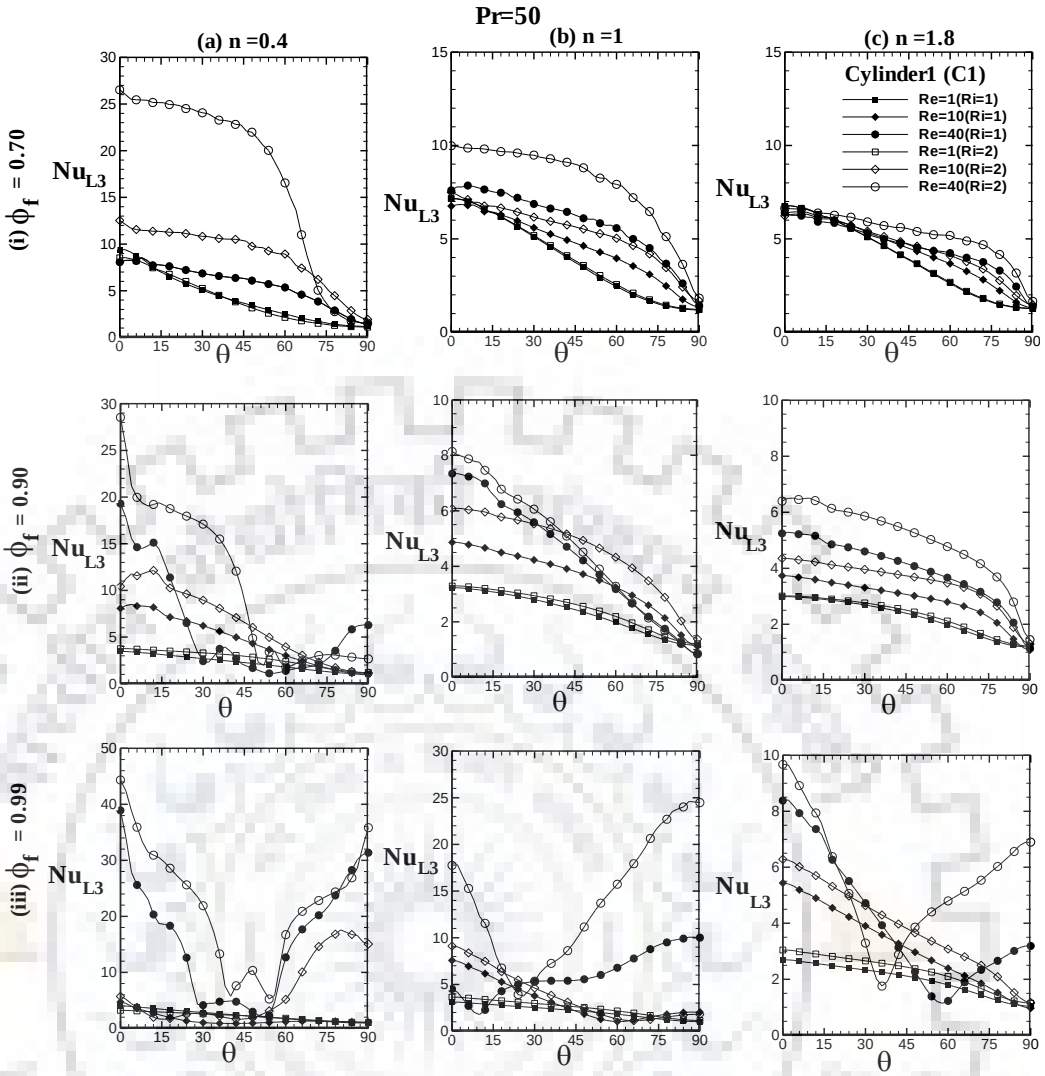

Figure 9.17: Variation of local Nusselt number (Nu_{L3}) over the surface of cylinder (C_1) for power-law index (n = 0.4, 1and 1.8), fluid volume fractions (ϕ_f = 0.70, 0.90 and 0.99), Reynolds number (Re = 1, 10 and 40), Richardson number (Ri = 1 and 2) at a fixed Prandtl number (Pr = 50)

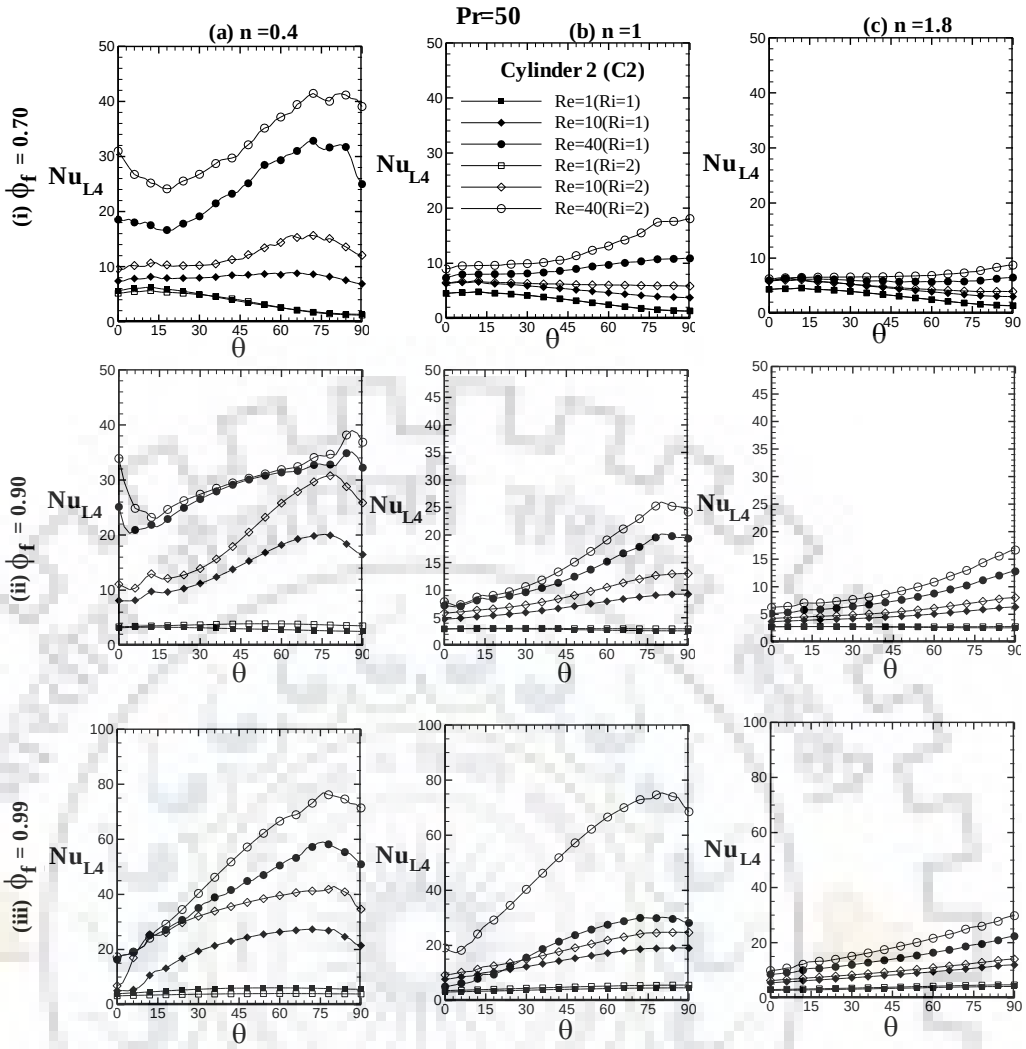

Figure 9.18: Variation of local Nusselt number (Nu_{L4}) over the surface of cylinder (C_2) for power-law index (n = 0.4, 1and 1.8), fluid volume fractions (ϕ_f = 0.70, 0.90 and 0.99), Reynolds number (Re = 1, 10 and 40), Richardson number (Ri = 1 and 2) at a fixed Prandtl number (Pr = 50)

9.3 Macroscopic characteristics

This section presents the nature of flow and thermal features in terms of pressure, friction and total drag coefficients and average Nusselt number. The dependence of these features on the governing parameters have also been presented using statistical correlations for both of the drag coefficients and average Nusselt number.

9.3.1 Pressure drag coefficient (C_{DP})

The variations of pressure drag coefficient (C_{DP}) on dimensionless parameters (n, ϕ_f , Re, Pr, and Ri) are shown in Table D1-D5 (Appendix-D). As can be observed in these Tables D1-

D5, the pressure drag coefficient (C_{DP}) has a strong dependence on aforementioned dimensionless parameters, but the dependence on flow behavior index (n), fluid volume fraction (ϕ_f) and Reynolds number (Re) are more prominent than the other parameters (Pr and Ri). For a fixed value of fluid volume fraction (ϕ_f), Reynolds number (Re), the Richardson number (Ri) and Prandtl number (Pr), the pressure drag coefficient (C_{DP}) increases as the value of the power-law index (n) gradually increases. For instance, an opposite trend can be seen in Table D1-D5 for both of the shear-thinning as well as shear-thickening fluids when compared with Newtonian fluids. The pressure drag coefficient (C_{DP}) of shear-thickening fluid is greater than the corresponding Newtonian fluid, whereas it is lower for the shear-thinning fluids; both these interpretations are directly associated with the nature of the surface pressure (Cp) profiles presented in the previous section. Further, the pressure drag coefficient (C_{DP}) shows a strong dependence on fluid volume fraction (ϕ_f), but an opposite trend was observed herein as compared to the dependence of power-law index (n). Thus, for a fixed value of Reynolds (Re), Prandtl (Pr) and Richardson (Ri) numbers, the pressure drag coefficient (C_{DP}) decreases as the value of fluid volume fraction (ϕ_f) gradually increases from ϕ_f = 0.70 to 0.99, irrespective of the value of the power-law index (n). As a consequence, the influences are greater in the region of lower fluid volume fraction (ϕ_f) as compared to higher fluid volume fraction (ϕ_f). For instance, for a fixed value of n = 0.4, Re = 1, Pr = 1 and Ri = 1, the C_{DP} value is 80.3642 for ϕ_f = 0.70 against the C_{DP} value of 31.0422 of ϕ_f = 0.80 and 10.2817 of ϕ_f = 0.99, etc. (Table D1). The influence of Richardson number (Ri) on pressure drag coefficient (C_{DP}) is also more stimulating and especially in the case of non-Newtonian mixed convection flow with the periodic geometry which consists a lot of complexity due to the varying fluid volume fraction (ϕ_f). Due to the buoyancy effect, the pressure drag coefficient (C_{DP}) varied significantly with the increased value of Richardson number. An increasing value of C_{DP} can be observed with the increased value of Richardson number in Tables D1-D5. Further, at higher Prandtl number, the influence of Richardson number was found to be more prominent. For instance, for a fixed value of n = 0.4, Pr = 1, ϕ_f = 0.70 and Re = 1, the C_{DP} value is 80.3642 for Ri = 1 and 85.8542 for Ri = 2 (Table D1). These C_{DP} values were improved at higher Prandtl number. For instance, at n = 0.4, Pr = 50, the above C_{DP} value was altered from 80.3642 to 89.6320 for Ri = 1 and 85.8542 to 92.8105 for Ri = 2 (Table D1). Similarly, at maximum fluid volume fraction of ϕ_f = 0.99 and at n = 0.4, Pr = 1, Re = 1, the C_{DP} value was 10.2817 for Ri = 1 and 10.5701 for Ri = 2. These value again altered at higher Prandtl number of n = 0.4, Pr = 50. For instance, the C_{DP} value is altered from 10.2817 to 15.3532 for Ri = 1 and from 10.5701 to 16.2882 for Ri = 2 under the identical

conditions. The above increase can be observed for all the values of n, Pr, Re and ϕ_f in Table D1-D5. This enhancement in C_{DP} value revealed that as the Richardson number increases, the more mixing (buoyancy) takes place in the vicinity of periodic cylinders which further improves with the increased Prandtl number. Additionally, when compared with forced convection (Ri=0), the mixed convection provides more distortion in the vicinity of flow and therefore a sharper velocity gradient appears which gives rise to pressure drag coefficient (C_{DP}).

Additionally, the influence of Reynolds number and Prandtl number have play an important role in such a complex system. It can be seen in Table D1-D5, as the Reynolds number is increasing, the pressure drag coefficient (C_{DP}) is decreasing accordingly irrespective of the other pertinent dimensionless parameters (n, ϕ_f , Pr and Ri). Thus, a higher value of C_{DP} can be seen at lower Reynolds number for any of the power law index (n), fluid volume fractions (ϕ_f), Prandtl (Pr) and Richardson (Ri) numbers. For instance, for a fixed value of n = 0.4, ϕ_f = 0.70, Pr = 1 and Ri = 1, the C_{DP} value is 80.3642 for Re = 1, 44.2844 for Re = 2 and 20.8522 for Re = 5, etc. This feature reveals that as the Reynolds number increases, the inertial forces are dominating over viscous forces and so the pressure drag coefficient (C_{DP}) getting reduced. Further, in contrast to forced convection, where Prandtl number does not influence the drag coefficients, there is a significant influence of Prandtl number in the case of mixed convection (Ri>0). In Tables D1-D5, it can be seen that the value of pressure drag coefficient (C_{DP}) increases as the Prandtl number increases. For instance, for a fixed value of n = 0.4, ϕ_f = 0.70, Re = 1 and Ri = 1, the C_{DP} value is 80.3642 for Pr = 1, 83.2135 for Pr = 10 and 89.6320 for Pr = 50, etc. Noticeably, the influence of Prandtl number (Pr) is seen to be less significant than that of the fluid volume fraction (ϕ_f), Reynolds number (Re) or Richardson number (Ri).

9.3.2 Friction drag coefficient (C_{DF})

The dependence of friction drag coefficient (C_{DF}) on dimensionless parameters (n, ϕ_f , Re, Pr and Ri) is also displayed in Table D1-D5. Similar to pressure drag coefficient (C_{DP}), the friction drag coefficient (C_{DF}) has shown a strong dependence on dimensionless parameters such as power-law index (n), fluid volume fraction (ϕ_f), Reynolds number (Re), Prandtl number (Pr) and Richardson number (Ri). Here, again the dependence on the power-law index (n), fluid volume fraction (ϕ_f) and Reynolds number (Re) is more prominent as compared to the Prandtl number (Pr) and or Richardson number (Ri). For a fixed value of fluid volume fraction (ϕ_f), Reynolds number (Re), the Richardson number (Ri) and Prandtl number (Pr), the friction drag

coefficient (C_{DF}) increases as the value of the power-law index (n) is slowly increased. For instance, an opposite trend can be seen in Table D1-D5 for both of the shear-thinning as well as shear-thickening fluids when compared with Newtonian fluids. The friction drag coefficient (C_{DF}) of shear-thickening fluid is greater than the corresponding Newtonian value, whereas it is lower for the shear-thinning fluid. Similarly, for a fixed value of the power-law index (n), Reynolds number (Re), Prandtl number (Pr) and Richardson number (Ri), the friction drag coefficient (C_{DF}) always decreases as the value of fluid volume fraction (ϕ_f) is progressively increase from ϕ_f = 0.70 to 0.99. As a consequence, the influences are greater in the region of lower fluid volume fraction (ϕ_f) as compared to higher fluid volume fraction (ϕ_f). Further, a significant role of buoyancy effect in terms of Richardson is seen here in the case of friction drag coefficient (C_{DF}). An increasing value of C_{DF} can be observed in Table D1-D5 as the Richardson number is increasing. Further, at higher Prandtl number, the influence of Richardson number is more prominent. For instance, for a fixed value of n = 0.4, Pr = 1, ϕ_f = 0.70 and Re = 1, the C_{DF} value is 44.8675 for Ri = 1 and 53.7376 for Ri = 2 (Table D1). These C_{DF} values are improved at higher Prandtl number as such for instance, at Pr = 50, the above C_{DF} value is altered from 44.8675 to 49.1211 for Ri = 1 and from 53.7376 to 59.5200 for Ri = 2 under the identical conditions. Additionally, the dependence of friction drag coefficient (C_{DF}) on Reynolds number and Prandtl number have been shown in Table D1-D5. Analogous to pressure drag coefficient (C_{DP}), the friction drag coefficient (C_{DF}) is decreasing as the Reynolds number is increasing. Thus a higher value of friction drag coefficient (C_{DF}) can be seen at lower Reynolds number in any of the fluid volume fractions for a given n, Pr and Ri. As far as the influence of Prandtl number is concerned, a similar trend to pressure drag coefficient (C_{DP}) can be seen in Table D1-D5.

9.3.3 Total drag coefficient (C_D)

Table D1-D5 shows the variations of total drag coefficient (C_D) also on the pertinent dimensionless parameters (n, ϕ_f, Re, Pr and Ri). As can be observed in these tables, the total drag coefficient (C_D) also exhibits the similar kind of dependence as that of pressure drag coefficient (C_{DP}) and friction drag coefficient (C_{DF}). So a strong dependence of total drag coefficient (C_D) on above dimensionless parameters can be seen in Tables D1-D5. Further, as discussed earlier, the dependence on the power-law index (n) and fluid volume fraction (ϕ_f) is more prominent than the other parameters. Additional efforts are made to develop a simple statistical correlation for the functional dependence of total drag coefficient over the governing

parameters (n, ϕ_f , Pr, Re and Ri) based on the 432 data points for each of the n. The correlation is expressed by Eq. (9.1) as follows:

$$C_D = a n^b \, Pr^c \, Ri^d \phi_f^e \, Re^g + \exp(Ri) \; ; \qquad (0.4 \le n \le 1.8) \qquad (9.1)$$

$$\text{and} \qquad \alpha = \sum_{i=1}^{5} \alpha_i n^{(5-i)} \text{ , where } \alpha = a, b, c, d, e, g \qquad (9.2)$$

The correlation coefficients and exponents (a, b, c, d, e and g) together with their statistical parameters are summarized in Table 9.2. The above correlation is developed by non-linear regression of the numerical data. The best fit of the current numerical data versus the correlation values of Eq. (9.1) is shown in Figs. 9.19 (a-b). The present numerical values show an excellent correspondence with the values predicted using Eq. 9.1. For instance, the above correlation has the average and maximum deviations of ~3.5% and ~8.25%, respectively for the 92% of the data points whereas the 5% of the data points have the average and maximum deviations of ~10.25 % and ~20.35%, respectively. Only 2% of the data points have the deviations within the 20 to 30%.

Table 9.2: Correlation coefficients and exponents for total drag coefficient (C_D) of Eq. (9.1)

	C_D				
α	α_1	α_2	α_3	α_4	α_5
a	215.92	-930.82	1371.7	-799.28	158.42
b	-10.065	5.4714	62.159	-80.565	21.137
c	0	0.0241	-0.0746	0.0454	0.0319
d	0	0	-0.1052	0.1715	-0.0054
e	0	0	1.2912	-0.2076	-5.9963
g	0	0.1373	-0.6821	0.9191	-1.2128
R^2	0.9844				

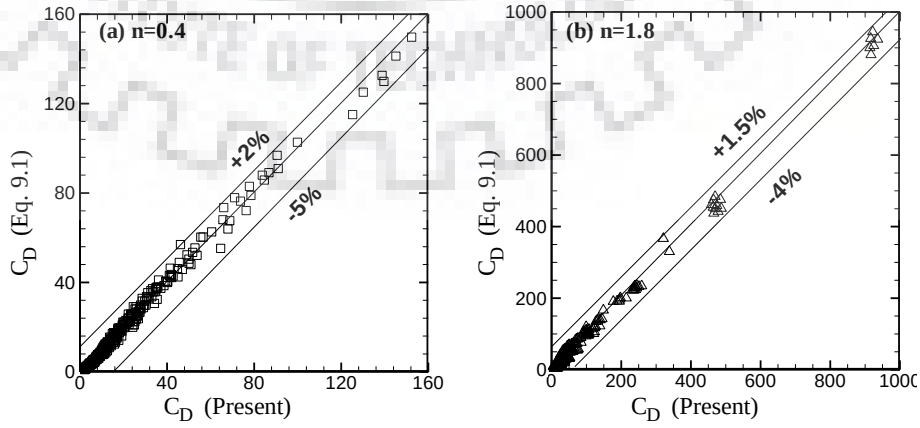

Figure 9.19: Best fit of present numerical vs. correlation values for total drag coefficient (C_D) (a) n = 0.4 and (b) n = 1.8

9.3.4 Influence of buoyancy parameter (Ri)

Although, the influence of buoyancy parameter (Ri) on the drag coefficients has been discussed briefly earlier, perhaps, it is beneficial to delineate the influence of Ri on the individual and total drag coefficients. In view of above, Newtonian and non-Newtonian mixed convection values of drag coefficients have been normalized using the corresponding forced convection values (Ri = 0) in the manner as defined in Chapter 8 (Section 8.3.4). The normalized plots of pressure drag coefficient (C_{DP}), friction drag coefficient (C_{DF}) and total drag coefficient (C_{DP}) vs. fluid volume fraction (ϕ_f) are shown in Figs. 9.20-9.22, respectively with the systematic variations of the power-law index (n), Reynolds number (Re), Prandtl number (Pr) and Richardson number (Ri). An examination of these plots discloses that the similar pattern is being followed for each of the normalized values of C_{DP}, C_{DF} and/or C_D. As expected, an opposite trend is seen for shear-thinning fluids in contrast to the Newtonian as well as shear-thickening fluids. For shear-thinning fluids, the normalized values (X^N) are decreased as the fluid volume fraction (ϕ_f) is increased for all values of Pr, Re and Ri. Further, these values are lower than Newtonian as well as shear-thickening fluids. The above decrease is more significant for Re= 10 and 40 as compared to Re = 1 (Figs. 9.20-9.22). On the contrary, the normalized value (X^N = C_{DP}, C_{DF} and/or C_D) for Newtonian as well as shear-thickening fluids are increasing as the fluid volume fractions and the power-law index is increasing. So the lowest and the highest normalized values (X^N) are observed in shear-thinning fluids and shear-thickening fluids, respectively (Figs. 9.20-9.22). Furthermore, the influence of Ri is clearly visible in these plots. The solid and dashed lines represent the behavior at Ri = 1 and 2, respectively. A higher normalized value (X^N) can be seen at Ri = 2 as compared to Ri = 1 for all the values of the power-law index, Reynolds number and Prandtl number. Additional information includes the unsteady behavior at a higher fluid volume fraction of ϕ_f = 0.99. For instance, the behavior was observed to be unsteady for shear-thinning and Newtonian fluids at Re = 40 and ϕ_f = 0.99 for all the values of Prandtl number (Pr = 1, 10 and 50) and Richardson number (1 and 2) (Figs. 9.20-9.21). However, under the similar conditions, the behavior is steady for Re = 1 and 10. The unsteady behavior was found to be increased with an increase in Prandtl number. For instance, at Pr = 50, an unsteady behavior at ϕ_f = 0.96 and 0.98 was also noticed for Re = 40. Moreover, Fig. 9.22 shows the normalized plot for total drag coefficients (C_D) which includes the complete ranges of parameters studied herein. Both of the steady as well unsteady behaviors are exhibited for the total drag coefficients (C_D) in a different way. Here, the influence of power-law index (n) and buoyancy parameter (Ri) is shown in the

plot which displays the dependence of normalized parameters. In summary, the normalized values of drag coefficients increase consistently for Newtonian as well as shear thickening fluids whereas decreases for shear-thinning fluids as the value of fluid volume fraction (ϕ_f) increases irrespective of the values of Reynolds number (Re), Prandtl number (Pr) and Richardson number (Ri). Also, under the identical conditions, drag coefficients (C_D, C_{DP} and C_{DF}) increase with increasing Richardson number (Ri). This behavior can generally be attributed to higher stresses owing to aiding buoyancy. Finally, qualitatively similar behavior has been observed for both of the individual and total drag coefficients.

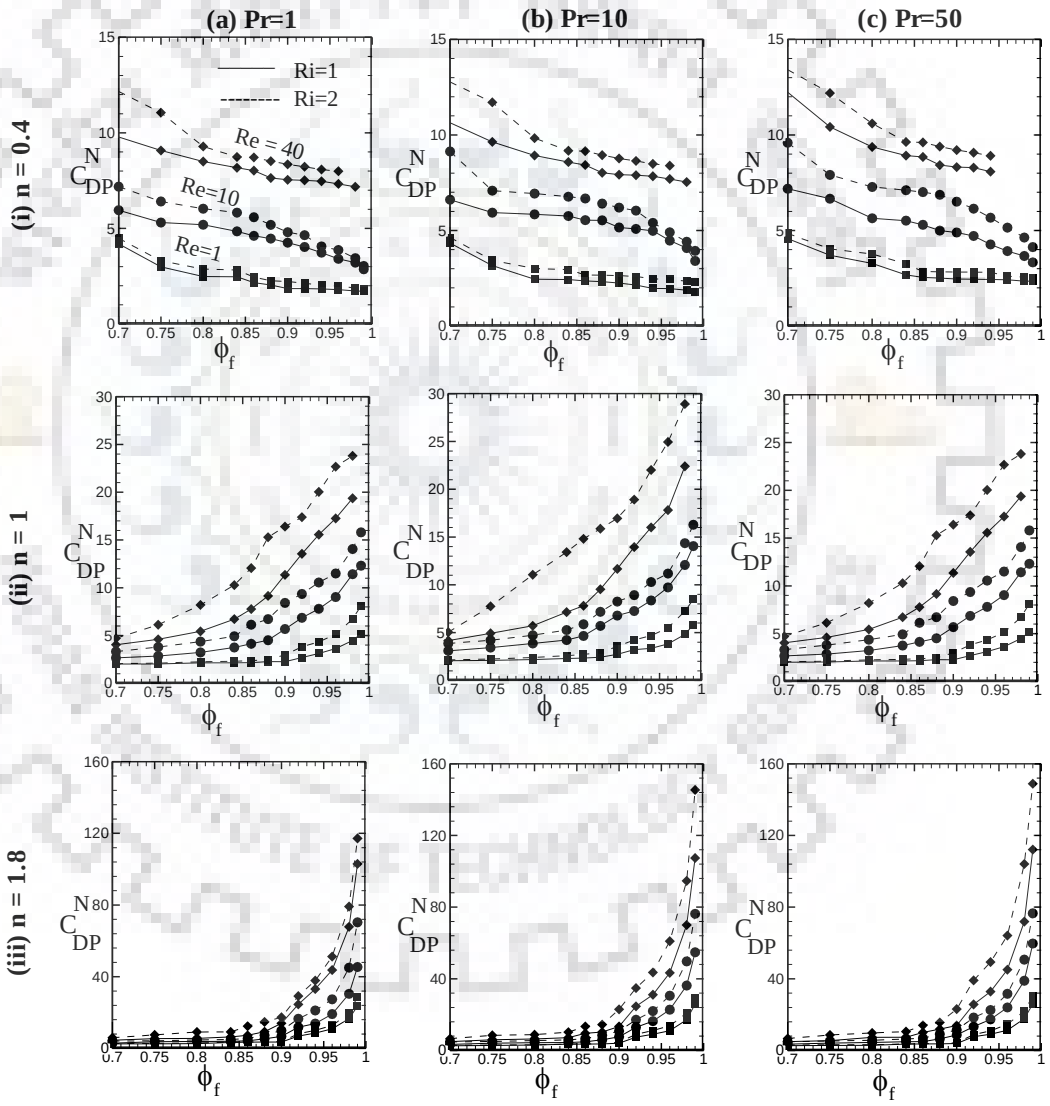

Figure 9.20: Dependence of normalized pressure drag coefficient (C_{DP}^N) over the fluid volume fractions (ϕ_f = 0.70-0.99), power-law index (n = 0.4, 1and 1.8), Reynolds number (Re = 1, 10 and 40), Richardson number (Ri = 1 and 2) and Prandtl number (Pr = 1, 10 and 50)

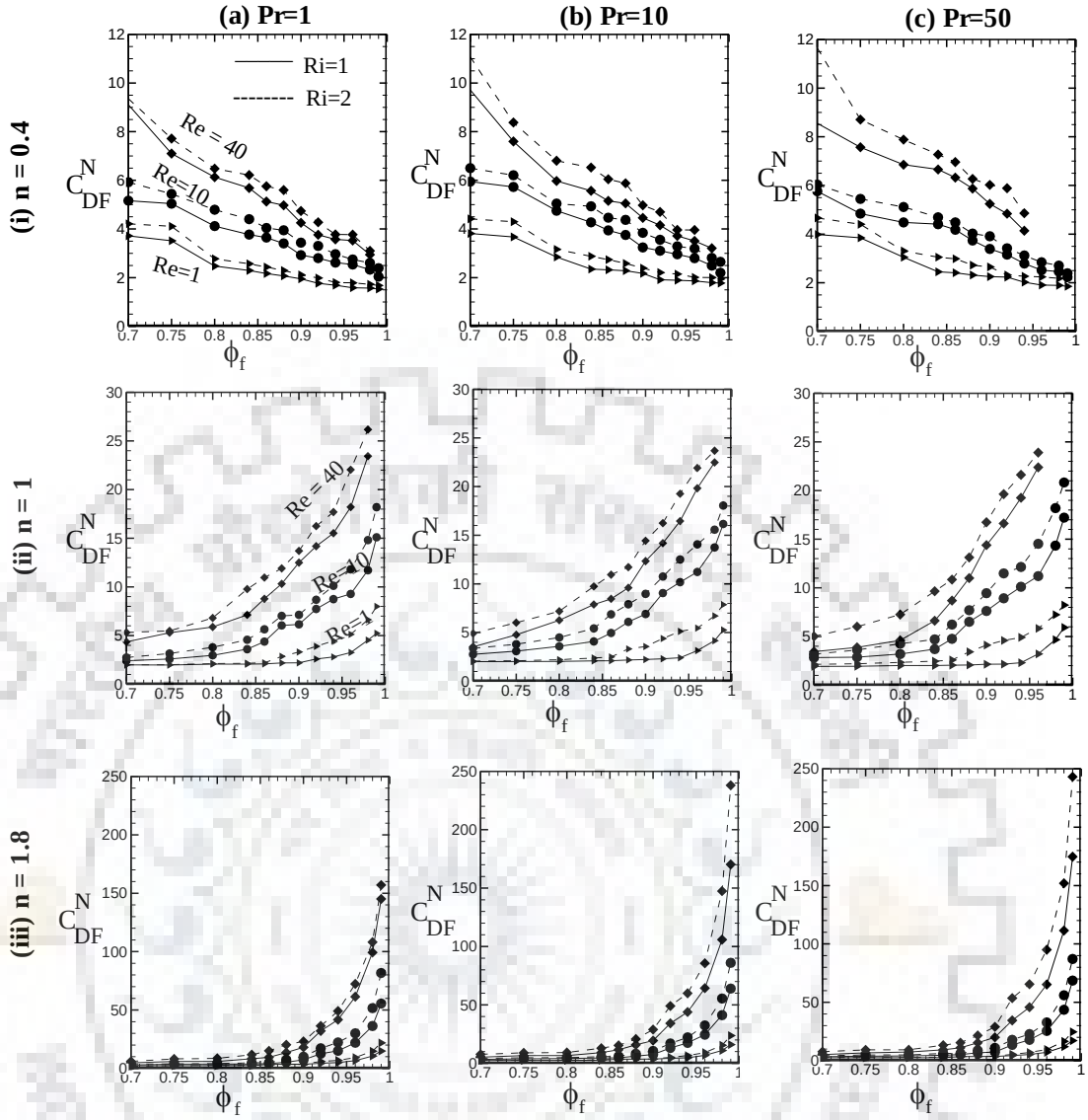

Figure 9.21: Variation of normalized friction drag coefficient (C_{DF}^{N}) versus fluid volume fractions (ϕ_f) over the surface of cylinders (C_1 and C_2) for power-law index (n = 0.4, 1and 1.8), Reynolds number (Re = 1, 10 and 40), Richardson number (Ri = 1 and 2) and Prandtl number (Pr = 1, 10 and 50)

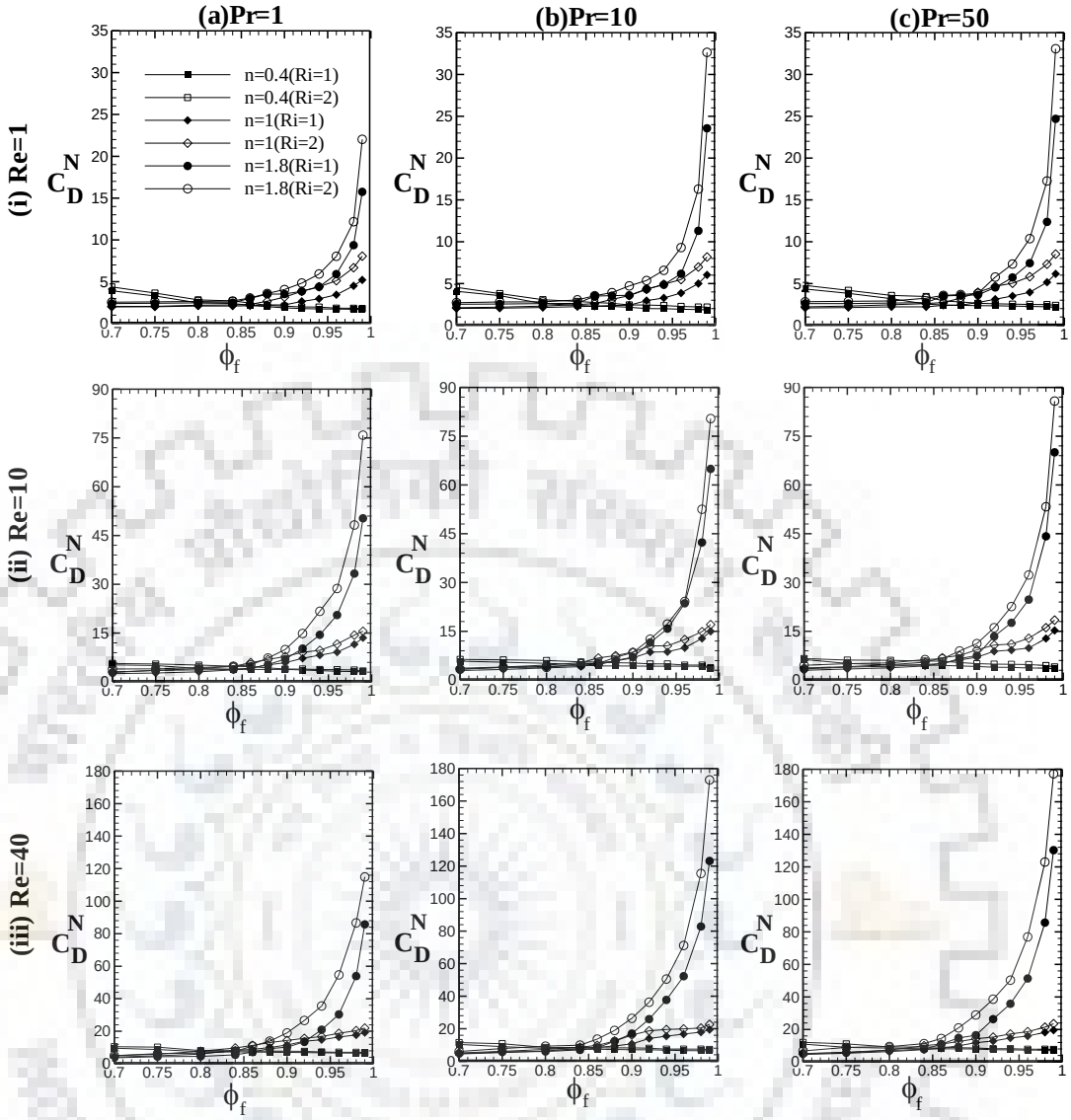

Figure 9.22: Variation of normalized total drag coefficient (C_D^N) versus fluid volume fractions (ϕ_f) over the surface of cylinders (C_1 and C_2) for power-law index (n = 0.4, 1 and 1.8), Reynolds number (Re = 1, 10 and 40), Richardson number (Ri = 1 and 2) and Prandtl number (Pr = 1, 10 and 50)

9.3.5 Average Nusselt number

The dependence of surface average Nusselt number (Nu) on the governing parameter (n, ϕ_f , Pr, Re and Ri) is shown in Table E1-E5. An improvement in the average Nusselt number (Nu) has been observed in with the increasing value of above governing parameters except for the power-law index (n). As expected, an opposite trend is observed herein between the shear-thinning and shear-thickening fluids. The value of average Nusselt number is seen to be higher and lower for shear-thinning and shear thickening fluids, respectively than the corresponding Newtonian values. For instance, at a given value of ϕ_f = 0.70, Re = 1, Pr = 1 and Ri = 1, the average Nusselt

number was found to be 1.0110 for shear-thinning (n = 0.4) (Table E1) and 0.9255 for shear-thickening (n = 1.8) fluids (Table E5). Of course, Newtonian value (Nu = 0.9518) lies in between these fluids under the identical conditions. The dependence of Nu on fluid volume fraction is also much interesting. For mixed convection of non-Newtonian case, an opposite dependence of Nu on ϕ_f was observed in contrast to forced convection, i.e., Nu increases with increasing ϕ_f, irrespective of the values of n, Re, Pr and Ri. In other words, heat transfer improved when the cylinders were gone away. This is exactly the opposite of forced convection case where the heat transfer improves when the cylinders come closer (Martin et al., 1998). Further, for a fixed value of the power-law index (n), the average Nusselt number (Nu) increases with increasing value of fluid volume fraction, Reynolds number, Prandtl number and buoyancy parameter (Ri). Additionally, the effect of n and ϕ_f on Nu is more pronounced than either of Re, Pr or Ri. Additional improvement in heat transfer was observed due to the buoyancy parameter (Ri). An increased value of the average Nusselt number can be observed in Table E1-E5 for Ri = 2 as compared to Ri = 1. The reason for above enhancement is that as the buoyancy parameter (Ri) increases, the potential energy of the molecules increases which gives rise to mixing and finally heat transfer improves. This can be observed in isotherms also where the sharp and dense thermal gradients appear with the increase in Ri. Thus, the maximum value of the average Nusselt number was found to be about 26.9526 for n = 0.4, ϕ_f = 0.99 at Pr = 50, Re = 40 and Ri = 2, whereas the minimum value was about 0.9255 for n = 1.8, ϕ_f = 0.70 at Pr = 1, Re = 1and Ri = 1.

The aforementioned behavior is further delineated by normalizing the average Nusselt number as shown in Fig. 9.23. It has also been normalized in a similar way as defined in Chapter 8 (Section 8.3.4) corresponding to their forced convection values (Ri = 0). An examination of these plots (Fig. 9.23) discloses that the normalized values (Nu^N) are increasing with the corresponding increase in fluid volume fractions (ϕ_f). This increase is more significant for Re= 10 and 40 as compared to Re = 1 for all the values of n, ϕ_f, Pr and Ri. Here, again the higher value of normalized Nu is seen for shear-thinning fluids than the corresponding Newtonian fluids, however, an opposite trend is seen for shear-thickening fluids. Additionally, the effect of buoyancy parameter (Ri) is clearly visible in the plots. The solid and dashed lines represent the behavior at Ri = 1 and 2, respectively. A greater normalized value (Nu^N) can be seen at Ri = 2 as compared to Ri = 1 for all the values of Reynolds number as well as Prandtl number. Further information includes the unsteady behavior at a higher fluid volume fraction of ϕ_f = 0.99. For ϕ_f = 0.99, an unsteady behavior was observed above Re = 10 (i.e. at Re = 20 and 40) for the Pr = 1, 10 and Ri = 1, 2. Further, with the increased Pr, the unsteady behavior was found to be

increased. For instance, at Pr = 50, an unsteady behavior at ϕ_f = 0.96 and 0.98 was also noticed. This behavior can generally be ascribed to higher stresses owing to aiding buoyancy and/or mixing.

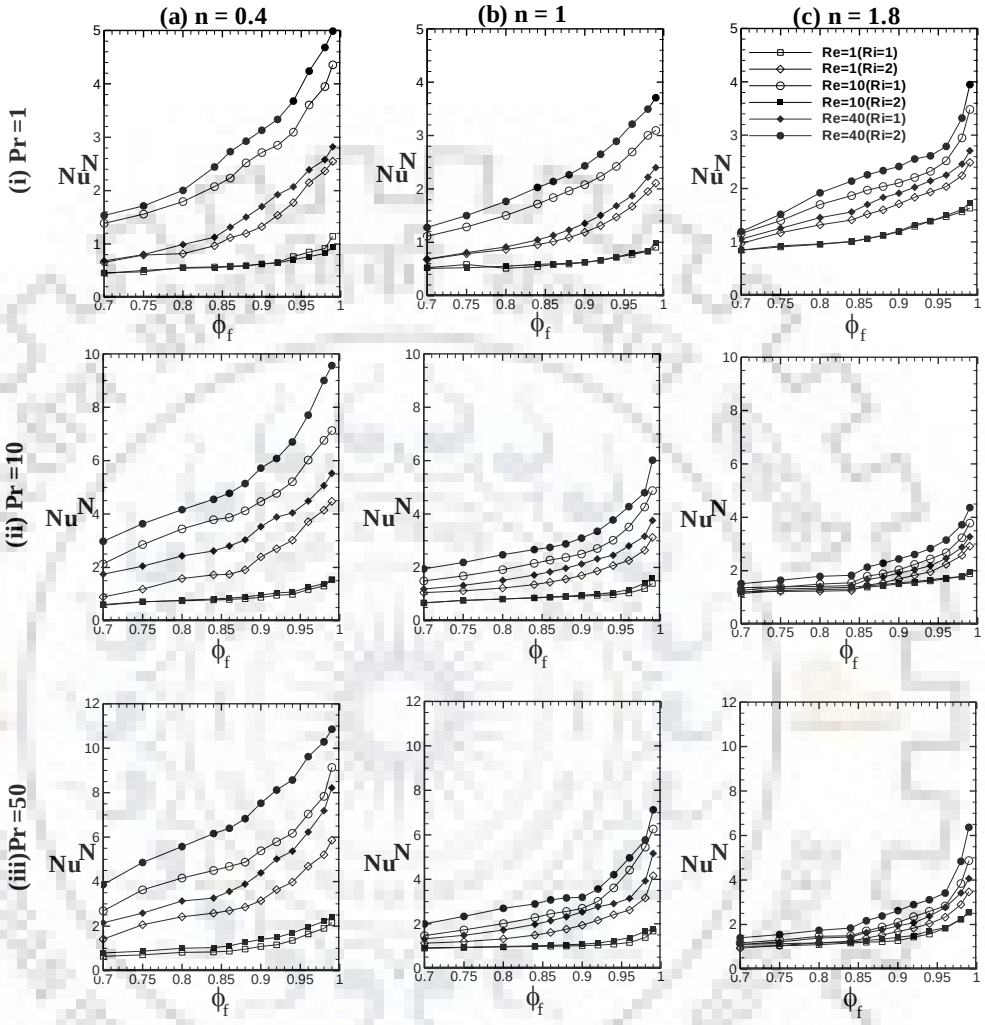

Figure 9.23: Variation of normalized average Nusselt number (Nu^N) vs. fluid volume fractions (ϕ_f) for power-law index (n = 0.4, 1and 1.8), Reynolds number (Re = 1, 10 and 40), Richardson number (Ri = 1 and 2) and Prandtl number (Pr = 1, 10 and 50)

Additional efforts have been made to develop a correlation for the average Nusselt number in terms of governing parameters (n, ϕ_f , Ri, Pr and Re). The statistical analysis of the results based on the 432 data points for each of the n, returned the following correlation for Nu:

$$Nu = an^b \, Pr^c \, Ri^d \phi_f^e \, Re^g + h \exp(nRi) \; ; \qquad (0.4 \le n \le 1.8) \qquad (9.3)$$

and $$\alpha = \sum_{i=1}^{5} \alpha_i n^{(5-i)} \text{ , where } \alpha = a, b, c, d, e, g \text{ and } h \qquad (9.4)$$

The correlation coefficients and exponents (a, b, c, d, e, g and h) together with their statistical parameters are listed in Table 9.3. The best fit of the present numerical vs. the correlation values of Eq. (9.3) is shown in Fig. 9.24. An excellent agreement was found between the present numerical results and the predictions of Eq. (9.3) in Fig 9.24. For instance, this correlation has shown the average and maximum deviations within 2% and 6% respectively for 95% of the data points, whereas the deviations were within 7-16% for rest 4% of the data points.

Table 9.3: Correlation coefficients and exponents for average Nusselt number (Nu) of Eq. (9.3)

	Nu				
α	α_1	α_2	α_3	α_4	α_5
a	11.2030	-49.5090	76.0990	-48.2481	11.9282
b	-8.8544	24.5430	-10.8830	-9.4621	4.0725
c	0	0	0.0337	-0.1208	0.2503
d	-0.7516	3.0398	-4.1457	2.1912	0.0309
e	1.3092	-5.6994	8.5555	-5.2031	2.1063
g	0	0.1172	-0.3999	0.2914	0.3437
h	0	1.5202	-6.0266	7.7396	-3.2833
R^2	0.9953				

Broadly speaking, in the case of mixed convection, an increase in Prandtl number, Reynolds number, shear-thinning behavior and fluid volume fractions enhances the rate of heat transfer and reduces the drag except Prandtl number as reported by many researchers (Duli et al., 1995; Gowda et al., 1998; Haldar, 2000; Fornarelli et al., 2016). Further, in the case of forced convection across periodic array of cylinders, the above feature has been reported (Zukauskas, 1972, 1987a; Martin et al., 1998; Mandhani et al., 2002; Gamrat et al., 2008, etc.). In addition, some different characteristics which were found in this investigation are the influence of fluid volume fraction (ϕ_f) and Prandtl number over the Nusselt numbers and drag coefficients, respectively. Firstly, as discussed above, an increase in Nusselt number was observed with the increasing value of fluid volume fractions (ϕ_f) in the case of mixed convection. This is in contrast to forced convection where the opposite trend has been observed. This might happen because as the fluid volume fractions (ϕ_f) increases, the fluids gets more time to distort and swirl in the increased vicinity of periodic cylinders, results the more heat transfer takes place. Secondly, an increase in individual and total drag coefficients was observed with the increase in Prandtl number. This is again in contrast to forced convection where the Prandtl number does not influence the flow characteristics such as individual and total drag coefficients.

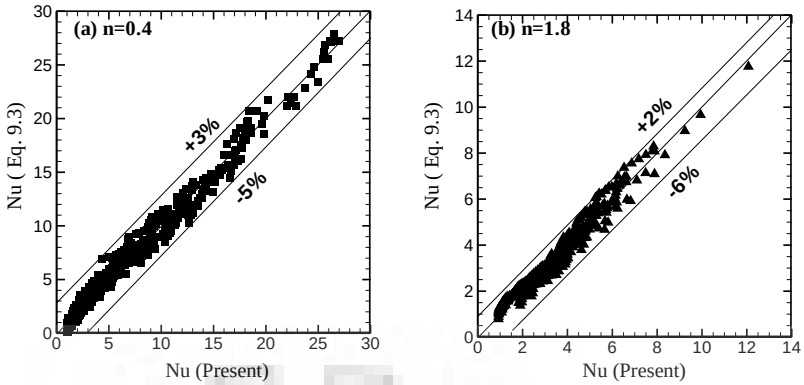

Figure 9.24: Best fit of present numerical vs. correlation values for average Nusselt number (Nu) of (a) n=0.4 and (b) n=1.8

In summary, the flow and heat transfer characteristics of non-Newtonian fluids across a periodic array of cylinders in cross-flow are seen to be influenced in an intricate manner with the power-law index (n), fluid volume fraction (ϕ_f), Reynolds (Re), Prandtl (Pr) and Richardson (Ri) numbers. At high values of Re, the wake interferences are more prominent when the fluid volume fraction (ϕ_f) is high. On the other hand, when the cylinders are sufficiently far away from each other i.e. maximum fluid volume fraction ($\phi_f = 0.99$), no wake interference phenomena will occur and both cylinders would act individually as a single cylinder. Finally, it needs to be emphasized here that, while the periodic array of cylinders in square geometry has been considered, the interactions in the other types of arrangements, e.g., triangular, rectangular, hexagonal are also equally important depending upon the fluid volume fraction or porosity of the cylinders. Indeed, a satisfactory understanding of both types of interactions (in line or staggered) is desirable to develop sound design strategies for shell-and-tube heat exchangers, tubular modules of membranes, etc. Further, the idealized flow geometry considered can serve us a launching pad to undertake the modeling of multi-cylinder arrays as encountered in process equipment.

Chapter 10

CONCLUSIONS AND SCOPE FOR FUTURE WORKS

The forced and mixed convection flow and heat transfer characteristics of Newtonian and non-Newtonian power-law fluids across the periodic array of circular cylinders have been investigated in a square geometrical configuration. Extensive numerical results have been obtained and presented with the systematic variations of pertinent dimensionless parameters (n, ϕ_f , Re, Pr and Ri). The impact of these parameters on the pressure coefficient, individual and total drag coefficients, local and average Nusselt numbers and the Colburn heat transfer factors, etc. have been examined and communicated. The qualitative features of flow and the thermal fields have been represented by the streamlines and isotherm profiles, respectively. The key findings of the various problems investigated herein are as follows:

10.1 Forced convection flow and heat transfer characteristics of Newtonian fluids across periodic array of circular cylinders

Fluid flow and heat transfer characteristics across the periodic array of circular cylinders have been examined to explore the influences of flow governing parameters (Re, Pr and ϕ_f) on the local and global characteristics of flow and thermal parameters. The local flow phenomenon describes that the dense arrays offer high resistances to flow of fluids and hence sparse array is required to minimize the flow resistances. A strong dependence of drag coefficients on Reynolds number and fluid volume fraction was observed. The drag coefficients decrease gradually with increasing Re for all the value of fluid volume fractions. Further, a drastic reduction in drag coefficient was observed with increasing value of fluid volume fractions. Also, in the region of higher inertial flow, the pressure forces are dominating over friction forces. The isotherm patterns reveal that the increasing inertial effects enhance the rate of heat transfer due to the dense clustering of the isotherms near the cylinder surfaces. The dependence of fluid volume fractions on the average Nusselt number is more prominent than the Reynolds number. The relative heat transfer enhancement was approximately 47% between the minimum and maximum fluid volume fractions. Additionally, a statistical correlations for the drag coefficients as well as Nusselt number have been presented for the best utilization of the results in the design and

engineering analysis. Finally, the present results of drag coefficient and Nusselt number have been compared with available literature which displayed an excellent agreement.

10.2 Forced convection momentum transfer characteristics of power-law fluids across periodic array of circular cylinders

The steady flow of power-law fluids has been examined across the periodic array of circular cylinders to explore the momentum transfer characteristics. The effects of Reynolds number, fluid volume fractions and power-law index on the local and global characteristics of momentum transfer has been elaborated. The drag coefficient was always seen to increase with increase in power-law index over the range of $0.40 \leq n \leq 1.8$ (i.e. decreasing shear-thinning or increasing shear-thickening behaviours). Further, with the increasing fluid volume fractions, the drag coefficients decreases rapidly, whereas, a gradual decrease was observed with the increasing value of Reynolds number. Also, in the region of higher inertial flow, the pressure forces are dominating over friction forces. The variation of the pressure coefficient on the surfaces of the cylinders with Reynolds number, fluid volume fraction and the power-law index has also been explained. Additionally, the results were used to develop the statistical correlations for the individual and total drag coefficients to give a further physical insight of the fluid behaviors. Finally, findings have been compared with scant available literature which displayed the excellent agreement

10.3 Forced convection heat transfer characteristics of power-law fluids across periodic array of circular cylinders

The flow and thermal energy equations have been solved to inculcate the dependence of heat transfer characteristics over the power-law index, fluid volume fraction, Reynolds and Prandtl numbers for the flow of power-law fluids across the periodic array of circular cylinders. The implications of frequently used constant temperature boundary condition on the thermal features have been investigated. The Nusselt number is greatly influenced by Re, Pr, n and ϕ_f. Particularly, the shear-thinning behavior improves the rate of heat transfer and the magnitude of improvement augments with the increasing value of Re and/or Pr and decreasing fluid volume fraction and the power-law index. In contrast, a reverse trend was observed for shear-thickening fluids under the alike situations. An enhancement of about 97% was noticed in the shear-thinning region between the extreme fluid volume fractions for the highest value of Pr and the lowest values of Re and n. Under the identical conditions, the enhancement was about 83% in the shear-thickening region. However, in many cases, the enhancement was noticed even more than 100%. Overall, different levels of improvement in local and average Nusselt numbers were noticed

because of the shear-thinning and shear-thickening natures of the fluids. The results have been further used to develop the statistical correlations for average Nusselt number and the Colburn heat transfer factor to give additional physical insight of the fluid behaviors. Moreover the findings have been shown the good contrast with scant available literature.

10.4 Aiding buoyancy mixed convection characteristics of Newtonian fluids across periodic array of circular cylinders

The aiding buoyancy mixed convection features of Newtonian fluids have been examined across periodic array of circular cylinders. The flow and thermal characteristics have shown the strong dependence over the governing parameters (ϕ_f , Re, Pr and Ri). The streamline patterns have shown the non-monotonous behavior. Further, the pressure drag coefficient was dominating over friction drag coefficient for both of Richardson (Ri) as well as Prandtl (Pr) numbers, but the influences were found to be more prominent at lower Reynolds numbers and higher buoyancy parameter. The total drag coefficient was also seen to decrease with increase in Reynolds number and fluid volume fraction for the given value of Prandtl and Richardson numbers. The additional feature was found with the influence of Prandtl number on drag coefficient. Here, an increase in the drag coefficients was observed with the increasing value of Prandtl numbers for the case mixed convection (Ri > 0) which is opposite to forced convection (Ri = 0) where Prandtl number does not influence the drag coefficient. The denser isotherm patterns at higher Reynolds and Prandtl numbers suggested an improvement in the rate of heat transfer. The average Nusselt number was observed to be increased with the increasing value of ϕ_f , Re, Pr and Ri. Additionally, aiding buoyancy enhances both of the flow and thermal parameters in the vicinity of periodic cylinders. An unsteady behavior was also observed at higher Re and ϕ_f for all the values of Pr. Moreover, a statistical correlation for the drag coefficients and average Nusselt numbers was developed for gaining the more physical insights of the results. Lastly, the findings were compared with the scant available literature which displayed a good agreement with the present results.

10.5 Aiding buoyancy mixed convection characteristics of power-law fluids across periodic array of circular cylinders

The mixed convection flow and heat transfer characteristics of power-law fluids have been investigated across the periodic array of circular cylinders numerically for a wide range of governing parameters (n, ϕ_f , Re, Pr and Ri) under the aiding buoyancy conditions. The influences of these parameters over the streamlines, pressure coefficient, isotherm patterns and

individual and total drag coefficients, local and average Nusselt number were explored and presented. The local flow phenomenon (streamlines, pressure coefficient and isotherm patterns) describes that the dense arrays offer higher resistances to flow of fluids and hence sparse array is required to minimize the flow resistances. Further, the drag coefficients decrease gradually with increasing value of Re for all the values of fluid volume fractions and power-law index. However, an increase in drag coefficients was observed with increasing value of Prandtl number in the mixed convection (Ri > 0) case as opposed to forced convection cases (Ri = 0).

The isotherm patterns reveal that the increasing inertial effects enhance the rate of heat transfer due to the dense clustering of the isotherms near the cylinder surfaces. The average Nusselt number was observed to be increased with the increasing values of ϕ_f , Re, Pr and Ri and decreasing value of n (i.e., increasing shear-thinning behavior). A transient behavior was observed for both of the drag coefficients as well as average Nusselt number at higher fluid volume fractions and Reynolds numbers. Additionally, aiding buoyancy, enhances both of the flow and thermal parameters in the vicinity of periodic cylinders. Moreover, a statistical correlations for the drag coefficients and average Nusselt numbers are developed for gaining the more physical insights of the results.

10.6 Scope for future works

The present work has contributed to the numerical understanding of the two-dimensional laminar flow and thermal characteristics of incompressible Newtonian and non-Newtonian fluids across a periodic array of circular cylinders in a square geometry for a wide ranges of engineering parameters and specially the fluid volume fraction and/or porosity of the cylinders. To gain more physical insights in different aspects of the present area, the following suggestions and recommendations are made for the future course of work;

- It needs to be emphasized here that, while the periodic array of cylinders in square geometry has been considered here, the interactions in the other types of arrangements such as triangular, rectangular, hexagonal etc. can be studied.
- In present studies, only in-line arrangements have been considered. The staggered configurations are also equally important and can be studied separately for the different aspects of the flow and heat transfer parameters.
- The non-Newtonian mixed convection flow and heat transfer characteristics across a periodic array of circular cylinders and/or over tube banks are almost negligible and can be studied extensively.

- The present work is limited to 2-D flow of Newtonian and power-law fluids. This study can be extended for 3-D flow also. Further, the other non-Newtonian models such as Carreau and Ellis models can be used to explore the different behaviors.

BIBLIOGRAPHY

Abrate, S., 2002, Resin flow in fiber preforms, App. Mech. Rev., 55, 579-599.

Abrate, S., 2007, Introduction of new concepts and problem solving in Engineering Dynamics, Int. Mech. Eng. Congress Exposition, Nov.11-15, Seattle, Washington , USA.

Abrate, S., 2011, Impact Engineering of Composite Structures, vol. 526, Springer.

Adams, D., Bell, K. J., 1968, Fluid friction and heat transfer for flow of sodium carboxy-methyl cellulose solutions across banks of tubes, Chem. Eng. Prog. Sympo. Series, 64, 133-145.

Alam, I., Ghoshdastidar, P. S., 2002, A study of heat transfer effectiveness of circular tubes with internal longitudinal fins having tapered lateral profiles, Int. J. Heat Mass Transfer, 45, 1371-1376.

Alcocer, F. J., Singh, P., 2002, Permeability of periodic arrays of cylinders for viscoelastic flows, Phys. Fluids, 14, 2578-2581.

Amiri, A., Vafai, K., 1994, Analysis of dispersion effects and non-thermal equilibrium, non-Darcian, variable porosity incompressible flow through porous media, Int. J. Heat Mass Transfer, 37, 939-934.

Andjelic, M., Popp, K., 1989, Stability effects in a normal triangular cylinder array, J. Fluids and Structures, 3, 165-185.

ANSYS User Manual, Ansys, Inc., 2009, Canonsburg, PA, 2009.

Arora, K., Kumar, S. S., Khomami, B., 2002, Experimental investigation of purely elastic instabilities in periodic flows, J. Non-Newt. Fluid Mech., 108, 209-226.

Astrom, B., Pipes, R., Advani, S., 1992, On flow through aligned fiber beds and its applications to composite processing's, J. Composite Materials, 26, 1351-1373.

Badr, H. M., 1982, A theoretical study of laminar mixed convection from a horizontal cylinder in a cross-stream, Int. J. Heat Mass Transfer, 26, 639–653.

Badr, H. M., 1984, Laminar combined convection from a horizontal cylinder-parallel and contra flow regimes, Int. J. Heat Mass Transfer, 27, 15-27.

Beale, S. B., Spadling, D. B., 1998, Numerical study of fluid flow and heat transfer in tube banks with streamwise periodic boundary conditions, Trans. Can. Soc. Mech. Eng., 22, 397-416.

Bergelin, O. P., Brown, G. A., Doberstein, S. C., 1952, Heat transfer and fluid frictions during flow across banks of tubes-IV: A study of the transition zone between viscous and turbulent flow, ASME J. Heat Transfer, 74, 953-959.

Bharti, R. P., Chhabra, R. P., Eswaran, V., 2007a, Steady forced convection heat transfer from a heated circular cylinder to power-law fluid, Int. J. Heat Mass Transfer, 50, 977-990.

Bharti, R. P., Chhabra, R. P., Eswaran, V., 2007b, A numerical study of the steady forced convection heat transfer from an unconfined circular cylinder, Heat Mass Transfer, 43, 639-648.

Bharti, R. P., Chhabra, R. P., Eswaran, V., 2006, Steady flow of power-law fluids across a circular cylinder, Can. J. Chem. Eng. 84, 406-421.

Bharti, R. P., Sivakumar, P., Chhabra, R. P., 2008, Forced convection heat transfer from an elliptical cylinder to power law fluids, Int. J. Heat Mass Transfer, 51, 1838-1849.

Bhowmick, S., Molla, M. M., Mustak, M., Saha, S.C., 2014, Non-Newtonian mixed convection flow from a horizontal circular cylinder with uniform surface heat flux, Procedia Eng., 90, 510-516.

Bird, R. B., Stewart, W. E., Lightfoot, E. N., 2002, Transport Phenomena, 2nd Edition. Wiley, New York, pp. 113.

Bruschke, M. V., Advani, S. G., 1993, Studied the flow of generalized Newtonian fluids across a periodic array of cylinders, J. Rheo., 37, 479- 498.

Chandra, A., Chhabra, R. P., 2012, Mixed convection from a heated semi-circular cylinder to power-law fluids in the steady flow regime, Int. J. Heat Mass Transfer, 55, 214-234.

Chang, K. S., Sa, J. Y., 1989, Numerical study of the unsteady mixed convection heat transfer from a circular cylinder, Int. Comm. Heat Mass Transfer, 16, 427-434.

Chen, C. J., Wung, T. S., 1989, Finite analytic solution of convective heat transfer for tube arrays in cross flow: Part-II, Heat transfer analysis, J. Heat Transfer, 111, 641-648.

Chhabra, R. P., Richardson, J. F., 1999, Non-Newtonian Flow in the Process Industries, Butterworth-Heinemann, Oxford.

Chhabra, R. P., Richardson, J. F., 2008, Non-Newtonian Flow and Applied Rheology, second edition, Butterworth-Heinemann, Oxford.

Chhabra, R. P., Comiti, J., Machac, I., 2001, Flow of non-Newtonian fluids in fixed and fluidized beds: a review, Chem. Eng. Sci., 56, 1-27.

Chhabra, R. P., Dhotkar, B. N., Eswaran, V., Satheesh, V. K., Vijaysri, M., 2000, Steady flow of Newtonian and dilatant fluids over an array of long circular cylinders, J. Chem. Eng. Japan, 33, 832–841.

Chatterjee, D., 2010, Mixed convection heat transfer from tandem square cylinders in a vertical channel at low Reynolds numbers, Numerical Heat Transfer, Part-A: 58, 740-755.

Chatterjee, D., Raja, M., 2013, Mixed convection heat transfer past in-line square cylinders in a vertical duct, Therm. Sci., 17, 567−580.

Chmielewski, C., Petty, C. A., Jayaraman, K., 1990, Cross-flow of elastic liquid through arrays of cylinders, J. Non-Newt. Fluid Mech. 35, 309-325.

Colburn, A. P., 1933, A method of correlating equation for forced convection heat transfer data and a comparison with fluid friction, Trans. AIChE, 29, 174-210.

Crowdy, D. G., 2016, Uniform flow past a periodic array of cylinders, European J. Mech. B/Fluids, 56, 120-129.

Daniel, A., Dhiman, A., 2013, Aiding-buoyancy mixed convection from a pair of side-by-side heated circular cylinders in power-law fluids, Ind. Eng. Chem. Res., 52, 17294-17314.

De, A. K., Dalal, A., 2006a, Numerical simulation of unconfined flow past a triangular cylinder, Int. J. Num. Meth. Fluids, 52, 801-821.

De, A. K., Dalal, A., 2006b, A numerical study of natural convection around a square horizontal heated cylinder placed in an enclosure, Heat Mass Transfer, 49, 4608-4623.

De, A. K., Dalal, A., 2007, Numerical study of laminar forced convection fluid flow and heat transfer from a triangular cylinder placed in a channel, Trans. ASME, 129, 646-656.

Dhiman, A. K., Anjaiah, N., Chhabra, R. P., Eswaran, V., 2007, Mixed convection from a heated square cylinder to Newtonian and power-law fluids, J. Fluids Eng., 129, 506-513.

Dhiman, A. K., Chhabra, R. P., Eswaran, V., 2008, Steady mixed convection across a confined square cylinder, Int. Comm. Heat Mass Transfer, 35, 47-55.

Dhiman, A. K., Chhabra, R. P., Sharma, A., Eswaran, V., 2006, Effect of Reynolds number and Prandtl numbers on the heat transfer across a square cylinder in the steady flow regime, Num. Heat Transfer, Part-A, 49, 717-731.

Dhotkar, B. N., Chhabra, R. P., Eswaran, V., 2000, Flow of non-Newtonian polymeric solutions in fibrous media, J. Applied Polymer Sci., 76, 1171-1185.

Drummond, J. E., Tahir, M. I., 1984, Laminar viscous flow through regular arrays of parallel solid cylinders, Int. J. Multiphase Flow, 10, 515- 540.

Duli, Y., Randall, F. B., Ameel, T. A., Warrington, R. O., 1995, Mixed convection from horizontal tube banks between two vertical parallel plates, Num. Heat Transfer, Part A, 27, 473-486.

Dybbs, A., Edwards, R. V., 1984, A new look at porous media fluid mechanics-Darcy to turbulent, Fundamental of Transport Phenomena in Porous Media, Martinus Nijhoff Publishers, pp. 199-254.

Eckert, E. R. G., Soehngen, E., 1952, Distribution of heat transfer coefficients around circular cylinders in cross-flow at Reynolds numbers from 20 to 500, Trans. ASME, 74, 343-347.

Edwards, D. A., Shapiro, M., Bar-Yoseph, P., Shapira, M., 1990, The influence of Reynolds number upon the apparent permeability of spatially periodic arrays of cylinders, Phys. Fluids, 2, 45-55.

Emersleben, O., 1925, Das Darcysche Filtergeseta, Physikalishe Zeitschr, 26, 601-610.

Fowler, A. J., Bejan, A., 1994, Forced convection in banks of inclined cylinders at low Reynolds numbers, Int. J. Heat Fluid Flow, 14, 90-99.

Fornarelli, F., Oresta, P., Lippolis, A., 2015, Flow pattern and heat transfer around six in-line circular cylinders at low Reynolds number, JP J. Heat Mass Transfer, 11, 1-28.

Fornarelli, F., Lippolis, A., Oresta, P., 2016, Buoyancy effect on the flow pattern and the thermal performance of an array of circular cylinders, J. Heat Transfer, 139, 1-10.

Ferreira, J. M., Chhabra, R. P., 2004, An analytical study of drag and mass transfer in creeping power-law flow across tube banks, Ind. Eng. Chem. Res., 43, 3439-3450.

Gamrat, G., Marinet, M. F., Stephane, L. P., 2008, Numerical study of heat transfer over banks of rods in small Reynolds number cross flow, Int. J. Heat Mass Transfer, 51, 853-864.

Geoffrey, R. M., Jonathan, P. R., 2010, Flow of wormlike micelle solutions through a periodic array of cylinders, J. Non-Newt. Fluid Mech., 165, 1-13.

Geonkoplis, C. J., 1993, Transport Processes and Unit Operations, Prentice-Hall Int. Inc., third edition, New Jersey, Chapter-3.

Georgiou, G., Momani, S., Chrochet, M. J., Walters, K., 1991, Newtonian and Non-Newtonian flow in a channel obstructed by an antisymmetric array of cylinders, J. Non-Newt. Fluid Mech., 40, 231-260.

Ghaddar, C. K., 1995, On the permeability of unidirectional fiberous media: a parallel computational approach, Phys. Fluids, 7, 2563-2586.

Ghosh, U. K., Upadhyay, S. N., Chhabra, R. P., 1994, Heat and mass transfer from immersed bodies to non-Newtonian fluids, Adv. Heat Transfer, 25, 251-319.

Ghoshdastidar, P. S., 1998, Computer Simulation of Flow and Heat Transfer", Tata McGraw Hill Publishing House, New Delhi.

Ghoshdastidar, P. S., 2012, Heat Transfer, Oxford University Press, 2nd edition.

Ghoshdastidar, P. S., 2017, Computational Fluid Dynamics and Heat Transfer, Cengage Learning India Pvt. Ltd.

Gillissen, J. J. J., 2013, Viscoelastic flow simulations through an array of cylinders, Phys. Rev., E 87, 023003, 1-7.

Gowda, Y. T. K., Narayana, P. A. A., Seetharamu, K. N., 1998, Finite element analysis of mixed convection over in-line tube bundles, Int. J. Heat Mass Transfer, 41, 1613-1619.

Grimison, E. D., 1937, Correlation and utilization of new data on flow resistance and heat transfer for cross flow of gases over tube banks, Trans. ASME, 59, 583-594.

Haldar, S. C., 2000, Fully developed combined convection in a seven-rod horizontal bundle, Int. J. Heat Mass Transfer, 43, 3735-3742.

Hantsch, A., Gross, U., Martin, A. R., 2010, Heat transfer augmentation: radiative-convective heat transfer in a tube with fiber array inserts, J. Heat Transfer, 132, 1-6.

Happel, J., 1964, An analytical study of heat and mass transfer in multi-particle systems at low Reynolds numbers, AIChE J., 10, 605-611.

Happel, J., 1959, Viscous flow relative to arrays of cylinders, AIChE J., 5, 174-177.

Hashimoto, H., 1959, On the periodic fundamental solution of the Stokes equations and their application to viscous flow past a cubic array of spheres, J. Fluid. Mech., 5, 317-328.

Hendricks, R. C., Braun, M. J., Canacci, V., Mullen, R. L., 1991, Simulation of brush inserts for leading-edge-passage convective heat transfer, In fourth Int. Sympo. Transport Phenomena, Sydney.

Hovart, A., Leskover, M., Mavko, B., 2006, Comparison of heat transfer conditions in tube bundles cross flow for different tube shapes, Int. J. Heat Mass Transfer, 49, 1027-1038.

Huge, E. C., 1937, Experimental investigation of effects of equipment size on convection heat transfer and flow resistance in cross flow of gases over tube banks, Trans. ASME, 59, 573-581.

Im, K. H., Ahluwalia, R. K., 1994, Radiative enhancement of tube side heat transfer. Int. J. Heat Mass Transfer, 37, 2635-2646.

James, D. F., Yip, R., Currie, I. G., 2012, Slow flow of bogger fluids through model fibrous porous media, J. Rheol., 56, 1249-1277.

James, S., Markus, J., Martin, A. R., 2012, Thermal modeling of a solar steam turbine with a focus on start-up time reduction, J. Eng. Gas Turbine Power, 134, 013001:1-8.

Johnson, A. A., Tezduyar, T. E., Liou, J., 1993, Numerical simulation of flow past periodic arrays of cylinders, Comp. Mech., 11, 371-383.

Kakac, S., Shah, R. K., Win, A., 1987, Handbook of Single Phase Convective Heat transfer, John Wiley and Sons, New York, Chapter 7.

Kawase, Y., Ulbrecht, J., 1981a, Drag and mass transfer in non-Newtonian flows through multi-particle systems at low Reynolds number, Chem. Eng. Sci., 36, 1193-1205.

Kawase, Y., Ulbrecht, J., 1981b, Motion of the mass transfer from an assemblage of solid spheres moving in a Non-Newtonian fluid at high Reynolds numbers, Chem. Eng. Com., 8, 233-245.

Khan, W.A., Culham, J. R., Yovanovich, 2006a, Convection heat transfer from tube banks in cross-flow, analytical approach, Int. J. Heat Mass transfer, 49, 4831-4838.

Khan, W.A., Culham, J. R., Yovanovich, 2006b, Fluid flow and heat transfer in power-law fluids across circular cylinders: analytical study, Trans. ASME, 128, 870-878.

Koch, D. L., Ladd, A. J. C., 1997, Moderate Reynolds number flows through periodic and random arrays of aligned cylinders, J. Fluid Mech., 349, 31-66.

Khomami, B., Morena, L. D., 1997, Stability of viscoelastic flow around periodic arrays of cylinders, Rheol. Acta. 36, 367-383.

Kreith, F., Bohn, M. S., 1993, Principles of Heat Transfer, fifth edition, West Publishing Company, New York, 469-485.

Kumar, R. S., Jayadev S., 2017, Influence of flow shedding frequency on convection heat transfer from banks of circular tubes in heat exchangers under cross flow, Int. J. Heat Mass Transfer, 105, 376-393.

Kuwabara, S., 1959, The forces experienced by randomly distributed parallel circular cylinders or spheres in a viscous flow at small Reynolds numbers, J. Phys. Society Japan, 14, 527-532.

Kuwahara, F., Shirota, M., Nakayama, A. A., 2001, Numerical study of interfacial convective heat transfer coefficient in two-energy equation model for convection in porous media, Int. J. Heat Mass Transfer, 44, 1153-1159.

Lange, C. F., Durst, F., Breuer, M., 1998, Momentum and heat transfer from cylinders in laminar cross flow at $10^{-4} \leq Re \leq 2000$, Int. J. Heat Mass Transfer, 41, 3409-3430.

Launder, B. E., Massey, T. H., 1978, The numerical predictions of viscous flow and heat transfer in tube banks, J. Heat Transfer, 100, 565-571.

Mandhani, V. K., Chhabra, R. P., Eswaran V., 2002, Forced convection heat transfer in tube banks in cross flow, Chem. Eng. Sci., 57, 379-391.

Mangadoddy, N., Bharti, R. P., Chhabra, R. P., Eswaran, V., 2004, Forced convection in cross flow of power law fluids over a tube bank, Chem. Eng. Sci., 59, 2213-2222.

Malleswara Rao, T.V., Chhabra, R. P., 2003, A note on pressure drop for the cross flow of power-law liquids and air/power law liquid mixtures past a bundle of circular rods, Chem. Eng. Sci., 58, 1365-1372.

Mangrulkar, C. K., Dhoble, A. S., Chakrabarty, S. G., Wankhede U. S., 2017, Experimental and CFD predictions of heat transfer and friction factor characteristics in cross flow tube bank with integral splitter plate, Int. J. Heat Mass Transfer, 104, 964-978.

Martin, A. R., Saltiel, C., Shyy, W., 1998, Frictional losses and convective heat transfer in sparse, periodic cylinder arrays in cross flow, Int. J. Heat Mass Transfer, 41, 2383- 2397.

Martin, A. R., Drotz, M., Talja, R., Kaijaluoto, S., Puumalainen, T., 2004, Energy analysis of impulse technology: research-scale experimental papermaking trials and simulations of industrial applications, Applied Thermal Eng., 24, 2411-2425.

McPhedran, R. C., 1986, Transport properties of cylinder pairs and of the square array of the cylinders, Proc. R. Soc. London, A 408, 31-43.

Merkin, J. H., 1977, Mixed convection from a horizontal circular cylinder, Int. J. Heat Mass Transfer, 20, 73−77.

Nagelhout, D., Bhatt, M. S., Heinrich, J. C., Poirier, D. R., 1995, Permeability for flow normal to a sparse array of fibers," Material Sci. Eng., A191, 203-208.

Nguyen, T. K., Vincent, M., Bonnet, G. A., 2013, Fourier based numerical method for computing the dynamic permeability of periodic porous media, European J. Mech. B/Fluids, 37, 90-98.

Nishimura, T., 1986, Flow across tube banks, Encyclopedia Fluid Mech., 1, 763-785.

Nishimura, T., Itoh, H., Ohya, K., Miyashita, H., 1991, Experimental validation of numerical analysis of flow across tube banks for laminar flow, J. Chem. Eng. Japan, 24, 666-669.

Nishimura, T., Itoh, H., Ohya, K., Miyashita, H., 1993, The influence of tube layout on flow and mass transfer characteristics in tube banks in the transitional flow regime, Int. J. Heat Mass Transfer, 36, 553-563.

Patankar, S. V., Liu, C. H., Sparrow, E.M., 1977, Fully developed flow and heat transfer in ducts having stream-wise-periodic variations of cross-sectional area, J. Heat Transfer, 99, 180-186.

Patil, R. C., Bharti, R. P., Chhabra, R. P., 2008, Forced convection heat transfer in power-law liquids from a pair of cylinders in tandem arrangement, Ind. Eng. Chem. Res. 47, 9141-9164.

Patnaik, B. S. V., Narayana, P. A. A., Seetharamu, K. N., 1999, Numerical simulation of vortex shedding past a circular cylinder under the influence of buoyancy, Int. J. Heat Mass Transfer, 42, 3495-3507.

Perry, R. H., 1997, Chemical Engineering Handbook, McGraw Hill, New York, 7th edition.

Pierson, O. L., 1937, Experimental investigation of the influence of tube arrangement on convection heat transfer and flow resistance in cross flow of gases over tube banks, Trans. ASME, 59, 563-572.

Prasad, D.V.N., Chhabra, R. P., 2001, An experimental investigation of the cross-flow of power law liquids past a bundle of cylinders and in a bed of stacked screens, Can. J. Chem. Eng., 79, 28-35.

Quesada, A.V., Ellero, M., 2012, SPH simulations of a viscoelastic flow around a periodic array of cylinders confined in a channel, J. Non-Newt. Fluid Mech., 167, 1-8.

Roychowdhury, D. G., Das, S. K., Sundararajan, T., 2002, Numerical simulation of laminar flow and heat transfer over banks of staggered cylinders, Int. J. Num. Method Fluids, 39, 23-40.

Salcedo, E., Cajas, J. C., Trevino, C., Lorenzo, M. S., 2016, Numerical investigation of mixed convection heat transfer from two isothermal circular cylinders in tandem arrangement: Buoyancy, spacing ratio and confinement effects, Theor. Comput. Fluid Dyn. 30, 1-29.

Sangani, A. S., Acrivos, A., 1982, Slow flow past periodic arrays of cylinders with application to heat transfer, Int. J. Multiphase Flow, 8, 193-206.

Sarkar, S., Dalal, A., Biswas, G., 2010, Mixed convective heat transfer from two identical square cylinders in cross flow at Re = 100, Int. J. Heat Mass Transfer, 53, 2628-2642.

Sarkar, S., Dalal, A., Biswas, G., 2011, Unsteady wake dynamics and heat transfer in forced and mixed convection past a circular cylinders in cross-flow for high Prandtl numbers, Int. J. Heat Mass Transfer, 54, 3536-3551.

Satish, M. G., Zhu, J., 1992, Flow resistance and mass transfer in slow non-Newtonian flow through multi-particle systems, J. Applied Mech., 59, 431-437.

Sharma, A., 2016, Introduction to Computational Fluid Dynamics, Development, Applications and Analysis, Wiley International Publishing Co. Ltd.

Sharma A, Eswaran, V., 2005a, Effect of channel confinement on the two-dimensional laminar flow and heat transfer across a square cylinder, Num. Heat Transfer, Part-A, 47, 79-107.

Sharma, A., Eswaran, V., 2005b, Effect of channel confinement and aiding/opposing buoyancy on the two-dimensional laminar flow and heat transfer across a square cylinder, Int. J. Heat Mass Transfer, 48, 5310-5322.

Sharma, A., Eswaran, V., 2004, Effect of aiding/opposing buoyancy on the heat and fluid flow across a square cylinder at Re=100, Num. Heat Transfer, Part-A, 45, 601-624.

Sharma, N., Dhiman, A. K., Kumar S., 2012, Mixed convection flow and heat transfer across a square cylinder under the influence of aiding buoyancy at low Reynolds numbers, Int. J. Heat Mass Transfer, 55, 2601-2614.

Shibu, S., Chhabra, R. P., Eswaran, V., 2001, Power-law fluid flow over a bundle of cylinders at intermediate Reynolds numbers, Chem. Eng. Sci., 56, 5545-5554.

Singh, John P., Padhy, S., Eric, S. G., Shaqfeh, Koch, D. L., 2012, Flow of power-law fluids in the fixed beds of cylinders or spheres, J. Fluid Mech., 713, 491-527.

Singh, P., Caussigna, P. H., Fortes, A., Joseph, D. D., Lundgren, T., 1989, Stability of arrays of cylinders across the stream by direct simulation, J. Fluid Mech., 205, 553-571.

Sivakumar, P., Bharti, R. P., Chhabra, R. P., 2006, Effect of power-law index on critical parameters for power-law flow across an unconfined circular cylinder. Chem. Eng. Sci., 61, 6035-6046.

Sivakumar, P., Bharti, R. P., Chhabra, R. P., 2007, Steady flow of power-law fluids across an unconfined elliptic cylinder, Chem. Eng. Sci., 62, 1682-1702.

Skartsis, L., Kardos, J. L, Khomami, B., 1992a, Resin flow through fiber beds during composite manufacturing processes, Part-I: Review of Newtonian flow through fiber beds, Polymer Eng. Sci., 32, 221-230

Skartsis, L., Khomami, B., Kardos, J. L., 1992b, Polymeric flow through fibrous media, J. Rheo., 36, 589-608.

Slattery, J. C., 1972, Mass, momentum and energy transfer in continua, New York: McGraw-Hill.

Soares, A. A., Ferreira, J. M., Chhabra, R. P., 2005a, Steady two dimensional non-Newtonian flow past an array of long circular cylinders up to Reynolds number 500: A numerical study, Can. J. Chem. Eng., 83, 437-450.

Soares, A. A., Ferreira, J. M., Chhabra, R. P., 2005b, Flow and forced convection heat transfer in cross-flow of non-Newtonian fluids over a circular cylinder, Ind. Eng. Chem. Res., 44, 5815-5827.

Soares, A. A., Ferreira, J. M., Caramelo, L., Anacleto, J., Chhabra, R. P., 2010, Effect of temperature dependent viscosity on forced convection heat transfer from a cylinder in crossflow of power-law fluids, Int. J. Heat mass transfer, 53, 4728-4740.

Soares, A. A., Anacleto, J., Caramelo, L., Ferreira, J. M., Chhabra, R. P., 2009, Mixed convection from a circular cylinder to power-law fluids, Ind. Eng. Chem. Res., 48, 8219-8231.

Sparrow, E. M., Lee, L., 1976, Analysis of mixed convection about a horizontal cylinder, Int. J. Heat Mass transfer, 19, 229-232.

Sparrow, E. M., Loeffler, A. L., 1959, Longitudinal laminar flow between cylinders arranged in regular array, AIChE J., 5, 325-330.

Spelt, P. D. M., Selerland, T., Lawrence, C. J., Lee, P. D., 2005a, Flow of inelastic Non-Newtonian fluids through arrays of aligned cylinders, Part I (Creeping flow), J. Eng. Math., 51, 57-80.

Spelt, P. D. M., Selerland, T., Lawrence, C. J., Lee, P. D., 2005b, Flow of inelastic Non-Newtonian fluids through arrays of aligned cylinders, Part-II (Inertial effects for square arrays), J. Eng. Math., 51, 81-97.

Spelt, P. D. M., Selerland, T., Lawrence, C. J., Lee, P. D., 2005c, Creeping flow of Bingham fluids through arrays of aligned cylinders, J. Non-Newt. Fluid Mech., 129, 66-74.

Srinivas, A. T., Bharti, R. P., Chhabra, R. P., 2009, Mixed convection heat transfer from a cylinder in power-law fluids: Effect of aiding buoyancy, Ind. Eng. Chem. Res., 48, 9735-9754.

Tahseen, A., Ishak, M., Rahman, M. M., 2013, Laminar forced convection heat transfer over staggered circular tube banks, J. Mech. Eng. Sci., 4, 418-430.

Talwar, K. K., Khomami, B., 1995, Flow of viscoelastic fluids past periodic arrays of cylinders: inertial and shear thinning viscosity and elasticity effects, J. Non-Newt. Fluid Mech., 57, 177-202.

Tamayol, A., Bahrami, M., 2009, Analytical determination of viscous permeability of fibrous porous media, Int. J. Heat Mass Transfer, 52, 2407-2414.

Tripathi, A., Chhabra, R. P., 1992, Slow power-law fluid flow relative to an array of infinite cylinders, Ind. Eng. Chem. Res., 31, 2754-2759.

Tripathi, A., Chhabra, R. P., 1996, Transverse laminar flow of non-Newtonian fluids over a bank of long cylinders, Chem. Eng. Comm., 147, 197-212.

Vijaysri, M., Chhabra, R. P., Eswaran, V., 1999, Power-law fluid across an array of infinite circular cylinder: a numerical study, J. Non- Newt. Fluid Mech., 87, 263-282.

Wang Y., Shao, X. M., 2012, Study on flow of power-law fluid through an infinite array of circular cylinders with immersed boundary-Lattice Boltzmann Method, Thermal Sci., 16, 1451-1455.

Wilson, A. S., Bassiouny, M. K., 2000, Modeling of heat transfer for flow across a tube banks, Chem. Eng. Processing, 39, 1-14.

Wung, T. S., Chen, C. J., 1989, Finite analytic solution of convective heat transfer for tube arrays in cross-flow: Part I-Flow field analysis, J. Heat Transfer, 111, 633-640.

Yazdchi, K., Srivastava, S., Luding, S., 2011, Microstructural effects on the permeability of periodic fiberous porous media, Int. J. Multiphase Flow, 37, 956-966.

Zhu, J., 1995, Drag and mass transfer for flow of a Carreau fluid past a swarm of Newtonian drops, Int. J. Multiphase Flow, 21, 935-940.

Zukaukas, A., 1972, Heat transfer from tubes in cross flow, Adv. Heat Transfer, 8, 93-160.

Zukaukas, A., 1987a, Heat transfer from tubes in cross-flow, Adv. Heat Transfer, 18, 87-159.

Zukauskas, A., 1987b, Convective heat transfer in cross flow, Handbook of Single-Phase Convective Heat Transfer, Wiley, New York (Chapter 6).

APPENDIX-A

Non-Newtonian Forced Convection Data for Drag Coefficients

Table A1: Dependence of pressure (C_{DP}), friction (C_{DF}) and total (C_D) drag coefficients on the fluid volume fractions (ϕ_f), power-law index (n) and Reynolds number (Re)

	n	ϕ_f	0.70	0.75	0.80	0.84	0.86	0.88	0.90	0.92	0.94	0.96	0.98	0.99
C_{DP}		Re ↓												
	0.4	1	19.1597	13.8266	12.5756	10.9784	10.0242	8.2838	8.0981	7.3502	7.3800	6.8305	6.5018	5.7355
		2	9.4901	7.0427	6.1090	5.1632	5.0705	4.5904	3.9783	3.9690	3.8328	3.4615	3.3195	3.1973
		5	3.1409	2.7251	2.5716	2.2756	2.0665	1.7972	1.6208	2.1445	1.8106	2.2460	1.5043	1.4488
		10	2.2162	1.5305	1.3976	1.2895	1.2298	1.0516	1.0345	0.9403	0.9310	0.8609	0.8324	0.8233
		20	0.9854	0.8560	0.7825	0.7168	0.6493	0.5873	0.5808	0.5003	0.4896	0.4777	0.4725	0.4101
		40	0.5122	0.4552	0.4307	0.4014	0.3406	0.3283	0.2908	0.2721	0.2616	0.2588	0.2399	0.2100
	0.6	1	34.0285	27.9697	22.6443	13.6872	11.95	9.2084	8.2734	6.6092	6.5929	5.4197	5.3433	3.8894
		2	17.0743	14.0631	11.4018	6.9772	6.0349	4.8022	4.2372	3.7587	3.4886	2.8796	2.6472	2.6164
		5	6.9926	5.8125	4.7748	2.3544	2.6338	1.9523	1.6752	1.6358	1.4875	1.3337	1.1714	1.1999
		10	3.7168	3.1305	2.6058	1.4764	1.3560	1.1040	0.9601	0.8843	0.8109	0.7352	0.6602	0.6490
		20	2.0748	1.7614	1.4708	0.8097	0.7564	0.6997	0.5318	0.4717	0.4531	0.4142	0.3740	0.4028
		40	1.1636	0.9788	0.8230	0.4542	0.4262	0.3465	0.2972	0.2658	0.2549	0.2341	0.2132	0.2057
	0.8	1	53.7668	41.6880	25.8589	14.7258	11.9795	9.5731	8.4567	5.9120	5.7344	4.4852	3.8192	3.1713
		2	26.9502	20.9387	13.0184	7.4402	6.0589	4.8620	4.3188	3.3795	2.9474	2.5039	2.0254	1.7035
		5	10.9916	8.6108	5.4071	3.1247	2.5624	2.0705	1.7102	1.4651	1.2927	1.1148	0.9250	0.7876
		10	5.7926	4.5975	2.9204	1.6975	1.6029	1.2794	0.9817	0.8091	0.7182	0.6243	0.5216	0.4529
		20	3.1968	2,5416	1.6184	1.1012	0.3963	0.7177	0.5674	0.4566	0.4065	0.3549	0.2983	0.2648
		40	1.7962	1.4216	0.9023	0.6134	0.4996	0.4007	0.3020	0.2590	0.2300	0.2017	0.1710	0.1519
	1.0	1	71.0562	43.4821	25.5881	16.4529	12.9038	9.9281	7.5446	5.7412	4.8105	3.8755	2.8971	2.3332
		2	35.6386	22.0360	13.0071	8.2438	6.5553	5.0672	3.8252	2.9731	2.5163	2.0616	1.5693	1.2822
		5	14.9532	9.1417	5.4966	3.5525	2.8293	2.2097	1.6854	1.3250	1.1358	0.9375	0.7261	0.6015
		10	7.9041	4.9473	3.0451	2.0541	1.5790	1.2363	0.9459	0.7546	0.6408	0.5334	0.4136	0.3453
		20	4.3985	2.7792	1.7264	1.1188	0.8918	0.7009	0.5383	0.4257	0.3665	0.3068	0.2407	0.1995
		40	2.4904	1.5468	0.9533	0.6284	0.4990	0.3924	0.3020	0.2398	0.2019	0.1747	0.1380	0.1148
	1.4	1	92.9915	49.5865	26.4478	19.7852	13.9975	10.2226	7.2736	4.3948	3.4628	2.5980	1.7720	1.2814
		2	45.6162	24.9236	13.3640	10.1816	7.2024	5.3146	3.8240	2.3414	1.8812	1.4402	0.9867	0.7109
		5	18.5012	10.3218	5.6962	4.7223	3.2902	2.4816	1.8170	1.1048	0.8921	0.6845	0.4708	0.3403
		10	9.7825	5.6266	3.2334	2.9130	1.9460	1.4678	1.0720	0.6406	0.5175	0.3915	0.2729	0.1982
		20	5.4712	3.2134	1.8510	1.6948	1.1326	0.8562	0.6290	0.3704	0.3002	0.2308	0.1586	0.1143
		40	3.1556	1.8423	1.0514	0.9576	0.6466	0.4884	0.3372	0.2098	0.1702	0.1308	0.0914	0.0669
	1.8	1	116.8942	57.1925	27.5807	21.1817	15.3020	11.8107	7.6601	3.4426	2.5789	1.8289	1.1142	0.7267
		2	58.5698	28.7997	13.9414	10.9712	7.5436	5.6758	3.8012	1.9124	1.4670	1.0468	0.6362	0.4091
		5	23.7590	11.9145	5.9912	5.2855	3.6046	2.5670	1.6560	0.9497	0.7243	0.5140	0.3109	0.1993
		10	12.3700	6.4280	3.4614	3.3554	2.2015	1.4026	0.9989	0.5614	0.4275	0.3026	0.1825	0.1167
		20	6.8431	3.7524	2.0330	1.9634	1.2968	0.8248	0.5875	0.3264	0.2492	0.1769	0.1067	0.0657
		40	3.9972	2.1978	1.3118	1.1734	0.7478	0.5744	0.3586	0.1855	0.1418	0.1010	0.0618	0.0454
C_{DF}	0.4	1	12.7656	10.0034	8.7959	7.7818	7.1438	6.0411	5.8575	5.6696	5.2976	4.5073	3.7170	3.8046
		2	6.3573	5.1368	4.3611	3.7590	3.5899	3.3689	2.8874	2.7696	2.7298	2.2892	2.0998	1.9892
		5	2.2901	1.9905	1.7535	1.5599	1.3314	1.1970	1.0923	1.2383	1.1382	1.1964	0.8754	0.8595
		10	1.3606	1.0232	0.8812	0.7801	0.6230	0.6205	0.6203	0.6098	0.5790	0.5775	0.4392	0.4112
		20	0.5680	0.4876	0.4443	0.3531	0.3510	0.3182	0.3176	0.2918	0.2826	0.2551	0.2241	0.2153
		40	0.2518	0.2130	0.1851	0.1598	0.1680	0.1105	0.1255	0.1254	0.1279	0.1119	0.1022	0.0944
	0.6	1	27.7404	22.9263	18.5592	11.1030	9.6102	7.4833	6.4515	6.1570	5.2592	4.3124	3.4791	3.8047
		2	13.8791	11.4782	9.3084	5.5812	4.8061	3.6368	3.4138	3.0418	2.7099	2.2102	2.0190	1.9733
		5	5.5687	4.6248	3.7702	1.6822	1.9965	1.5091	1.2806	1.2871	1.1064	0.9742	0.8260	0.8097
		10	2.7948	2,3384	1.9208	1.0795	0.9772	0.7419	0.6746	0.6122	0.5492	0.4864	0.4189	0.4088
		20	1.3730	1.1548	0.9532	0.5198	0.4767	0.4367	0.3262	0.3168	0.2671	0.2381	0.2063	0.1971
		40	0.6282	0.5247	0.4366	0.2388	0.2221	0.2049	0.1566	0.1388	0.1267	0.1089	0.0989	0.0928
	0.8	1	48.4987	38.2438	23.9502	13.6871	11.1529	8.9106	6.5006	6.2330	5.2011	4.0356	3.4019	2.8712
		2	24.2452	19.1239	11.9751	6.8556	5.5823	4.4702	3.4960	3.0788	2.6434	1.9127	1.7787	1.4857
		5	9.6890	7,6462	4.7910	2.7476	2.2406	1.7975	1.4090	1.3152	1.0825	0.9189	0.7429	0.6252
		10	4.8161	3.8062	2.3882	1.3704	1.2819	1.0132	0.7043	0.6435	0.5432	0.4033	0.3764	0.3237
		20	2.3395	1.8435	1.1572	0.7761	0.6245	0.4944	0.3443	0.3053	0.2667	0.2284	0.1070	0.1644
		40	1.0914	0.8564	0.5368	0.3604	0.2904	0.2307	0.1614	0.1440	0.1256	0.1014	0.0901	0.0797
	1.0	1	73.6701	44.1688	26.4367	17.0605	13.3938	10.3209	7.7389	5.9606	4.9723	3.9821	2.9296	2.3693
		2	36.8435	22.0939	13.2774	8.5102	6.7195	5.1871	3.8983	3.0134	2.5195	2.0448	1.5168	1.2428
		5	14.3575	8.8812	5.3578	3.4527	2.7270	2.1132	1.5945	1.2392	1.0447	0.8498	0.6407	0.5298
		10	7.1772	4.4665	2.7085	1.7745	1.3787	1.0685	0.8067	0.6272	0.5297	0.4329	0.3277	0.2726
		20	3.5236	2.1309	1.3348	0.8569	0.6758	0.5251	0.3972	0.3094	0.2615	0.2148	0.1652	0.1365
		40	1.6769	1.0309	0.6241	0.4045	0.3182	0.2472	0.1874	0.1463	0.1244	0.1025	0.0792	0.0661
	1.4	1	101.8366	58.1354	32.0279	24.5932	17.4674	12.8097	9.1298	5.5020	4.3057	3.1832	2.1044	1.5229
		2	50.9518	29.1088	16.0638	12.5005	8.8446	6.5232	4.6742	2.8354	2.2484	1.6894	1.1188	0.8033
		5	20.4624	11.7492	6.5430	5.4238	3.7380	2.7878	2.0156	1.2075	0.9594	0.7214	0.4782	0.3448
		10	10.3063	5.9651	3.3620	2.9867	1.9683	1.4658	1.0558	0.6204	0.4916	0.3620	0.2445	0.1774
		20	5.1556	2.9782	1.6720	1.5044	0.9904	0.7374	0.5295	0.3075	0.2437	0.1828	0.1210	0.0871
		40	2.5308	1.4544	0.8115	0.7244	0.4814	0.3574	0.2562	0.1468	0.1156	0.0859	0.0577	0.0423
	1.8	1	144.6101	75.2704	38.1029	30.3448	22.0489	17.1148	11.1138	4.9665	3.6749	2.5512	1.4902	0.9509
		2	72.3536	37.7886	19.1198	15.4974	10.6630	8.0096	5.3224	2.6360	1.9830	1.3814	0.8012	0.5091
		5	29.0660	15.3359	7.8534	6.9156	4.6398	3.2475	2.0574	1.1569	0.8632	0.5952	0.3424	0.2165
		10	14.6734	7.8472	4.0930	3.8706	2.4916	1.5598	1.0902	0.5988	0.4442	0.3044	0.1738	0.1096
		20	7.4273	3.9897	2.0810	1.9770	1.2695	0.7908	0.5504	0.2974	0.2198	0.1499	0.0850	0.0512
		40	3.7270	1.9994	1.0350	1.1258	0.6288	0.3900	0.2702	0.1440	0.1056	0.0714	0.0403	0.0247

Table A1 (Continued)

	n	ϕ_f	0.70	0.75	0.80	0.84	0.86	0.88	0.90	0.92	0.94	0.96	0.98	0.99
C_D	0.4	1	31.9253	23.8300	21.3715	18.7602	17.1680	14.3249	13.9556	13.0198	12.6776	11.3378	10.2188	9.5401
		2	15.8474	12.1795	10.4701	8.9222	8.6604	7.9593	6.8657	6.7386	6.5626	5.7507	5.4193	5.1865
		5	5.4310	4.7156	4.3251	3.8355	3.3979	2.9942	2.7131	3.3828	2.9488	3.4424	2.3797	2.3083
		10	3.5768	2.5537	2.2788	2.0696	1.8528	1.6721	1.6548	1.5501	1.5100	1.4384	1.2716	1.2345
		20	1.5534	1.3436	1.2268	1.0699	1.0003	0.9055	0.8984	0.7921	0.7722	0.7328	0.6966	0.6254
		40	0.7640	0.6682	0.6158	0.5612	0.5086	0.4388	0.4163	0.3975	0.3895	0.3707	0.3421	0.3044
	0.6	1	61.7689	61.7689	41.2035	24.7902	21.5600	16.6917	14.7249	12.7662	11.8521	9.7321	8.8224	7.0941
		2	30.9534	30.9534	20.7102	12.5584	10.8410	8.4390	7.6510	6.6988	6.1985	5.0898	4.6662	4.5897
		5	12.5613	12.5613	8.545	4.6303	4.0360	3.4614	2.9558	2.9229	2.5939	2.3079	2.0574	2.0096
		10	6.5116	6.5116	4.5266	2.5559	2.3332	1.8459	1.6347	1.4965	1.3601	1.2216	1.0791	1.0578
		20	3.4478	3.4478	2.4240	1.3295	1.2331	1.1364	0.8880	0.7885	0.7202	0.6523	0.5803	0.5999
		40	1.7918	1.7918	1.2596	0.693	0.6483	0.5514	0.4538	0.4146	0.3816	0.343	0.3121	0.2985
	0.8	1	102.2655	79.9318	49.8091	28.4129	23.1324	18.4837	14.9573	12.1450	10.9355	8.5208	7.2211	6.0425
		2	51.1954	40.0626	24.9935	14.2958	11.6412	9.3322	7.8148	6.4583	5.5908	4.4166	3.8041	3.1892
		5	20.6806	16.2570	10.1981	5.8723	4.8030	3.8680	3.1192	2.7803	2.3752	2.0337	1.6679	1.4128
		10	10.6087	8.4037	5.3086	3.0679	2.8848	2.2926	1.6860	1.4526	1.2614	1.0276	0.8980	0.7766
		20	5.5363	4.3851	2.7756	1.8773	1.0208	1.2121	0.9117	0.7619	0.6732	0.5833	0.4053	0.4292
		40	2.8876	2.2780	1.4391	0.9738	0.7900	0.6314	0.4634	0.4030	0.3556	0.3031	0.2611	0.2316
	1.0	1	144.7263	87.6509	52.0248	33.5134	26.2976	20.2490	15.2835	11.7018	9.7828	7.8576	5.8267	4.7025
		2	72.4821	44.1299	26.2845	16.7540	13.2748	10.2543	7.7235	5.9865	5.0358	4.1064	3.0861	2.5250
		5	29.3107	18.0229	10.8544	7.0052	5.5563	4.3229	3.2799	2.5642	2.1805	1.7873	1.3668	1.1313
		10	15.0813	9.4138	5.7536	3.8286	2.9577	2.3048	1.7526	1.3818	1.1705	0.9663	0.7413	0.6179
		20	7.9221	4.9101	3.0612	1.9757	1.5676	1.2260	0.9355	0.7351	0.6280	0.5216	0.4059	0.3360
		40	4.1673	2.5777	1.5774	1.0329	0.8172	0.6396	0.4894	0.3861	0.3263	0.2772	0.2172	0.1809
	1.4	1	194.8281	107.7219	58.4757	44.3784	31.4649	23.0323	16.4034	9.8968	7.7685	5.7812	3.8764	2.8043
		2	96.5680	54.0324	29.4278	22.6821	16.0470	11.8378	8.4982	5.1768	4.1296	3.1296	2.1055	1.5142
		5	38.9636	22.0710	12.2392	10.1461	7.0282	5.2694	3.8326	2.3123	1.8515	1.4059	0.9490	0.6851
		10	20.0888	11.5917	6.5954	5.8997	3.9143	2.9336	2.1278	1.2610	1.0091	0.7535	0.5174	0.3756
		20	10.6268	6.1916	3.5230	3.1992	2.1230	1.5936	1.1585	0.6779	0.5439	0.4136	0.2796	0.2014
		40	5.6864	3.2967	1.8629	1.6820	1.1280	0.8458	0.5934	0.3566	0.2858	0.2167	0.1491	0.1092
	1.8	1	261.5043	132.4629	65.6836	51.5265	37.3509	28.9255	18.7739	8.4091	6.2538	4.3801	2.6044	1.6776
		2	130.9234	66.5883	33.0612	26.4686	18.2066	13.6854	9.1236	4.5484	3.4500	2.4282	1.4374	0.9182
		5	52.8250	27.2504	13.8446	12.2011	8.2444	5.8145	3.7134	2.1066	1.5875	1.1092	0.6533	0.4158
		10	27.0434	14.2752	7.5544	7.2260	4.6931	2.9624	2.0891	1.1602	0.8717	0.6070	0.3563	0.2263
		20	14.2704	7.7421	4.1140	3.9404	2.5663	1.6156	1.1379	0.6238	0.4690	0.3268	0.1917	0.1169
		40	7.7242	4.1972	2.3468	2.2992	1.3766	0.9644	0.6288	0.3295	0.2474	0.1724	0.1021	0.0701

APPENDIX-B

Non-Newtonian Forced Convection Data for Average Nusselt Number (Nu)

Table B1: Dependence of average Nusselt number (Nu) on the power-law index (n), fluid volume fractions (ϕ_f) and Reynolds number (Re) at Pr = 1 and 5

Pr	n	ϕ_f	0.70	0.75	0.80	0.84	0.86	0.88	0.90	0.92	0.94	0.96	0.98	0.99
		Re↓												
		1	2.2128	2.1276	1.9814	1.9506	1.9117	1.8919	1.8161	1.7767	1.6257	1.5448	1.4804	1.3256
		2	2.4294	2.3884	2.1526	2.1036	2.0577	1.9622	1.8924	1.8605	1.7832	1.6221	1.5834	1.4781
	0.4	5	2.8137	2.6132	2.5684	2.4732	2.4232	2.3842	2.2020	2.1652	1.9824	1.8432	1.6938	1.6454
		10	3.1591	2.8076	2.7617	2.7161	2.6363	2.5131	2.4094	2.3218	2.2094	1.9875	1.8626	1.7846
		20	3.6028	3.4055	3.2606	2.9870	2.9213	2.8836	2.5846	2.5221	2.4382	2.1244	2.0082	1.9416
		40	4.2372	3.9223	3.7193	3.2398	3.0497	2.9824	2.8295	2.7750	2.6148	2.2774	2.1628	2.1198
		1	2.1644	1.9985	1.9492	1.8642	1.8045	1.7552	1.6946	1.6482	1.5631	1.5092	1.4487	1.3045
		2	2.3328	2.3062	2.0965	2.0548	1.9452	1.8597	1.8016	1.7586	1.6541	1.5692	1.5243	1.4269
	0.6	5	2.7787	2.5691	2.4908	2.4163	2.3738	2.2991	2.1002	2.0531	1.8954	1.7836	1.6357	1.6054
		10	3.0248	2.7519	2.6524	2.5748	2.4748	2.4712	2.3272	2.2512	2.0724	1.9378	1.7824	1.7148
		20	3.3986	3.2450	3.0343	2.8350	2.7257	2.6086	2.4862	2.4264	2.2181	2.0697	1.9020	1.8245
		40	3.9206	3.6342	3.3254	3.1667	2.9334	2.8794	2.6578	2.5432	2.3482	2.1860	2.0070	1.9194
		1	2.1281	1.9539	1.9076	1.8079	1.7488	1.7091	1.6419	1.6088	1.5237	1.4518	1.3985	1.2769
		2	2.2861	2.2484	1.9782	1.9574	1.8441	1.8195	1.7561	1.6869	1.5864	1.5070	1.4932	1.3848
	0.8	5	2.7328	2.4818	2.4217	2.3273	2.3096	2.2046	2.0240	1.9743	1.8634	1.7460	1.5901	1.5678
		10	2.9625	2.7123	2.6215	2.5110	2.4398	2.3850	2.2597	2.1817	2.0295	1.8889	1.7161	1.6972
		20	3.3584	3.2002	2.9876	2.7877	2.6788	2.5695	2.4385	2.3573	2.1664	2.0114	1.8298	1.7998
1		40	3.8620	3.5770	3.2705	3.0144	2.8823	2.7732	2.6002	2.4803	2.2928	2.1244	1.9344	1.8876
		1	2.1025	1.9249	1.8572	1.7764	1.6768	1.6635	1.6131	1.5537	1.4656	1.4008	1.3610	1.2346
		2	2.3845	2.1856	1.9183	1.8852	1.8126	1.7558	1.6982	1.6241	1.5490	1.4858	1.4560	1.3637
	1	5	2.6714	2.4398	2.3477	2.2812	2.2129	2.1567	2.0048	1.9326	1.8384	1.7152	1.5423	1.4331
		10	2.8668	2.6735	2.5987	2.4868	2.4138	2.3282	2.2316	2.1222	1.9972	1.8511	1.6650	1.6520
		20	3.3300	3.1680	2.9609	2.7535	2.6457	2.5283	2.4049	2.2728	2.1295	1.9703	1.7795	1.7607
		40	3.8215	3.5363	3.2362	2.9778	2.8490	2.7107	2.5675	2.4142	2.2558	2.0830	1.9028	1.8404
		1	1.7028	1.6561	1.6083	1.5298	1.4419	1.3976	1.3472	1.3037	1.2614	1.2411	1.1949	0.7667
		2	1.7597	1.7319	1.6933	1.6433	1.5973	1.5424	1.6074	1.5562	1.5096	1.4622	1.3371	0.9270
	1.4	5	2.2574	2.2022	2.1504	2.0915	2.0687	2.0302	1.9559	1.9006	1.8035	1.6780	1.5021	0.9978
		10	2.7474	2.6474	2.5622	2.4514	2.3773	2.2902	2.1921	2.0807	1.9530	1.7906	1.6121	1.1021
		20	3.2956	3.1276	2.9164	2.7127	2.6030	2.4857	2.3615	2.2277	2.0817	1.9183	1.7171	1.1792
		40	3.7696	3.4870	3.1879	2.9406	2.7809	2.6747	2.5024	2.3802	2.2137	2.0265	1.8188	1.2822
		1	1.0941	1.0034	0.9858	0.9552	0.9212	0.8911	0.8576	0.8139	0.7786	0.7563	0.7236	0.7195
		2	1.2505	1.2087	1.1631	1.1254	1.1055	1.0537	0.9992	0.9669	0.9323	0.9099	0.8725	0.8484
	1.8	5	1.8974	1.4016	1.3788	1.3304	1.2013	1.1688	1.1887	1.1152	1.0820	1.0309	1.0115	0.9622
		10	2.6378	2.1920	1.5038	1.4723	1.2648	1.3419	1.3055	1.2744	1.2459	1.2289	1.1514	1.0683
		20	3.2792	2.6412	1.9426	1.6587	1.6227	1.5902	1.5574	1.5176	1.4831	1.4115	1.2749	1.1268
		40	3.7374	3.6046	2.0769	1.9871	1.9096	1.8663	1.8269	1.7677	1.6828	1.5629	1.3840	1.2240
		1	2.5921	2.5034	2.4107	2.3568	2.3115	2.2587	2.2001	2.1566	2.0544	1.9051	1.6617	1.5055
		2	2.8772	2.8065	2.7645	2.6582	2.6016	2.5194	2.3694	2.2764	2.1220	1.9878	1.7976	1.6597
	0.4	5	3.6638	3.3981	3.1507	2.9435	2.9182	2.9539	2.5913	2.5315	2.3761	2.1202	2.0230	1.9598
		10	4.2923	3.7783	3.4257	3.1621	3.0300	3.1264	2.8001	2.5919	2.5134	2.2527	2.1868	2.1546
		20	4.6895	4.1236	3.8589	3.4222	3.3742	3.2852	2.9319	2.7067	2.6243	2.3139	2.2646	2.2260
		40	5.0703	4.2715	3.8224	3.5152	3.4579	3.2765	2.9914	2.8953	2.8195	2.4914	2.3765	2.3295
		1	2.5272	2.4673	2.3382	2.2489	2.2042	2.1816	2.1059	1.9960	1.9878	1.8703	1.6179	1.4743
		2	2.8181	2.7628	2.7042	2.5812	2.5436	2.4388	2.2895	2.1724	2.0638	1.9365	1.7630	1.6182
	0.6	5	3.5958	3.3789	3.1159	2.8975	2.7709	2.6357	2.5065	2.3729	2.2343	2.0900	1.9357	1.8513
		10	4.0220	3.6798	3.3297	3.0474	2.9093	2.7674	2.6262	2.4835	2.3394	2.1940	2.0505	1.9663
		20	4.3043	3.8948	3.5027	3.1905	3.0502	2.8991	2.7489	2.5968	2.4435	2.2899	2.1376	2.0712
		40	4.5939	4.1499	3.7265	3.4322	3.3452	3.1543	2.9129	2.7944	2.6717	2.3943	2.2182	2.1559
		1	2.4507	2.4095	2.2712	2.1648	2.1492	2.0944	2.0231	1.9525	1.8597	1.7819	1.5742	1.4519
		2	2.7871	2.7298	2.6660	2.5156	2.4732	2.3764	2.2590	2.1491	2.0247	1.8816	1.7078	1.5875
	0.8	5	3.5576	3.3372	3.0722	2.8395	2.7187	2.5920	2.4624	2.3277	2.1864	2.0354	1.8686	1.7547
		10	3.9633	3.6198	3.2634	2.9938	2.8557	2.7156	2.5755	2.4328	2.2860	2.1328	1.9567	1.8672
		20	4.2302	3.8300	3.4434	3.1440	2.9966	2.8471	2.6977	2.5452	2.3891	2.2266	2.0549	1.9671
		40	4.5196	4.0878	3.6764	3.3988	3.2523	3.1088	2.8731	2.7515	2.5772	2.3418	2.1467	2.0489
		1	2.4095	2.3372	2.2162	2.1118	2.0940	2.0579	2.0048	1.9320	1.7085	1.8361	1.5333	1.4217
		2	2.7427	2.6829	2.6106	2.4953	2.4285	2.3348	2.2357	2.1237	1.8481	1.9960	1.6612	1.5476
	1	5	3.5332	3.3109	3.0433	2.8092	2.6883	2.5612	2.4322	2.2951	1.9954	2.1494	1.8098	1.7047
		10	3.8257	3.5797	3.2378	2.9570	2.8199	2.6808	2.5409	2.3977	2.0901	2.2487	1.9118	1.8067
		20	4.1817	3.7879	3.4287	3.1156	2.9673	2.8184	2.6691	2.5160	2.1883	2.3574	2.0022	1.8974
		40	4.4702	4.0475	3.6459	3.3356	3.1825	3.0218	2.8577	2.6840	2.3148	2.5040	2.1043	1.9878
		1	2.2052	2.1221	2.0877	2.0008	1.9938	1.9562	1.8812	1.8106	1.7807	1.6768	1.5007	1.0724
		2	2.6952	2.6626	2.5879	2.4660	2.3956	2.3045	2.2036	2.0883	1.9579	1.8056	1.6146	1.1160
	1.4	5	3.5054	3.2791	3.0076	2.7697	2.6483	2.5200	2.3887	2.2512	2.1050	1.9439	1.7516	1.2848
		10	3.7884	3.5337	3.1847	2.9132	2.7783	2.6405	2.5012	2.3574	2.2060	2.0344	1.8475	1.3563
		20	4.1206	3.7373	3.3708	3.0891	2.9038	2.7967	2.6167	2.4915	2.3295	2.1536	1.9487	1.4635
		40	4.4047	3.9973	3.6118	3.3043	3.1183	3.0016	2.8045	2.6152	2.4978	2.2803	2.0666	1.5642
		1	1.5002	1.4607	1.4247	1.3952	1.3534	1.3004	1.2745	1.2474	1.2162	1.1833	1.1215	1.0486
		2	1.6457	1.5939	1.5407	1.5009	1.4446	1.3813	1.3316	1.3052	1.2757	1.2454	1.1730	1.0799
	1.8	5	2.4203	2.2442	2.1134	2.0610	1.7442	1.6956	1.6536	1.6304	1.5799	1.4920	1.3419	1.2142
		10	2.5897	2.5086	2.4671	2.4136	2.0379	1.9976	1.9412	1.8655	1.7665	1.6362	1.4524	1.3125
		20	2.6368	2.6127	2.5696	2.5172	2.3422	2.2563	2.1586	2.0462	1.9154	1.7592	1.5560	1.4025
		40	3.2537	3.0920	2.8839	2.6905	2.5853	2.4699	2.3460	2.2096	2.0565	1.8792	1.6599	1.5087

Table B2: Dependence of average Nusselt number (Nu) on the power-law index (n), fluid volume fractions (ϕ_f) and Reynolds number (Re) at Pr = 10 and 20

Pr	n	ϕ_f	0.70	0.75	0.80	0.84	0.86	0.88	0.90	0.92	0.94	0.96	0.98	0.99
		Re↓												
10	0.4	1	3.1265	2.8231	2.7465	2.6604	2.6123	2.5399	2.4102	2.2562	2.1971	1.9636	1.7915	1.6488
		2	3.4398	3.2904	3.1253	2.9316	2.7889	2.7294	2.5323	2.3625	2.2726	2.1014	1.9276	1.7945
		5	4.1021	3.7113	3.3767	3.1655	3.1203	3.0325	2.6922	2.6031	2.4776	2.2525	2.1425	2.0917
		10	4.6045	3.9732	3.5075	3.3026	3.2690	3.1915	2.8903	2.6744	2.5948	2.3582	2.2593	2.2305
		20	4.9203	4.2728	3.9822	3.5327	3.4698	3.3873	3.0407	2.7758	2.7151	2.4127	2.3500	2.2615
		40	5.2934	4.4080	3.9311	3.6714	3.5923	3.4323	3.1696	2.9834	2.8981	2.5524	2.4593	2.4185
	0.6	1	3.0181	2.7866	2.6946	2.5469	2.5056	2.4653	2.3754	2.1781	2.1224	1.9224	1.7558	1.5823
		2	3.4129	3.2491	3.1054	2.8211	2.7041	2.6228	2.4956	2.3152	2.1934	2.0234	1.8918	1.7473
		5	4.0197	3.6712	3.3140	3.0716	2.8947	2.7471	2.6566	2.4661	2.3261	2.1867	2.0465	1.9761
		10	4.2712	3.8528	3.4514	3.2074	2.9945	2.8447	2.7281	2.5532	2.4113	2.2737	2.1459	2.0418
		20	4.4653	4.0126	3.5951	3.4195	3.1243	3.0275	2.8429	2.6576	2.5041	2.3553	2.2174	2.1668
		40	4.7555	4.2823	3.8390	3.5038	3.4417	3.2426	3.1014	2.8824	2.7427	2.5184	2.2875	2.2318
	0.8	1	2.9068	2.7485	2.6581	2.5160	2.4727	2.3958	2.2782	2.1479	2.0228	1.8926	1.7030	1.5482
		2	3.3805	3.2136	3.0582	2.7773	2.6645	2.5841	2.4593	2.2881	2.1487	1.9982	1.8277	1.7197
		5	3.9661	3.6163	3.2598	2.9784	2.8391	2.6985	2.5987	2.4175	2.2744	2.1268	1.9719	1.8739
		10	4.1986	3.7827	3.3838	3.0842	2.9374	2.7906	2.6759	2.5011	2.3556	2.2082	2.0561	1.9768
		20	4.3873	3.9512	3.5406	3.2279	3.0964	2.9518	2.7874	2.6112	2.4530	2.2917	2.1311	2.0573
		40	4.6800	4.2207	3.7944	3.4659	3.3585	3.2090	3.0012	2.8176	2.6681	2.4540	2.2182	2.1341
	1	1	2.8626	2.6827	2.6100	2.4963	2.4225	2.3342	2.2345	2.1220	1.9935	1.8463	1.6510	1.5440
		2	3.3595	3.1912	2.9640	2.7499	2.6394	2.5180	2.3920	2.2586	2.1159	1.9608	1.7720	1.6657
		5	3.8332	3.5822	3.2250	2.9440	2.8052	2.6650	2.5269	2.3827	2.2354	2.0812	1.9095	1.8122
		10	4.1530	3.7382	3.3435	3.0490	2.9016	2.7563	2.6121	2.4663	2.3178	2.1634	1.9960	1.9032
		20	4.3382	3.9128	3.5131	3.2063	3.0563	2.9020	2.7482	2.5903	2.4286	2.2579	2.0786	1.9848
		40	4.6298	4.1817	3.7648	3.4474	3.2935	3.1284	2.9607	2.7792	2.5926	2.3958	2.1840	2.0730
	1.4	1	2.7147	2.6625	2.5880	2.4222	2.3967	2.3060	2.1848	2.0894	1.9575	1.8024	1.6116	1.1447
		2	3.3350	3.1647	2.9356	2.6914	2.6068	2.4834	2.3446	2.2183	2.0718	1.9097	1.7174	1.2188
		5	3.8078	3.5435	3.1839	2.9012	2.7621	2.6215	2.4808	2.3370	2.1877	2.0272	1.8414	1.3528
		10	4.1035	3.6863	3.2971	2.9808	2.8664	2.7235	2.5602	2.4035	2.2814	2.1003	1.9302	1.4792
		20	4.2757	3.8688	3.4878	3.1439	3.0007	2.8584	2.6744	2.5142	2.3886	2.2386	2.0330	1.5809
		40	4.5626	4.1346	3.7365	3.4033	3.1873	3.0886	2.9274	2.6951	2.5205	2.3759	2.1581	1.6933
	1.8	1	1.5951	1.4946	1.4666	1.4499	1.4019	1.3792	1.3263	1.2979	1.2527	1.2067	1.1782	1.1102
		2	2.2303	2.1081	2.0209	1.9832	1.7572	1.7022	1.6625	1.5440	1.5148	1.4463	1.3126	1.1924
		5	2.5874	2.5112	2.4755	2.4280	2.0518	2.0111	1.9540	1.8774	1.7778	1.6478	1.4657	1.3209
		10	2.7817	2.7443	2.7174	2.6849	2.3529	2.2647	2.1031	2.0529	1.9234	1.7699	1.5712	1.4291
		20	3.2796	3.1042	2.9549	2.9172	2.5773	2.4606	2.3211	2.2019	2.0527	1.8833	1.6735	1.5180
		40	3.7374	3.4561	3.2113	3.1689	2.7912	2.6571	2.5170	2.3660	2.1988	2.0076	1.7789	1.6264
20	0.4	1	3.4991	3.2882	3.1063	2.9367	2.8416	2.7317	2.5684	2.3974	2.3025	2.0726	1.9870	1.7918
		2	3.9405	3.6600	3.2914	3.1119	3.0141	3.0252	2.6212	2.4740	2.3612	2.2057	2.0912	2.0384
		5	4.3154	3.8966	3.5395	3.3445	3.2010	3.2555	2.7668	2.6562	2.5534	2.3797	2.2510	2.2130
		10	4.7794	4.0851	3.6364	3.4555	3.3422	3.3927	2.9543	2.7278	2.6628	2.4013	2.3516	2.3315
		20	5.0864	4.3791	3.9347	3.6344	3.5668	3.4708	3.0858	2.8217	2.7341	2.4829	2.4565	2.4031
		40	5.4921	4.5272	4.0249	3.8058	3.7157	3.5935	3.2410	3.0518	2.9465	2.6057	2.4823	2.4563
	0.6	1	3.4131	3.2487	3.0249	2.8164	2.7052	2.6051	2.5091	2.3221	2.2434	2.0217	1.8862	1.7635
		2	3.9064	3.5917	3.2569	2.9884	2.8623	2.6924	2.5679	2.4180	2.2955	2.1570	2.0129	1.9279
		5	4.2613	3.8354	3.4264	3.1408	2.9732	2.8188	2.6754	2.5359	2.4014	2.2724	2.1497	2.0924
		10	4.4084	3.9494	3.5230	3.2948	3.0502	2.8971	2.7498	2.6067	2.4713	2.3435	2.2334	2.1404
		20	4.5694	4.0926	3.6632	3.4778	3.2230	3.1208	2.9640	2.7849	2.5852	2.4131	2.2904	2.2442
		40	4.8965	4.3965	3.9357	3.7499	3.5347	3.3230	3.2082	2.9512	2.8061	2.5755	2.3517	2.3080
	0.8	1	3.3805	3.2137	2.9878	2.7877	2.6642	2.5438	2.4590	2.2878	2.1481	1.9825	1.8262	1.7364
		2	3.8596	3.5436	3.2093	2.9399	2.8036	2.6660	2.5426	2.3897	2.2476	2.1005	1.9417	1.8379
		5	4.1947	3.7700	3.3658	3.0606	2.9139	2.7682	2.6260	2.4855	2.3468	2.2080	2.0689	1.9800
		10	4.3269	3.8728	3.4458	3.1415	2.9922	2.8427	2.7012	2.5547	2.4133	2.2747	2.1385	2.0655
		20	4.4951	4.0386	3.6176	3.3470	3.1947	3.0485	2.9258	2.6962	2.5407	2.3494	2.2032	2.1442
		40	4.8197	4.3364	3.8942	3.5960	3.4562	3.2902	3.1560	2.8987	2.7790	2.5165	2.3033	2.2249
	1	1	3.3597	3.1914	2.9634	2.7523	2.6395	2.5181	2.3915	2.2583	2.1154	1.9310	1.7658	1.6671
		2	3.7308	3.4143	3.1794	2.9072	2.7754	2.6374	2.4988	2.3579	2.2123	2.0590	1.8861	1.7826
		5	4.1545	3.7302	3.3286	3.0242	2.8787	2.7335	2.5911	2.4490	2.3053	2.1600	1.9993	1.9160
		10	4.2770	3.8287	3.4148	3.1082	2.9587	2.8106	2.6654	2.5201	2.3754	2.2277	2.0747	1.9944
		20	4.4495	4.0086	3.5977	3.2846	3.1342	2.9751	2.8185	2.6548	2.4942	2.3207	2.1536	2.0699
		40	4.7707	4.3012	3.8712	3.5469	3.3962	3.2248	3.0554	2.8658	2.6712	2.4670	2.2562	2.1550
	1.4	1	3.3354	3.1652	2.9358	2.7234	2.6091	2.4861	2.3275	2.2012	2.0743	1.9101	1.7176	1.2545
		2	3.7097	3.3819	3.1469	2.8755	2.7396	2.6000	2.4115	2.2843	2.1926	2.0006	1.8145	1.3269
		5	4.1132	3.6869	3.2829	2.9799	2.8346	2.6897	2.5465	2.4024	2.2550	2.0995	1.9252	1.4633
		10	4.2235	3.7745	3.3713	3.0766	2.9051	2.7602	2.5959	2.4980	2.3369	2.1774	2.0059	1.5919
		20	4.3885	3.9708	3.5836	3.2173	3.0835	2.9087	2.7515	2.5701	2.4145	2.3144	2.1101	1.7062
		40	4.7063	4.2599	3.8497	3.4927	3.3001	3.1853	3.0019	2.8124	2.6022	2.4599	2.2409	1.8137
	1.8	1	1.7549	1.7132	1.6882	1.6466	1.6144	1.5811	1.5428	1.5457	1.5149	1.4492	1.3171	1.2283
		2	2.7884	2.7079	2.6509	2.6008	2.0341	1.9941	1.9714	1.8156	1.7279	1.6106	1.4370	1.2898
		5	2.8134	2.7473	2.7164	2.6819	2.3659	2.2747	2.1733	2.0951	1.9290	1.7762	1.5799	1.4354
		10	3.3057	3.1256	2.9117	2.8812	2.5712	2.4524	2.3245	2.1954	2.0502	1.8862	1.6821	1.5430
		20	3.7403	3.4372	3.1307	3.1055	2.7540	2.6204	2.4169	2.3343	2.1748	1.9983	1.7852	1.6305
		40	4.0667	3.7189	3.3765	3.4055	2.9687	2.8248	2.6760	2.5166	2.3413	2.1388	1.8979	1.7412

Table B3: Dependence of average Nusselt number (Nu) on the power-law index (n), fluid volume fractions (ϕ_f) and Reynolds number (Re) at Pr = 50 and 100

Pr	n	ϕ_f	0.70	0.75	0.80	0.84	0.86	0.88	0.90	0.92	0.94	0.96	0.98	0.99
50	0.4	Re↓												
		1	4.0528	3.7038	3.2321	3.1955	3.1106	2.8162	2.6515	2.5027	2.2643	2.1924	2.0937	1.9495
		2	4.2953	3.9307	3.4459	3.2586	3.2132	3.2034	2.7289	2.5554	2.4983	2.3582	2.3212	2.2103
		5	4.4472	4.0979	3.6091	3.4628	3.2728	3.3712	2.7967	2.7195	2.6332	2.4269	2.3785	2.3037
		10	4.9093	4.1760	3.6741	3.5256	3.4056	3.4512	3.0194	2.7805	2.7445	2.4969	2.4622	2.4153
		20	5.2848	4.5053	4.0777	3.7289	3.6856	3.5733	3.1568	2.9114	2.8715	2.5543	2.5231	2.4884
		40	5.8002	4.7020	4.2553	3.9486	3.8446	3.7269	3.3882	3.1607	3.0210	2.6979	2.5819	2.4823
	0.6	1	4.0193	3.6677	3.3073	3.0215	2.8949	2.7575	2.6171	2.4541	2.1931	2.2021	2.0493	1.8944
		2	4.2588	3.8296	3.4182	3.1156	2.9798	2.8135	2.6966	2.5172	2.4231	2.2796	2.1617	2.0938
		5	4.4198	3.9437	3.5051	3.2080	3.0852	2.8832	2.7435	2.6111	2.4886	2.3748	2.2744	2.2322
		10	4.5133	4.0255	3.5825	3.3529	3.1451	2.9499	2.9062	2.6686	2.5624	2.4296	2.3401	2.2601
		20	4.7952	4.3888	3.7426	3.6086	3.3594	3.2063	3.0566	2.7650	2.6512	2.4861	2.3817	2.3514
		40	5.2219	4.5668	4.1689	3.8021	3.6758	3.4423	3.3294	3.0727	2.8913	2.6591	2.4855	2.4280
	0.8	1	3.9680	3.6163	3.2580	2.9751	2.8358	2.6956	2.5871	2.4185	2.2789	2.1574	1.9823	1.8668
		2	4.1951	3.7682	3.3615	3.0565	2.9109	2.7666	2.6514	2.4906	2.3561	2.2260	2.0844	1.9957
		5	4.3419	3.8701	3.4398	3.1241	2.9782	2.8324	2.7036	2.5593	2.4315	2.3064	2.1887	2.1292
		10	4.4261	3.9466	3.4996	3.1932	3.0476	2.8960	2.8525	2.6154	2.4837	2.3567	2.2427	2.1847
		20	4.7283	4.3147	3.7080	3.4092	3.2928	3.1646	2.9817	2.7925	2.6276	2.4227	2.2900	2.2566
		40	5.1467	4.5126	4.0914	3.7493	3.6043	3.4252	3.2841	3.0271	2.8761	2.5937	2.4148	2.3651
	1	1	3.9370	3.5856	3.2269	2.9460	2.8078	2.6677	2.5284	2.3883	2.2440	2.0958	1.9299	1.8295
		2	4.0574	3.7320	3.3265	3.0230	2.8812	2.7375	2.5967	2.4578	2.3190	2.1765	2.0224	1.9336
		5	4.2964	3.8275	3.4052	3.0878	2.9428	2.7977	2.6579	2.5210	2.3880	2.2518	2.1139	2.0492
		10	4.3750	3.9021	3.4782	3.1686	3.0194	2.8687	2.7245	2.5820	2.4452	2.3061	2.1738	2.1172
		20	4.6867	4.2228	3.6982	3.3790	3.2336	3.0644	2.9047	2.7420	2.5771	2.3969	2.2506	2.1926
		40	5.1021	4.4846	4.0178	3.6980	3.5521	3.3650	3.1921	2.9819	2.7780	2.5534	2.3520	2.2710
	1.4	1	3.9042	3.5521	3.1954	2.9140	2.7749	2.6336	2.4921	2.2982	2.1988	2.0371	1.8542	1.3916
		2	4.0188	3.6943	3.2926	2.9914	2.8454	2.7000	2.5514	2.3420	2.2236	2.1096	1.9376	1.4708
		5	4.2506	3.7802	3.3549	3.0452	2.8999	2.7547	2.6134	2.3925	2.3317	2.1856	2.0273	1.6001
		10	4.3219	3.8548	3.4463	3.1028	2.9747	2.8172	2.6526	2.4775	2.3936	2.2598	2.1010	1.7218
		20	4.5286	4.0946	3.6974	3.3190	3.2025	3.0004	2.8012	2.6658	2.5009	2.3194	2.1991	1.8223
		40	4.9438	4.4530	4.0106	3.6184	3.4720	3.3016	3.1246	2.9229	2.7295	2.5085	2.3257	1.9426
	1.8	1	2.2175	2.1814	2.1542	2.1079	2.0608	2.0239	1.9650	1.8914	1.7878	1.6566	1.4741	1.3755
		2	2.7841	2.7515	2.7148	2.6591	2.3790	2.2869	2.1694	2.0653	1.9322	1.7774	1.5812	1.4409
		5	3.4914	3.2638	2.9982	2.9857	2.6232	2.4941	2.3624	2.2246	2.0772	1.9133	1.7137	1.5758
		10	3.8659	3.5100	3.1590	3.0574	2.7571	2.6206	2.4258	2.3384	2.1855	2.0168	1.8142	1.6770
		20	4.0841	3.7047	3.3513	3.2164	2.9384	2.7955	2.6665	2.4925	2.3248	2.1412	1.9247	1.7702
		40	4.3529	3.9644	3.5938	3.5513	3.1663	3.0164	2.8620	2.6983	2.5198	2.3106	2.0538	1.8954
100	0.4	1	4.2920	3.8858	3.3138	3.2536	3.1987	2.9045	2.7015	2.5614	2.4490	2.3474	2.2059	2.1768
		2	4.4210	4.0358	3.5535	3.3786	3.2715	3.1654	2.7626	2.6298	2.5595	2.4483	2.3843	2.3382
		5	4.5273	4.0890	3.6422	3.5824	3.3071	3.4645	2.8924	2.7672	2.6884	2.5213	2.4617	2.4161
		10	4.9987	4.3372	3.7241	3.6256	3.4455	3.5817	3.0667	2.8332	2.8071	2.5985	2.5672	2.5398
		20	5.4765	4.6230	4.2690	3.8558	3.8014	3.6670	3.3618	2.9882	2.9381	2.7291	2.6922	2.5982
		40	6.1657	4.8991	4.4894	4.1123	3.9710	3.8192	3.4670	3.2740	3.1110	2.9484	2.8091	2.6606
	0.6	1	4.2336	3.8288	3.4163	3.1081	2.9708	2.8191	2.6848	2.5287	2.4065	2.2946	2.1637	2.0914
		2	4.3870	3.9159	3.4801	3.2014	3.0444	2.8602	2.7233	2.5790	2.4810	2.3631	2.2652	2.2160
		5	4.4887	3.9923	3.5419	3.2512	3.0940	2.9248	2.8523	2.6645	2.5512	2.4473	2.3619	2.3060
		10	4.7884	4.2798	3.6230	3.3518	3.1488	3.1014	2.9959	2.7181	2.6625	2.4932	2.4174	2.3881
		20	5.1504	4.5859	3.8955	3.6386	3.4352	3.3251	3.1781	2.8192	2.7621	2.5454	2.4925	2.4604
		40	5.3987	4.7606	4.2869	3.8923	3.7362	3.6263	3.3841	3.1797	2.9766	2.7558	2.5820	2.5087
	0.8	1	4.1952	3.7681	3.3612	3.0566	2.9112	2.7678	2.6593	2.4944	2.3625	2.2493	2.1053	2.0086
		2	4.3147	3.8484	3.4208	3.1078	2.9632	2.8240	2.6814	2.5552	2.4295	2.3075	2.1855	2.1083
		5	4.4060	3.9151	3.4759	3.1589	3.0190	2.8740	2.7397	2.6118	2.4924	2.3765	2.2747	2.2185
		10	4.7297	4.2096	3.5873	3.2295	3.0918	2.9980	2.9415	2.6596	2.5383	2.4172	2.3546	2.3054
		20	5.0554	4.4701	3.8482	3.5091	3.3948	3.1917	3.1017	2.7901	2.6869	2.4824	2.4266	2.3589
		40	5.3233	4.7113	4.2076	3.8253	3.8019	3.5841	3.3225	3.1218	2.9392	2.6902	2.5390	2.4946
	1	1	4.1578	3.7324	3.3287	3.0272	2.8832	2.7404	2.6014	2.4645	2.3284	2.1890	2.0388	1.9506
		2	4.2733	3.8095	3.3842	3.0766	2.9345	2.7925	2.6556	2.5220	2.3913	2.2595	2.1195	2.0479
		5	4.3582	3.8710	3.4452	3.1267	2.9839	2.8399	2.7050	2.5719	2.4462	2.3212	2.1999	2.1506
		10	4.6912	4.1535	3.5262	3.2051	3.0684	2.9140	2.7721	2.6299	2.4997	2.3649	2.2527	2.2157
		20	4.9966	4.4325	3.7848	3.4583	3.3268	3.1409	2.9776	2.7978	2.6408	2.4695	2.3324	2.2914
		40	5.2823	4.6884	4.1682	3.8283	3.7270	3.5160	3.3557	3.0934	2.8840	2.6428	2.4318	2.4144
	1.4	1	4.1199	3.6957	3.2953	2.9949	2.8510	2.7073	2.5659	2.3247	2.2806	2.1265	1.9559	1.5077
		2	4.2311	3.7700	3.3513	3.0439	2.9004	2.7561	2.6085	2.3750	2.3412	2.1865	2.0282	1.5759
		5	4.3121	3.8237	3.3924	3.1013	2.9424	2.7978	2.6592	2.4216	2.3891	2.2479	2.1029	1.7188
		10	4.3999	3.9177	3.5017	3.1754	3.0052	2.8726	2.7121	2.5283	2.4154	2.3186	2.1714	1.8130
		20	4.6714	4.2114	3.7955	3.3910	3.2795	3.0852	2.9014	2.7423	2.5771	2.4110	2.2607	1.9051
		40	5.2301	4.6674	4.1722	3.7859	3.6563	3.4560	3.2886	3.0475	2.8116	2.6093	2.3989	2.0212
	1.8	1	2.7069	2.6613	2.2825	2.2548	2.2212	2.1707	2.1854	2.0699	1.9335	1.7769	1.5789	1.4820
		2	3.3215	3.1522	3.0515	2.9922	2.5876	2.4620	2.3541	2.1914	2.0224	1.8776	1.6784	1.5421
		5	3.8817	3.5260	3.1623	3.0152	2.7366	2.5963	2.5461	2.3125	2.1620	1.9778	1.8026	1.6726
		10	4.0818	3.6599	3.2742	3.1033	2.8549	2.7147	2.6514	2.4270	2.2728	2.1035	1.9035	1.7712
		20	4.2319	3.8369	3.4756	3.2714	3.0566	2.9113	2.8756	2.6024	2.4314	2.2427	2.0237	1.8687
		40	4.5061	4.1031	3.7234	3.6748	3.2922	3.1386	2.9828	2.8147	2.6359	2.4262	2.1609	2.0012

APPENDIX-C

Mixed Convection Newtonian Data for Drag Coefficients

Table C1: Dependence of pressure drag coefficients (C_{DP}) on the fluid volume fractions (ϕ_f), Reynolds (Re), Prandtl (Pr) and Richardson (Ri) numbers (NC-results not converged possibly due to unsteadiness in the flow)

C_{DP}													
Pr	ϕ_f	Ri=1						Ri=2					
		Re→1	2	5	10	20	40	1	2	5	10	20	40
0.7	0.70	147.0031	75.5807	33.3814	19.5496	13.6948	9.6724	150.6507	79.4862	37.9541	24.9215	18.1371	11.9476
	0.75	88.3842	46.1470	21.3492	13.9754	10.1050	7.0398	91.7965	49.8001	25.5492	17.7810	12.9337	8.5964
	0.80	54.7158	29.0938	14.0014	9.6534	7.0938	5.1062	57.7034	32.4001	17.886	13.0311	9.1227	6.6462
	0.84	35.0610	19.2133	10.2804	7.3504	5.5640	4.0892	37.6176	22.2051	13.0991	9.7420	7.7582	5.4514
	0.86	27.2972	15.4650	9.6340	6.2940	4.7786	3.7371	30.3709	18.3048	11.3470	8.5989	6.9495	4.8878
	0.88	21.8412	13.4336	8.1158	5.4528	4.2670	3.4622	24.3004	15.1394	9.6678	7.4465	6.0341	4.6475
	0.90	16.9482	12.9345	7.3576	5.4439	4.2064	3.2405	22.2699	14.1824	9.3162	7.3679	5.6368	4.5169
	0.92	15.4000	11.3270	6.8971	4.7480	3.7530	3.1320	21.7204	13.6620	8.3863	6.1360	5.2723	4.1282
	0.94	14.8847	10.8862	5.7666	4.6848	3.7080	3.0324	20.0118	12.8321	7.5989	5.8521	4.8072	4.0455
	0.96	13.8116	10.0900	5.4184	4.4444	3.4728	2.5897	19.5582	11.6421	7.5666	5.5502	4.7309	3.8745
	0.98	12.8521	9.7958	5.2610	4.3092	3.1841	2.3248	18.9590	10.4420	7.3825	5.5087	4.3760	3.2137
	0.99	11.7483	9.4171	4.8018	3.9875	NC	NC	17.5621	10.8311	6.9651	5.4902	NC	NC
1	0.70	147.0720	75.7800	33.7804	21.0280	13.9044	10.0503	150.8284	79.8615	38.8658	26.2950	18.2362	11.7180
	0.75	88.3984	46.2145	21.7974	14.1482	10.2040	7.1178	91.8472	49.8631	26.4070	18.7805	13.8653	9.4860
	0.80	54.7572	29.3480	14.4756	9.8458	8.2031	5.1860	57.7399	32.839	18.162	13.291	10.161	8.7708
	0.84	35.1782	19.4165	10.3605	7.7096	6.1859	4.2227	38.0156	22.599	13.749	10.114	8.9092	7.5771
	0.86	27.9064	15.6800	9.7699	6.5340	5.6016	3.8781	30.5900	18.7322	11.6451	9.6864	7.0884	5.1287
	0.88	23.5877	13.6549	8.4680	5.5795	4.9532	3.5914	24.5247	15.6229	10.2054	8.3088	6.9196	6.0000
	0.90	20.0606	12.9584	7.5788	5.3735	4.3948	3.4278	22.5106	14.5984	9.6842	7.9628	5.8392	4.9538
	0.92	18.9265	11.4088	6.9135	5.1755	4.3054	3.2501	21.9625	13.832	8.7451	7.0594	5.5837	4.1691
	0.94	17.1325	10.9704	6.0261	4.9988	3.8882	3.1418	20.8752	12.336	8.0518	6.7624	5.0243	4.0453
	0.96	16.9904	10.3521	5.6940	4.8174	3.8455	3.0512	19.8506	11.92	7.9558	6.1326	4.9014	4.1588
	0.98	15.2744	9.8702	5.5364	4.7244	3.6036	2.4739	19.4710	10.907	7.6216	5.813	4.4824	3.267
	0.99	14.8390	9.6897	5.4568	4.2514	NC	NC	18.9554	10.688	7.4546	5.4568	NC	NC
10	0.70	149.9247	80.4692	38.4434	24.4748	15.5376	10.3667	156.5641	89.1109	46.4445	30.5454	18.7453	12.562
	0.75	90.9954	50.3572	25.5312	16.9632	11.0178	7.6115	97.2448	57.9001	32.3365	20.7573	13.3023	11.985
	0.80	55.7632	31.8966	17.3050	11.7518	8.3006	5.4438	61.2281	38.378	22.277	14.38	10.404	10.5387
	0.84	37.7528	22.2644	12.5462	8.6648	6.8676	4.4886	42.5985	27.289	16.263	10.823	9.4748	8.4323
	0.86	30.1698	18.37	10.688	7.3418	6.2478	3.896	35.0626	22.4638	13.6672	9.2703	8.5864	8.239
	0.88	24.0910	15.0756	8.8846	7.0477	5.3923	3.7409	28.7095	18.9851	11.5008	8.8715	6.9726	6.2055
	0.90	20.5571	13.1039	8.4066	6.4148	5.0674	3.5228	26.8088	15.6065	9.6687	7.7980	6.1790	4.7924
	0.92	18.4708	12.216	8.0408	5.4777	4.8278	3.3453	24.2421	13.603	8.9009	6.7325	5.9502	4.5354
	0.94	16.0847	11.1444	7.8519	5.3595	4.1648	3.2319	22.5296	13.134	8.4263	6.5939	5.4075	4.4453
	0.96	15.8075	10.7940	7.1532	5.1888	4.0993	3.1127	21.2845	13.001	8.2628	5.9624	4.9268	4.3588
	0.98	14.9148	9.9465	6.9652	4.9958	3.8706	3.0914	20.9751	12.723	8.1938	5.938	4.5823	4.267
	0.99	14.6174	10.0790	6.7225	4.8526	NC	NC	19.7894	11.2472	7.8808	5.6223	NC	NC
50	0.70	154.7525	84.3262	40.2992	25.2065	16.5286	10.6354	166.0560	96.3839	49.5430	31.0704	18.9970	14.451
	0.75	94.7092	52.9922	26.7860	17.6452	11.3905	7.6302	104.2015	62.8126	33.4135	21.2345	13.7118	12.6362
	0.80	58.1935	33.6878	18.1930	13.9256	8.5868	5.4964	66.1757	44.44	23.103	14.826	10.587	11.2989
	0.84	39.5272	22.9955	12.8686	10.1132	6.9741	4.5012	45.0899	32.8982	18.0642	10.9745	9.8866	9.2083
	0.86	33.7925	18.927	10.999	8.748	6.5182	4.4443	37.0932	28.3830	14.2815	9.726	8.7075	8.6633
	0.88	28.7660	15.5788	9.4447	7.307	5.9774	4.3127	30.4716	24.0680	13.034	9.2113	7.1512	6.3195
	0.90	24.2318	12.4562	8.9195	6.9674	5.3627	3.832	28.6136	20.5378	12.0729	7.8854	6.2015	5.1664
	0.92	20.0534	10.928	8.5662	5.8401	4.8756	3.4098	26.0734	18.74	9.9732	7.2805	5.9918	4.8106
	0.94	18.8350	10.736	7.9825	5.4298	4.3775	3.2952	24.8253	16.46	8.5775	6.8635	5.5208	4.5485
	0.96	16.0604	10.5910	7.6049	5.2246	4.1693	3.1921	22.4848	15.04	8.4054	6.1174	5.0481	4.4112
	0.98	15.6622	10.5836	6.9978	5.1095	3.9742	NC	21.4195	14.644	8.2229	5.9796	4.8338	NC
	0.99	14.9318	10.349	6.5398	4.7316	NC	NC	20.5888	13.8665	7.9791	5.7154	NC	NC

Table C2: Dependence of friction drag coefficients (C_{DF}) on the fluid volume fractions (ϕ_f), Reynolds (Re), Prandtl (Pr) and Richardson (Ri) numbers (NC-results not converged possibly due to unsteadiness in the flow)

C_{DF}													
Pr	ϕ_f	Ri=1						Ri=2					
		Re→1	2	5	10	20	40	1	2	5	10	20	40
0.7	0.70	142.1439	71.7954	30.0058	16.1454	10.1483	7.2560	143.2847	73.1094	31.8105	18.6238	12.4870	8.5797
	0.75	87.3522	44.5387	19.1642	11.4124	7.5964	5.4290	88.8520	46.1688	21.1322	13.1988	9.3180	6.4218
	0.80	54.5746	28.1622	12.4698	7.8620	5.5510	4.1176	55.8994	29.7539	14.5982	9.8465	6.9297	5.1399
	0.84	34.9566	18.5058	9.0651	6.0384	6.7784	3.3001	36.1945	20.1904	10.6602	7.5838	4.7746	4.2854
	0.86	27.8020	14.8666	6.6262	5.4863	5.2984	2.9887	29.2216	16.5516	9.3055	7.8862	5.4550	3.8690
	0.88	21.7975	13.9104	5.2946	6.0827	4.4625	2.7005	23.2718	13.6378	8.0099	7.9881	6.3473	3.4238
	0.90	16.8632	12.1848	5.4277	4.6116	3.6250	2.2230	19.3644	8.9596	8.0547	6.1123	5.2217	2.7669
	0.92	14.2875	12.6654	5.0269	4.8405	3.4600	2.1412	17.9328	8.8622	8.6534	6.8515	4.4969	2.9045
	0.94	12.7520	10.1584	5.3665	4.0387	3.4360	2.1505	17.3634	8.7670	7.8258	5.3317	4.7428	1.9085
	0.96	11.7095	9.9280	5.5711	4.2404	3.3950	2.4865	15.7590	9.2278	6.5550	5.1627	3.8500	1.2214
	0.98	12.0929	9.5138	5.0394	3.9564	3.6837	2.093	15.5642	9.8159	6.7118	4.7107	4.1978	1.2024
	0.99	11.7226	9.0371	5.1700	4.0459	NC	NC	16.2415	9.1277	6.8996	4.6343	NC	NC
1	0.70	142.1961	71.9289	26.4940	17.2995	10.3958	7.2994	143.4064	73.3662	32.4677	19.6862	13.0455	8.9218
	0.75	87.1802	44.4843	19.5155	11.5422	7.8060	5.4580	88.3732	46.0230	21.8110	14.1054	8.7084	5.6470
	0.80	54.6332	28.3610	12.8520	8.0504	6.7148	4.2510	56.0098	28.1884	14.8456	10.2748	6.0788	3.4198
	0.84	35.1414	18.6758	9.1486	6.3890	4.0347	4.4330	36.6498	20.5176	11.2795	8.1047	4.0710	2.4806
	0.86	27.9095	15.0758	6.7600	6.0369	3.9014	3.1112	29.4367	16.9644	9.6645	7.7818	5.4687	4.8300
	0.88	21.5470	14.1308	5.6252	6.4535	4.3282	2.7976	29.5030	14.0600	8.5734	7.5008	5.6010	2.9424
	0.90	16.9838	12.3742	5.9725	4.9629	4.7156	2.5289	25.6229	9.3840	7.9275	5.7530	5.2777	2.5678
	0.92	15.525	13.3484	5.4171	4.8507	3.6360	2.3772	23.1996	8.9998	7.3337	6.3439	4.6191	3.0785
	0.94	15.0457	10.5505	5.7202	4.6325	3.6104	2.2009	22.1684	9.6396	7.0906	4.5972	5.0929	3.1311
	0.96	14.0751	10.3923	5.7880	4.0164	3.2875	2.2762	20.3996	9.9319	6.4925	5.1080	4.0642	0.8996
	0.98	13.9824	10.0062	5.2918	3.8371	3.1949	2.0937	19.4111	10.0106	6.7286	4.8534	4.3701	1.2291
	0.99	13.1132	9.2476	5.0466	4.1163	NC	NC	18.8500	10.1251	6.6938	4.9596	NC	NC
10	0.70	144.2265	75.1820	33.2798	19.7906	12.0862	8.2281	147.4697	79.8507	37.9274	24.2338	15.4558	8.8301
	0.75	89.2110	47.4896	22.1198	13.8094	8.7718	6.2001	92.6315	51.9885	26.6502	16.9692	11.2368	3.6390
	0.80	55.0953	30.1521	15.0146	9.7063	6.7656	4.4845	58.5038	34.4485	18.7161	12.1682	7.8311	2.9767
	0.84	37.2525	20.9910	10.8984	7.2500	4.5618	4.4274	40.6970	24.4482	13.9232	9.6254	8.0835	3.4232
	0.86	29.8594	20.2865	9.3422	8.2104	4.4372	3.0993	33.3514	20.1735	11.8844	10.8549	7.0847	2.7366
	0.88	23.7875	18.1468	7.7970	6.5139	4.5055	2.8959	34.2326	17.0929	10.1115	8.4446	6.1492	3.7540
	0.90	16.2518	16.1241	7.3217	5.5661	3.7784	2.7051	27.5603	14.0956	10.2588	7.2396	5.2878	4.0900
	0.92	16.1490	13.8420	5.8838	6.4135	3.6172	2.3761	26.1540	12.3788	9.3188	7.8453	5.2970	3.2889
	0.94	15.9723	12.5526	5.5095	4.7978	3.2461	2.3960	25.4510	12.0304	7.7362	5.6974	5.0106	2.0468
	0.96	14.5118	10.8216	5.7115	4.4052	3.2206	2.4278	21.7200	12.0262	7.6523	6.0871	4.5694	1.3674
	0.98	14.1914	10.9725	5.6089	4.5052	3.3406	1.5768	19.6594	10.6326	7.3598	5.1020	4.4605	0.5609
	0.99	13.7087	9.2022	5.6547	4.4040	NC	NC	18.5610	10.0682	7.4462	4.9208	NC	NC
50	0.70	147.2794	77.5338	34.4648	20.2764	12.8259	8.4057	153.5886	84.5818	40.3038	24.7221	15.6375	7.1402
	0.75	91.5578	49.1322	22.9390	14.2780	9.0375	6.1951	97.2510	55.3175	27.4452	17.3473	12.6220	3.2773
	0.80	56.7190	31.3026	15.6100	7.7816	6.8526	4.5306	61.9147	35.6927	19.3217	12.4830	9.9720	2.2584
	0.84	34.4738	21.2786	11.0525	6.5690	4.6592	5.3090	42.0324	21.4996	15.4416	9.9744	8.4750	2.7610
	0.86	28.9658	17.5258	9.5071	6.5644	3.5899	3.4515	34.5968	17.6284	12.3226	10.6053	7.7090	1.4959
	0.88	20.0549	14.3924	8.1978	6.9567	3.6328	2.6335	35.3652	13.8595	10.4079	8.2250	7.7218	2.7187
	0.90	17.5676	11.4712	7.2295	5.3435	3.2627	3.0715	31.8570	10.7676	10.5156	8.4330	6.3957	3.3250
	0.92	16.4642	9.9897	6.2455	6.4017	3.5045	2.4308	28.5702	11.1434	11.7190	7.6173	5.4083	3.3939
	0.94	15.4690	9.7467	6.0909	5.3545	3.2028	2.3953	24.4148	12.2247	10.1094	6.0834	5.0725	2.4419
	0.96	14.9896	9.7480	5.6634	4.2962	3.4026	2.3966	23.2310	12.4325	7.6959	6.2893	4.3344	2.1133
	0.98	14.3744	9.7264	6.1442	4.3720	3.5419	NC	21.1936	12.0977	7.4005	5.9622	4.5332	NC
	0.99	13.9747	9.5522	6.3972	4.6927	NC	NC	19.4197	12.2068	7.3978	5.6771	NC	NC

Table C3: Dependence of total drag coefficients (C_D) on the fluid volume fractions (ϕ_f), Reynolds (Re), Prandtl (Pr) and Richardson (Ri) numbers

C_D													
Pr	ϕ_f	Ri=1						Ri=2					
		Re→1	2	5	10	20	40	1	2	5	10	20	40
0.7	0.70	289.1470	147.3761	63.3872	35.6950	23.8431	16.9284	293.9354	152.5956	69.7646	43.5453	30.6241	20.5273
	0.75	175.7364	90.6857	40.5134	25.3878	17.7014	12.4688	180.6485	95.9689	46.6814	30.9798	22.2517	15.0182
	0.80	109.2904	57.2560	26.4712	17.5154	12.6448	9.2238	113.6028	62.1537	32.4844	22.8779	16.0524	11.7861
	0.84	70.0176	37.7191	19.3455	13.3888	12.3424	7.3893	73.8121	42.3958	23.7591	17.3258	12.5328	9.7368
	0.86	55.0992	30.3316	16.2602	11.7803	10.0770	6.7258	59.5925	34.8564	20.6525	16.4851	12.4045	8.7568
	0.88	43.6387	27.3440	13.4104	11.5355	8.7295	6.1627	47.5722	28.7772	17.6777	15.4346	12.3814	8.0713
	0.90	33.8114	25.1193	12.7853	10.0555	7.8314	5.4635	41.6343	23.1420	17.3709	13.4802	10.8585	7.2838
	0.92	29.6875	23.9924	11.9240	9.5885	7.2130	5.2732	39.6532	22.5242	17.0397	12.9875	9.7692	7.0327
	0.94	27.6367	21.0446	11.1331	8.7235	7.1440	5.1829	37.3752	21.5994	15.4247	11.1837	9.5500	5.9540
	0.96	25.5211	20.0180	10.9895	8.6848	6.8678	5.0762	35.3172	20.8700	14.1216	10.7129	8.5809	5.0959
	0.98	24.9450	19.3096	10.3004	8.2656	6.5752	4.4178	34.5232	20.2576	14.0943	10.2194	8.5738	4.4461
	0.99	23.4709	18.4542	9.9718	8.0334	6.3037	1.9725	33.8036	19.9585	13.8647	10.1245	7.9336	3.5730
1	0.70	289.2681	147.7089	60.2744	38.3275	24.3002	17.3497	294.2348	153.2277	71.3335	45.9812	31.2817	20.6398
	0.75	175.5786	90.6988	41.3129	25.6904	18.0100	12.5758	180.2204	95.8861	48.2180	32.8859	22.5737	15.1330
	0.80	109.3904	57.7090	27.3276	17.8962	14.9179	9.4370	113.7497	61.0270	33.0078	23.5654	16.2400	12.1906
	0.84	70.3196	38.0923	19.5091	14.0986	10.2206	8.6557	74.6654	43.1170	25.0286	18.2189	12.9802	10.0577
	0.86	55.8159	30.7553	16.5299	12.5709	9.5030	6.9893	60.0267	35.6966	21.3096	17.4682	12.5571	9.9587
	0.88	45.1347	27.7857	14.0932	12.0330	9.2814	6.3890	54.0277	29.6829	18.7788	15.8096	12.5206	8.9424
	0.90	37.0444	25.3326	13.5513	10.3364	9.1104	5.9567	48.1335	23.9824	17.6117	13.7158	11.1169	7.5216
	0.92	34.4515	24.7572	12.3306	10.0262	7.9414	5.6273	45.1621	22.8318	16.0788	13.4033	10.2028	7.2476
	0.94	32.1782	21.5209	11.7463	9.6313	7.4986	5.3427	43.0436	21.9756	15.1424	11.3596	10.1172	7.1764
	0.96	31.0655	20.7441	11.4820	8.8338	7.1330	5.3274	40.2502	21.8522	14.4483	11.2406	8.9656	5.0584
	0.98	29.2568	19.8764	10.8282	8.5615	6.7985	4.5676	38.8821	20.9177	14.3502	10.6664	8.8525	4.4961
	0.99	27.9522	18.9373	10.5034	8.3677	6.5348	2.9814	37.8054	20.8134	14.1484	10.4164	8.3443	3.6980
10	0.70	294.1512	155.6512	71.7232	44.2654	27.6238	18.5948	304.0338	168.9616	84.3719	54.7792	34.2011	21.3919
	0.75	180.2064	97.8468	47.6510	30.7726	19.7896	13.8116	189.8763	109.8886	58.9867	37.7265	24.5391	15.6235
	0.80	110.8585	62.0487	32.3196	21.4581	15.0662	9.9283	119.7319	72.8260	40.9931	26.5478	18.2348	13.5154
	0.84	75.0053	43.2554	23.4446	15.9148	11.4294	8.9160	83.2955	51.7369	30.1862	20.4480	17.5583	11.8555
	0.86	60.0292	38.6561	20.0304	15.5522	10.6850	6.9953	68.4140	42.6373	25.5516	20.1252	15.6711	10.9756
	0.88	47.8785	33.2224	16.6816	13.5616	9.8978	6.6368	62.9421	36.0780	21.6123	17.3161	13.1218	9.9595
	0.90	36.8089	29.2280	15.7283	11.9809	8.8458	6.2279	54.3691	29.7021	19.9275	15.0376	11.4668	8.8824
	0.92	34.6198	26.0581	13.9246	11.8912	8.4450	5.7214	50.3961	25.9817	18.2197	14.5778	11.2472	7.8243
	0.94	32.0570	23.6970	13.3614	10.1573	7.4109	5.6279	47.9806	25.1648	16.1625	12.2913	10.4181	6.4921
	0.96	30.3193	21.6156	12.8647	9.5940	7.3199	5.5405	43.0045	25.0276	15.9151	12.0495	9.4962	5.7262
	0.98	29.1062	20.9190	12.5741	9.5010	7.2112	4.6682	40.6345	23.3554	15.5536	11.0400	9.0428	4.8279
	0.99	28.3261	19.2815	12.3772	9.2566	6.7351	3.0688	38.3504	21.3154	15.3270	10.5431	8.7522	3.7328
50	0.70	302.0319	161.8600	74.7640	45.4829	29.3545	19.0411	319.6446	180.9657	89.8468	55.7925	34.6345	21.5914
	0.75	186.2670	102.1244	49.7250	31.9232	20.4280	13.8253	201.4525	118.1301	60.8587	38.5818	26.3338	15.9135
	0.80	114.9125	64.9904	33.8030	21.7072	15.4394	10.0270	128.0904	80.1329	42.4243	27.3091	20.5591	13.5573
	0.84	74.0010	44.2741	23.9211	16.6822	11.6333	9.8102	87.1223	54.3978	33.5058	20.9489	18.3616	11.9693
	0.86	62.7583	36.4532	20.5058	15.3124	10.1081	7.8958	71.6900	46.0114	26.6041	20.3313	16.4165	10.1592
	0.88	48.8209	29.9712	17.6425	14.2637	9.6102	6.9462	65.8368	37.9275	23.4419	17.4363	14.8730	9.0382
	0.90	41.7994	23.9274	16.1490	12.3109	8.6254	6.9035	60.4706	31.3054	22.5885	16.3184	12.5972	8.4914
	0.92	36.5176	20.9178	14.8117	12.2418	8.3801	5.8406	54.6436	29.8832	21.6922	14.8978	11.4001	8.2045
	0.94	34.3040	20.4822	14.0734	10.7843	7.5803	5.6905	49.2401	28.6848	18.6869	12.9469	10.5933	6.9904
	0.96	31.0500	20.3390	13.2683	9.5208	7.5719	5.5887	45.7158	27.4721	16.1013	12.4067	9.3825	6.5245
	0.98	30.0366	20.3100	13.1420	9.4815	7.5161	4.7273	42.6131	26.7417	15.6234	11.9418	9.3670	4.9564
	0.99	28.9065	19.9014	12.9370	9.4243	6.9619	3.1526	40.0085	26.0733	15.3769	11.3925	8.9737	3.8827

Table C4: Dependence of average Nusselt number (Nu) on the fluid volume fractions (ϕ_f), Reynolds (Re), Prandtl (Pr) and Richardson (Ri) numbers

Nu (n = 1)													
Pr	ϕ_f	Ri=1						Ri=2					
		Re→1	2	5	10	20	40	1	2	5	10	20	40
0.7	0.70	0.8862	1.0128	1.2401	1.638	2.409	3.6596	0.8915	1.0159	1.2435	1.6492	2.5031	4.089
	0.75	0.9199	1.0154	1.292	1.7758	2.611	3.983	0.924	1.0161	1.299	1.805	2.8038	4.5335
	0.80	0.9228	1.0638	1.369	1.9248	2.8354	4.3305	0.9259	1.0712	1.3813	1.9955	3.1514	4.9846
	0.84	0.9300	1.0819	1.4575	2.058	3.0632	4.5658	0.9359	1.092	1.4847	2.1932	3.4648	5.3534
	0.86	0.9360	1.0881	1.4944	2.1081	3.1586	4.6136	0.9379	1.0966	1.5315	2.2825	3.5873	5.4184
	0.88	0.9486	1.1086	1.5446	2.1948	3.3015	4.7102	0.9574	1.1027	1.6001	2.4175	3.7657	5.4941
	0.90	0.9660	1.1100	1.603	2.3046	3.455	4.837	0.9802	1.1251	1.6882	2.5755	3.9523	5.6112
	0.92	0.9818	1.1539	1.6912	2.4691	3.6419	4.8804	1.0084	1.178	1.8248	2.7882	4.0954	5.818
	0.94	1.0138	1.1952	1.7879	2.6345	3.7314	4.885	1.0544	1.2328	1.9781	2.9817	4.2131	6.005
	0.96	1.0267	1.2390	1.9205	2.7871	3.8074	4.9793	1.0915	1.3175	2.1523	3.0789	4.3709	6.1128
	0.98	1.0394	1.3518	2.1408	2.9328	3.9556	5.0831	1.1001	1.4973	2.3483	3.3005	4.682	5.8026
	0.99	1.0415	1.4841	2.2511	3.1351	3.8516	5.2886	1.1008	1.6314	2.4908	3.5398	4.6673	6.2059
1	0.70	0.9518	1.0994	1.3838	1.9448	2.8602	4.2534	0.9534	1.103	1.3877	1.9671	3.0449	4.8885
	0.75	0.972	1.1184	1.476	2.1	3.049	4.5545	0.979	1.1197	1.4847	2.1578	3.3744	5.3094
	0.80	0.9801	1.1394	1.5878	2.2478	3.2662	4.8653	0.9835	1.1312	1.6078	2.3764	3.7308	5.7192
	0.84	0.9865	1.1712	1.688	2.374	3.4864	5.1135	0.991	1.1481	1.7308	2.5992	4.0308	6.0392
	0.86	1.004	1.1856	1.7404	2.4484	3.6114	5.1922	1.0104	1.1943	1.8049	2.7285	4.1886	6.0926
	0.88	1.0052	1.2146	1.7905	2.5367	3.7428	5.2357	1.0352	1.2272	1.885	2.868	4.3497	6.1424
	0.90	1.0058	1.2508	1.847	2.6489	3.882	5.3225	1.067	1.2701	1.9848	3.0233	4.5026	6.2476
	0.92	1.0082	1.2904	1.9165	2.785	4.0201	5.3414	1.1019	1.3223	2.1112	3.1914	4.5641	6.3975
	0.94	1.0105	1.334	2.0176	2.9422	4.0768	5.3922	1.1132	1.3899	2.2693	3.3634	4.6722	6.4627
	0.96	1.0204	1.3898	2.1744	3.0976	4.1891	5.464	1.1516	1.4948	2.4609	3.4603	4.8757	6.5246
	0.98	1.0382	1.5109	2.3856	3.2492	4.2911	5.5332	1.1731	1.6839	2.6322	3.697	4.918	6.8276
	0.99	1.0504	1.6487	2.5021	3.483	4.2814	5.7172	1.2108	1.8173	2.7905	3.9662	5.2032	6.904
10	0.70	1.9215	2.3982	3.234	4.1008	5.2868	6.9085	1.924	2.677	3.7423	4.9264	6.6408	8.9938
	0.75	1.9269	2.4042	3.2342	4.134	5.3272	7.0278	2.0486	2.6838	3.771	4.9505	6.7694	9.0098
	0.80	1.9467	2.4428	3.2562	4.1966	5.3834	7.2074	2.1098	2.6884	3.791	5.0663	6.9286	9.0444
	0.84	1.985	2.472	3.2748	4.201	5.557	7.4036	2.1145	2.7008	3.8358	5.2207	7.1094	9.139
	0.86	2.0183	2.4923	3.3568	4.2971	5.6689	7.4078	2.1327	2.7104	3.8545	5.3149	7.1459	9.1657
	0.88	2.0426	2.5457	3.366	4.3757	5.7999	7.4138	2.1334	2.7234	3.9355	5.4228	7.1822	9.194
	0.90	2.0659	2.5916	3.52	4.4284	5.9552	7.423	2.15	2.7398	4.0402	5.557	7.216	9.3097
	0.92	2.1022	2.673	3.5206	4.5903	5.9907	7.4867	2.155	2.7553	4.1654	5.6877	7.2886	9.3207
	0.94	2.1202	2.6913	3.6738	4.7944	6.0438	7.5208	2.1608	2.8108	4.3262	5.7163	7.3016	9.7906
	0.96	2.1266	2.7184	3.7547	4.8874	6.1576	7.8232	2.1616	2.9616	4.5044	6.266	7.7208	10.2437
	0.98	2.1374	2.7215	4.0051	5.2726	6.2758	9.9651	2.3154	3.2188	4.6206	7.0541	8.6239	10.4801
	0.99	2.1582	2.9671	4.3377	5.9464	6.3538	10.115	2.5008	3.362	5.0345	8.128	9.5411	13.0918
50	0.70	2.4228	2.8974	3.7348	4.6018	5.8164	7.496	2.7122	3.3406	4.5701	5.774	7.5572	10.1772
	0.75	2.4264	2.9115	3.7365	4.6754	5.8234	7.7316	2.7449	3.3521	4.7178	5.7825	7.7757	10.3412
	0.80	2.4858	2.959	3.7844	4.723	6.0214	8.075	2.7885	3.3792	4.7983	5.9804	8.0784	10.4647
	0.84	2.5752	2.967	3.8434	4.8668	6.3269	8.4224	2.8068	3.3933	4.8735	6.2562	8.4135	10.622
	0.86	2.6624	3.0488	3.9011	4.9268	6.5675	8.5912	2.8843	3.4872	4.9938	6.4491	8.6152	10.6928
	0.88	2.6751	3.1444	4.1023	5.0469	6.7766	8.6057	2.8868	3.5422	5.0694	6.6457	8.6364	10.7428
	0.90	2.7814	3.1764	4.1078	5.2768	7.0316	8.6505	2.9722	3.686	5.3194	6.8893	8.7208	10.8263
	0.92	2.8878	3.3692	4.4	5.5637	7.0796	8.7084	3.0592	3.8041	5.6276	7.1054	8.7659	10.9224
	0.94	2.9029	3.685	4.4586	5.8992	7.2274	8.9728	3.1037	3.9956	5.8812	7.147	9.0148	11.6788
	0.96	2.9398	3.6952	4.823	6.0306	7.8585	11.2707	3.1535	4.0963	6.1452	7.2325	9.3762	11.6939
	0.98	2.9608	4.0106	5.2034	6.8727	9.2825	13.7561	3.2039	4.4864	7.3598	8.5354	11.2497	14.7376
	0.99	3.0529	4.115	6.033	8.8066	11.0577	14.8162	3.235	4.7695	4..4952	10.9318	12.484	16.1826

APPENDIX-D

Mixed Convection Non-Newtonian Data for Drag Coefficients

Table D1: Dependence of pressure (C_{DP}), friction (C_{DF}) and total (C_D) drag coefficients on the fluid volume fraction (ϕ_f), Reynolds (Re), Prandtl (Pr) and Richardson (Ri) numbers for the power-law index of n = 0.4 (NC-results not converged possibly due to unsteadiness in the flow)

C_{DP} (n = 0.4)													
Pr	ϕ_f	Ri = 1						Ri = 2					
		Re →1	2	5	10	20	40	1	2	5	10	20	40
1	0.70	80.3642	44.2844	20.8522	11.5064	7.1398	5.0104	85.8542	48.7929	21.9393	12.8166	8.4622	5.6636
	0.75	41.3430	24.5261	14.5874	8.1220	6.9441	4.1314	45.6910	27.4203	16.2912	9.8093	7.2792	5.5372
	0.80	31.0422	17.2410	9.4890	6.3052	5.3432	3.4564	36.1139	20.3418	12.4244	8.4296	6.0385	3.7534
	0.84	27.1999	15.6991	8.1924	5.4926	4.1931	2.9417	30.9743	17.4402	10.3836	7.2875	4.0151	3.2084
	0.86	21.6634	12.4158	7.4319	5.1239	3.9670	2.6017	24.6022	14.3850	9.5526	6.1854	3.7063	2.9756
	0.88	18.1389	10.8990	6.6396	4.6554	3.0575	2.4680	20.0697	12.1489	9.3251	5.0478	3.3864	2.7964
	0.90	14.6143	9.3821	6.5653	4.5115	2.8554	2.3766	17.5371	11.9127	8.0194	4.7345	3.2838	2.5845
	0.92	13.4864	8.9561	5.6987	4.1868	2.6522	2.3126	15.6411	10.7413	7.4861	4.3682	3.2332	2.2725
	0.94	12.7507	7.7525	5.3640	3.8594	2.4416	1.9735	14.9243	10.0429	6.2285	4.0018	2.9441	2.1524
	0.96	12.6517	7.2213	5.0154	3.0474	2.1235	1.8572	13.6056	9.1895	5.7072	3.9101	2.7600	2.0914
	0.98	11.1186	6.8195	4.5519	2.9473	1.9435	1.7909	12.2075	8.9654	5.4195	3.3772	2.5018	NC
	0.99	10.2817	6.3824	4.0884	2.8472	NC	NC	10.5701	8.6162	5.1318	2.7526	NC	NC
10	0.70	83.2125	36.5814	21.3488	12.9540	7.4968	5.4490	88.7534	52.0622	22.9962	13.7569	9.0546	5.9961
	0.75	46.5124	29.9032	15.9240	8.4664	7.2913	4.3868	47.5507	30.2598	16.8924	10.2154	7.7887	5.8141
	0.80	30.4561	18.3978	9.6217	8.0460	5.6104	3.6292	37.8369	25.0585	12.9144	9.9010	6.4612	3.9411
	0.84	26.7291	15.6650	9.3674	7.2983	4.4028	3.0888	32.4524	21.9553	10.7561	8.5254	4.2962	3.3688
	0.86	22.5627	12.2596	8.9044	5.6915	4.1654	2.7318	26.4512	15.9843	10.5236	7.8639	3.9657	3.1244
	0.88	20.6096	11.6258	8.0124	5.2403	3.1254	2.5914	23.7417	13.3886	8.3632	6.5177	3.6234	2.9362
	0.90	18.6565	10.6500	7.3362	5.1595	3.0684	2.4954	21.0321	12.9183	7.0038	6.3019	3.5137	2.7137
	0.92	15.7554	9.9920	6.6599	4.7797	2.9557	2.4282	17.2641	11.7928	6.8322	5.6793	3.4595	2.3861
	0.94	14.4785	8.6569	5.7832	4.6274	2.8198	2.0722	17.1188	10.8315	6.3668	5.0745	3.1502	2.26
	0.96	13.4785	7.5499	5.5755	4.3932	2.4787	1.9501	16.8687	10.3686	6.3668	5.0745	2.9532	2.196
	0.98	12.2015	6.5499	5.2469	4.2934	2.2297	1.8804	15.8687	9.3867	6.2027	4.4948	2.6769	NC
	0.99	10.1864	5.4428	4.5677	3.6071	NC	NC	14.8732	7.9057	5.9014	3.6312	NC	NC
50	0.70	89.6320	38.9342	25.4850	14.7668	9.3296	6.2664	92.8105	54.7344	25.0708	15.4447	10.0796	6.2959
	0.75	51.1994	30.3310	16.4925	8.6324	8.0253	4.6061	55.8154	31.4542	17.2151	10.7262	8.1781	6.1048
	0.80	41.1663	21.7478	10.8046	6.8429	6.6574	3.8107	47.2513	25.8511	17.1528	10.4961	6.7843	4.1382
	0.84	27.5633	17.6153	10.4841	6.7822	4.4266	3.2432	41.3958	22.7096	12.5227	8.9517	4.511	3.5372
	0.86	23.5434	12.5929	8.5747	6.1866	4.0862	2.8684	28.2745	16.3724	11.8335	8.2571	4.164	3.2806
	0.88	21.5031	11.9479	8.1560	5.2525	3.7335	2.721	25.3006	15.1928	11.2137	6.8436	3.8046	3.083
	0.90	19.4628	11.3028	8.1287	4.9320	3.6204	2.6202	22.3266	14.2773	9.3859	6.6170	3.6894	2.8494
	0.92	18.6981	10.6791	7.8660	4.4324	3.5646	2.5496	20.6885	12.1822	7.4681	5.9633	3.6325	2.5054
	0.94	17.3495	9.8886	7.5760	3.9751	3.2459	2.1758	18.8998	11.9018	6.4518	5.3282	3.3077	2.373
	0.96	16.7501	8.8567	5.7238	3.9108	3.0429	NC	17.1111	10.9818	6.4205	5.3282	NC	NC
	0.98	15.8771	7.2274	5.5883	3.3892	NC	NC	16.9497	9.7963	6.3891	4.7195	NC	NC
	0.99	15.3532	7.0980	5.4528	3.0181	NC	NC	16.2882	8.9107	5.5502	3.8128	NC	NC
C_{DF} (n = 0.4)													
Pr	ϕ_f	Ri = 1						Ri = 2					
		Re →1	2	5	10	20	40	1	2	5	10	20	40
1	0.70	44.8675	24.5128	9.7304	7.2134	4.1370	2.2930	53.7376	24.9449	13.0186	6.8588	3.8972	2.3563
	0.75	37.1842	16.9324	8.6252	5.2601	3.2504	1.7250	41.0983	21.7077	9.6174	5.2423	3.0366	1.3238
	0.80	21.7618	14.3658	7.1292	3.4476	2.4602	1.1344	24.3894	14.5337	6.8995	3.8804	2.2268	1.1994
	0.84	17.8385	10.6856	4.8697	2.8446	1.4428	0.8033	19.9803	10.6132	5.3997	3.1516	1.7909	1.1225
	0.86	15.4988	9.4535	3.9355	2.3388	1.2102	0.6319	17.4042	9.5788	4.7331	2.9725	1.7395	0.9670
	0.88	12.6931	7.4564	3.4139	2.0767	1.1378	0.6280	13.2259	8.0651	4.1404	2.4058	0.8698	0.6187
	0.90	9.8874	5.4592	2.8923	1.8146	1.0653	0.6241	11.0476	6.5513	3.5476	1.8390	0.6529	0.5946
	0.92	8.6797	4.8802	2.3805	1.4666	0.9245	0.5334	10.1285	5.2521	2.9626	1.5288	0.3999	0.5613
	0.94	8.3186	4.8073	2.3134	1.3486	0.6896	0.4571	8.3590	5.1638	2.7112	1.5090	0.2400	0.4828
	0.96	7.9575	4.7441	2.1941	1.2716	0.5408	0.3945	8.1214	4.6851	2.6503	1.4891	0.2113	0.4218
	0.98	7.7573	3.9577	2.1606	1.2306	0.4546	0.2807	7.2366	4.6409	2.5246	1.4513	0.1913	NC
	0.99	6.2557	3.7080	2.0077	1.0766	NC	NC	6.8142	4.1180	2.3380	1.4134	NC	NC

Table D1 (Contd.)

Pr	ϕ_f	Ri = 1						Ri = 2					
		Re →1	2	5	10	20	40	1	2	5	10	20	40
10	0.70	46.8898	29.4452	11.2206	7.7922	4.3708	2.4455	56.3616	25.7480	13.1003	8.4468	4.8878	2.7888
	0.75	38.1742	20.1420	9.4715	6.0848	3.0105	1.6184	42.9954	15.9173	8.3422	6.6520	3.1884	1.3900
	0.80	25.0492	12.7234	5.7560	4.1858	2.2718	0.8795	27.8225	15.1318	7.3604	4.4441	2.3381	1.2594
	0.84	18.0624	11.2660	5.1494	3.0750	1.7545	0.7940	21.3067	12.2581	6.2861	3.4119	1.8804	1.1786
	0.86	16.7918	9.9504	4.1994	2.6508	1.4155	0.7092	20.5497	10.6535	5.7701	3.0596	1.8265	1.0154
	0.88	13.9412	7.8255	3.4684	2.2889	1.2528	0.5970	16.5611	8.9197	4.7461	2.7218	0.9133	0.6496
	0.90	11.0906	6.7006	2.7374	1.9270	1.0900	0.4847	12.5724	7.1858	3.7220	2.3839	0.6855	0.6243
	0.92	10.1655	5.3430	2.7333	1.8723	0.8665	0.3773	11.3595	6.7797	3.2957	2.0535	0.4199	0.5894
	0.94	9.3962	5.2541	2.5926	1.7136	0.7006	0.3685	10.6604	6.3555	3.0706	1.9025	0.2520	0.5069
	0.96	8.6268	5.1652	2.5807	1.5548	0.5347	0.3597	9.9613	6.0782	2.8455	1.7514	0.2219	0.4429
	0.98	8.4972	5.1589	2.4518	1.2297	0.5142	0.3377	8.5125	6.0047	2.2612	1.4030	0.2009	NC
	0.99	7.3675	5.1525	2.4281	0.9045	NC	NC	7.6586	5.9312	1.2266	1.0546	NC	NC
50	0.70	49.1211	32.0889	13.0777	7.8381	4.2292	2.1538	59.5200	29.0195	16.9588	8.2094	4.9370	2.9324
	0.75	39.8736	21.4082	9.0126	4.9554	2.6258	1.4178	44.0482	25.0708	10.6310	5.5722	2.9620	1.3352
	0.80	26.8040	13.4410	6.6232	3.8842	1.8214	1.1703	29.0747	15.5910	7.7687	3.9490	2.2443	1.5518
	0.84	18.0391	11.5414	5.9350	3.3389	1.9636	0.9382	23.2270	12.7439	6.6413	3.6592	1.5500	1.1124
	0.86	17.4988	10.9453	4.4570	2.7794	1.5025	0.8129	21.8042	10.9788	6.0131	3.1725	1.4016	1.0118
	0.88	14.2971	8.2547	3.8920	2.2795	1.5114	0.8365	17.4629	9.2269	4.6825	2.4522	1.3837	0.9622
	0.90	11.0954	6.5640	3.3270	1.9796	1.5202	0.8601	13.1215	7.4750	3.3519	1.7318	1.3658	0.9126
	0.92	10.8166	5.7525	3.1805	1.6423	1.3665	0.6324	12.3595	7.1794	3.0655	1.4538	1.2705	0.7381
	0.94	9.8185	5.5712	2.8752	1.5658	1.0420	0.5421	11.4044	6.2324	3.0271	1.4238	1.1165	0.6214
	0.96	9.1192	4.7899	2.5699	1.4893	0.7175	NC	10.4492	6.1082	2.9887	1.3938	NC	NC
	0.98	8.9655	4.2149	2.4655	1.3863	NC	NC	9.8499	5.6347	2.8618	1.5010	NC	NC
	0.99	8.8915	3.9398	2.3610	1.2833	NC	NC	8.9506	5.0370	2.7349	1.6081	NC	NC

C_D (n = 0.4)

Pr	ϕ_f	Ri = 1						Ri = 2					
		Re →1	2	5	10	20	40	1	2	5	10	20	40
1	0.70	125.2317	68.7972	30.5826	18.7198	11.2768	7.3034	139.5918	73.7378	34.9579	19.6754	12.3594	8.0199
	0.75	78.5272	41.4585	23.2126	13.3821	10.1945	5.8564	86.7893	49.1280	25.9086	15.0516	10.3158	6.8610
	0.80	52.8040	31.6068	16.6182	9.7528	7.8034	4.5908	60.5033	34.8755	19.3239	12.3100	8.2653	4.9528
	0.84	45.0384	26.3847	13.0621	8.3372	5.6359	3.7450	50.9546	28.0534	15.7833	10.4391	5.8060	4.3309
	0.86	37.1622	21.8693	11.3674	7.4627	5.1772	3.2336	42.0064	23.9638	14.2857	9.1579	5.4458	3.9426
	0.88	30.8320	18.3554	10.0535	6.7321	4.1953	3.0960	33.2956	20.2140	13.4655	7.4536	4.2562	3.4151
	0.90	24.5017	14.8413	9.4576	6.3261	3.9207	3.0007	28.5847	18.4640	11.5670	6.5735	3.9367	3.1791
	0.92	22.1661	13.8363	8.0792	5.6534	3.5767	2.8460	25.7696	15.9934	10.4487	5.8970	3.6331	2.8338
	0.94	21.0693	12.5598	7.6774	5.2080	3.1312	2.4306	23.2833	15.2067	8.9397	5.5108	3.1841	2.6352
	0.96	20.6092	11.9654	7.2095	4.3190	2.6643	2.3945	21.7270	13.8746	8.3575	5.3992	2.9713	2.5132
	0.98	18.8759	10.7772	6.7125	4.1779	2.3981	2.3516	19.4441	13.6063	7.9441	4.8285	2.6931	2.4856
	0.99	16.5374	10.0904	6.0961	3.9238	2.3051	2.2051	17.3843	12.7342	7.4698	4.1660	2.1054	2.4153
10	0.70	130.1023	66.0266	32.5694	20.7462	11.8676	7.8945	145.1150	77.8102	36.0965	22.2037	13.9424	8.7849
	0.75	84.6866	50.0452	25.3955	14.5512	10.3018	6.0052	90.5461	46.1771	25.2346	16.8674	10.9771	7.2041
	0.80	55.5053	31.1212	15.3777	12.2318	7.8822	4.5087	65.6594	40.1903	20.2748	14.3451	8.7993	5.2005
	0.84	44.7915	26.9310	14.5168	10.3733	6.1573	3.8828	53.7591	34.2134	17.0422	11.9373	6.1766	4.5474
	0.86	39.3545	22.2100	13.1038	8.3423	5.5809	3.4410	47.0009	26.6378	16.2937	10.9235	5.7922	4.1398
	0.88	34.5508	19.4513	11.4808	7.5292	4.3782	3.1884	40.3028	22.3083	13.1093	9.2395	4.5367	3.5858
	0.90	29.7471	17.3506	10.0736	7.0865	4.1584	2.9801	33.6045	20.1041	10.7258	8.6858	4.1992	3.3380
	0.92	25.9209	15.3350	9.3932	6.6520	3.8222	2.8055	28.6236	18.5725	10.1279	7.7328	3.8794	2.9755
	0.94	23.8747	13.9110	8.3758	6.3410	3.3240	2.4407	27.7792	17.1870	9.4374	6.9770	3.4022	2.7669
	0.96	22.1053	12.7151	8.1562	5.9480	3.0134	2.3098	26.8300	16.4468	9.2123	6.8259	3.1751	2.6389
	0.98	20.6987	11.7088	7.6987	5.5231	2.7439	2.2181	24.3812	15.3914	8.4639	5.8978	2.8778	2.5514
	0.99	17.5539	10.5953	6.9958	4.5116	2.5138	2.4035	22.5318	13.8369	7.1280	4.6858	2.7546	2.5198
50	0.70	138.7531	71.0231	38.5627	22.6049	13.5588	8.4202	152.3305	83.7539	42.0296	23.6541	15.0166	9.2283
	0.75	91.0730	51.7392	25.5051	13.5878	10.6511	6.0239	99.8636	56.5250	27.8461	16.2984	11.1401	7.4400
	0.80	67.9703	35.1888	17.4278	10.7271	8.4788	4.9810	76.3260	41.4421	24.9215	14.4451	9.0286	5.6900
	0.84	45.6024	29.1567	16.4191	10.1211	6.3902	4.1814	64.6228	35.4535	19.1640	12.6109	6.0610	4.6496
	0.86	41.0422	23.5382	13.0317	8.9660	5.5887	3.6813	50.0787	27.3512	17.8466	11.4296	5.5656	4.2924
	0.88	35.8002	20.2026	12.0480	7.5320	5.2449	3.5575	42.7635	24.4197	15.8962	9.2958	5.1883	4.0452
	0.90	30.5582	17.8668	11.4557	6.9116	5.1406	3.4803	35.4481	21.7523	12.7378	8.3488	5.0552	3.7620
	0.92	29.5147	16.4316	11.0465	6.0747	4.9311	3.1820	33.0480	19.3616	10.5336	7.4171	4.9030	3.2435
	0.94	27.1680	15.4598	10.4512	5.5409	4.2879	2.7179	30.3042	18.1342	9.4789	6.7520	4.4242	2.9944
	0.96	25.8693	13.6466	8.2937	5.4001	3.7604	2.6047	27.5603	17.0900	9.4092	6.7220	3.8546	2.7418
	0.98	24.8426	11.4423	8.0538	4.7755	3.5148	2.5535	26.7996	15.4310	9.2509	6.2205	3.3015	2.6879
	0.99	24.2447	11.0378	7.8138	4.3014	3.1267	2.4838	25.2388	13.9477	8.2851	5.4209	3.0158	2.6145

Table D2: Dependence of pressure (C_{DP}), friction (C_{DF}) and total (C_D) drag coefficients on the fluid volume fraction (ϕ_f), Reynolds (Re), Prandtl (Pr) and Richardson (Ri) numbers for the power-law index of n = 0.6 (NC-results not converged possibly due to unsteadiness in the flow)

C_{DP} (n = 0.6)													
Pr	ϕ_f	Ri = 1						Ri = 2					
		Re→1	2	5	10	20	40	1	2	5	10	20	40
1	0.70	95.0724	49.8600	23.4960	15.2668	10.5716	6.1484	108.4204	57.3998	28.9872	18.3498	11.7675	7.6078
	0.75	62.6768	34.1838	17.3012	11.4270	7.4145	4.7124	68.0317	37.9020	19.6894	15.2948	10.1898	6.3549
	0.80	42.2041	23.2160	11.3335	8.3068	5.2778	3.8105	43.1164	32.4571	14.8976	10.0156	8.3081	5.0000
	0.84	29.5580	16.3644	9.2276	6.2445	4.1488	3.2562	30.7622	19.1250	11.5961	7.4103	6.8413	4.6461
	0.86	23.5627	13.2596	8.0124	5.6915	3.9842	3.1259	28.4512	14.9843	10.5236	6.0264	5.6987	3.9541
	0.88	19.7163	11.3082	6.8845	5.0815	2.9771	2.9772	24.5699	12.9831	8.9563	4.7967	4.3048	3.8253
	0.90	16.8698	9.3567	6.8681	4.8548	2.3478	2.7284	22.6885	11.1017	7.7535	4.7304	3.9109	3.5631
	0.92	14.5898	9.2568	6.1458	4.6780	2.1269	2.5992	16.8659	10.9818	7.3890	4.5213	3.7748	3.1721
	0.94	13.5630	9.0991	5.7238	4.6291	2.0198	2.4528	15.8330	10.6100	6.6554	4.4632	3.5147	3.1721
	0.96	12.5361	8.6804	5.4070	4.4273	1.8286	2.3171	14.6485	9.3104	5.5573	4.3121	2.9118	3.0933
	0.98	11.3579	7.6016	4.4025	4.1766	1.7544	2.1814	13.8321	9.0645	5.0423	4.1960	2.5525	NC
	0.99	10.8797	6.1041	3.3935	3.8581	NC	NC	13.4311	7.5190	4.5272	3.9567	NC	NC
10	0.70	98.4196	54.5488	24.6224	15.8538	10.8051	6.6982	110.5231	62.2424	29.6557	18.8407	12.0966	8.3686
	0.75	66.7765	37.1972	17.5103	12.2098	7.7239	5.5580	71.4390	39.5317	20.5395	16.0329	11.1069	6.9904
	0.80	47.9690	25.1707	12.3108	8.6216	6.3832	3.9524	45.5993	33.7065	15.9718	11.3102	9.0558	5.5112
	0.84	32.1668	19.1304	10.3699	7.4911	5.3444	3.9114	32.4487	23.8292	12.9014	8.2670	7.4575	5.1107
	0.86	26.3259	14.3923	9.1832	6.3475	4.8760	3.8090	29.3594	16.2583	12.0362	7.7312	6.2116	4.6495
	0.88	22.1841	13.1476	8.6824	5.8070	4.6018	3.4985	26.6558	14.9295	11.0522	7.6265	4.6922	4.0165
	0.90	18.0423	11.9028	7.5932	5.4134	4.0380	3.4377	23.9521	13.6008	9.7072	6.7526	4.2629	3.7413
	0.92	14.1915	10.4428	7.4690	5.0474	3.9666	3.1575	19.5824	12.8315	9.1298	6.2976	4.1523	3.3307
	0.94	13.9664	9.1812	7.0154	4.4793	3.7067	2.5336	17.3774	11.5861	7.2074	5.7740	3.8662	3.3307
	0.96	12.9817	8.1753	6.2556	4.2878	3.1572	2.3625	15.9233	10.7413	6.5130	5.2769	3.203	3.2479
	0.98	11.8692	7.1945	6.2204	4.1712	2.1053	2.2194	14.4208	10.1186	6.4694	4.9687	2.8078	NC
	0.99	10.7719	6.5077	4.8476	4.0545	NC	NC	13.2641	8.6511	5.4257	4.7797	NC	NC
50	0.70	101.3789	58.1366	25.9095	18.4738	11.1125	7.4350	115.4975	69.4954	31.2803	19.7827	13.7014	9.7870
	0.75	70.0496	39.0511	20.5880	13.3783	8.6585	6.8694	76.5772	52.7858	25.6724	16.8345	11.6622	7.3399
	0.80	49.0528	30.8292	14.5764	8.7405	7.1556	5.3872	59.0499	31.2814	15.9198	11.8757	9.5086	5.7868
	0.84	36.7870	21.6162	10.7322	8.5384	5.9911	4.7417	47.5497	24.0112	14.6738	8.6803	7.8304	5.3662
	0.86	32.2456	16.2574	10.4671	7.7184	5.4660	4.5228	37.9279	23.5850	12.7330	8.1178	6.5222	4.5670
	0.88	28.5531	15.0963	9.2135	6.5944	5.1586	3.8833	29.0257	18.8513	12.5894	8.0078	4.9268	3.4385
	0.90	22.8606	11.9351	8.5056	6.5921	4.5266	3.8158	26.5733	15.1794	10.8655	7.0902	4.4760	2.7117
	0.92	20.4032	10.6405	7.8621	5.5134	4.4466	3.5048	24.9262	13.6914	9.5981	6.6125	4.0913	2.6566
	0.94	18.2936	9.8925	7.7976	4.6458	4.1552	2.8122	21.8383	12.3499	7.0572	6.0627	3.6792	2.5484
	0.96	17.8214	8.8330	6.7808	4.4324	3.9876	2.6224	20.5147	11.9212	6.6068	5.5407	2.9892	2.1121
	0.98	16.2666	8.4590	6.0189	4.3472	3.7837	NC	18.8234	10.7208	6.5570	5.2171	2.4635	NC
	0.99	15.2396	7.0254	5.2570	4.0487	NC	NC	16.5032	9.5204	6.2567	5.0187	NC	NC
C_{DF} (n = 0.6)													
Pr	ϕ_f	Ri = 1						Ri = 2					
		Re→1	2	5	10	20	40	1	2	5	10	20	40
1	0.70	75.5052	38.4615	16.6068	10.4190	6.1436	3.8290	79.4662	41.1628	18.5704	11.3961	7.4638	3.8952
	0.75	50.1918	25.4930	11.8045	7.3545	4.5370	2.9058	50.7518	27.0945	12.7174	8.7382	5.3904	3.4036
	0.80	33.1554	17.4745	7.9762	5.1784	3.3871	2.2528	33.5282	25.5745	9.4786	5.9482	3.8148	2.7444
	0.84	22.9434	12.4999	6.8392	4.4324	3.0215	2.2081	22.7450	13.6914	7.3859	4.5455	3.6605	2.2929
	0.86	18.8259	11.3651	6.1560	4.0045	2.6470	1.8064	14.4850	13.3724	6.6068	4.4440	3.0112	2.1514
	0.88	15.4988	8.9454	5.9351	3.3389	2.2103	1.2241	13.8042	10.5788	5.7331	3.3973	2.7395	2.0050
	0.90	12.1716	6.5256	3.8938	2.6732	1.7735	0.6897	13.1234	7.4662	4.8594	2.7046	1.8622	1.7242
	0.92	10.8699	6.4720	3.6525	2.4003	1.7735	0.6418	12.6981	6.9365	4.0250	2.6571	1.8622	1.4739
	0.94	10.0779	6.3996	3.6416	2.1712	1.6844	0.6262	9.9846	6.1345	3.8129	2.6097	1.7686	1.3576
	0.96	9.4100	6.1569	3.6332	1.9422	1.5953	0.5628	7.7397	5.7552	3.6009	2.2490	1.6751	1.1909
	0.98	8.3480	6.1207	3.4255	1.7363	1.4455	0.5231	6.4948	5.5439	2.9232	1.9391	1.3078	NC
	0.99	7.8859	5.8418	3.2178	1.5303	NC	NC	5.7474	5.3326	2.2455	1.5685	NC	NC
10	0.70	77.5135	41.0117	17.2910	11.1794	6.8182	4.1903	80.3512	45.6058	21.3882	12.6070	7.5065	3.3253
	0.75	52.2722	29.0862	11.2125	7.9740	5.0477	3.5788	53.4588	34.1224	16.1798	9.6924	5.5759	2.8915
	0.80	31.8807	16.7722	9.3282	6.8426	4.9129	3.0544	35.0127	22.1075	10.9212	6.7378	4.2303	2.8590
	0.84	24.6050	12.8974	7.2518	5.8504	3.7201	2.1970	31.1070	17.3353	8.5581	6.5428	4.0386	2.2351
	0.86	20.5518	11.7564	6.0044	4.4964	2.8602	1.7282	24.0904	14.2368	7.3316	5.2636	3.3239	1.7532
	0.88	16.6918	9.5004	5.1994	3.6508	2.3155	1.1592	20.4970	11.9653	6.7701	5.0596	2.3921	1.7499
	0.90	14.8318	7.2444	4.3944	2.8052	1.7708	0.9562	16.9036	9.6939	5.5526	3.3814	1.8593	1.1040
	0.92	13.1382	7.0267	4.2384	2.5988	1.6159	0.7902	13.4437	8.4325	5.2086	3.1270	1.6967	0.8297
	0.94	12.4718	6.8985	3.9444	2.4040	1.4015	0.7528	12.6270	8.1782	4.8626	3.0659	1.4716	0.7904
	0.96	11.6302	5.8714	3.6805	2.2092	1.1872	0.7154	11.2212	7.3792	4.5828	3.0049	1.2466	0.7512
	0.98	10.7976	5.8073	3.5335	1.8306	1.0615	0.5334	10.8129	7.2521	4.3777	2.3288	1.1145	NC
	0.99	9.1222	4.7161	3.6226	1.7452	NC	NC	9.9987	6.3260	3.1726	1.6527	NC	NC

Table D2 (Contd.)

Pr	ϕ_f	Ri = 1						Ri = 2					
		Re→1	2	5	10	20	40	1	2	5	10	20	40
50	0.70	80.3789	44.1366	23.9095	11.3783	10.0976	5.7770	83.9794	47.9480	21.1500	13.2374	7.8818	4.0415
	0.75	53.8005	28.3904	13.0488	8.5654	5.4604	2.9099	56.1188	32.9109	16.7642	10.1770	5.8547	2.9508
	0.80	37.9270	20.5003	9.6925	6.9435	3.6485	2.0149	41.1698	21.9098	11.2292	7.0747	4.4418	2.7207
	0.84	26.1470	15.3218	8.7976	5.5494	2.9615	2.0146	34.4065	17.6628	9.0632	6.8699	4.2405	2.3698
	0.86	22.6915	13.9351	7.3014	4.7765	2.9415	1.8670	26.6225	14.8645	8.1577	5.5268	3.4901	1.7884
	0.88	20.7761	11.1945	7.0352	4.6045	2.8998	1.7190	20.8410	12.3565	7.4479	5.3126	2.5117	1.1259
	0.90	18.8606	9.4539	5.7808	3.8874	2.7390	1.5983	18.0075	10.8485	6.7380	3.5505	1.9523	1.0928
	0.92	15.5987	7.2425	5.5529	3.4324	2.2558	1.5739	14.3924	9.2292	5.6738	3.2834	1.7815	1.0528
	0.94	13.2197	6.7767	4.4951	2.8723	1.8665	0.8130	12.7130	8.7202	5.2868	3.2192	1.5452	0.9385
	0.96	12.0166	6.1525	4.4281	2.4168	1.4772	0.7726	12.0360	7.7797	4.8455	3.1551	1.3089	0.8243
	0.98	11.2157	5.3675	3.3927	2.3122	1.1124	NC	9.9542	6.8757	4.4042	2.4452	1.1702	NC
	0.99	10.4344	5.0625	3.3032	2.1145	NC	NC	9.6795	5.8392	3.6388	1.7353	NC	NC

C_D (n = 0.6)

Pr	ϕ_f	Ri = 1						Ri = 2					
		Re→1	2	5	10	20	40	1	2	5	10	20	40
1	0.70	170.5776	88.3215	40.1028	25.6858	16.7152	9.9774	187.8866	98.5626	47.5576	29.7459	19.2313	11.5030
	0.75	112.8686	59.6768	29.1057	18.7815	11.9515	7.6182	118.7835	64.9965	32.4068	24.0330	15.5802	9.7585
	0.80	75.3595	40.6905	19.3097	13.4852	8.6649	6.0633	76.6446	58.0316	24.3762	15.9638	12.1229	7.7444
	0.84	52.5014	28.8643	16.0668	10.6769	7.1703	5.4643	53.5072	32.8164	18.9820	11.9558	10.5018	6.9390
	0.86	42.3886	24.6247	14.1684	9.6960	6.6312	4.9323	42.9362	28.3567	17.1304	10.4704	8.7099	6.1055
	0.88	35.2150	20.2535	12.8196	8.4204	5.1874	4.2013	38.3741	23.5619	14.6894	8.1939	7.0443	5.8303
	0.90	29.0414	15.8823	10.7619	7.5280	4.1213	3.4181	35.8119	18.5679	12.6129	7.4350	5.7731	5.2873
	0.92	25.4597	15.7288	9.7983	7.0783	3.9004	3.2410	29.5640	17.9183	11.4140	7.1784	5.6370	4.6460
	0.94	23.6409	15.4987	9.3654	6.8003	3.7042	3.0790	25.8176	16.7445	10.4683	7.0729	5.2833	4.5297
	0.96	21.9461	14.8373	9.0402	6.3695	3.4239	2.8799	22.3882	15.0656	9.1582	6.5611	4.5869	3.2439
	0.98	19.7059	13.7223	7.8280	5.9129	3.1999	2.7045	20.3269	14.6084	7.9655	6.1351	3.8603	3.0645
	0.99	18.7656	11.9459	6.6113	5.3884	3.1245	2.6128	19.1785	12.8516	6.7727	5.5252	3.3529	2.9145
10	0.70	175.9331	95.5605	41.9134	27.0332	17.6233	10.8885	190.8743	107.8482	51.0439	31.4477	19.6031	11.6939
	0.75	119.0487	66.2834	28.7228	20.1838	12.7716	9.1368	124.8978	73.6541	36.7193	25.7253	16.6828	9.8819
	0.80	79.8497	41.9429	21.6390	15.4642	11.2961	7.0068	80.6120	55.8140	26.8930	18.0480	13.2861	8.3702
	0.84	56.7718	32.0278	17.6217	13.3415	9.0645	6.1084	63.5557	41.1645	21.4595	14.8098	11.4961	7.3458
	0.86	46.8777	26.1487	15.1876	10.8439	7.7362	5.5372	53.4498	30.4951	19.3678	12.9948	9.5355	6.4027
	0.88	38.8759	22.6480	13.8818	9.4578	6.9173	4.6577	47.1528	26.8948	17.8223	12.6861	7.0843	5.7664
	0.90	32.8741	19.1472	11.9876	8.2186	5.8088	4.3939	40.8557	23.2947	15.2598	10.1340	6.1222	4.8453
	0.92	27.3297	17.4695	11.7074	7.6462	5.5825	3.9477	33.0261	21.2640	14.3384	9.4246	5.8490	4.1604
	0.94	26.4382	16.0797	10.9598	6.8833	5.1082	3.2864	30.0044	19.7643	12.0700	8.8399	5.3378	4.1211
	0.96	24.6119	14.0467	9.9361	6.4970	4.3444	3.0779	27.1445	18.1205	11.0958	8.2818	4.4496	3.9991
	0.98	22.6668	13.0018	9.7539	6.0018	3.2668	2.7528	25.2336	17.3707	10.8471	7.2975	3.9223	3.1542
	0.99	19.8941	11.2238	8.4702	5.7997	3.1807	2.6434	23.2628	14.9771	8.5983	6.4324	3.4155	2.9824
50	0.70	181.7578	102.2732	49.8190	29.8521	21.2101	13.2120	199.4769	117.4434	52.4303	33.0201	21.5832	13.8285
	0.75	123.8501	67.4415	33.6368	21.9437	14.1189	9.7793	132.6960	85.6967	42.4366	27.0115	17.5169	10.2907
	0.80	86.9798	51.3295	24.2689	15.6840	10.8041	7.4021	100.2197	53.1912	27.1490	18.9504	13.9504	8.5075
	0.84	62.9340	36.9380	19.5298	14.0878	8.9526	6.7563	81.9562	41.6740	23.7370	15.5502	12.0709	7.7360
	0.86	54.9371	30.1925	17.7685	12.4949	8.4075	6.3898	64.5504	38.4495	20.8907	13.6446	10.0123	6.3554
	0.88	49.3292	26.2908	16.2487	11.1989	8.0584	5.6023	49.8667	31.2078	20.0373	13.3204	7.4385	4.5644
	0.90	41.7212	21.3890	14.2864	10.4795	7.2656	5.4141	44.5808	26.0279	17.6035	10.6407	6.4283	3.8045
	0.92	36.0019	17.8830	13.4150	8.9458	6.7024	5.0787	39.3186	22.9206	15.2719	9.8959	5.8728	3.7094
	0.94	31.5133	16.6692	12.2927	7.5181	6.0217	3.6252	34.5513	21.0701	12.3440	9.2819	5.2244	3.4869
	0.96	29.8380	14.9855	11.2089	6.8492	5.4648	3.3950	32.5507	19.7009	11.4523	8.6958	4.2981	3.4129
	0.98	27.4823	13.8265	9.4116	6.6594	4.8961	2.8305	28.7776	17.5965	10.9612	7.6623	3.6337	3.3119
	0.99	25.6740	12.0879	8.5602	6.1632	4.1528	2.7546	26.1827	15.3596	9.8955	6.7540	3.4813	3.1415

Table D3: Dependence of pressure (C_{DP}), friction (C_{DF}) and total (C_D) drag coefficients on the fluid volume fraction (ϕ_f), Reynolds (Re), Prandtl (Pr) and Richardson (Ri) numbers for the power-law index of n = 0.8 (NC-results not converged possibly due to unsteadiness in the flow)

C_{DP} (n = 0.8)													
Pr	ϕ_f	Ri = 1						Ri = 2					
		Re→1	2	5	10	20	40	1	2	5	10	20	40
1	0.70	118.8887	61.7618	28.1522	17.7324	12.4590	7.9581	122.9529	65.9728	32.9248	22.7191	15.0756	9.4716
	0.75	75.9348	40.0039	19.2030	12.8123	8.8834	5.7474	79.5292	43.7255	23.4607	16.5148	10.5512	7.2796
	0.80	47.9470	25.9790	13.1860	9.1092	6.2155	4.4142	51.0995	29.2666	16.8303	12.8032	9.1840	5.8312
	0.84	32.1150	17.9225	9.7772	6.9912	5.1868	3.7626	34.5796	21.0080	12.8158	9.7414	7.5412	4.1409
	0.86	26.7911	14.9023	8.6248	6.3475	4.8760	3.4985	28.3594	16.2583	11.0522	9.2670	6.7869	4.0018
	0.88	21.7664	12.6416	7.3198	5.3458	4.7063	3.4968	24.5603	14.3850	9.9556	8.7854	5.9670	3.4084
	0.90	18.7416	10.3808	7.1563	5.2475	4.2258	3.4339	20.7611	14.3333	9.5309	7.1694	5.1443	3.2151
	0.92	15.5314	9.8432	6.4494	5.0385	4.2026	3.2364	18.4164	12.7043	8.3976	6.5152	4.7343	3.0231
	0.94	14.6471	9.3786	6.0148	4.5475	3.8752	2.9760	16.6490	12.4083	8.0095	5.7307	4.3898	2.8512
	0.96	13.6262	8.7253	5.4425	4.4638	3.7418	2.7493	16.1095	11.0236	7.1068	5.4866	4.3243	2.3554
	0.98	12.1840	7.9665	5.3644	4.3158	3.5477	2.7170	15.4955	10.7812	6.9732	5.3330	3.2704	2.1016
	0.99	11.7209	7.4073	4.9862	4.0841	NC	NC	14.8815	10.5388	5.8395	4.9353	NC	NC
10	0.70	121.4910	65.9998	33.1318	21.1260	13.2244	8.1019	128.4055	74.0232	40.2723	24.5506	15.1210	10.4188
	0.75	79.0140	43.9646	22.9575	14.7920	9.3360	5.9695	84.3154	50.8121	28.0632	16.8092	10.2144	8.0076
	0.80	50.5903	29.1194	15.8018	10.2954	7.1975	5.9616	55.6427	34.7915	19.1294	11.9818	9.1398	6.4143
	0.84	34.6480	20.7182	11.5082	9.6312	6.7165	4.9565	41.1540	26.9399	15.3047	10.8012	7.6736	4.555
	0.86	28.2456	16.2574	10.2135	7.7184	6.0459	4.5067	33.2790	20.0112	12.5894	9.4129	6.8708	4.4021
	0.88	23.8987	14.0069	9.3886	7.4020	5.2258	3.9514	28.1847	17.4174	11.4530	8.2635	5.9520	3.7492
	0.90	19.5518	11.7564	9.3281	6.8426	4.9129	3.5788	23.0904	14.8236	10.484	7.9737	5.6303	3.5366
	0.92	15.6286	10.5940	9.2674	5.9483	4.8943	3.2247	20.6520	13.5634	9.2373	6.8782	4.8967	3.3254
	0.94	14.6843	10.0653	8.5723	5.1728	4.2620	3.0774	19.2845	12.7811	8.8105	6.1567	4.4666	3.1363
	0.96	14.2772	9.9913	7.7605	5.0539	4.1504	2.9301	19.1844	12.7628	7.8175	6.0282	4.4142	3.0115
	0.98	14.0086	9.7270	6.9311	4.8693	3.6110	2.5336	18.5006	12.3808	7.4437	5.7198	4.3618	2.9218
	0.99	13.7399	9.3886	5.1324	4.1659	NC	NC	17.7167	11.9988	7.3611	4.1828	NC	NC
50	0.70	124.4021	69.3558	34.7160	21.6544	13.4690	8.6582	136.9560	80.1064	41.9346	25.0250	16.0331	11.5589
	0.75	82.0672	46.3122	23.9244	15.1299	9.5307	6.3874	90.7915	54.8534	29.8217	17.2324	10.2411	8.8842
	0.80	51.8303	30.6065	16.3510	11.0161	7.7733	6.3789	59.9937	37.2056	19.7107	12.6590	7.0855	7.0614
	0.84	36.6590	21.6620	12.1388	10.3054	7.2538	5.3035	42.5017	31.1966	16.0280	11.4338	6.8098	6.2534
	0.86	30.2215	17.3361	10.9284	8.2587	6.5296	4.8222	34.2651	27.4576	15.0874	9.1332	6.1660	5.8469
	0.88	25.2546	15.8402	10.0458	7.9201	5.6439	4.2280	29.0670	21.5050	13.9826	8.1769	5.9221	4.7548
	0.90	20.2878	13.3442	9.9811	7.3216	5.3059	3.8293	23.8688	15.9437	11.4090	7.9686	5.3942	4.5113
	0.92	16.5006	11.9794	9.9161	6.3646	5.2858	3.4504	23.1495	15.5524	11.1824	7.7937	5.2878	4.2678
	0.94	15.5048	10.5056	9.1724	5.5349	4.6029	3.2928	20.9817	14.1496	8.3822	7.5188	4.8743	3.6261
	0.96	15.4198	10.2502	8.3037	5.4077	4.4824	3.1352	20.5654	13.3915	7.7305	6.8686	4.8662	3.2899
	0.98	14.9644	10.1681	7.4163	5.2102	3.8999	NC	19.6897	12.8735	7.5116	5.8905	4.4965	NC
	0.99	14.5091	10.0306	5.4971	4.5421	NC	NC	18.8139	11.3540	7.2926	4.9584	NC	NC
C_{DF} (n = 0.8)													
Pr	ϕ_f	Ri = 1						Ri = 2					
		Re→1	2	5	10	20	40	1	2	5	10	20	40
1	0.70	105.2510	53.4154	22.6924	12.9412	8.3014	5.5874	106.4659	54.7895	24.4209	14.9786	9.6922	6.3108
	0.75	67.8338	34.6808	15.3012	9.2354	6.1275	4.2108	69.1062	36.0520	17.0766	10.9633	7.1250	4.9764
	0.80	42.9122	22.4154	10.3664	6.5944	4.5262	3.2299	44.2294	23.8031	12.1192	8.1018	5.2974	4.0698
	0.84	28.6298	15.3299	8.5723	5.9483	4.2620	3.0774	29.2072	17.4174	10.4530	6.9164	4.4142	3.1744
	0.86	23.8987	14.0069	7.6188	5.1572	3.6506	2.6328	28.1847	16.9174	9.2792	6.2972	4.2856	3.1128
	0.88	19.3636	9.4287	6.6636	4.6996	3.3823	2.4390	22.7091	13.6557	8.2736	5.5679	3.7663	2.8562
	0.90	14.8284	7.9044	4.9395	3.6282	2.5028	1.8005	17.2334	11.7754	6.7601	5.3183	3.6491	2.4429
	0.92	11.2777	7.3450	4.7655	3.4511	2.3785	1.1999	15.9496	10.4369	6.0942	5.0791	3.6360	2.1943
	0.94	11.1584	7.0293	4.7548	3.4237	2.3709	0.9864	14.2752	9.8940	6.0465	4.5903	3.2837	1.8756
	0.96	10.7674	6.9074	4.5915	3.2192	2.3201	0.9721	13.5238	9.0984	5.5041	3.7565	3.1183	1.5422
	0.98	10.7077	6.7855	3.9839	3.1918	2.2617	0.7443	13.0623	8.5401	5.4185	3.2802	2.9182	1.1267
	0.99	10.2570	4.8505	3.3762	3.1644	NC	NC	12.6007	7.9818	5.3328	2.7731	NC	NC
10	0.70	106.8300	55.9448	25.6720	15.3190	9.5254	6.1943	109.9412	59.6856	29.5254	18.1312	11.2047	7.0729
	0.75	69.9118	37.2001	17.6958	10.8314	6.9544	4.5859	72.1858	40.6414	20.8392	12.9415	8.1438	5.2120
	0.80	44.7909	24.5025	12.1834	7.7158	5.1454	3.3822	47.4326	27.6864	14.5368	9.0852	5.5282	3.8228
	0.84	30.5184	17.2877	8.9028	5.9014	3.9880	3.1112	34.4446	22.6984	12.1574	7.7818	5.4687	3.3014
	0.86	26.8095	15.1758	7.8603	5.2369	3.3282	2.5520	29.5030	16.9644	9.6645	7.0229	4.6046	3.1311
	0.88	22.6692	12.4539	6.8529	4.5777	2.9418	2.1492	24.4122	14.4865	8.2158	6.1394	4.3542	2.9547
	0.90	17.5288	9.7320	6.7619	4.4397	2.5621	1.7464	19.3214	12.0085	6.7670	5.4970	3.2430	2.4435
	0.92	13.5570	8.4925	6.3864	3.9374	2.5553	1.1108	17.6496	10.4966	5.9788	4.7234	3.2397	2.1229
	0.94	12.6722	8.3304	6.1332	3.9184	2.4208	1.0280	16.3362	10.2778	5.8783	4.3099	3.2144	1.9245
	0.96	12.3698	8.1764	5.8455	3.4778	2.2795	1.0004	16.1085	10.0590	5.7777	3.9964	3.1858	1.2574
	0.98	12.0786	8.0954	5.5045	3.4564	2.2056	0.9452	15.5656	9.6306	5.0993	3.2776	1.9431	0.4128
	0.99	11.7874	7.8603	4.9125	3.4350	NC	NC	15.0227	8.2022	4.4209	2.8318	NC	NC

Table D3 (Contd.)

Pr	ϕ_f	Ri = 1						Ri = 2					
		Re→1	2	5	10	20	40	1	2	5	10	20	40
50	0.70	107.8395	57.5886	26.5255	15.6392	9.7020	6.2258	114.5890	63.0170	30.7556	18.6554	11.3744	7.8934
	0.75	71.4356	38.3882	18.2221	11.0382	7.0889	4.5527	75.8422	42.9965	22.3778	13.3171	8.4456	5.8166
	0.80	45.1110	25.2625	12.4820	7.8968	5.2042	3.2226	49.9007	29.1738	15.2018	9.2748	5.6916	4.2662
	0.84	31.7176	17.7564	9.3099	6.0190	3.9920	2.4319	35.8325	24.4675	12.6500	8.6530	5.5299	3.6844
	0.86	27.9095	15.0758	7.8776	5.9622	3.0288	2.1492	30.7503	16.4144	10.2531	8.1206	4.6587	3.4943
	0.88	22.6692	12.4539	6.8529	4.5777	2.9418	2.1112	24.4122	14.4865	8.7408	6.1394	4.4042	3.2974
	0.90	17.5580	10.0807	6.3864	3.9374	2.4208	1.5138	19.6684	12.5540	8.2158	4.5768	3.9958	2.7269
	0.92	14.0798	8.9860	6.1332	3.9292	2.2174	1.1589	19.4497	12.0914	6.7435	4.1102	3.3053	2.3692
	0.94	13.2030	8.3213	6.0432	3.6618	2.2056	1.0280	16.9948	10.9725	5.8783	4.1099	3.2347	2.1477
	0.96	12.6722	8.2186	5.7124	3.4564	2.1667	1.0004	16.3362	10.2778	5.8520	3.6318	3.2168	1.4033
	0.98	12.3300	8.1764	5.1583	3.4252	2.0020	NC	15.8854	10.2046	5.8354	3.2776	2.1531	NC
	0.99	12.0786	8.0954	5.0226	3.3289	NC	NC	15.5656	9.6306	5.0993	2.6340	NC	NC

C_D (n = 0.8)

Pr	ϕ_f	Ri = 1						Ri = 2					
		Re→1	2	5	10	20	40	1	2	5	10	20	40
1	0.70	224.1397	115.1772	50.8446	30.6736	20.7604	13.5455	229.4188	120.7623	57.3457	37.6977	24.7678	15.7824
	0.75	143.7686	74.6847	34.5042	22.0477	15.0109	9.9582	148.6354	79.7775	40.5373	27.4781	17.6762	12.2560
	0.80	90.8592	48.3944	23.5524	15.7036	10.7417	7.6441	95.3289	53.0697	28.9495	20.9050	14.4814	9.9010
	0.84	60.7448	33.2524	18.3495	12.9395	9.4488	6.8400	63.7868	38.4254	23.2688	16.6578	11.9554	7.3153
	0.86	50.6898	28.9092	16.2436	11.5047	8.5266	6.1313	56.5441	33.1757	20.3314	15.5642	11.0725	7.1146
	0.88	41.1299	22.0703	13.9834	10.0454	8.0886	5.9358	47.2693	28.0407	18.2292	14.3533	9.7333	6.2646
	0.90	33.5700	18.2852	12.0958	8.8757	6.7286	5.2344	37.9945	26.1087	16.2910	12.4877	8.7934	5.6580
	0.92	26.8091	17.1882	11.2149	8.4896	6.5811	4.4363	34.3660	23.1412	14.4918	11.5943	8.3703	5.2174
	0.94	25.8055	16.4079	10.7696	7.9712	6.2460	3.9624	30.9241	22.3023	14.0560	10.3210	7.6735	4.7268
	0.96	24.3935	15.6327	10.0340	7.6830	6.0619	3.7214	29.6333	20.1220	12.6109	9.2431	7.4426	4.1439
	0.98	22.8917	14.7520	9.3482	7.5076	5.8094	3.4613	28.5578	19.3213	12.3916	8.6132	6.1886	3.2283
	0.99	21.9779	12.2578	8.3624	7.2485	4.3551	2.9551	27.4822	18.5206	11.1723	7.7084	5.2536	3.1142
10	0.70	228.3210	121.9446	58.8038	36.4450	22.7498	14.2962	238.3467	133.7088	69.7977	42.6818	26.3257	17.4917
	0.75	148.9258	81.1647	40.6533	25.6234	16.2904	10.5554	156.5012	91.4535	48.9024	29.7507	18.3582	13.2196
	0.80	95.3812	53.6219	27.9852	18.0112	12.3429	9.3438	103.0753	62.4779	33.6662	21.0670	14.6680	10.2371
	0.84	65.1664	38.0059	20.4110	15.5326	10.7045	8.0677	75.5986	49.6383	27.4621	18.5830	13.1423	7.8564
	0.86	55.0551	31.4332	18.0738	12.9553	9.3741	7.0587	62.7820	36.9756	22.2539	16.4358	11.4754	7.5331
	0.88	46.5679	26.4608	16.2415	11.9797	8.1676	6.1006	52.5969	31.9039	19.6687	14.4029	10.3062	6.7039
	0.90	37.0806	21.4884	16.0900	11.2823	7.4750	5.3252	42.4118	26.8321	17.2509	13.4707	8.8733	6.7701
	0.92	29.1856	19.0865	15.6538	9.8856	7.4496	4.3355	38.3016	24.0600	15.2161	11.6016	8.1364	5.4483
	0.94	27.3565	18.3957	14.7055	9.0912	6.6828	4.1054	35.6207	23.0589	14.6888	10.4666	7.6810	5.0608
	0.96	26.6470	18.1677	13.6060	8.5317	6.4299	3.9305	35.2929	22.8218	13.5952	10.0246	7.6000	4.2689
	0.98	26.0872	17.8223	12.4356	8.3257	5.8166	3.6024	34.0662	22.0114	12.5430	8.9974	6.3049	3.3346
	0.99	25.5273	17.2489	10.0449	7.6009	4.6856	3.0112	32.7394	20.2010	11.7820	7.0146	5.9125	3.1526
50	0.70	232.2416	126.9444	61.2415	37.2936	23.1710	14.8840	251.5450	143.1234	72.6902	43.6804	27.4075	19.4523
	0.75	153.5028	84.7004	42.1465	26.1681	16.6196	10.9401	166.6337	97.8499	52.1995	30.5495	18.6867	14.7008
	0.80	96.9413	55.8690	28.8330	18.9129	12.9775	9.6015	109.8944	66.3794	34.9125	21.9338	12.7771	11.3276
	0.84	68.3766	39.4184	21.4487	16.3244	11.2458	7.7354	78.3342	55.6641	28.6780	20.0868	12.3397	9.9378
	0.86	58.1310	32.4119	18.8060	14.2209	9.5584	6.9714	65.0154	43.8720	25.3405	17.2538	10.8247	9.3412
	0.88	47.9238	28.2941	16.8987	12.4978	8.5857	6.3392	53.4792	35.9915	22.7234	14.3163	10.3263	8.0522
	0.90	37.8458	23.4249	16.3675	11.2590	7.7267	5.3431	43.5372	28.4977	19.6247	12.5454	9.3900	7.2382
	0.92	30.5804	20.9654	16.0493	10.2938	7.5032	4.6093	42.5992	27.6438	17.9259	11.9039	8.5931	6.6370
	0.94	28.7078	18.8269	15.2156	9.1967	6.8085	4.3208	37.9765	25.1221	14.2605	11.6287	8.1090	5.7738
	0.96	28.0920	18.4688	14.0161	8.8641	6.6491	4.1356	36.9016	23.6693	13.5825	10.5004	8.0830	5.3129
	0.98	27.2944	18.3445	12.5746	8.6354	5.9019	3.8566	35.5751	23.0781	13.3470	9.1681	6.6496	4.0522
	0.99	26.5877	18.1260	10.5197	7.8710	4.7225	3.2018	34.3795	20.9846	12.3919	7.5924	6.1241	3.3569

Table D4: Dependence of pressure (C_{DP}), friction (C_{DF}) and total (C_D) drag coefficients on the fluid volume fraction (ϕ_f), Reynolds (Re), Prandtl (Pr) and Richardson (Ri) numbers for the power-law index of n = 1.4

C_{DP} (n = 1.4)													
Pr	ϕ_f	Ri = 1						Ri = 2					
		Re→1	2	5	10	20	40	1	2	5	10	20	40
1	0.70	242.973	123.6595	52.6738	29.9175	19.2694	13.6061	246.7329	127.5285	57.2654	35.3555	24.6619	17.3011
	0.75	133.2575	68.6748	30.4922	18.5425	12.9125	9.6148	136.5896	72.1624	34.7224	23.3974	17.2030	12.4124
	0.80	72.1900	37.8904	17.9788	11.9401	8.9536	6.9624	75.0983	41.0438	21.8393	16.0844	12.2611	9.0638
	0.84	42.9121	23.2256	11.9198	8.5989	7.8820	5.4166	45.6638	26.1146	15.4790	12.1842	10.9132	7.1879
	0.86	36.2548	18.2456	10.2645	7.4869	6.8115	5.2795	39.5582	21.3574	12.3125	10.2587	9.3820	6.9046
	0.88	27.0853	16.3571	9.9052	7.3885	5.8594	4.5067	29.8974	17.2150	10.9574	10.2189	8.4561	6.8512
	0.90	23.9159	14.4686	8.5951	6.4561	5.7832	4.4867	26.2367	15.0726	10.1637	9.0592	8.0826	6.4997
	0.92	21.1252	12.8448	7.0317	6.0533	5.1625	3.8955	24.5348	14.9348	9.6024	8.2251	7.2482	6.0948
	0.94	19.0120	11.7591	6.5459	5.4365	4.8108	3.7168	22.9047	13.3296	9.0222	7.8597	6.3011	5.8491
	0.96	17.7945	11.3998	6.3748	5.4254	4.5418	3.6224	20.5571	12.6811	9.0041	7.1220	5.9932	4.9203
	0.98	16.2978	10.6908	5.9205	5.1414	4.4231	3.4420	20.4106	11.0092	8.8948	6.9481	5.5628	4.4599
	0.99	15.8901	10.1863	5.7884	4.9581	4.0928	3.2168	19.5944	10.9871	8.7595	6.9051	5.5412	4.2450
10	0.70	245.7450	127.3743	57.3844	33.8631	21.6220	14.8172	251.2515	134.7828	65.8922	41.6692	27.8485	18.9868
	0.75	135.7400	72.0600	34.2303	21.4039	14.5846	10.5543	141.2912	78.7656	41.3610	27.3610	19.4796	13.5304
	0.80	74.3875	40.7922	20.8016	13.9658	10.1899	7.6890	79.4533	46.6711	26.7549	19.1245	13.8190	9.6730
	0.84	45.2093	25.6772	14.1294	10.1872	7.9032	6.6067	49.6684	30.9408	19.2634	14.3353	10.5761	8.9712
	0.86	38.2694	20.3656	11.3845	9.6069	7.7480	6.0706	41.6782	23.4774	14.4325	12.3787	10.4236	7.3158
	0.88	30.7851	17.1653	9.9000	7.9730	6.4167	5.9557	32.6864	20.1339	13.1341	11.2850	9.0084	7.1204
	0.90	25.3009	13.9649	8.4310	7.3294	6.3765	5.1145	30.6947	16.7904	12.2215	10.6304	8.8042	6.7155
	0.92	21.5016	12.2676	8.4155	6.6174	5.1806	4.1992	27.5273	14.5648	11.8357	8.8821	7.3198	6.4847
	0.94	19.9377	11.8772	7.9693	6.3392	4.8498	3.9282	25.1681	14.5322	10.5021	7.8404	6.8631	5.9109
	0.96	18.5084	11.7677	7.7654	6.0011	4.5118	3.9118	23.9818	14.4138	10.2575	7.7412	6.1222	5.4669
	0.98	17.0119	10.9651	7.4540	5.8345	4.4161	3.7505	21.3864	14.3170	9.9196	7.5608	5.8846	5.3222
	0.99	16.9457	10.6199	7.4184	5.7332	4.386	3.6468	20.2871	13.4232	9.3562	7.4991	5.7005	4.8894
50	0.70	249.1978	130.3943	58.9099	34.4995	21.9608	14.991	258.7355	140.5376	68.3697	42.8854	28.5038	19.4244
	0.75	138.6408	74.1481	35.2341	21.936	14.8955	10.7406	146.9085	82.6624	43.1055	28.7758	20.0336	13.7862
	0.80	76.4681	42.2290	21.5229	14.4123	10.481	7.8746	83.4761	49.3109	28.0709	19.9247	14.2645	10.0922
	0.84	46.6701	26.7226	14.7842	10.7279	9.0242	7.7394	52.9192	39.8718	20.3981	15.0104	11.6971	9.7591
	0.86	39.3904	21.4866	12.5055	10.586	8.0564	7.7277	42.7992	34.5984	15.5535	13.4997	10.6647	7.2880
	0.88	30.0298	17.2975	10.5555	8.7625	7.2214	6.0857	34.1941	29.3627	14.0951	11.3286	10.0231	7.2805
	0.90	26.6692	13.1084	9.6054	7.9824	7.1481	5.8490	30.5891	25.1270	13.2372	10.1576	8.4728	7.1571
	0.92	24.3041	12.6353	8.9282	6.7972	5.2721	5.0819	28.2842	21.8554	12.6368	9.0332	8.0081	6.5994
	0.94	20.6462	11.9707	8.0877	6.5172	5.0884	5.0814	26.0074	18.8115	11.2152	8.9970	7.3696	6.0019
	0.96	19.4872	11.8406	8.0175	6.2355	4.7827	4.0081	23.1920	15.7912	10.7360	8.5604	6.4404	5.7245
	0.98	18.3450	10.7886	7.8456	6.2102	4.7395	3.9703	22.1460	15.2460	10.0195	7.8542	6.0808	5.5526
	0.99	17.5161	10.6512	7.6725	6.1693	4.5127	3.7595	21.7586	14.7858	9.8652	7.6552	5.8797	4.9835
C_{DF} (n = 1.4)													
Pr	ϕ_f	Ri = 1						Ri = 2					
		Re→1	2	5	10	20	40	1	2	5	10	20	40
1	0.70	269.6539	135.6860	55.7131	29.7384	17.4496	11.6266	270.9850	137.0398	57.6444	32.4522	20.8448	14.9310
	0.75	153.8682	77.9512	32.8198	18.4336	11.7823	8.5302	155.3009	79.4796	35.0045	21.3755	15.0580	11.2004
	0.80	85.6822	43.8599	19.3842	11.8407	8.3693	6.4117	87.1234	45.5704	21.8164	14.8838	11.2315	8.4044
	0.84	51.5308	26.9932	12.7767	8.5792	6.5058	5.0889	53.2242	28.8234	15.4236	11.5394	8.8339	6.7382
	0.86	42.1537	20.1526	10.2584	7.5214	6.2662	4.3462	44.2687	22.2676	12.3734	9.6434	8.7626	5.2458
	0.88	31.8136	16.1049	8.6407	6.9510	5.4565	4.1596	33.7801	18.2648	11.0557	9.6364	7.5715	5.2625
	0.90	21.4736	14.0572	8.0135	6.5153	5.0193	3.9035	28.2916	14.2621	10.6765	8.6682	7.0262	4.7179
	0.92	17.1005	13.1795	7.4791	5.9347	4.9492	3.6465	25.2338	14.1958	9.7381	8.0658	6.7038	4.1872
	0.94	16.0152	12.8886	7.0230	5.5366	4.4712	3.6402	23.2085	13.7945	9.4623	7.7001	5.9115	4.1794
	0.96	15.6464	11.6456	6.8163	5.5092	4.4420	3.3816	21.7698	12.8292	9.2184	7.1674	5.8362	4.1733
	0.98	14.7754	10.8262	6.6234	5.2398	4.2637	3.3092	20.4718	12.0552	9.2183	6.8832	5.6742	3.8717
	0.99	13.7691	9.7052	6.3430	5.0544	4.0104	2.6161	19.6150	12.0402	8.9348	6.8748	5.4220	3.0580
10	0.70	271.8534	138.3523	59.0644	32.7644	19.6571	12.9704	274.2866	142.2938	64.2448	38.3378	25.0038	17.2564
	0.75	155.9091	80.5656	35.7260	20.8652	13.4230	9.4387	159.0796	84.6694	40.6959	26.0082	17.9184	12.5109
	0.80	87.6258	46.3332	21.8051	13.7061	9.5172	7.0195	90.9984	50.4972	26.5794	18.2427	12.9846	9.0165
	0.84	53.7542	29.2064	14.7854	10.0335	7.6015	6.3046	57.0374	33.4144	19.2710	13.8220	9.8605	6.8355
	0.86	44.2987	25.2976	12.4034	9.6664	7.2976	5.4890	46.4137	24.4126	14.5184	11.7814	8.7165	5.3164
	0.88	33.7998	21.1313	10.4095	8.0028	6.2256	4.9635	36.6787	21.2281	13.2054	10.2071	7.6675	5.0932
	0.90	23.3009	18.9649	8.4310	7.3294	5.2254	3.9599	26.9438	18.0434	12.1376	9.9854	7.38245	5.0896
	0.92	16.0121	14.2676	8.4155	6.3392	5.1806	3.8955	22.0893	15.4944	11.8925	8.6328	6.5193	5.0860
	0.94	15.7945	13.4605	8.1072	6.1745	4.8498	3.7168	21.0283	15.3610	10.5540	7.5375	6.0484	5.0371
	0.96	15.4157	11.7677	7.7654	6.0011	4.6336	3.6242	20.9610	15.2960	10.2906	7.3342	5.9712	4.8282
	0.98	14.8568	10.9651	7.4540	5.8345	4.5118	3.6224	20.6258	15.1451	9.9941	7.2805	5.7289	4.6304
	0.99	14.2978	10.2603	7.1592	5.8166	4.4161	3.4421	20.2668	14.4324	9.4017	7.264	5.5894	4.4524

Table D4 (Contd.)

Pr	ϕ_f	Ri = 1						Ri = 2					
		Re→1	2	5	10	20	40	1	2	5	10	20	40
50	0.70	273.9433	140.2389	60.0818	33.2006	19.8939	13.0743	279.2325	146.1418	66.1994	39.3985	25.5265	17.556
	0.75	157.908	81.9504	36.4054	21.2372	13.6342	9.5654	163.042	87.4766	42.1125	26.798	18.3292	12.6804
	0.80	89.1482	47.3371	22.3113	14.0206	9.7224	7.9575	94.0544	52.5305	27.6412	18.8473	13.2979	9.0549
	0.84	54.8070	29.9504	15.2830	10.3178	8.5324	6.587	59.6807	34.9512	20.1631	14.3204	10.0033	6.9796
	0.86	45.8587	23.8576	13.9634	9.7825	7.1615	5.2566	47.9737	25.9726	16.0784	13.3414	9.2765	6.4545
	0.88	34.9631	19.1818	11.3927	8.2011	6.5638	4.1769	38.2500	22.5515	14.2861	11.0650	7.62005	6.1274
	0.90	24.0676	14.5060	8.8220	6.6198	5.9662	4.0954	33.5263	19.1305	12.9708	10.7887	6.9636	5.8956
	0.92	18.8416	12.3600	8.3680	6.3798	5.7196	3.9891	30.5851	16.5938	12.4938	9.6932	6.7125	5.3669
	0.94	17.3435	12.3524	8.1804	6.1250	5.2058	3.9142	26.5283	16.4292	11.0868	9.1615	6.3032	5.1667
	0.96	16.5682	12.0278	8.0644	6.0252	4.9602	3.8894	24.0923	16.4009	10.5935	8.2926	6.0926	4.9296
	0.98	15.7866	11.5440	7.9340	6.0138	4.7186	3.7632	21.8482	16.172	10.1144	7.6924	5.9728	4.5868
	0.99	15.2544	11.4616	7.8228	6.0101	4.5772	3.5527	21.5346	15.3758	10.0083	7.4692	5.8675	4.5565

C_D (n = 1.4)

Pr	ϕ_f	Ri = 1						Ri = 2					
		Re→1	2	5	10	20	40	1	2	5	10	20	40
1	0.70	512.6269	259.3455	108.3869	59.6559	36.7190	25.2327	517.7179	264.5683	114.9098	67.8077	45.5067	32.2321
	0.75	287.1257	146.6260	63.3120	36.9761	24.6948	18.1450	291.8905	151.6420	69.7269	44.7729	32.2610	23.6128
	0.80	157.8722	81.7503	37.3630	23.7808	17.3229	13.3741	162.2217	86.6142	43.6557	30.9682	23.4926	17.4682
	0.84	94.4429	50.2188	24.6965	17.1781	14.3878	10.5055	98.8880	54.9380	30.9026	23.7236	19.7471	13.9261
	0.86	78.4085	38.3982	20.5229	15.0083	13.0777	9.6257	83.8269	43.6250	24.6859	19.9021	18.1446	12.1504
	0.88	58.8990	32.4620	18.5459	14.3395	11.3159	8.6663	63.6776	35.4799	22.0132	19.8553	16.0276	12.1137
	0.90	45.3895	28.5258	16.6085	12.9715	10.8025	8.3898	54.5283	29.3347	20.8402	17.7275	15.1088	11.2176
	0.92	38.2257	26.0243	14.5107	11.9880	10.1118	7.5420	49.7686	29.1306	19.3405	16.2909	13.9521	10.2820
	0.94	35.0272	24.6477	13.5689	10.9731	9.2820	7.3570	46.1132	27.1241	18.4845	15.5598	12.2125	10.0285
	0.96	33.4409	23.0454	13.1911	10.9346	8.9838	7.0040	42.3269	25.5102	18.2224	14.2894	11.8294	9.0936
	0.98	31.0732	21.5170	12.5439	10.3812	8.6867	6.7512	40.8824	23.0644	18.1131	13.8312	11.2370	8.3316
	0.99	29.6591	19.8915	12.1314	10.0125	8.1032	5.8329	39.2094	23.0272	17.6943	13.7799	10.9632	7.3030
10	0.70	517.5984	265.7266	116.4488	66.6275	41.2791	27.7876	525.5381	277.0766	130.1370	80.0070	52.8523	36.2432
	0.75	291.6491	152.6256	69.9563	42.2691	28.0076	19.9930	300.3708	163.4350	82.0569	53.3692	37.3980	26.0413
	0.80	162.0133	87.1254	42.6067	27.6719	19.7071	14.7085	170.4517	97.1683	53.3343	37.3672	26.8036	18.6895
	0.84	98.9635	54.8836	28.9148	20.2207	15.5047	12.9113	106.7058	64.3552	38.5344	28.1573	20.4366	15.8067
	0.86	82.5681	45.6632	23.7879	19.2733	15.0456	11.5596	88.0919	47.8900	28.9509	24.1601	19.1401	12.6322
	0.88	64.5850	38.2966	20.3095	15.9759	12.6424	10.9192	69.3652	41.3619	26.3396	21.4921	16.6760	12.2136
	0.90	48.6018	32.9298	16.8620	14.6588	11.6019	9.0745	57.6385	34.8338	24.3591	20.6158	16.1867	11.8052
	0.92	37.5136	26.5352	16.8310	12.9566	10.3612	8.0948	49.6166	30.0592	23.7282	17.5149	13.8392	11.5708
	0.94	35.7322	25.3377	16.0765	12.5137	9.6996	7.6450	46.1964	29.8932	21.0560	15.3779	12.9115	10.9479
	0.96	33.9241	23.5354	15.5308	12.0022	9.1454	7.5360	44.9428	29.7098	20.5481	15.0754	12.0934	10.2951
	0.98	31.8687	21.9302	14.9080	11.6690	8.9279	7.3729	42.0122	29.4620	19.9136	14.8413	11.6135	9.9526
	0.99	31.2435	20.8802	14.5776	11.5498	8.8021	7.0888	40.5539	27.8556	18.7579	14.7630	11.2899	9.3418
50	0.70	523.1411	270.6332	118.9917	67.7001	41.8547	28.0653	537.9680	286.6794	134.5691	82.2839	54.0303	36.9804
	0.75	296.5488	156.0985	71.6395	43.1732	28.5297	20.3060	309.9505	170.1390	85.2175	55.5738	38.3628	26.4666
	0.80	165.6162	89.5661	43.8342	28.4329	20.2034	15.8321	177.5305	101.8414	55.7121	38.7720	27.5624	19.1471
	0.84	101.4771	56.6730	30.0672	21.0457	17.5566	14.3264	112.5997	74.8230	40.5610	29.3308	21.7004	16.7387
	0.86	85.2491	45.3442	26.4689	20.3685	15.2179	12.9843	90.7729	60.5710	31.6319	26.8411	19.9412	13.7425
	0.88	64.9930	36.4793	21.9482	16.9637	13.7853	10.2626	72.4442	51.9143	28.3813	22.3937	17.6432	13.4079
	0.90	50.7368	27.6144	18.4274	14.6022	13.1144	9.9444	64.1154	44.2575	26.2080	20.9463	15.4365	13.0527
	0.92	43.1457	24.9953	17.2962	13.1770	10.9917	9.0710	58.8692	38.4492	25.1306	18.7264	14.7207	11.9664
	0.94	37.9897	24.3231	16.2681	12.5422	10.2942	8.9956	52.5357	35.2407	22.3020	18.1585	13.6728	11.1686
	0.96	36.0554	23.8684	16.0819	12.2605	9.7429	7.8974	47.2843	32.1921	21.3295	16.8530	12.5331	10.6541
	0.98	34.1316	22.3326	15.7796	12.2240	9.4581	7.7335	43.9942	31.4180	20.1339	15.5466	12.0536	10.1394
	0.99	32.7705	22.1128	15.4953	12.1794	9.0899	7.3122	43.2932	30.1616	19.8735	15.1244	11.7472	9.5400

Table D5: Dependence of pressure (C_{DP}), friction (C_{DF}) and total (C_D) drag coefficients on the fluid volume fraction (ϕ_f), Reynolds (Re), Prandtl (Pr) and Richardson (Ri) numbers for the power-law index of n = 1.8

C_{DP} (n = 1.8)													
Pr	ϕ_f	Ri = 1						Ri = 2					
		Re→1	2	5	10	20	40	1	2	5	10	20	40
1	0.70	409.514	206.4924	85.6915	46.2554	27.4649	18.2363	412.2945	210.2921	90.1615	51.7221	33.6471	23.7631
	0.75	202.072	102.9064	44.0734	25.2843	16.4745	11.9945	205.6135	106.3368	48.2475	30.3345	21.7845	16.5634
	0.80	97.9808	50.7202	23.0419	14.5032	10.2936	8.4096	100.8199	53.8375	26.9109	19.0371	15.0232	11.9912
	0.84	53.2618	28.2452	13.9062	9.6785	7.7435	6.5158	55.8801	31.1564	17.5488	13.8443	11.5154	10.7862
	0.86	40.3425	25.3578	10.2642	8.4881	7.4745	5.4355	45.6652	24.3696	13.9553	10.8462	10.4431	9.2549
	0.88	29.6830	23.1868	9.5450	7.4418	6.8429	5.3400	33.4677	21.9953	12.0820	10.2661	9.1555	8.4728
	0.90	25.0234	20.0157	8.8953	6.6770	6.4050	5.0184	29.2702	19.6210	10.7204	9.9416	8.7710	6.2262
	0.92	23.6246	18.1100	7.3410	6.6395	5.9768	4.9254	27.8585	17.3711	10.4264	9.2758	8.3038	5.4174
	0.94	21.9814	16.7255	6.8258	5.9122	5.3355	4.6968	25.9804	15.6012	10.2087	9.0370	7.4522	5.3654
	0.96	19.9898	14.4342	6.5868	5.7909	5.1108	4.4154	23.4248	14.8312	10.1324	8.2855	7.0990	5.1738
	0.98	18.5513	12.4818	6.0128	5.5541	4.8618	4.1930	21.7836	13.1080	9.7846	8.2160	6.7383	4.8915
	0.99	17.1211	11.3411	5.8930	5.3001	4.7104	4.0567	20.9911	11.9372	9.3310	8.2104	6.7285	4.6176
10	0.70	411.0128	209.9234	90.0535	50.2064	30.0125	19.6183	416.6803	216.9906	98.5935	58.6857	37.7845	26.2628
	0.75	204.2072	106.0626	47.6698	28.2044	18.3082	13.1282	209.5072	112.5970	55.0559	35.4330	24.9554	18.5552
	0.80	100.0518	53.4868	25.8304	16.6102	11.9527	9.3267	104.9587	59.2962	32.1882	22.8366	17.4397	13.3839
	0.84	55.2526	30.6701	16.1699	11.4017	8.9629	7.5555	59.8066	35.8926	21.8276	16.8336	13.3502	10.3464
	0.86	42.4625	25.4778	12.3842	9.6081	8.9045	7.1795	47.7852	26.4896	16.0753	12.9662	11.2755	10.0284
	0.88	35.6173	23.2070	10.4392	8.2995	8.5321	5.8936	36.2804	21.9763	14.6018	11.8863	11.0139	8.2863
	0.90	30.7721	20.9361	8.6812	7.6292	7.4423	4.8071	34.7757	17.4630	13.1283	10.8064	9.8370	8.2264
	0.92	25.5105	18.7698	8.4942	7.2552	7.0626	4.5666	31.1011	15.5667	11.9608	9.6154	8.6229	7.1992
	0.94	23.3828	16.7608	8.3986	6.9910	5.9218	4.4128	28.6628	15.1889	11.7705	9.3920	8.3985	6.1721
	0.96	20.0987	14.8292	8.1160	6.8812	5.5932	4.3720	25.1793	15.0494	11.6758	9.2435	7.3262	6.1594
	0.98	19.0792	12.7518	7.6064	6.6124	5.5174	4.3262	23.2575	14.9791	11.0083	9.0716	7.0158	5.8486
	0.99	18.8146	11.6386	7.5648	6.3944	5.3976	4.2318	21.1430	14.8110	10.2460	8.8997	6.8232	5.7290
50	0.70	414.4440	212.6355	91.2812	50.8668	30.3395	19.7771	423.5432	222.3190	101.4110	59.8884	38.4437	26.6318
	0.75	206.8540	108.0059	48.628	28.7276	18.6284	12.0165	214.7476	116.3200	56.7962	36.4527	25.6234	18.9978
	0.80	101.9810	54.8367	26.5401	17.0867	12.2844	9.5733	108.7558	61.8692	33.4954	23.7731	18.0859	13.7995
	0.84	56.7276	31.6380	16.7758	11.7662	10.0839	8.6765	62.6996	47.9148	23.0247	17.7093	13.9558	11.4674
	0.86	43.5835	26.5988	13.5052	10.7291	9.1719	7.5196	48.9062	37.6106	17.1963	14.0872	12.3965	10.4822
	0.88	32.6546	24.1245	11.2708	9.0846	8.1441	6.8325	37.7647	31.2705	15.6673	12.7729	11.5513	8.9716
	0.90	29.7256	22.6501	10.0364	8.5942	7.7575	4.9886	32.6232	28.9303	14.1382	11.4586	10.7061	8.2771
	0.92	26.3818	20.8118	9.8897	7.4401	7.4543	4.7657	30.4504	25.3695	12.9885	10.2981	9.4921	7.9973
	0.94	23.3101	18.8742	8.7421	7.4262	6.2044	4.6595	28.0951	22.5296	12.8519	9.6368	9.0418	6.9966
	0.96	20.6579	16.4082	8.5946	7.2582	5.7305	4.5534	26.7945	19.4293	12.4288	9.5713	8.4072	6.4758
	0.98	19.7368	14.8366	8.3464	7.0992	5.6794	4.4436	24.4940	17.8847	11.9924	9.2514	7.3911	6.4312
	0.99	18.9057	12.7021	8.0092	6.9648	5.6512	4.4165	22.0257	15.3999	10.5560	8.9316	7.0175	5.8652
C_{DF} (n = 1.8)													
Pr	ϕ_f	Ri = 1						Ri = 2					
		Re→1	2	5	10	20	40	1	2	5	10	20	40
1	0.70	504.3750	252.5900	102.4524	53.0468	29.1635	17.8206	504.6128	253.9480	104.3444	55.8188	33.0176	22.4064
	0.75	263.7368	132.7994	54.7666	29.4898	17.5267	11.9528	135.0345	134.3524	57.0101	32.6554	21.6362	16.2499
	0.80	133.5404	67.8205	29.0481	16.8450	11.0315	8.5943	132.5412	69.6054	31.6491	20.4007	15.3687	12.1184
	0.84	74.1272	38.2664	17.4388	11.1109	8.3978	6.7468	75.8778	40.2758	20.3965	14.9904	12.0162	9.686
	0.86	52.3648	30.2695	14.2564	9.2551	7.5695	5.9606	54.9068	32.8115	16.7984	11.7971	10.6090	9.4584
	0.88	39.4020	22.4755	11.3344	8.3288	7.3695	5.2968	41.6426	24.9742	14.3125	11.4622	9.9115	7.8992
	0.90	26.4392	18.6815	9.6882	7.9704	6.6608	4.8786	34.3784	17.1368	12.7202	10.8385	9.0877	6.2327
	0.92	21.7451	14.6705	8.7747	7.5148	6.4632	4.6164	29.7835	16.5194	12.1448	10.3014	8.8797	5.2368
	0.94	18.5014	13.8118	8.4124	6.7009	5.7522	4.4052	25.0638	15.5621	11.8265	9.8798	7.8479	5.1827
	0.96	16.8975	12.0770	7.8612	6.6858	5.5570	4.3832	23.7860	14.6046	11.5694	9.1405	7.5665	4.4516
	0.98	15.8346	11.7645	7.2925	6.3091	5.2554	3.9999	21.9254	13.8922	11.1979	8.9701	7.1367	4.3573
	0.99	14.1678	10.4834	7.2324	6.0821	5.1144	3.5835	20.7886	13.6244	10.7766	8.9544	7.1082	3.8778
10	0.70	505.2063	255.1061	105.5985	56.0774	31.4692	19.3087	507.9882	258.8853	110.7864	61.9751	37.7765	28.5188
	0.75	265.5582	135.3440	57.6801	32.0066	19.3330	13.0846	268.6840	139.5024	62.9428	37.8287	25.3442	18.3640
	0.80	135.5073	70.3486	31.5908	18.8910	12.6870	9.3993	138.9855	74.7165	36.8896	24.5933	17.9282	13.3966
	0.84	76.1990	40.6494	19.6667	12.9062	9.5145	7.3994	79.9195	45.1252	25.0042	18.1490	13.7564	10.0534
	0.86	54.5098	32.4145	16.4014	11.4001	9.4491	7.2669	57.0518	34.9565	18.9434	13.9421	12.0565	9.6414
	0.88	41.4732	24.5885	13.2447	9.5742	8.2597	6.1390	44.7542	28.2009	16.8436	12.7018	10.7108	8.0870
	0.90	28.4365	16.7625	10.0880	8.1944	7.8601	5.2544	32.4566	21.4452	14.7438	11.4614	10.3182	7.7964
	0.92	20.9533	14.0021	9.9354	7.8229	7.0327	4.9244	25.4061	18.2380	13.0624	10.1360	8.7780	7.0628
	0.94	17.4818	13.1932	9.5486	7.7484	6.2057	4.6330	24.0360	17.9957	12.9402	9.8580	8.5799	6.3292
	0.96	17.3168	12.9241	9.1618	7.4514	5.8058	4.5945	23.2557	17.7538	12.8355	9.8538	7.8872	6.1124
	0.98	16.3430	12.0586	8.7178	7.1635	5.7323	4.2660	22.9936	17.6741	12.2172	9.6393	7.4768	5.9414
	0.99	15.2042	11.8458	8.6212	7.0090	5.6380	4.2060	22.4754	16.3525	11.5988	9.4248	7.1852	5.8795
50	0.70	507.4500	256.8337	106.3378	56.5525	31.7021	19.3978	512.5971	262.519	113.113	63.0381	38.3195	28.7768
	0.75	267.4950	136.7208	58.3628	32.3826	19.5585	14.9196	272.6008	142.314	64.4018	38.6888	25.8696	18.6990
	0.80	137.0470	71.3704	32.1165	19.2296	12.9401	9.5939	142.1074	76.8271	38.0490	25.3657	18.4380	13.7207
	0.84	77.4232	41.3708	30.1504	13.1760	9.6462	7.5657	82.4188	46.8900	26.0373	18.8630	14.2451	10.4364
	0.86	56.0698	33.9745	17.9614	12.9601	8.2546	6.9594	58.6118	36.5165	20.5034	15.5021	13.6165	9.7014
	0.88	42.6624	25.6779	14.2601	10.5445	7.3447	5.9847	46.3713	29.6496	18.0432	13.7368	11.2094	8.4325
	0.90	29.2549	17.3812	10.5588	8.1288	6.4348	5.4101	34.1308	22.7826	15.5829	11.9714	10.8022	7.8295
	0.92	21.7145	14.4588	9.8604	8.1025	6.0769	4.9686	27.0706	19.5867	13.9634	10.6966	9.5838	7.7172
	0.94	19.4879	13.8080	9.8145	7.9339	5.9558	4.8343	25.7629	19.4550	13.9110	10.1268	8.8147	6.9181
	0.96	18.1866	13.6595	9.7687	7.7654	5.9023	4.6597	24.6928	19.0898	13.3221	9.9738	7.9802	6.7851
	0.98	17.9081	12.8601	9.3833	7.5799	5.8732	4.4917	24.6175	18.1066	12.3851	9.7374	7.6828	6.1218
	0.99	16.3282	12.8588	9.2084	7.5214	5.8348	4.3148	23.4722	16.6265	11.7257	9.5481	7.3754	6.0055

Table D5 (Contd.)

Pr	ϕ_f	Ri = 1						Ri = 2					
		Re→1	2	5	10	20	40	1	2	5	10	20	40
1	0.70	913.8887	459.0824	188.1439	99.3022	56.6284	36.0569	916.9073	464.2401	194.5059	107.5409	66.6647	46.1695
	0.75	465.8084	235.7058	98.8400	54.7741	34.0012	23.9473	340.6480	240.6892	105.2576	62.9899	43.4207	32.8133
	0.80	231.5212	118.5407	52.0900	31.3482	21.3251	17.0039	233.3611	123.4429	58.5600	39.4378	30.3919	24.1096
	0.84	127.3890	66.5116	31.3450	20.7894	16.1413	13.2626	131.7579	71.4322	37.9453	28.8347	23.5316	20.4722
	0.86	92.7073	55.6273	24.5206	17.7432	15.0440	11.3961	100.5720	57.1811	30.7537	22.6433	21.0521	18.7133
	0.88	69.0850	45.6623	20.8794	15.7706	14.2124	10.6368	75.1103	46.9695	26.3945	21.7283	19.0670	16.3720
	0.90	51.4626	38.6972	18.5835	14.6475	13.0659	9.8970	63.6486	36.7578	23.4406	20.7801	17.8588	12.4589
	0.92	45.3697	32.7805	16.1158	14.1544	12.4401	9.5419	57.6420	33.8905	22.5712	19.5772	17.1836	10.6542
	0.94	40.4828	30.5374	15.2382	12.6131	11.0877	9.1020	51.0442	31.1632	22.0352	18.9168	15.3001	10.5481
	0.96	36.8873	26.5112	14.4480	12.4767	10.6678	8.7986	47.2109	29.4358	21.7018	17.4260	14.6655	9.6254
	0.98	34.3859	24.2463	13.3053	11.8632	10.1172	8.1930	43.7090	27.0002	20.9825	17.1861	13.8750	9.2488
	0.99	31.2889	21.8245	13.1254	11.3822	9.8248	7.6402	41.7797	25.5616	20.1076	17.1648	13.8367	8.4954
10	0.70	916.2191	465.0295	195.6520	106.2838	61.4817	38.9270	924.6685	475.8759	209.3799	120.6608	75.5610	54.7816
	0.75	469.7654	241.4066	105.3499	60.2110	37.6412	26.2128	478.1912	252.0994	117.9987	73.2617	50.2996	36.9192
	0.80	235.5591	123.8354	57.4212	35.5012	24.6397	18.7260	243.9442	134.0127	69.0778	47.4299	35.3679	26.7805
	0.84	131.4516	71.3195	35.8366	24.3079	18.4774	14.9549	139.7261	81.0178	46.8318	34.9826	27.1066	20.3998
	0.86	96.9723	57.8923	28.7856	21.0082	18.3536	14.4464	104.8370	61.4461	35.0187	26.9083	23.3320	19.6698
	0.88	77.0905	47.7955	23.6839	17.8738	16.7918	12.0327	81.0347	50.1772	31.4454	24.5881	21.7247	16.3734
	0.90	59.2086	37.6986	18.7692	15.8236	15.3025	10.0615	67.2323	38.9082	27.8721	22.2678	20.1552	16.0228
	0.92	46.4638	32.7719	18.4296	15.0781	14.0954	9.4911	56.5072	33.8047	25.0232	19.7514	17.4010	14.2621
	0.94	40.8646	29.9540	17.9472	14.7394	12.1275	9.0458	52.6988	33.1846	24.7107	19.2500	16.9784	12.5013
	0.96	37.4155	27.7532	17.2778	14.3326	11.3990	8.9665	48.4350	32.8032	24.5113	19.0973	15.2134	12.2718
	0.98	35.4222	24.8104	16.3242	13.7759	11.2497	8.5922	46.2511	32.6532	23.2254	18.7109	14.4926	11.7900
	0.99	34.0188	23.4844	16.1860	13.4034	11.0356	8.4378	43.6184	31.1635	21.8448	18.3245	14.0084	11.6085
50	0.70	921.8946	469.4692	197.6190	107.4193	62.0416	39.1749	936.1403	484.8379	214.5239	122.9265	76.7632	55.4086
	0.75	474.3490	244.7267	106.9908	61.1102	38.1869	26.9361	487.3484	258.6333	121.1980	75.1415	51.4930	37.6968
	0.80	239.0279	126.2071	58.6566	36.3163	25.2245	19.1672	250.8632	138.6963	71.5444	49.1388	36.5239	27.5202
	0.84	134.1508	73.0088	46.9262	24.9422	19.7301	16.2422	145.1184	94.8048	49.0620	36.5723	28.2009	21.9038
	0.86	99.6533	60.5733	31.4666	23.6892	17.4265	14.4790	107.5180	74.1271	37.6997	29.5893	26.0130	20.1836
	0.88	75.3169	49.8024	25.5309	19.6291	15.4889	12.8173	84.1360	60.9201	33.7104	26.5097	22.7607	17.4041
	0.90	58.9805	40.0313	20.5952	16.7230	14.1923	10.3987	66.7540	51.7129	29.7211	23.4300	21.5083	16.1066
	0.92	48.0963	35.2706	19.7501	15.5426	13.5313	9.7343	57.5210	44.9562	26.9519	20.9947	19.0759	15.7145
	0.94	42.7980	32.6822	18.5567	15.3602	12.1603	9.4939	53.8580	41.9846	26.7629	19.7636	17.8565	13.9147
	0.96	38.8445	30.0677	18.3633	15.0236	11.6328	9.2131	51.4874	38.5191	25.7508	19.5451	16.3874	13.2609
	0.98	37.6449	27.6967	17.7297	14.6791	11.5526	8.9353	49.1116	35.9913	24.3775	18.9889	15.0739	12.5531
	0.99	35.2339	25.5609	17.2176	14.4862	11.4860	8.7313	45.4979	32.0264	22.2817	18.4797	14.3929	11.8707

APPENDIX-E

Mixed Convection Non-Newtonian Data for Average Nusselt Number

TABLE E1: Dependence of average Nusselt number (Nu) on the fluid volume fraction (ϕ_f), Reynolds (Re), Prandtl (Pr) and Richardson (Ri) numbers for power-law index of n = 0.4

Nu														
n	Pr	ϕ_f	Ri = 1						Ri = 2					
			Re→1	2	5	10	20	40	1	2	5	10	20	40
0.4	1	0.70	1.0110	1.1535	1.4462	2.0696	3.2404	5.8762	0.9972	1.1652	1.4782	2.1585	3.5918	6.5001
		0.75	1.0160	1.1591	1.4690	2.2250	3.3868	6.1182	1.0756	1.1892	1.5547	2.2526	3.9875	6.7225
		0.80	1.1062	1.1891	1.6046	2.2595	3.4215	6.6728	1.0811	1.2097	1.6795	2.7340	5.0415	6.8567
		0.84	1.1128	1.2025	1.7214	2.8881	5.3069	6.7230	1.0866	1.2248	1.8440	3.0579	5.5904	7.9145
		0.86	1.1170	1.2045	1.7930	2.9469	5.4053	6.8153	1.0943	1.2635	2.1162	3.4625	5.8562	8.6321
		0.88	1.1237	1.2090	1.8645	3.0056	5.5037	7.5124	1.1125	1.3034	2.2496	3.7791	5.9308	8.7287
		0.90	1.1345	1.2134	1.9325	3.1944	5.5419	7.6764	1.1365	1.3433	2.3829	4.0956	5.9332	8.8565
		0.92	1.1613	1.2856	1.9735	3.5689	5.5622	7.9080	1.1459	1.5283	2.4261	4.4674	6.0053	8.9746
		0.94	1.2443	1.3826	2.0816	3.9202	5.5719	8.0924	1.1465	1.6596	2.4516	4.5768	6.5112	9.0927
		0.96	1.3116	1.4796	2.2306	4.2714	5.5816	8.2086	1.1804	1.7908	2.4770	4.7508	6.7595	9.6527
		0.98	1.3540	1.6940	2.7919	4.4094	5.6110	8.3247	1.2166	2.0072	3.2177	4.8055	7.0485	10.1267
		0.99	1.5152	1.9084	3.3532	4.5474	5.7769	9.2345	1.2528	2.2236	3.9584	5.0342	7.5857	10.6007
	10	0.70	1.8944	2.3294	2.7050	4.1092	9.2706	11.2780	1.8220	2.6304	3.4874	8.0408	12.2372	15.7582
		0.75	2.0166	2.4288	3.1211	4.7074	9.3085	12.5870	1.9881	2.8034	5.2874	8.1396	12.6459	16.0186
		0.80	2.0568	2.5256	3.5134	5.5501	10.3889	13.5245	2.1132	2.8786	5.3036	8.5242	13.0228	16.3641
		0.84	2.0818	2.5281	3.6527	5.6830	10.6360	13.8963	2.1715	2.9027	5.4105	8.6388	13.0960	16.7096
		0.86	2.0850	2.6725	3.7264	5.6953	10.8459	13.9042	2.2200	3.1259	5.7565	9.1558	13.5460	17.1591
		0.88	2.1068	2.7994	4.1552	6.0920	10.8745	14.1390	2.2706	3.2361	6.1475	9.6748	13.6815	17.6462
		0.90	2.1124	2.8232	4.1994	6.9198	10.9660	14.1548	2.3256	3.3462	6.5385	10.1938	13.8812	18.1270
		0.92	2.1534	2.8345	4.3218	7.2207	11.0650	14.2430	2.3483	3.7558	6.8957	10.3982	13.9875	18.1332
		0.94	2.1718	2.9725	4.7370	7.2568	11.0855	14.4470	2.3710	3.9455	7.2597	10.4858	14.2800	18.5515
		0.96	2.2934	3.0731	5.8212	8.7460	11.2546	15.3692	2.4562	4.1352	7.6236	10.5734	14.5720	19.6671
		0.98	2.3278	3.5989	6.5968	9.3625	11.5760	16.6232	2.4886	4.6537	8.1788	11.4432	16.5880	22.1386
		0.99	2.5488	4.1247	7.3724	9.9790	12.2770	16.9995	2.5210	5.1721	8.7340	12.3130	18.6030	26.1439
	50	0.70	2.6016	3.1228	3.3726	6.9477	11.6190	15.5850	3.2122	3.9302	5.3082	10.5494	15.1174	22.4355
		0.75	2.6215	3.2587	3.8745	8.6139	11.6834	17.0712	3.2343	4.2467	7.1526	10.7943	15.6843	22.8561
		0.80	2.6571	3.3628	4.1180	8.8951	12.5698	17.7090	3.2564	4.2622	7.1344	11.4968	15.9740	23.7283
		0.84	2.6729	3.4668	4.3614	9.1126	12.9590	17.7802	3.3025	4.4862	6.9418	11.5022	16.2632	24.3306
		0.86	2.7125	3.8621	4.9818	9.2820	12.9692	18.0170	3.4527	4.7256	7.5634	12.1108	16.9916	24.6004
		0.88	2.7243	4.1131	5.6329	9.3066	13.0239	18.1745	3.5826	4.9724	8.3061	12.3873	17.1524	25.4590
		0.90	2.8730	4.3495	6.1776	9.5006	14.2346	18.2547	3.7124	5.2518	9.0488	13.2723	17.5612	25.4989
		0.92	2.8977	4.3640	6.4748	10.1256	14.7780	18.2941	3.7254	5.3816	9.4584	13.9456	18.1490	25.6677
		0.94	3.0710	4.9898	6.6861	10.9218	15.5348	18.3468	3.8294	5.7248	10.0780	14.7516	18.5853	25.8896
		0.96	3.6198	5.0059	7.7392	11.7180	16.9861	19.7962	3.8417	6.1978	10.6976	15.5576	19.1450	26.2256
		0.98	3.9779	5.2340	9.3419	12.3388	17.3150	20.2300	3.9710	7.1348	12.8040	17.7013	22.0440	26.5515
		0.99	4.2158	6.1040	10.9446	12.9596	17.6442	22.6795	4.6665	8.0718	14.9108	19.8449	24.9435	26.9526

TABLE E2: Dependence of average Nusselt number (Nu) on the fluid volume fraction (ϕ_f), Reynolds (Re), Prandtl (Pr) and Richardson (Ri) numbers for power-law index of n = 0.6

Nu														
n	Pr	ϕ_f	Ri = 1						Ri = 2					
			Re→1	2	5	10	20	40	1	2	5	10	20	40
0.6	1	0.70	0.9814	1.1318	1.4174	2.0808	3.0558	5.1528	0.9667	1.1530	1.4280	2.0025	3.2144	5.7906
		0.75	1.0148	1.1477	1.5045	2.1764	3.4119	5.6115	0.9898	1.1706	1.5385	2.1998	3.6988	6.7027
		0.80	1.0169	1.1528	1.6834	2.3750	3.8721	5.7722	1.0156	1.1714	1.6508	2.5942	4.4577	7.3787
		0.84	1.0187	1.1634	1.7395	2.5928	4.2890	5.9332	1.0832	1.2158	1.7882	2.8819	5.1224	7.9280
		0.86	1.0204	1.1956	1.8219	2.9467	4.5026	6.2548	1.1220	1.2637	1.9842	3.1121	5.2264	8.1684
		0.88	1.0371	1.2099	1.8786	3.0299	4.6967	6.3784	1.1443	1.3115	2.0876	3.3707	5.4428	8.3284
		0.90	1.0371	1.2242	1.8925	3.1130	4.8907	6.5702	1.1507	1.4115	2.1910	3.6292	5.6592	8.4884
		0.92	1.0739	1.3295	1.9630	3.3307	4.9315	6.7152	1.2014	1.4476	2.3958	3.9547	5.7214	8.1665
		0.94	1.1107	1.3852	2.1831	3.5339	4.9840	6.7280	1.2195	1.5086	2.6224	4.1544	5.7774	8.0791
		0.96	1.1268	1.4409	2.4875	3.7371	5.0364	6.7307	1.2882	1.6056	2.6394	4.3540	5.8334	7.9917
		0.98	1.1668	1.6149	2.7320	4.0166	5.1292	6.7462	1.3218	1.6521	2.7527	4.6359	6.0763	8.3691
		0.99	1.2229	1.7888	2.9764	4.2961	5.3269	7.5288	1.5466	1.6985	2.8830	4.9177	6.3191	8.7464
	10	0.70	1.9518	2.2678	3.6420	4.9359	7.0129	9.7200	1.9524	2.7862	4.2562	6.2080	9.6986	13.4758
		0.75	1.9860	2.5103	3.6898	5.1528	7.3830	9.8895	2.0694	2.8192	4.5132	6.2647	9.8971	13.5670
		0.80	1.9996	2.5946	3.8015	5.3308	7.7590	10.0150	2.2080	3.0232	4.7692	6.7962	9.9754	13.6582
		0.84	2.0132	2.6805	3.8876	5.3644	8.0931	10.1400	2.5832	3.1265	4.7802	7.2599	10.1292	13.8882
		0.86	2.0181	2.6820	3.9736	5.4296	8.1726	10.1860	2.4126	3.2144	4.9659	7.4052	10.1574	13.9082
		0.88	2.0244	2.7417	3.9905	5.5102	8.1832	10.5834	2.3599	3.2245	5.1082	7.5175	10.4165	14.2450
		0.90	2.0306	2.7468	4.0556	5.6895	8.2646	10.6525	2.3072	3.3354	5.2504	7.6298	10.5110	14.3262
		0.92	2.0781	2.7528	4.1872	6.2082	8.3326	10.9606	2.3816	3.4257	5.3982	8.1121	10.6470	14.6983
		0.94	2.1594	2.7694	4.4837	6.4456	8.3460	10.9825	2.3632	3.4828	5.6383	8.3597	10.8782	14.9610
		0.96	2.1865	2.7712	4.7802	6.6830	8.4925	11.0003	2.3448	3.5443	5.8784	8.6072	11.1254	15.2244
		0.98	2.1945	3.1517	5.3091	7.4573	8.9561	11.9250	2.6114	3.8857	6.5601	9.2434	11.8870	15.5400
		0.99	2.3584	3.5340	5.8380	8.2316	9.7395	13.7095	2.8779	4.2270	7.2418	9.8795	13.8778	15.8552
	50	0.70	2.4418	3.0108	3.5393	5.3280	7.6070	12.2982	3.0124	4.0832	5.2308	7.7503	12.2642	15.8185
		0.75	2.5031	3.1112	3.8121	6.1354	8.1304	12.6535	3.1582	4.0842	5.9409	8.1124	12.4316	15.9690
		0.80	2.5465	3.1517	3.8331	6.5335	9.1194	12.7462	3.2403	4.2526	6.0543	8.2356	12.4362	16.1195
		0.84	2.5517	3.2115	4.1268	6.8945	9.5571	12.7850	3.3223	4.3678	6.3515	8.3142	12.6587	16.2162
		0.86	2.6002	3.2355	4.3654	7.0702	9.7658	12.7922	3.4126	4.5126	6.6759	8.5927	12.8021	16.5642
		0.88	2.6512	3.3844	4.4534	7.2458	10.1320	12.8234	3.5626	4.6524	6.9008	8.8066	12.9684	17.1196
		0.90	2.9862	3.4877	4.5624	7.5637	10.1344	12.8340	3.6534	4.7830	7.0002	9.4660	13.1020	17.2880
		0.92	2.9994	3.7398	5.3406	7.6132	10.4982	13.2248	3.8323	4.9284	7.2154	9.5008	13.3320	17.5032
		0.94	3.0408	3.8829	5.7479	7.9791	11.5305	14.0100	4.1128	5.0500	7.5010	9.5893	13.5452	18.5090
		0.96	3.4814	4.1435	6.1552	8.3944	12.9265	14.7946	4.3422	5.0534	7.7865	9.7125	13.6958	20.4541
		0.98	3.5758	4.3835	7.3833	10.5130	13.5980	17.0050	4.4288	5.6350	9.5962	11.3630	14.5460	21.7600
		0.99	3.6400	5.0272	8.6114	12.6308	14.2695	19.2148	4.4325	6.2166	11.4058	13.2598	16.1243	23.0661

TABLE E3: Dependence of average Nusselt number (Nu) on the fluid volume fraction (ϕ_f), Reynolds (Re), Prandtl (Pr) and Richardson (Ri) numbers for power-law index of n = 0.8

Nu														
n	Pr	ϕ_f	Ri = 1						Ri = 2					
			Re→1	2	5	10	20	40	1	2	5	10	20	40
0.8	1	0.70	0.9641	1.1128	1.3975	1.9650	2.9402	4.6220	0.9665	1.1187	1.4034	1.9950	3.1772	5.3209
		0.75	0.9904	1.1304	1.4921	2.1318	3.1922	5.0596	1.0061	1.1324	1.5043	2.2070	3.5860	5.9004
		0.80	1.0047	1.1435	1.6064	2.3018	3.5078	5.5007	1.0476	1.1484	1.6312	2.4698	4.0362	6.4915
		0.84	1.0136	1.1565	1.7136	2.4621	3.8262	5.8058	1.0880	1.1632	1.7610	2.7428	4.4345	6.7584
		0.86	1.0150	1.1968	1.7614	2.5021	4.0129	5.8302	1.1125	1.2135	1.8529	2.8254	4.6221	6.7718
		0.88	1.0162	1.2273	1.8024	2.6676	4.1680	5.8728	1.1288	1.2511	1.9606	3.0500	4.7951	6.8988
		0.90	1.0500	1.2578	1.8467	2.8330	4.3232	5.9397	1.1945	1.2886	2.0683	3.2745	4.9680	6.9714
		0.92	1.0946	1.2940	1.8909	3.0104	4.4417	5.9631	1.2100	1.3132	2.2230	3.4850	5.1273	7.0391
		0.94	1.1117	1.3532	2.7025	3.1858	4.5810	6.0362	1.2470	1.3364	2.4327	3.6565	5.3816	7.0932
		0.96	1.1520	1.4124	4.6473	3.3612	4.7201	6.1093	1.3650	1.3595	2.6423	3.8280	5.6358	7.2150
		0.98	1.1882	1.5600	5.1179	3.6008	4.8330	6.2276	1.4129	1.6345	2.8690	4.0696	5.7878	7.5660
		0.99	1.2101	1.7076	7.5332	3.8404	4.9466	6.5155	1.5680	1.9095	3.0957	4.3112	5.9398	8.0929
	10	0.70	1.9339	2.4829	3.4240	4.4662	5.9130	8.2326	1.9370	2.7376	3.9708	5.4038	7.7602	10.5125
		0.75	1.9716	2.5075	3.4728	4.4768	6.0411	8.4784	2.0652	2.7954	3.9730	5.5782	7.9932	10.9586
		0.80	2.0120	2.5301	3.4796	4.5762	6.2703	8.6889	2.1544	2.7988	4.0961	5.8448	8.2278	10.9877
		0.84	2.0522	2.5375	3.5100	4.6192	6.5116	8.7405	2.1662	2.8224	4.5127	6.0046	8.4145	10.9994
		0.86	2.0575	2.5526	3.5472	4.8978	6.6166	8.7768	2.2000	2.8886	4.5227	6.2540	8.4253	11.0001
		0.88	2.1060	2.5920	3.6109	4.9653	6.7211	8.7925	2.2338	2.9725	4.5326	6.3468	8.4361	11.0125
		0.90	2.1301	2.6340	3.6829	5.0327	6.8261	8.8041	2.3419	3.0414	4.5935	6.4265	8.4624	11.1313
		0.92	2.1360	2.7084	3.7432	5.2315	6.8869	8.8156	2.3490	3.1225	4.6740	6.5395	8.6457	11.2460
		0.94	2.1374	2.7120	3.9241	5.3918	7.1885	8.8209	2.3554	3.1942	4.8298	6.6203	9.1109	11.2501
		0.96	2.1415	2.7446	4.1652	5.5520	7.4898	8.9529	2.3662	3.2522	4.9855	6.8141	9.5761	11.4628
		0.98	2.1575	2.8919	4.5454	6.2798	7.9480	9.9051	2.4440	3.3102	5.1163	6.9832	10.0651	13.4351
		0.99	2.2404	3.1917	4.9255	7.0075	8.4054	10.8572	2.6536	3.3372	5.2470	7.1522	10.5540	15.4074
	50	0.70	2.5050	3.0244	3.9993	5.0684	6.5945	9.1534	2.8276	3.6552	5.0015	6.5592	9.1716	12.7035
		0.75	2.5250	3.0345	4.0375	5.1392	6.7942	9.4744	2.8405	3.6738	5.0842	6.7614	9.4895	12.8935
		0.80	2.5458	3.0675	4.1566	5.2258	7.1482	9.5467	2.9430	3.8065	5.1524	7.1478	9.8586	12.9289
		0.84	2.6663	3.1106	4.2425	5.3950	7.5245	9.5494	3.0584	3.8853	5.7182	7.2490	10.0560	13.2585
		0.86	2.7260	3.2154	4.2575	5.6862	7.5788	9.6163	3.2030	3.9052	5.7952	7.4586	10.0810	13.2816
		0.88	2.7851	3.2214	4.3284	5.8803	7.5960	9.7581	3.2144	4.1084	5.8046	7.7292	10.1015	13.4665
		0.90	2.8650	3.3962	4.5793	6.0743	7.6126	9.9824	3.4362	4.1154	5.8140	7.9605	10.1055	13.7585
		0.92	2.9292	3.4345	4.5832	6.3999	8.1216	9.9922	3.4870	4.1788	6.0974	7.9998	10.6805	14.2585
		0.94	3.1380	3.7422	4.9802	6.6375	9.1450	11.0290	3.5662	4.4102	6.2987	8.3417	11.0830	14.7119
		0.96	3.2248	3.9291	5.3810	6.8750	10.1675	12.5092	3.6236	4.6885	6.5000	8.7229	11.4864	15.9572
		0.98	3.3863	4.0630	6.1857	8.4505	13.0500	15.5340	3.6274	4.8449	7.6322	9.3642	15.4480	19.8701
		0.99	3.5927	4.4619	6.9903	10.0259	15.9354	18.5587	3.9150	5.2795	8.7644	10.0055	19.4090	23.7829

TABLE E4: Dependence of average Nusselt number (Nu) on the fluid volume fraction (ϕ_f), Reynolds (Re), Prandtl (Pr) and Richardson (Ri) numbers for power-law index of n = 1.4

Nu														
n	Pr	ϕ_f	Ri = 1						Ri = 2					
			Re→1	2	5	10	20	40	1	2	5	10	20	40
1.4	1	0.70	0.9356	1.0815	1.3666	1.9194	2.7627	3.8303	0.9364	1.0834	1.3684	1.9318	2.8706	4.2770
		0.75	0.9454	1.1034	1.4547	2.0585	2.8784	3.9452	0.9503	1.1040	1.4592	2.0929	3.0845	4.5244
		0.80	0.9538	1.1073	1.5624	2.1780	2.9832	4.0847	0.9635	1.1089	1.5745	2.2615	3.3107	4.7421
		0.84	0.9707	1.1238	1.6548	2.2637	3.0881	4.2152	0.9776	1.1274	1.6835	2.4130	3.5020	4.9077
		0.86	0.9875	1.1626	1.7029	2.3157	3.1834	4.3658	0.9916	1.1753	1.7429	2.5231	3.6233	4.9821
		0.88	1.0087	1.1959	1.7442	2.3683	3.2504	4.4016	1.0154	1.2094	1.8122	2.6108	3.7112	5.0475
		0.90	1.0328	1.2292	1.7854	2.4208	3.3173	4.4374	1.0465	1.2434	1.8814	2.6984	3.7990	5.1128
		0.92	1.0634	1.2666	1.8347	2.5032	3.4115	4.4429	1.0886	1.2915	1.9703	2.8124	3.9023	5.0586
		0.94	1.0884	1.3077	1.9024	2.6081	3.5128	4.4660	1.0918	1.3517	2.0828	2.9338	3.9406	5.0821
		0.96	1.1181	1.3587	2.0089	2.7355	3.5300	4.5404	1.1484	1.4374	2.2228	3.0441	3.9544	5.2335
		0.98	1.1474	1.4598	2.1745	2.8168	3.6943	4.5920	1.1750	1.5867	2.3630	3.1104	4.1705	5.4529
		0.99	1.1849	1.5675	2.2382	2.9713	3.9162	4.7104	1.2790	1.6944	2.4370	3.2929	4.4096	5.7228
	10	0.70	1.8660	2.2738	2.9604	3.6246	4.4504	5.5132	1.9074	2.5168	3.3714	4.2391	5.3764	6.8195
		0.75	1.9061	2.3018	2.9916	3.6521	4.4937	5.5595	2.0243	2.5177	3.4129	4.2817	5.4201	6.8426
		0.80	1.9120	2.3122	2.9924	3.6883	4.5405	5.5909	2.0277	2.5352	3.4258	4.2971	5.4209	6.9406
		0.84	1.9134	2.3550	3.0228	3.7056	4.6028	5.6974	2.0441	2.5536	3.4338	4.3962	5.5362	6.9542
		0.86	1.9715	2.4593	3.0641	3.7244	4.6923	5.9567	2.0457	2.5614	3.4546	4.4361	5.6521	7.0625
		0.88	2.0241	2.4948	3.0878	3.8422	4.7482	6.0114	2.0732	2.6069	3.5480	4.4574	5.7523	7.0827
		0.90	2.0250	2.5360	3.2101	3.9044	4.7818	6.0418	2.1060	2.6690	3.5499	4.5186	5.8524	7.0991
		0.92	2.0480	2.5635	3.2645	4.0052	4.9375	6.0420	2.1084	2.6708	3.6712	4.6427	5.8626	7.1126
		0.94	2.0605	2.6288	3.4116	4.1544	5.0750	6.0660	2.1254	2.6772	3.6799	4.8014	5.8927	7.1778
		0.96	2.0729	2.6660	3.5147	4.2204	5.0902	6.3024	2.1435	2.7072	3.8444	4.8451	5.9844	7.2429
		0.98	2.0975	2.6849	3.5916	4.3468	5.5394	6.8220	2.1683	2.8648	3.9555	4.9358	6.5269	7.7925
		0.99	2.1087	2.6890	3.6760	4.8032	5.7046	7.1484	2.3054	2.9830	4.1232	5.5238	7.7058	9.3284
	50	0.70	2.3194	2.7270	3.4290	4.0280	4.8535	5.9223	2.5608	3.0646	3.9217	4.7965	5.9314	7.3978
		0.75	2.3308	2.7471	3.4342	4.0648	4.8809	5.9509	2.5680	3.0902	3.9720	4.8276	5.9426	7.5398
		0.80	2.4055	2.7686	3.4394	4.1164	5.0001	6.0850	2.6221	3.1059	3.9859	4.9286	6.0920	7.8234
		0.84	2.5035	2.8432	3.4480	4.2268	5.0963	6.3646	2.6604	3.1158	4.0788	5.0291	6.3635	8.1696
		0.86	2.5200	2.9016	3.5444	4.2758	5.2966	6.5875	2.6942	3.2001	4.1716	5.1147	6.6984	8.4452
		0.88	2.6163	2.9178	3.6223	4.3371	5.4432	6.8703	2.7663	3.2370	4.1829	5.2834	6.8889	8.5493
		0.90	2.7125	3.0481	3.7681	4.5760	5.5897	7.1530	2.8898	3.3944	4.3758	5.4521	7.0794	8.6369
		0.92	2.8328	3.2895	3.9369	4.6135	5.8935	7.1747	2.9686	3.4900	4.4980	5.7218	7.3152	8.6963
		0.94	2.8384	3.3206	4.1271	4.8926	6.1296	7.2810	3.0919	3.6884	4.6438	6.0644	7.3220	8.8285
		0.96	3.0543	3.6174	4.3173	5.2570	6.2024	7.2834	3.2852	3.9336	5.0212	6.1720	7.3512	10.0382
		0.98	3.3109	3.7008	4.5809	5.5439	6.6722	8.8313	3.3353	4.0005	5.2754	6.4760	8.3367	12.3659
		0.99	3.5259	3.9505	5.0254	7.1154	8.8902	9.2517	3.5420	4.1995	5.8216	7.6846	11.9814	15.3005

TABLE E5: Dependence of average Nusselt number (Nu) on the fluid volume fraction (ϕ_f), Reynolds (Re), Prandtl (Pr) and Richardson (Ri) numbers for power-law index of n = 1.8

Nu														
n	Pr	ϕ_f	Ri = 1						Ri = 2					
			Re→1	2	5	10	20	40	1	2	5	10	20	40
1.8	1	0.70	0.9255	1.0709	1.3567	1.9050	2.7101	3.6201	0.9259	1.0715	1.3576	1.9121	2.7733	3.8997
		0.75	0.9278	1.0943	1.4421	2.0343	2.7848	3.6294	0.9309	1.0948	1.4446	2.0550	2.9123	4.0312
		0.80	0.9411	1.0945	1.5477	2.1363	2.8288	3.6580	0.9498	1.0952	1.5545	2.1894	3.0515	4.1550
		0.84	0.9590	1.1145	1.6341	2.1966	2.8702	3.7115	0.9650	1.1147	1.6531	2.3002	3.1715	4.2507
		0.86	0.9769	1.1553	1.6828	2.2216	2.9027	3.7628	0.9799	1.1662	1.7156	2.4235	3.2598	4.3124
		0.88	0.9972	1.1853	1.7138	2.2557	2.9470	3.8050	1.0026	1.1958	1.7666	2.4607	3.3170	4.3611
		0.90	1.0214	1.2152	1.7447	2.2898	2.9906	3.8471	1.0330	1.2254	1.8175	2.4978	3.3741	4.4097
		0.92	1.0520	1.2508	1.7826	2.3398	3.0536	3.9030	1.0778	1.2705	1.8854	2.5805	3.4454	4.8685
		0.94	1.0807	1.2897	1.8316	2.4095	3.1281	3.9080	1.0808	1.3265	1.9697	2.6708	3.5202	4.3978
		0.96	1.1130	1.3385	1.9084	2.5035	3.1932	3.9384	1.1323	1.4016	2.0770	2.7692	3.5154	4.3597
		0.98	1.1318	1.4263	1.9939	2.5811	3.3060	4.0829	1.1630	1.5091	2.1544	2.8314	3.6390	4.5963
		0.99	1.1740	1.5140	2.0793	2.6586	3.4178	4.2627	1.2490	1.6165	2.2318	2.8935	3.7625	4.8328
	10	0.70	1.8268	2.1958	2.7874	3.3473	3.9603	4.7340	1.8979	2.3980	3.1290	3.7899	4.6224	5.6547
		0.75	1.8762	2.2118	2.7887	3.3497	4.0068	4.7927	1.9690	2.4125	3.1358	3.8322	4.6670	5.6744
		0.80	1.8972	2.2364	2.8157	3.3521	4.0115	4.8048	1.9748	2.4178	3.1426	3.8328	4.6895	5.7356
		0.84	1.9020	2.2997	2.8403	3.3683	4.0690	4.9006	1.9980	2.4604	3.1548	3.8754	4.8036	5.7920
		0.86	1.9407	2.3512	2.8426	3.4208	4.1274	5.0080	2.0152	2.4894	3.1836	3.9186	4.8621	5.9515
		0.88	1.9766	2.3675	2.9568	3.5058	4.1950	5.0131	2.0350	2.5029	3.2616	3.9868	4.8680	6.0618
		0.90	1.9991	2.4026	2.9792	3.5548	4.2650	5.1153	2.0480	2.5495	3.2854	4.0277	4.9324	6.1432
		0.92	2.0130	2.5031	3.1295	3.7580	4.4488	5.2897	2.0612	2.6282	3.4360	4.1720	5.0806	6.1721
		0.94	2.0260	2.5231	3.1581	3.7618	4.4829	5.3660	2.0800	2.6296	3.6002	4.2056	5.2270	6.2237
		0.96	2.0525	2.6027	3.3369	3.9664	4.5819	5.3662	2.0893	2.6586	3.6885	4.3646	5.2602	6.3179
		0.98	2.0840	2.6519	3.3532	4.0436	4.9860	5.7583	2.1035	2.6796	3.7137	4.5197	5.7300	6.6193
		0.99	2.0921	2.6657	3.5480	4.1710	5.3897	6.1503	2.1855	2.7670	3.7388	4.6748	6.2330	7.0954
	50	0.70	2.2520	2.6226	3.1832	3.6005	4.3107	5.1024	2.4546	2.8940	3.5969	4.2454	5.0711	6.0978
		0.75	2.2718	2.6252	3.1994	3.6922	4.3346	5.1084	2.4796	2.8992	3.6251	4.2560	5.0767	6.1248
		0.80	2.3540	2.6826	3.2156	3.7131	4.4016	5.2721	2.5205	2.9264	3.6523	4.3855	5.2318	6.2464
		0.84	2.4551	2.7046	3.2448	3.8045	4.4612	5.2966	2.5471	2.9587	3.6795	4.4002	5.2448	6.5282
		0.86	2.4780	2.7265	3.2960	3.8257	4.5770	5.4156	2.6310	2.9782	3.7191	4.4997	5.5126	6.8659
		0.88	2.4800	2.7340	3.5056	4.0038	4.7530	5.6980	2.7145	3.0932	3.8270	4.6138	5.6775	7.1817
		0.90	2.5012	2.9929	3.7149	4.0815	4.7738	5.9804	2.7960	3.1852	3.9948	4.6994	5.8424	7.4975
		0.92	2.7072	3.0953	3.8475	4.2844	5.0308	6.3427	2.8418	3.3122	4.0642	4.8580	6.1834	7.8039
		0.94	2.8035	3.2450	4.1398	4.4606	5.3961	6.5338	3.0535	3.5305	4.3520	5.1801	6.5747	7.8429
		0.96	3.0286	3.4565	4.2446	4.6967	5.6474	6.5407	3.0723	3.6260	4.4128	5.5788	6.6270	7.8848
		0.98	3.2895	3.5812	4.2587	5.2552	6.1490	7.8847	3.3051	3.8757	4.8106	6.1976	7.4866	9.9365
		0.99	3.5073	3.9195	4.5647	5.8137	6.6508	9.2355	3.5174	3.9504	5.2084	6.8164	8.3462	12.0691